WAVE CLIMATE AND SEDIMENT TRANSPORT WITHIN TAURANGA HARBOUR, IN THE VICINITY OF PILOT BAY.

A thesis

submitted in fulfillment

of the requirements for the degree

of

Doctor of Philosophy in Earth Sciences

at the

University of Waikato

by

WILLEM PIETER DE LANGE

Department of Earth Sciences
University of Waikato
Hamilton, New Zealand

February, 1988

Abstract

Previous studies of hydrodynamics and circulation in Tauranga Harbour, a meso-tidal estuarine lagoon (168km^2 total area), have concentrated on tidally-induced processes. However, non-tidal processes, such as wind-generated waves, are also responsible for sediment transport in estuaries. This study was initiated to characterise the wave climate and investigate the effect waves have on sediment transport and deposition within the southern basin of the harbour (112km^2), particularly adjacent to the Port of Tauranga in the vicinity of Pilot Bay.

A review of previous investigations of the hydrodynamics and sedimentology of Tauranga Harbour was undertaken, and predictions concerning tidal circulation patterns and sediment transport pathways were examined in light of more recent data. Two model-based studies were considered in detail: the physical model run by the Wallingford Hydraulic Research Station; and the numerical models used by the Tauranga Harbour Study (THS). Both methods simulated large-scale circulation patterns reasonably well, the numerical model results being more exact than those of the earlier physical model. However, discrepancies were evident when considering more local circulation patterns, such as in Pilot Bay.

Tidal circulation patterns and sediment facies distributions for Pilot Bay were compared with detailed model predictions from the two previous studies. Both failed to correctly define the circulation present, although the THS numerical sediment transport model did agree with the facies distribution. However, the facies distribution is relict, resulting from flow conditions prior to port development.

Wind and pressure parameters were measured to assess the role local weather conditions play in determining the wave climate within the harbour. The harbour weather patterns are dominated by a diurnal sea breeze cycle which results in a relatively high average speed of 4ms^{-1} compared to inland locations.

To define the wave climate, two main groups of waves were considered: high-frequency (short-period) waves, including wind-generated waves; and low-frequency (long-period) non-tidal waves, including seiches, storm surges and tsunamis. The wave climate within Tauranga Harbour is

dominated by wave energy transmitted through the harbour entrance. This source accounts for ~70% of the energy in the average harbour spectrum; local wind-generated waves account for ~9%; and the rest represents low-frequency waves, including tides. A relationship, based on the JONSWAP spectral form, was derived to predict the local wind-generated component of the wave field. The equation is more peaked than the normal JONSWAP form, reflecting the extreme limiting conditions found inside the harbour.

Seiching occurs frequently, usually in association with local winds exceeding $9.5ms^{-1}$, but also in response to external forcing by tsunamis and large swell waves. Analysis of the seiche frequencies indicates that seiches are not controlled by harbour channels and dredged shipping basins. The largest oscillations within the harbour are caused by tsunamis and storm surges.

Normally high-frequency waves inside the harbour are too small to move significant quantities of sediment, except when breaking or in very shallow water. However, wave-induced suspension of sediment combined with tidal currents can produce large sediment fluxes, particularly over the extensive intertidal regions of the southern basin ($64km^2$). This process is most significant for regions where tidal velocities are below sediment threshold ($<0.35ms^{-1}$). The annual sediment fluxes for shallow regions with low tidal velocities are comparable to those occurring in major tidal channels within the harbour.

A renourished beach in Pilot Bay was monitored between 1983 and 1987. Based on measured volumetric changes the renourished beach is expected to last for between 7 and 16 years. The net sediment flux measured within the nearshore zone is in close agreement with the Tauranga Harbour Study numerical model predictions. Textural analyses of monthly sediment samples were used to predict sediment transport directions. The method employed produced directions consistent with the observed patterns of erosion and accretion.

Acknowledgements

First and foremost I would like to thank the Bay of Plenty Harbour Board, especially John Palmer, John Stephenson and Owen Mainard, for their support during this study, and my supervisors, Associate-professors Terry Healy and Cam Nelson, for their assistance and comments throughout this study.

I am indebted to Dr. Kerry Black for his assistance with the SUBTLE wave probe system employed during the initial stages of this study and the additional numerical modelling he undertook to check circulation patterns within Pilot Bay. I wish to acknowledge the contributions made by Dr. Alistair Barnett and the Ministry of Works and Development Water Quality Centre in terms of access to raw data from the THS numerical model simulations and the Moturiki Island tide gauge data.

I thank Eduoard Devanouges for his help during the data collection programme in the winter of 1983. Bruce Shakespeare and Malcolm Greig of the New Zealand Oceanographic Institute maintained the Aanderaa current meters used and also transcribed the data from the Aanderaa tapes to media compatible with the University computers. Dr. Steve Reid, New Zealand Meteorological Service, provided wind data from Tauranga Airport for the winter of 1983.

Finally I would like to thank Carole Keenan and the other staff of the Computer Centre for their assistance with transferring unusually formatted data to the University computer system.

Contents

List of Plates

List of Figures

List of Tables

Notation

a	constant in power function
B	basin length (m)
b	constant in power function
C	wave phase velocity (ms^{-1})
c	concentration of suspended sediment
	constant in power function
c_a	sediment concentration at height a
c_b	near-bed sediment concentration
c_0	near-bed sediment concentration
D	duration (s)
	grain diameter (m)
	half tidal cycle duration (~22350s)
D_{50}	median grain diameter (m)
D_{65}	65th percentile grain diameter (m)
d	constant in power function
d_0	wave orbital diameter (m)
E	energy (J)
E_{max}	peak energy (J)
E_t	total wave energy (J)
$E(f)$	energy function
e_o	energy contribution per radian ($J.rad^{-1}$)
F	fetch (m)
$F(k)$	energy density in wave number space
$F(x)$	Weibull probability function
F_{eff}	effective fetch (m)
F_o	Liu dimensionless fetch
f	frequency (Hz)
f_i	inertial frequency
f_m	mean frequency (Hz)
f_n	free oscillation frequency (Hz)
f_p	peak frequency (Hz)
f_w	wave friction factor
f_0	fundamental frequency (Hz)
g	gravitation constant ($9.81ms^{-2}$)
H	wave height (m)
H_b	breaking wave height (m)
H_c	component wave height (m)
H_e	monochromatic wave height (m)
H_m	mean wave height (m)
H_{max}	maximum wave height (m)
H_{m0}	spectral wave height (m)
H_{rms}	root mean square wave height (m)
H_s	significant wave height (m) - statistical
H_{10}	average height of highest 10% of wave heights (m)
H_o	significant wave height (m) - energy based
h	water depth (m)
k	constant
	roughness length (m)
	wave number ($2\pi/L$) (m^{-1})
L	wave length (m)
L_e	edge wave length (m)
m_n	nth spectral moment
N	number of waves

n	mode of oscillation
	scaling factor relating phase velocity to group velocity
p	pressure (Pa)
	probability
p_o	sea level pressure (hPa)
p_z	pressure at altitude z (hPa)
Q_p	Goda's peakedness parameter
q	JONSWAP peak scaling power
q_b	bedload flux ($kgm^{-1}s^{-1}$)
q_s	suspended sediment flux ($kgm^{-1}s^{-1}$)
R	tidal range (m)
	gas constant ($287Jkg^{-1}K^{-1}$)
r	correlation coefficient
	grain radius (cm)
r^2	determination coefficient
S	generalised wave energy function
S_{ds}	energy dissipation function
S_{in}	momentum transfer function
S_{nl}	non-linear transfer functions
$S(f)$	Spectral energy density function (m^2Hz^{-1})
$S(f_p)$	Energy density at spectral peak (m^2Hz^{-1})
Sk	skewness
$Sn(f)$	non-dimensional energy density function
s	beach slope
	settling velocity (ms^{-1})
	sheltering coefficient
s_m	measured settling velocity (ms^{-1})
s_o	standard settling velocity ($1ms^{-1}$)
s_s	suspended sediment load (kgm^{-2})
T	temperature (°K or °C)
	wave period (s)
T_c	crest wave period (s)
T_{max}	maximum wave period (s)
T_p	peak period (s)
T_s	significant wave period
T_z	mean wave period (s)
T_{10}	average period of longest 10%
t	time (s)
U	wind speed (ms^{-1})
U_A	SMB adjusted wind speed
U_*	Liu wind friction velocity
u	current velocity (ms^{-1})
u_{max}	maximum wave orbital velocity (ms^{-1})
u_1	current velocity 1m above bed (ms^{-1})
u_{1cr}	critical velocity 1m above bed (ms^{-1})
u_*	skin friction velocity (ms^{-1})
u_{*cr}	critical skin friction velocity (ms^{-1})
V	peak tidal velocity (ms^{-1})
v	current velocity (ms^{-1})
y	distance above bed (m)
x	distance along a basin (m)
	distance to the origin of the boundary layer
x_i	radial distance to shoreline (m)
z	Rouse number

α	Phillips' equilibrium constant (0.008)
	Weibull distribution location parameter
α_b	breaker angle (°)
β	angle between wave recorders
	constant
	Weibull distribution shape parameter
ψ	Shields parameter
ψ_c	critical Shields parameter
ψ_r	Shields parameter adjusted for flow contraction
ψ'	Shields parameter over rippled or duned bed
Φ	TMA depth scaling factor
ϕ	cospectral phase lag
	latitude (°)
	non-dimensional grain size
ϕ_{50}	median grain size
ϵ	non-dimensional surface variance
	turbulent viscosity (m^2s^{-1})
ϵ_s	spectral width
Λ	JONSWAP shape function
λ	non-dimensional spectral shape
	ripple length (m)
λ_b	linear concentration
η_t	surface displacement (m)
κ	von Kármáns constant (≈0.4)
ω	angular frequency (rad)
μ	dynamic viscosity (Poise)
ν	kinematic viscosity (m^2s^{-1})
	non-dimensional peak frequency
ℓ	concentration gradient
ρ	fluid density (kgm^{-3})
ρ_a	density of air (kgm^{-3})
ρ_s	grain density (kgm^{-3})
ρ_w	density of water (kgm^{-3})
γ	JONSWAP peak enhancement parameter
θ	angle to direction of wave propagation (rad)
	wave orthogonal approach angle
θ_i	angle between wind axis and radii (°)
σ	sorting
	width of the spectral peak
σ^2	water surface variance (m^2)
τ	shear stress (Nm^{-2})
τ_{max}	maximum shear stress (Nm^{-2})
τ_0	shear stress (Nm^{-2})
τ_*	shear stress over rippled or duned bed (Nm^{-2})
ξ	dynamic friction angle (°)
Δf	frequency interval
$\Delta\theta$	angular width of segment
δ	boundary layer thickness (m)
	non-dimensional duration
χ	non-dimensional settling velocity
χ_{50}	median settling velocity
ζ	non-dimensional fetch
	ripple height (m)
π	constant

Abbreviations

A/D	analog to digital
BOPHB	Bay of Plenty Harbour Board
df	degrees of freedom
HRS	Hydraulic Research Station
JONSWAP	Joint North Sea Wave Project
MHW	mean high water
MHWS	mean high water spring
MLW	mean low water
MLWS	mean low water spring
MSL	mean sea level
NZMS	New Zealand map series
	New Zealand Meteorological Service
RSA	Rapid sediment analyser
SMB	Sverdrup-Munk-Bretschneider
SPM	Shore Protection Manual

Chapter 1 - Introduction

Tauranga Harbour is located in the north-western Bay of Plenty (Fig. 1.1). The harbour complex has been described as a meso-tidal estuarine lagoon impounded by a barrier island and two barrier-tombolo's (Healy & Kirk, 1981; Dahm, 1983). The harbour can be considered as two almost independent basins (Davies-Colley, 1976; Barnett, 1985) with the southern basin possessing the largest tidal compartment (Hydraulics Research Station, 1963; Dahm, 1983). The Port of Tauranga is located within the southern basin and it is in the vicinity of the port and the southern harbour entrance that most previous work has been concentrated.

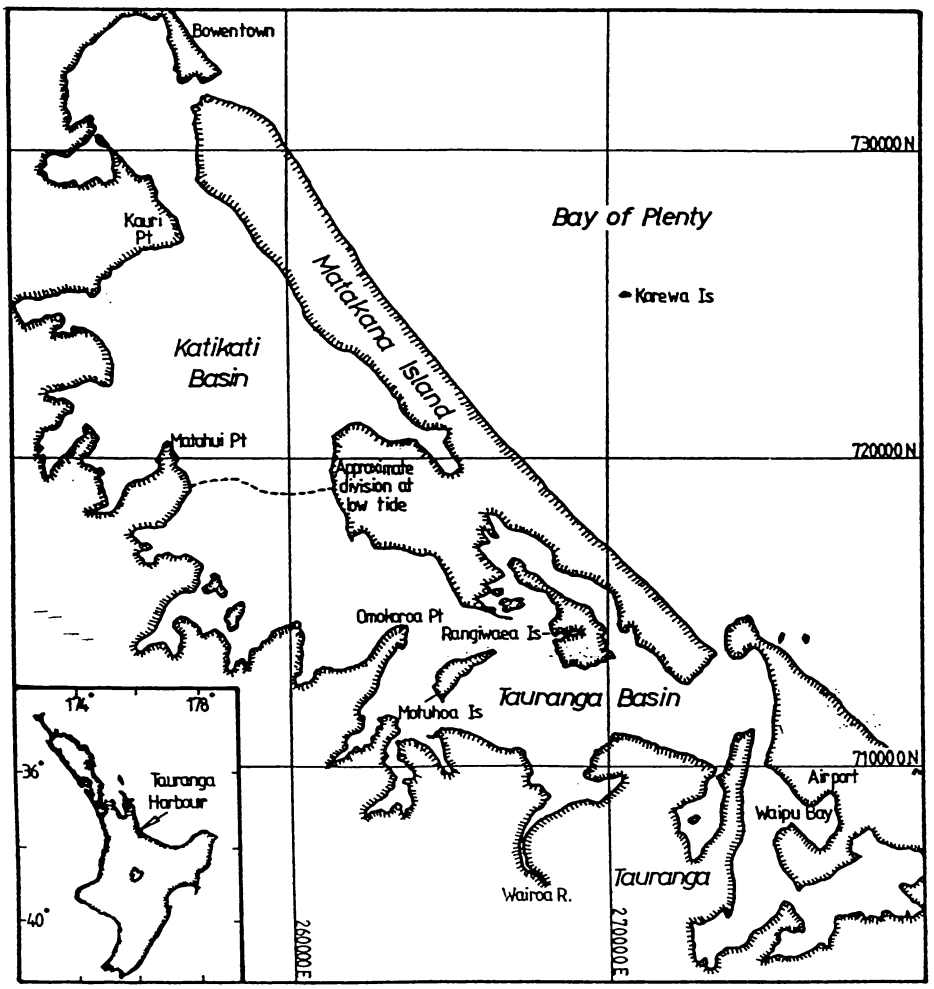

Figure 1.1 - Location diagram of the Tauranga Harbour showing the division of the harbour into the northern Katikati Basin and southern Tauranga Basin.

From research into historical morphological changes within the harbour, Dahm (1983) expressed concern over the future of the lower

Western Channel (Fig. 1.2). Arising from this, and to ascertain whether port development had influenced, or exacerbated, major hydrodynamic and sedimentological changes, the Bay of Plenty Harbour Board (BOPHB) commissioned the Tauranga Harbour Study (THS). The primary aims of the study were (Black, 1984) to:

(i) investigate the past and present patterns of sediment transport in Tauranga Harbour with particular reference to the Western Channel;

(ii) ascertain past effects and predict future effects of construction work on sediment transport in Tauranga Harbour, with particular consideration to the Sulphur Point construction and the construction of a cross-harbour bridge; and

(iii) predict shipping channel maintenance dredging requirements in Tauranga Harbour.

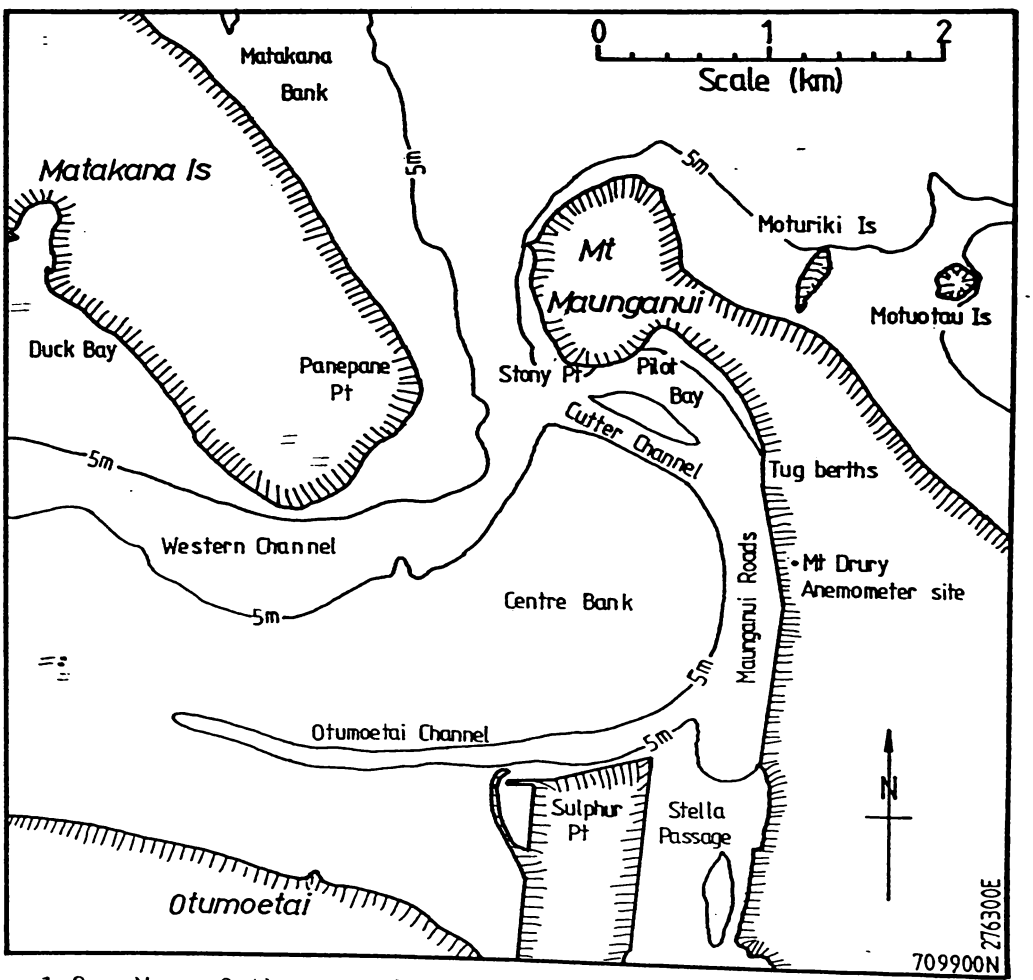

Figure 1.2 - Map of the southern basin of Tauranga Harbour showing the major features referred to in this report.

1.1 - Study objectives

Although the THS did consider by inference the influence of waves on sediment transport for the ebb tidal delta, within the harbour the study was restricted to tidal current induced sediment transport. Consequently, recognising the possible influence of non-tidal processes on sediment transport, this research project was initiated to:

(a) characterise the wave climate within the harbour, particularly for the region affected by port development; and

(b) investigate the role of waves in entraining and transporting sediment within the harbour.

As this study progressed, two additional objectives were added:

(c) to review the application of the Hydraulic Research Station (HRS) physical model and the THS numerical model studies of Tauranga Harbour, in light of subsequent data; and

(d) to monitor and assess in relation to the wave climate, and other factors, the long term response of the renourished beach in Pilot Bay.

These objectives were largely constrained to Pilot Bay and the adjacent inner harbour, for a number of reasons:

(1) The interactions between waves and currents within most of inner harbour area covered by the THS were deemed too complex to be tackled by the limited resources of this project. The three main factors complicating analysis in regions other than Pilot Bay, such as Centre Bank, are high tidal velocities, extreme depth-limited conditions, and exposure to ocean swell propagating directly through the entrance. These problems are not insurmountable and could be dealt with, given a more intensive monitoring programme;

(2) Pilot Bay is adjacent to the BOPHB offices and the main port facilities. The BOPHB tug berths afforded security, access to technical support, and were favourably located in relation to the two longest fetches within the harbour. Hence this site provided a suitable location for the installation of the equipment used to quantify the wave climate.

(3) Both the HRS and THS model studies made detailed predictions about the hydrodynamic behaviour in the vicinity of Pilot Bay

which could be examined to test the applicability of the models. Further, the two models considered the long term sedimentation patterns within this region; and

(4) Prior to the commencement of the study, a portion of Pilot Bay beach was artificially renourished by dredge spoil. By monitoring the response of the renourished beach a long term assessment of the total sediment transport induced by tidal and non-tidal (wave) processes could be made. This was not possible at any other location within the harbour.

Chapter 2 - Review of Harbour Studies

This chapter reviews earlier hydrodynamic and sedimentological studies of Tauranga Harbour as a background to the two major model studies undertaken of the harbour. Predictions and observations concerning sediment transport and tidal flow patterns are examined, in particular those relating to the Pilot Bay region. Finally the limitations of the two sediment transport models are considered.

2.1 - Early harbour studies

Early studies of Tauranga Harbour were concerned with the suitability of the harbour for port development (Coode, 1880; Blair-Mason, 1919; Lee, 1928). These studies were based primarily on visual observations of flow patterns and analysis of bathymetric surveys. The primary objective of the early reports was to determine the cost of potential harbour development and assess the relative economic viabilities of development options.

The review of survey data presented by Lee (1928) represents the first quantitative assessment of the historical morphological changes, although it is restricted to a comparison of the 1901 and 1927 bathymetric surveys. This study concluded that the shallow regions of the ebb delta (Matakana Bank) were highly mobile, whereas the inner harbour showed little change, with accretion being compensated by erosion, except for slight channel narrowing in Stella Passage.

In 1959, the Hydraulics Research Station (HRS) at Wallingford, United Kingdom, was commissioned to undertake a study of the hydrodynamics of Tauranga Harbour using a physical scale model of the harbour (HRS, 1963, 1968). This study considered a range of development options for the port and assessed their likely impact on the tidal currents within the harbour. These findings were extended to predict likely bathymetric responses to the changed harbour flows. This study is considered in more detail in Section 2.1.1.

The first major research into the sediment dynamics of Tauranga Harbour was undertaken by Davies-Colley (1976). His study was primarily concerned with sediment transport in the vicinity of the flood and ebb tidal delta systems, with the main emphasis being on the flood tide delta. This study proposed a general model for sediment movement (Fig.

2.1A), similar to the idealised model for sandy mesotidal inlets (Boothroyd, 1978), apart from perturbations to the sediment transport pathways in the lower Western Channel. The general circulation is indicative of a system dominated by sediment fluxes induced by a flood jet and associated eddies.

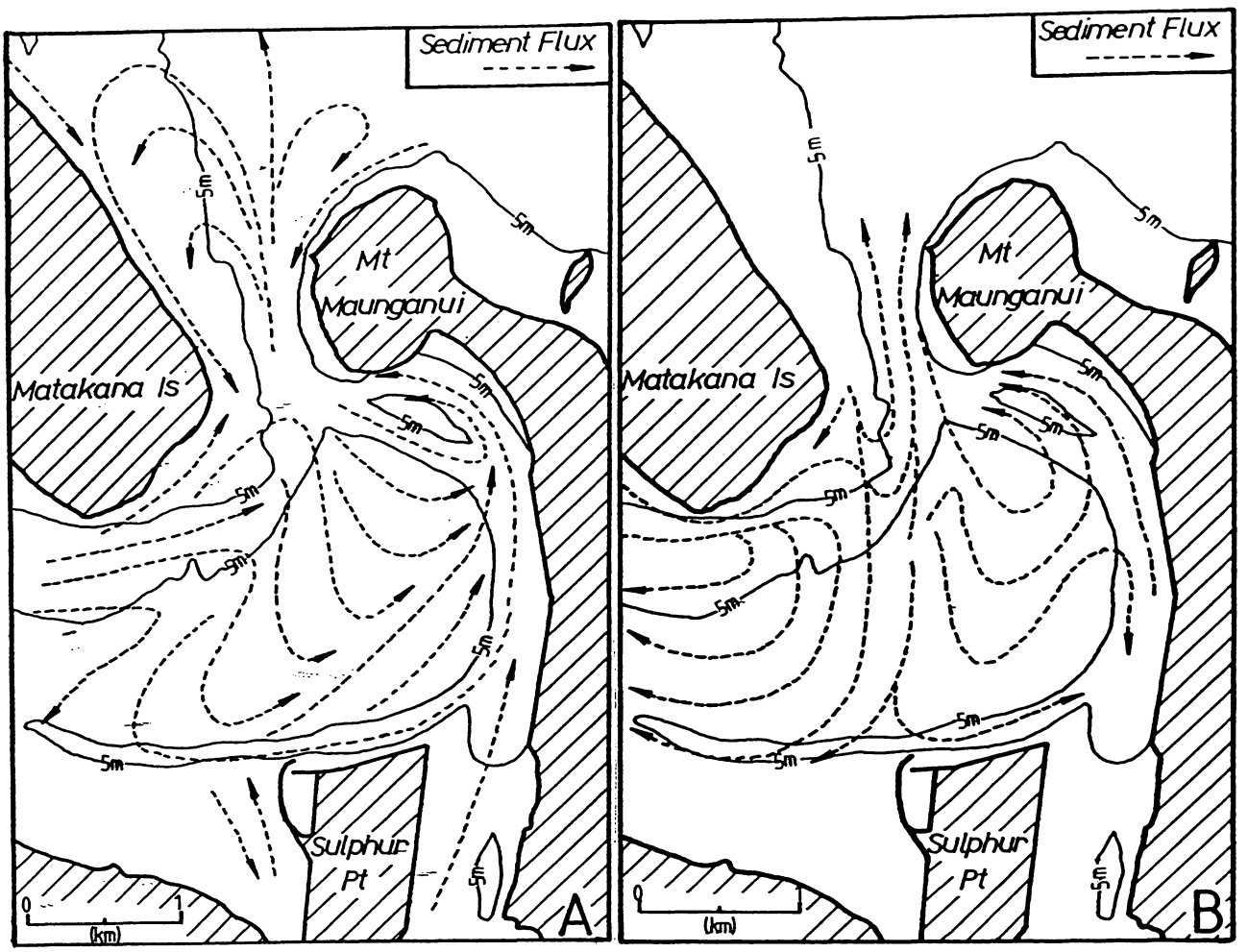

Figure 2.1 - The main sediment transport pathways within Tauranga Harbour as proposed by Davies-Colley (1976) and Black (1984). The Davies-Colley model is based on drogue observations and sediment trap data, whereas the Black model is derived from the predictions of the numerical model 2SS. Figure A is after Davies-Colley and Healy (1978).

The Davies-Colley model suggested sediment enters the harbour via the flood ramp and moves around the margin of the ebb shield (Centre Bank), eventually exiting the harbour through the Maunganui Roads and Pilot Bay Channel. In addition, some sediment discharge from an unspecified source occurs through the Western Channel. High net sediment fluxes (>10 kgm^{-1} per tidal cycle) occur in both the Maunganui Roads and the Pilot Bay Channel, representing more than 10 times the net sediment

flux up the flood ramp. Sediment transport pathways in the vicinity of the lower Western Channel were uncertain due to difficulties experienced in defining the influence of strong ebb flows from the western arm of Tauranga Harbour (Davies-Colley and Healy, 1978).

Davies-Colley (1976) noted the presence of two major eddies associated with the flood jet; one southwest of Panepane Point, and the other in Pilot Bay. The latter eddy would cause asymmetry of tidal flow within Pilot Bay involving longer periods of ebb flow, thereby making the channel ebb-dominant.

Dahm (1983) undertook further study into the sediment dynamics of the ebb-tidal delta, and also considered the geomorphic development and bathymetric stability of Tauranga Harbour in the vicinity of the entrance. He concluded that the harbour bathymetry was not stable, as evidenced by large scale infilling of the lower Western Channel. These findings indicated a need to modify the Davies-Colley model to account for the observed geomorphic responses in the lower Western Channel region.

Re-evaluating Davies-Colley's (1976) data, Dahm (1983) suggested that ebb flow from the upper Western Channel is diverted across Centre Bank by flood flow into the lower Western Channel, and enters the Otumoetai Channel or crosses the southeastern margin of Centre Bank via a blind ebb channel into the Maunganui Roads. He attributed the strength and nature of the interaction of flood and ebb flow at the southern end of Matakana Island to changes in the orientation of the ebb jet in response to both natural sedimentation and modifications to the ebb delta undertaken as part of the port development.

During 1982, a number of potential problems within the harbour was identified, including: bathymetric changes and reduced tidal discharges in the Western Channel; modifications in tidal circulation associated with dredging in Cutter Channel and the harbour entrance; and possible changes in current flows and sedimentation patterns caused by proposed port developments such as a harbour bridge. These and other concerns, were brought to the attention of the BOPHB (Healy, 1985) and a numerical model was suggested as a possible means for resolving some issues.

In May 1983, a joint team, comprising the Ministry of Works and Development, the Danish Hydraulics Institute, a private consultant, and the University of Waikato, was commissioned to undertake a major

investigation into the hydrodynamics and sediment transport patterns of the inner harbour. The Tauranga Harbour Study (THS) represents the most comprehensive study of Tauranga Harbour undertaken to date (Black, 1984; Barnett, 1985; Healy, 1985). The project involved a large scale field data collection programme and three numerical models, two for hydrodynamic simulations (S21 and 2DD) and the third for sediment transport simulations (2SS). The field programme provided calibration and verification data for the numerical models, and data for a morphological study (Healy, 1985).

2.1.1 - The Wallingford Hydraulic Research Station (HRS) physical model

The HRS study was commissioned to consider two main problems (HRS, 1963):

(1) how to improve and maintain depths in the harbour entrance and Maunganui Roads to allow high water access to the Mt Maunganui Wharves for ships with a minimum draft of 9m; and

(2) how future port development should proceed, particularly with regard to extension of wharf facilities, without endangering the existing port.

The HRS undertook an analysis of historical bathymetric charts, a field data collection programme and scale model simulations. The historical chart analysis suggested that transport processes and the harbour sediments were not in equilibrium (HRS, 1963). The major manifestations of this included progradation of the Matakana Island foreshore at Panepane Point, and scour in the Western Channel associated with accretion between the upper Western Channel and Otumoetai Channel. It was also noted that the ebb tidal delta, Pilot Bay Channel, Maunganui Roads and Stella Passage were relatively stable during the period 1852 to 1954 (HRS, 1963).

The physical modelling was undertaken in two stages, the first involving a pilot model which covered the entire harbour and provided the boundary conditions for a second, larger model. The second stage involved a scale model of the Tauranga Basin south of Omokoroa Point. This model had both fixed and mobile bed options, using granular coal to represent the harbour sediments. Various development options for the harbour were simulated within the scale model (HRS, 1968), in particular

reclamation of Sulphur Point and dredging of Cutter Channel. The model simulations predicted hydrodynamic changes in three main areas: Western Channel; Sulphur Point; and Pilot Bay.

The Western Channel region would experience a reduction in ebb and flood peak velocities due to the formation of a third major tidal channel (Cutter Channel). Since both ebb and flood flows would undergo similar reductions, it was suggested that the overall effect on the channel and banks would be negligible. The reclamation of Sulphur Point was predicted to have little influence on Western Channel, although a slight reduction in tidal range could be expected.

Flow patterns in the vicinity of Sulphur Point would be significantly changed, resulting in stronger ebb flows in the Maunganui Roads and modification of flood flow paths into Stella Passage. It was noted from the scale model that the reclamation would tend to divert ebb flow into the Cutter Channel. Before the inclusion of the reclamation this flow travelled obliquely across Centre Bank and entered the Cutter Channel near its mid-point. The other major change predicted was stabilisation of an existing eddy within Stella Passage. Prior to reclamation the position of this eddy changed with the state of the tide, traversing most of the length of Stella Passage. After reclamation, the eddy would be confined to one location adjacent to the middle of Sulphur Point.

For Pilot Bay, the physical modelling predicted a change from an ebb-dominated channel to a flood-dominated channel, with the Cutter Channel becoming the main ebb channel, concommitant with large reductions in flow velocities through most of Pilot Bay except in the vicinity of Stony Point where flood velocities would increase. It was also predicted that sediment would travel from the entrance, in a loop over Centre Bank and into the middle of the new channel. It was considered that the ebb flows, reinforced by flow diversion induced by the Sulphur Point reclamation, would remove most of the incoming sediment so that Cutter Channel would require very little maintenance dredging.

2.1.2 - Tauranga Harbour Study (THS) numerical models

The THS involved four main phases: a field data collection programme; a morphological study of the features present in the harbour related to sediment transport patterns; a hydrodynamic numerical model; and a

sediment transport model.

The morphological analysis (Healy, 1985) suggested the existence of a generalised recirculating sediment transport system, similar to that outlined by Davies-Colley (1976) (Fig. 2.1A). One major difference was the identification of a number of null points where sediment could be expected to accrete. Three such zones were identified: at the junction of Hunters Creek and the upper Western Channel; the lower Western Channel adjacent to the flood ramp; and the junction of the Maunganui Roads, Cutter and Pilot Bay channels. All these zones have shown marked accretion, with the latter requiring maintenance dredging in 1984.

Barnett (1985) reports on the findings of hydrodynamic model (S21), concentrating primarily on the calibration and verification of the model. He presents only summaries of the simulation results, details having been presented in informal reports to the BOPHB Chief Engineer. The calibration and verification results were deemed satisfactory with mention of only two problem areas (Barnett, 1985). The predicted tidal levels at Salisbury Wharf were not consistent with measured levels, and the model predicted unexpected variations in the timing of slack tides and peak flows in Stella Passage. These latter variations are probably associated with a tidal eddy in Stella Passage, although Barnett (1985) presents insufficient data to determine this with certainty.

The overall flow pattern presented by Barnett for peak flow conditions (Fig. 2.2B) indicates that no dominant flood jet exists during peak maximum flood flows. Instead there are two zones of maximum flow confined to the lower Western Channel and Cutter Channel. Pilot Bay Channel has a weak flood flow (<0.10 ms^{-1}) and Barnett (1985) states a small eddy is present adjacent to Salisbury Wharf, although this is not apparent from figure 2.2B. The shallow regions of Centre Bank are also subjected to relatively low speeds (<0.25 ms^{-1}).

This flow pattern is similar to that predicted by the numerical model 2DD used to derive friction coefficients for the sediment transport model. The major differences are that 2DD predicts higher velocities across Centre Bank, consistent with a rapidly diverging flood jet, and the presence of a strong eddy in Pilot Bay (Black, 1984).

The S21 flow pattern differs from those patterns previously predicted by the physical model of HRS (1963,1968) and described by Davies-Colley (1976). These works indicated the presence of one flood jet with two

main eddies (Fig. 2.2A), with the jet orientated so the dominant flow runs across Centre Bank and is not confined to the channels. This flow path suggests higher velocities across Centre Bank than predicted by S21. Seabed photographs taken by the THS (Healy, 1985) show that most of Centre Bank is covered by shell lag or active sand current ripples. These indicate velocities >0.35ms^{-1} operate during the tidal cycle, which is more consistent with the predictions of the physical model (HRS, 1968), or the numerical model 2DD (Black, 1984).

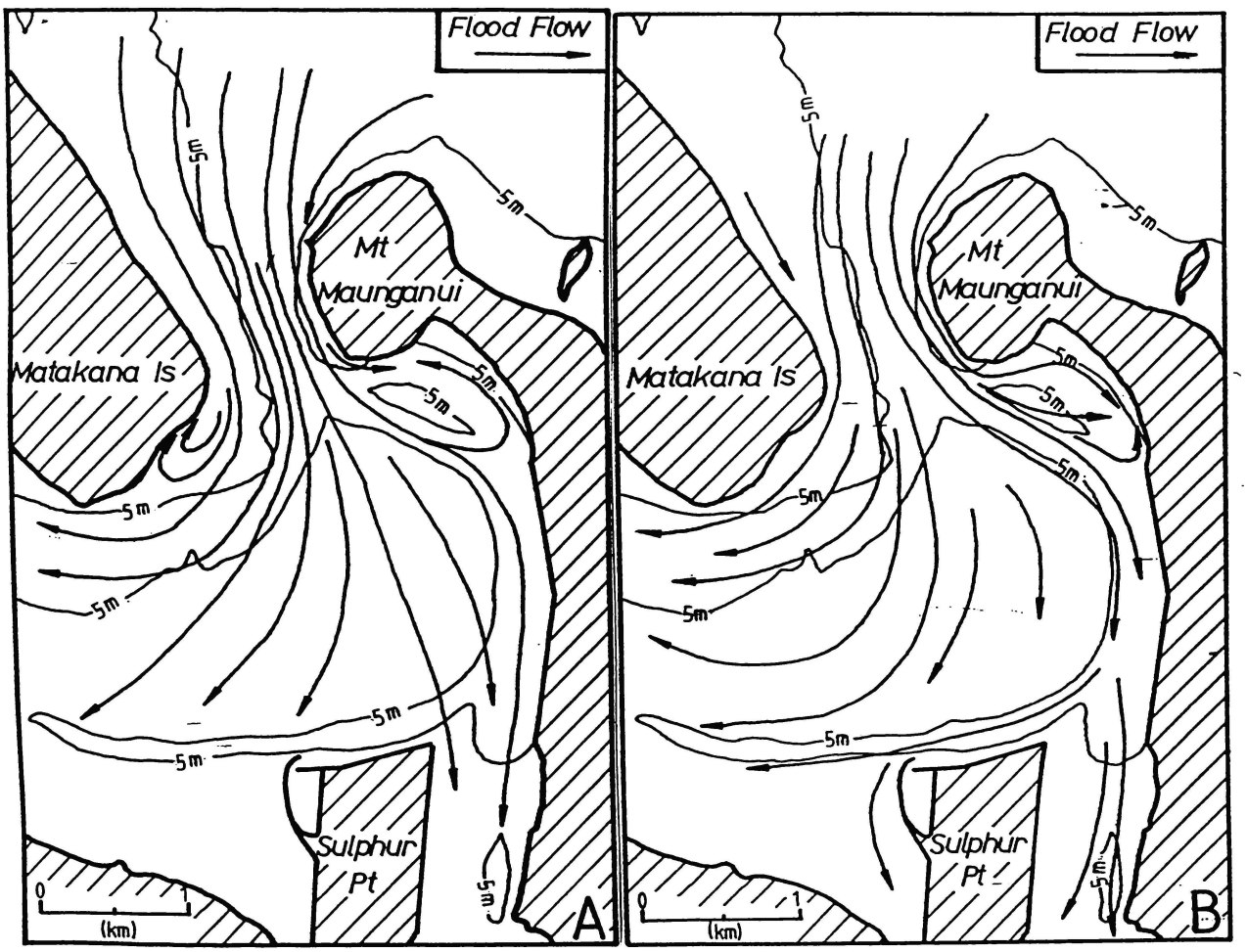

Figure 2.2 - Flood tide peak flow streamlines predicted by the HRS (1968) physical model and the S21 numerical model (Barnett, 1985). Davies-Colley (1976) obtained streamlines which closely matched the predictions made by HRS (1968).

The ebb flow distribution predicted by the S21 model (Barnett, 1985) agrees more closely with earlier studies than the flood flow pattern (Fig. 2.3). The main ebb flows occur in the lower Western Channel, Cutter Channel, and to a lesser extent, in Pilot Bay. An eddy is

present in Stella Passage, adjacent to the mid-point of the Sulphur Point reclamation. A smaller eddy occurs in the shallows offshore from the Pilot Bay boat ramp (Barnett, Pers. comm., 1985), although this is not evident in figure 2.3. The discharge from Western Channel flows in two arcs across Centre Bank to the entrance, one closely following the lower Western Channel, and the other following a blind channel on the southeastern margin of Centre Bank. The observations of Davies-Colley (1976) and Dahm (1983) suggest that the latter route is more significant than predicted by S21.

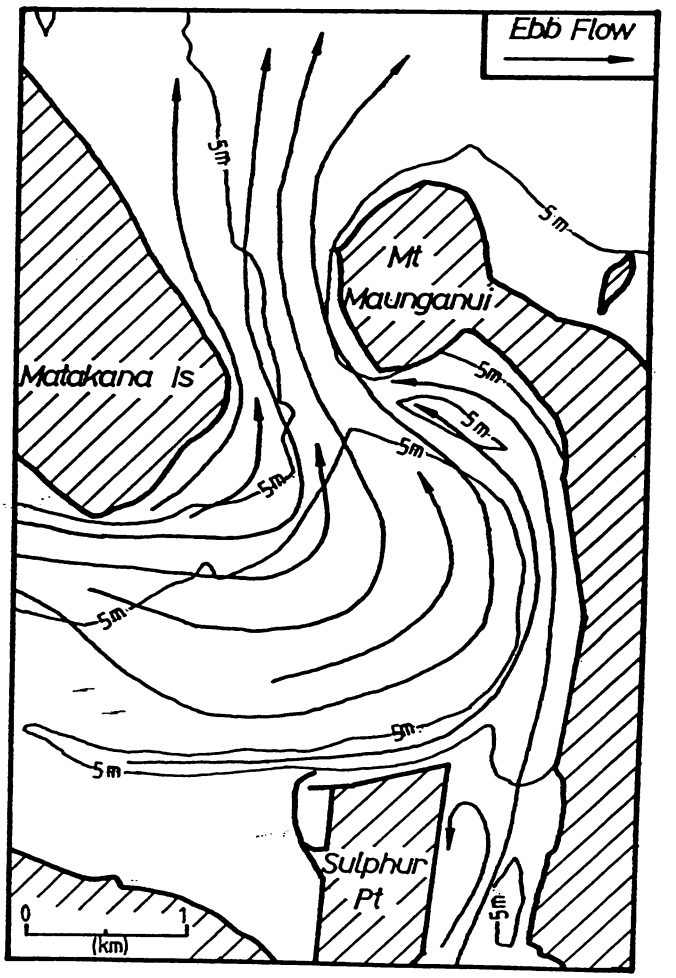

Figure 2.3 - Ebb tide peak flow streamlines predicted by S21 (Barnett, 1985). The overall pattern is consistent with previous works.

Black (1984) derived the net total-load sediment transport pathways for Tauranga Harbour from sediment transport fluxes computed by the numerical model 2SS (Fig. 2.1B) based on the above S21 flow results. The pathways are dominated by two major loops, similar to those proposed by Davies-Colley (1976). One loop follows an anticlockwise path from

the entrance gorge, over Centre Bank, into the Maunganui Roads, and exits via Cutter and Pilot Bay Channels. This is virtually identical to the loop proposed by Davies-Colley, except that more of the sediment flux is concentrated in Cutter Channel.

The second loop travels clockwise from the entrance gorge, over Centre Bank, westwards through the upper Otumoetai Channel and over the flanking shallow banks into the upper Western Channel. The return flow follows the deepest parts of the Western Channel onto the shallow banks adjacent to Matakana Island. At this point most of the sediment appears to be returned to the loop via Centre Bank.

Using the calculated sediment transport fluxes, Black (1984) predicted future erosion and accretion trends within the harbour. These indicated that the Maunganui Roads, Otumoetai Channel, Stella Passage and Centre Bank regions are relatively stable, with minor accretion and erosion occurring in Cutter Channel. The major region of expected change is the Western Channel, particularly the lower channel, as predicted by Dahm (1983) on geomorphic grounds.

2.1.3 - Review of model parameters used and their limitations

The physical models used by HRS (1963,1968) considered the propagation of tidal waves forced by changing the hydraulic head at the boundaries of the model. Therefore, only currents generated by the hydraulic forcing of the changing tide level were modelled for the region inside the harbour. The simulations did not incorporate progressive tidal wave components, although due to the good agreement between model tide levels and prototype data, HRS (1968) did not consider this a major problem.

Discharge from the Wairoa River, the largest freshwater input into the southern harbour, was modelled using average flow conditions. However, it was noted that the presence, or absence, of freshwater inputs did not affect the behaviour of the model (HRS, 1968). The only factor, other than hydraulic head, introduced into the model to control the fluid behaviour was bed resistance, which was modelled using wire mesh and pebbles.

Bedload sediment transport was modelled by adding granular coal to the scale models. Due to scale effects, HRS were unable to achieve the same ratio between the model sediment transport rates and prototype data at

all points within the model area (HRS, 1968). Consequently the HRS physical models only considered bedload transport within the vicinity of the harbour entrance, the most reliable data being obtained for the ebb-tidal delta. Sediment transport outside the harbour, as modelled by HRS (1968), resulted from both tidal currents produced by variations in hydraulic head, and waves generated to simulate the littoral drift system along Matakana Island.

The hydrodynamic numerical model S21 considered the hydraulic propagation of sea level variations induced at the free boundaries of the model in addition to progressive components of the open ocean tidal wave (Barnett, 1985). The model takes into account a number of factors which influence the mass and momentum of the fluid. The factors utilised in the Tauranga Harbour simulations were bed resistance, wind stress, eddy coefficients and latitude (for Coriolis effects). All these factors tend to dissipate the available energy and thereby reduce the potential sediment transport flux, except for the wind stress which may increase the available energy.

All the calibration runs undertaken were associated with periods of fine, calm weather, so that the wind stresses incorporated in the calibration were negligible. No freshwater inputs to the harbour are reported to have been considered, although S21 can handle these. Therefore S21 was driven entirely by tidal forcing for the simulations undertaken (Barnett, 1985).

The sediment transport model 2SS combined bedload and suspended load to derive the total sediment flux through each cell in the model. These two parameters were derived from the water velocities determined by S21 and the availability of sediment in each cell. The only mechanism capable of initiating sediment transport in 2SS is the effective shear stress exerted by the fluid. Therefore the behaviour of the sediment transport model is largely determined by the flow velocities provided by S21.

In summary, all previous sediment transport models of the inner harbour regions have been based principally on tidal forcing at the entrance, and additional energy inputs within the harbour, such as wave effects, were omitted for simplicity. Thus an important aim of this study has been to assess the effects of non-tidal processes on sediment transport in the inner harbour.

2.2 - Implications of the model studies for Pilot Bay

Evaluating the applicability of the models over the entire region examined by the previous studies is beyond the scope of this investigation. Therefore the evaluation is restricted to a smaller, more manageable area within the inner harbour. This section reviews the detailed modelling of Pilot Bay and Cutter Channel.

Pilot Bay is an embayment located adjacent to Mt Maunganui on the eastern side of the entrance. The beach fringing Pilot Bay has undergone significant erosion since the 1950's (Fraser, 1982), necessitating the installation of gabion basket seawalls to protect the foreshore and road. By the end of 1983, the position of the high tide mark coincided with the seawall for most of the southeastern end of the beach. The boat ramp at the northwestern end was subject to persistent sand accretion making the ramp difficult to negotiate by vehicles.

As noted previously, physical modelling of port developments undertaken by HRS (1963, 1968) indicated that the Cutter Channel dredging would change tidal flows within the Pilot Bay Channel resulting in a more flood-dominated channel. For example, it was estimated that peak flood velocities at 3' above the bed (comparable to u_1 velocities) would be reduced by 23% to 1.0 ft/s after the Cutter Channel dredging, whereas peak ebb velocities would showed a reduction of 46% to 1.5 ft/s. Therefore, as a result of the Cutter Channel dredging the bay would be ebb dominant, but less so than prior to dredging. The model also predicted eddying in the vicinity of Salisbury Wharf during the later part of the flood and deposition in the middle of the Cutter Channel due to ebb currents entering obliquely from Centre Bank.

Further simulations by HRS to include reclamation of Sulphur Point, predicted a further reduction in tidal velocities. More importantly, the main streamlines shifted northwards, causing the flood eddy to shift further into Pilot Bay and increasing convergence of flow into Cutter Channel during the ebb. Therefore, the study suggested that Pilot Bay Channel would tend towards flood dominance, whereas Cutter Channel would be strongly ebb-dominated.

The S21 results indicate the presence of a slight eddy within Pilot Bay, near Salisbury Wharf. Barnett (1985) suggests that the field data may be erroneous and states (p. 6.10):

> "Thus in terms of the field data Pilot Bay is better described as a backwater than an eddy zone during the flood tide, though of course the ebb tide runs quite strongly through the bay."

The S21 hydrodynamic model does not show any major difference in ebb and flood flow durations, although peak flood velocities are lower than ebb velocities. These results indicate that Pilot Bay is ebb-dominated and Cutter Channel tends towards flood dominance.

Black (1984) undertook simulations of the Pilot Bay region using his own hydrodynamic model (2DD). These simulations produced a strong eddy during flood flow which operated during 2/3 of the flood tide. The eddy involved flood flow in the Cutter Channel and ebb flow in Pilot Bay, suggesting that the presence of an eddy may be connected with the dredging of Cutter Channel as discussed above. Neither the S21 (Barnett, 1985) or 2DD (Black, 1984) numerical model predicts the ebb-dominance in Cutter Channel predicted by the physical model (HRS, 1968).

Although there is some disagreement between S21 and 2DD regarding the formation of an eddy, both models predict water velocities below sediment threshold (<0.30ms-1) within Pilot Bay Channel for all but ~30min during a tidal cycle. The only regions which do show high velocities are the entrance and exit of Pilot Bay Channel at Salisbury Wharf and in the vicinity of Stony Point. This is consistent with the HRS (1968) predictions.

The THS also undertook simulations, using bathymetric data obtained by previous surveys of the harbour, in an attempt to assess the influence of port developments. Of particular interest are the simulations based on the 1954 and 1970 bathymetric charts which bracket the time period covered by the HRS simulations, although the 1970 chart incorporates some development of Cutter Channel and the Sulphur Point reclamation.

The S21 results are not presented in a form which allows direct comparison with the HRS prototype data. However, comparison between residual water flows and float behaviour suggests that the S21 simulation based on the 1954 chart is consistent with the HRS large scale model, despite some obvious instabilities in the S21 flow patterns (indicated by zig-zagging streamlines along tidal channels). The predicted changes in flow patterns between 1954 and 1970 are also consistent with the predictions made by HRS (1968), except that the Cutter Channel region has no clear flow dominance.

2.3 - Summary

The HRS modelling was undertaken before the dredging of Cutter Channel and reclamation of Sulphur Point, whereas the Tauranga Model Study commenced after these works were completed. Both models suggested that as a result of the port developments Pilot Bay should experience reduced tidal velocities with the ebb values being somewhat higher than the flood. The HRS physical model and the 2DD numerical model of Black (1984) predict the presence of a large eddy in Pilot Bay during late flood tide. In contrast, the S21 model is interpreted by Barnett (1985) to indicate a tidal backwater in Pilot Bay with an insignificant eddy adjacent to Salisbury Wharf very late in the flood.

All three models, physical and numerical, indicate a flood-dominance in Cutter Channel and an ebb-dominance in Pilot Bay. However, the flood-dominance indicated by the physical model is not as strong as the numerical model predictions, since the physical model predicted significant diversion of the ebb flow through Cutter Channel.

The sediment transport model 2SS indicates high ebb sediment transport fluxes through Pilot Bay and high flood fluxes through Cutter Channel in accordance with the flow patterns. The physical model flow results suggested a slight accumulation of sediment would occur in the Cutter Channel, but this would be removed by ebb tidal scour when the Sulphur Point reclamation retaining wall was completed. This reflects a high ebb sediment flux through Cutter Channel, depending on the availability of sediment.

All the hydrodynamic models of the inner harbour, both physical and numerical, were driven entirely by tidal forcing at their ocean boundaries. The hydrodynamic models formed the basis of the sediment transport predictions, although wave-induced littoral drift on Matakana Bank was included in the HRS (1968) physical model. Additional energy inputs affecting sediment transport, such as atmospheric forcing, seiching, wind generated waves, and stormwater discharge, were not considered for the inner harbour.

Chapter 3 - Tides and Sedimentation in Pilot Bay

This chapter presents and reviews tidal current data collected by the author in conjunction with, and subsequent to, the THS field programme. These data are considered in terms of the overall flow pattern within Pilot Bay and compared to the model predictions discussed in Chapter 2. The observed flow patterns are also compared to the sublittoral sediment facies of Pilot Bay and Cutter Channel to determine if they are consistent with the tidal flows.

3.1 - Tidal current measurements

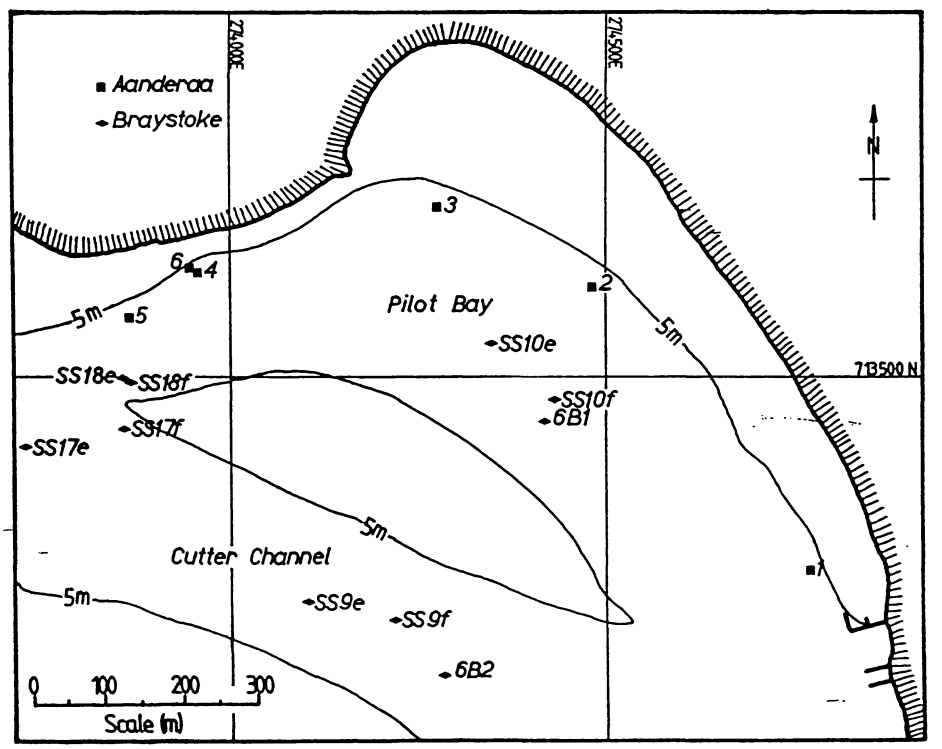

Figure 3.1 - Aanderaa current meter sites used during this study. Also marked are THS Braystoke measurement sites located within the study area and referred to in the text. The Braystoke sites identified with the letter B represent 13h monitoring stations, whereas the SS sites were measured only once at peak ebb (e) or flood (f) tide.

For the purposes of this study, the tidal currents within Pilot Bay were monitored with a continuous recording Aanderaa current meter deployed at 6 locations over several periods in 1984 and 1985 (Fig. 3.1 and Table 3.1). The meter was deployed with twin submersible floats, 200kg chain deadweights and a stainless steel strop, which positioned

the rotor at 1m above the bottom, providing u_1 current velocities for sediment transport calculations. The deflection of the meter at the peak flows encountered was negligible. BOPHB divers checked the meter approximately weekly, and removed any growth in the vicinity of the rotor.

Table 3.1 - Deployment data for Aanderaa current meter 6923 and the THS Braystoke sampling sites used in the study. The water depth is the approximate depth at MLWS.

Site	Location	Water depth (m)	Sampling period	Number of readings
1	713231N 274776E	7	14/ 8/84 - 17/ 9/84	9887
2	713620N 274485E	3	8/11/84 - 3/12/84	7212
3	713736N 274282E	8	12/ 2/85 - 5/ 3/85	0[a]
4	713643N 273962E	6	5/ 3/85 - 26/ 3/85	0[a]
5	713581N 273869E	14[b]	22/10/85 - 29/10/85	1981
6	713649N 273949E	6	29/10/85 - 15/11/85	4843
6B1	713434N 274417E	8	12/ 9/83	14
6B2	713087N 274287E	11	12/ 9/83	14
SS 9e	713187N 274102E	11	6/ 9/83	1
SS 9f	713164N 274223E	11	6/ 9/83	1
SS10e	713549N 274355E	9	6/ 9/83	1
SS10f	713463N 274438E	8	6/ 9/83	1
SS17e	713404N 273727E	12	6/ 9/83	1
SS17f	713428N 273859E	11	6/ 9/83	1
SS18e	713497N 273860E	14	6/ 9/83	1
SS18f	713494N 273868E	14	6/ 9/83	1

[a]The data recorded during these periods were destroyed accidentally.
[b]The mooring dragged during the flood tide following deployment before coming to rest at the bottom of the channel. The meter was redeployed the following week.

The Aanderaa current meter deployed in Pilot Bay during this study was fitted with standard sensors as follows:

a) Savonious rotor for current speed;
b) Flux-gate compass for current direction;
c) Thermocouple for water temperature;
d) Conductivity cell for salinity; and
e) Pressure transducer for water depth.

Each sensor was sampled at 5 min intervals and, with the exception of the current speed, each sample represents the instantaneous value recorded by the sensor. The recorded current speed represents the average speed during the preceding 5 min interval.

The current meter used was checked and calibrated by the New Zealand Oceanographic Institute, before and after the study period, and showed no deviations from the factory settings. These calibration checks did not involve the pressure transducer. From the results obtained it is clear that the water depth variations encountered were too small to be resolved by the transducer, and that pressure readings were incorrectly converted to depth. Therefore all the pressure readings were rejected.

The Savonious rotor was subject to fouling at all sites after a period of about 2-3 weeks, the most serious involving the growth of barnacles in the rotor bearings. Consequently, all current speed values were considered unreliable beyond 2 weeks after deployment. No problems were encountered with the other sensors.

The Braystoke data was obtained during the THS field programme. All the measurements made within Pilot Bay were made with Braystoke BFM010 Multiparameter current meters. This model is equipped with sensors for current speed and direction, salinity, and temperature, as well as a built in echo sounder. In conjunction with the winch distance meters, the echo sounder allowed accurate positioning of the current meter relative to the sea bed. At each site a velocity profile was determined by taking a sequence of measurements at fixed distances above the sea bed (0.5, 1, 2, 4, 6, 9, and 12m). During the full tidal cycle measurements, each site was measured 2-3 times an hour for at least 13h.

Suspended sediment samples were collected via a hose connected to the Braystoke Current meter, permitting simultaneous measurements of current parameters. The hose terminated in a 13mm copper pipe which protruded 100mm in front of the rotor safety cage on the current meter. To ensure minimal disturbance to the water flow around the intake, the leading 15mm of the pipe was bevelled. Samples were obtained by pumping 2ℓ of water through a 4ϕ seive. Any sediment retained on the seive was dried and weighed. The suspended sediment sites (prefixed by SS) were sampled twice during a tidal cycle, at times corresponding to the expected peak ebb and flood flows. All the suspended sediment sites listed in Table 3.1 were measured within the same tidal cycle during two 1h periods.

Additional data were obtained on tidal flow paths by deploying drogues during 4 ebb tides and 2 flood tides. The drogues utilised had 600mm square plates arranged in a cruciform pattern, and they were set for 60% of the water depth along the expected flow path. Each drogue deployed

was located by sextant fixes approximately every 4-7 min.

3.2 - Tidal currents in Pilot Bay

In terms of the possible sediment transport within Pilot Bay, the duration of velocities exceeding sediment threshold would normally be of prime importance. Therefore, tidal dominance would be considered in terms of the relative duration of flood and ebb velocities exceeding some critical velocity. However, the THS results indicate that a considerable volume of sediment may be transported in suspension and that the bulk of the sediment flux in Pilot Bay represents the advection of sediment entrained elsewhere (Black, 1984). Further, it is possible that sediment may be entrained by wave action within the bay, so that sediment transport may occur at velocities below threshold. For the purposes of this study, flow dominance will be considered in terms of the relative durations of all flow in the ebb and flood directions.

The Aanderaa and Braystoke sites at Pilot Bay (6B1, SS10) display a strong ebb flow dominance, whereas the other Braystoke sites (6B2, SS9, SS17, SS18) in the Cutter Channel and in the vicinity of No.1 Beacon show a flood dominance (Table 3.2). The duration of ebb and flood flow show the extent of the tidal asymmetry more clearly than the tidal velocities. In addition to the durations given in Table 3.2, ebb flow was observed 3.75h earlier at site 6B1 than at 6B2.

Residual distance vectors have been derived for the Braystoke data obtained from sites 6B1 and 6B2, and for the first complete tidal cycle in each set of Aanderaa data (Fig. 3.2). These vectors indicate the final distance, relative to the starting point, travelled by a particle of water during one tidal cycle as defined by the velocities and directions measured at the starting point (Black, 1984). This involves the same analysis as the program EULER described by Barnett (1985). The residual vectors from the Braystoke and Aanderaa current meters confirm that the Cutter Channel is flood dominated and Pilot Bay is ebb dominated.

3.2.1 - Relationship between peak velocity and tidal range

The velocity data derived from the current meters have not been scaled

Table 3.2 - Summary of tidal flow parameters measured by Braystoke and Aanderaa current meters in Pilot Bay for the period 1983-85. All measurements are peak velocities at 1m above the sea bed. The percentage of cycle values refer to the number of observations recorded within the range of flow directions, expressed as a percentage of the total number of observations made during a tidal cycle. The tidal range refers to the tidal range measured at Salisbury Wharf for the tidal half cycle corresponding to the velocity quoted.

	Flood tide					Ebb tide				
Site	Flow velocity (ms^{-1})	Tidal range (m)	Flow direction (°)	% of cycle	Duration (h:min)	Flow velocity (ms^{-1})	Tidal range (m)	Flow direction (°)	% of cycle	Duration (h:min)
1	0.31	1.31	145-155	8	2:45 ±0:03	0.34	1.30	335-345	39	9:41 ±0:03
2	0.25	1.40	105-115	8	4:05 ±0:07	0.44	1.26	315-325	12	8:21 ±0:09
5	0.31	1.20	45-55	7	2:00 ±0:06	0.83	1.45	255-265	23	10:28 ±0:06
6	0.16	1.49	55-65	6	1:27 ±0:03	0.82	1.49	275-285	42	10:56 ±0:03
6B1	0.16	1.75	175-185	14		0.58	1.63	300-310	36	
6B2	0.64	1.75	110-120	33		0.48	1.63	290-300	27	
SS9	0.55	1.81	104			0.40	1.67	298		
SS10	0.09	1.81	176			0.47	1.67	292		
SS17	0.68	1.81	120			0.60	1.67	304		
SS18	0.28	1.81	8			0.19	1.67	294		

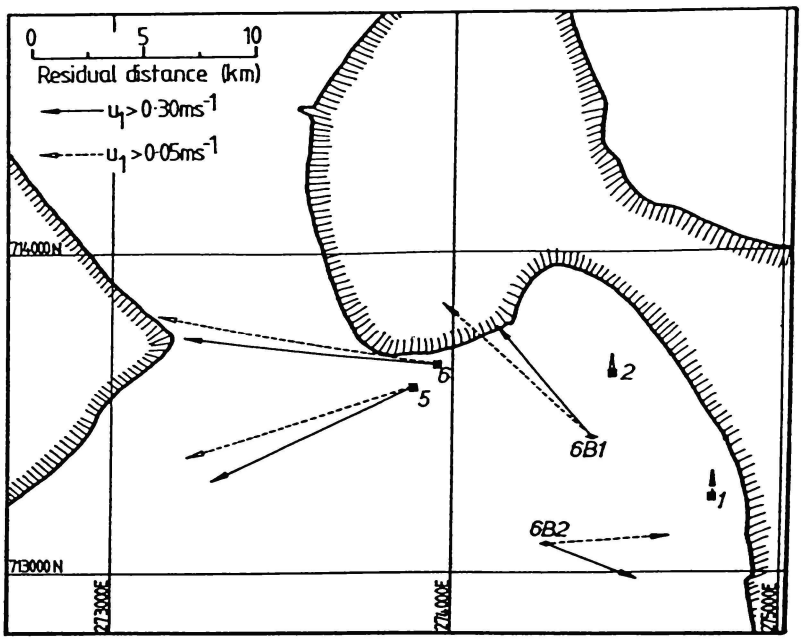

Figure 3.2 - Residual current distance vectors for the Pilot Bay region based on Aanderaa sites and Braystoke sites 6B1 and 6B2 (Table 3.2).
(See also Figures 3·6 and 3·7 on pages 3·25 and 3·26)

to a common tidal range. Black (1984) and Barnett (1985) consider that there is a clear relationship between tidal range (R) and measured peak velocity (V) for given locations in Tauranga Harbour. This relationship can be expressed as a power function of the form (Black, 1984):

$$V = aR^b \qquad \ldots 3.1$$

Given this relationship it is then possible to scale a measured velocity, obtained at one tidal range, to the velocity at another tidal range, using:

$$V_2 = V_1(R_2/R_1)^b \qquad \ldots 3.2$$

Black (1984) calculated the parameters a and b for two sites in Tauranga Harbour (Table 3.3) and recorded high correlation coefficients in the range 0.87-0.96, although the ebb relationship for Stella Passage had been determined from a subset of data which omitted badly fitting low velocities associated with the tidal eddy present in the channel. The same parameters were calculated from the Aanderaa data for both ebb and flood tides, and also the flood eddy. Due to the lower correlation

coefficients obtained, the relationship between tidal range and measured peak velocities for Pilot Bay is not as strong as for the locations considered by Black (1984).

Sternberg (1979) suggested that the ratio between the tidal range and the half cycle duration (D) is a better factor representing tidal conditions. Therefore the peak velocity is a function of the rate of change in water surface elevation during a half cycle. Equation 3.1 can be expressed as:

$$V = c(R/D)^d \qquad \ldots 3.3$$

The parameters c and d have been determined for the Aanderaa sites employed by this study (Table 3.3). Suitable data were not available from Black (1984) or Barnett (1985) to permit a similar analysis for the lower Western Channel or Stella Passage.

Table 3.3 - Summary of power function parameters for Equations 3.1 (a, b) and 3.3 (c, d), and correlation coefficients (r) derived from Aanderaa current meter data and Salisbury Wharf tide data. The data for the lower Western Channel and Stella Passage are from Black (1984).

Site	a	b	r	c	d	r
Stella Passage						
Ebb tide	0.35	0.88	0.95			
Flood tide	0.30	0.92	0.87			
Western Channel						
Ebb tide	0.54	0.60	0.97			
Flood tide	0.39	0.61	0.96			
Site 1						
Ebb tide	0.24	0.67	0.35	0.78	0.64	0.30
Flood tide	0.16	1.30	0.46	3.25	1.71	0.55
Eddy	0.32	-0.43	0.23	0.20	-0.23	0.11
Site 2						
Ebb tide	0.33	0.02	0.01	0.38	0.09	0.03
Flood tide	0.16	0.90	0.62	1.86	1.45	0.76
Eddy	0.09	0.14	0.02	0.14	0.30	0.04
Site 5						
Ebb tide	0.65	0.68	0.75	1.66	0.50	0.66
Flood tide	0.26	-0.09	0.05	0.26	0.01	0.00
Eddy	0.09	0.66	0.26	0.10	-0.02	0.01
Site 6						
Ebb tide	0.68	0.47	0.76	1.12	0.24	0.40
Flood tide	0.15	-0.24	0.20	0.15	0.02	0.02
Eddy	0.08	-0.05	0.02	0.14	0.41	0.17

The tidal range adequately characterises the peak velocities for all tides in the lower Western Channel and for flood tides in Stella Passage. This is not the case for tides in Pilot Bay, although there is a reasonable correlation between tidal range and peak ebb velocity closer to the harbour entrance at Aanderaa sites 5 and 6 (Fig. 3.1). When the peak velocity is characterised by the ratio of tidal range to half cycle duration, as suggested by Sternberg (1979), some results indicate a more significant relationship for flood tides, especially at site 2.

However, the results are not very different from those determined on the basis of tidal range alone. From the data presented in Table 3.3, the peak flood velocities can be predicted reasonably well from tidal parameters for sites 1 and 2, furtherest from the harbour entrance. At sites 5 and 6, closer to the harbour entrance, the peak ebb velocities can be predicted reasonably well from tidal conditions. Overall, tidal conditions characterised by tidal range and duration are not good predictors of tidal velocities in Pilot Bay

3.2.2 - Flow durations and directions within Pilot Bay

The onset of eddy circulation cannot be readily derived from tidal duration data (Table 3.2), since that data does not distinguish between ebb flow associated with the eddy and that associated with ebb tide. The S21 results indicate that the tide is still ebbing from Pilot Bay while the flood jet is being established (Black, pers. comm., 1984), so the onset of flood flow is delayed in some areas. Ebb flow, however, is established immediately after high tide. The lag associated with a delayed onset of flood flow within some regions of Pilot Bay may contribute to the extended duration of ebb flow. Table 3.4 summarises the average observed time of initiation and completion of ebb flow compared to the time of high and low water as recorded at Salisbury Wharf for each of the Aanderaa sites analysed.

The times presented in Table 3.4 are based on the period during which ebb flow is strongly established. Ebb flow within most of Pilot Bay tends to finish before dead low water, whereas the two sites closer to the harbour entrance show that ebb flow continues during the initial stages of the following flood tide, as indicated by the S21 results

(Barnett, 1985). Therefore, approximately 1h of the extended ebb duration recorded at sites 5 and 6 (Table 3.2) can be attributed to the continuation of ebb flow beyond dead low water.

Table 3.4 - Average time to the start of ebb flow after low water, and to the finish of ebb flow after high water, for the Aanderaa sites relative to Salisbury Wharf. Also given are the standard errors.

Site	Number of readings	Start time (h:min)	Finish time (h:min)
1	67	2:37 ±0:03	6:02 ±0:03
2	48	3:45 ±0:09	5:47 ±0:06
5	13	2:41 ±0:06	6:42 ±0:03
6	33	2:24 ±0:04	7:00 ±0:03

Aanderaa sites 5 and 6 also show a rapid switch from ebb flow to flood flow directions (Fig. 3.3). Within the rest of the bay, flows during the final stages of ebb tide are characterised by velocities $<0.05 ms^{-1}$ and a tendency for random flow directions. This condition continues until flood flow is strongly established. The time at which this occurs tends to be less consistent than the onset of ebb flow associated with the formation of the eddy in Pilot Bay.

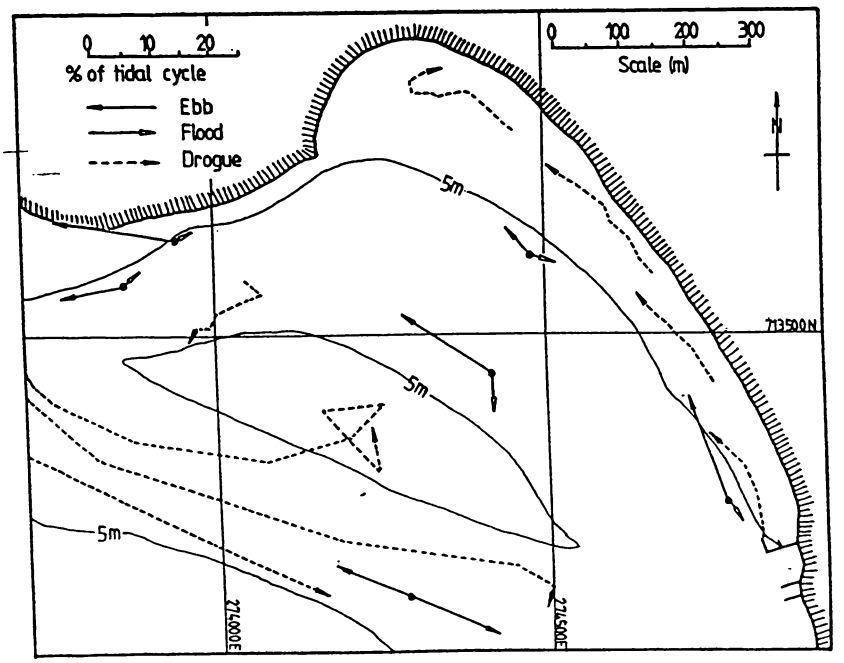

Figure 3.3 - Vector mean directions for ebb and flood flow derived from Aanderaa and Braystoke current meters. Also shown are flood tide drogue tracks obtained within the Pilot Bay area.

The transition from flood to ebb flow occurs more rapidly. The velocities drop to $<0.10ms^{-1}$ and the flow direction changes from flood to ebb without any marked tendency for random flow directions at sites 1, 5 and 6. The onset of ebb flow tends to show more scatter within the bay, compared to the regions close to Salisbury Wharf and the harbour entrance. This reflects the variation in size and strength of the flood tide eddy with time.

The transition between the two dominant flow directions at site 2 is difficult to define, since the flow direction tends to wander at velocities $<0.15ms^{-1}$, especially on windy days, with about 5% of the flow recorded as onshore-offshore. This effect tends to be less significant in the early hours of the morning and was quite pronounced during the passage of shipping through Pilot Bay. The velocity data obtained also show evidence of wave interference with the Savonious Rotor, resulting in anomalously high velocities. Therefore wave action has influenced data obtained from this site, especially for low tidal velocities.

Flow direction data from all sites (Table 3.2) and flood tide drogue tracking executed during the THS field programme (Fig. 3.3) define the shape of the eddy which forms during flood tide (Fig. 3.4). The eddy rotates about a centre located on the shallow bank separating Pilot Bay from Cutter Channel. Within the bay the flow is virtually all in the ebb direction once the eddy is established. The flow is essentially shore parallel in the nearshore region at the southeastern end. The movement of floats deployed in this work, indicates flow divergence from the shore, commencing in the vicinity of Aanderaa site 3 (Fig. 3.1) and becoming more pronounced towards the northeastern end.

3.2.3 Development and implications of the eddy

From the data presented it is clear that the eddy is established throughout Pilot Bay by mid-flood tide. The eddy appears to start between Salisbury Wharf and C4 beacon and extend progressively through Pilot Bay (Fig. 3.4). The general sequence of events during a flood tide appears to be:

(1) At dead low water the tide turns and initially flows along the margins of the entrance gorge. At this stage the ebb flow from

Pilot Bay dominates in the main channels, but flood flow starts to develop in the nearshore regions. All velocities are low ($<0.10 ms^{-1}$).

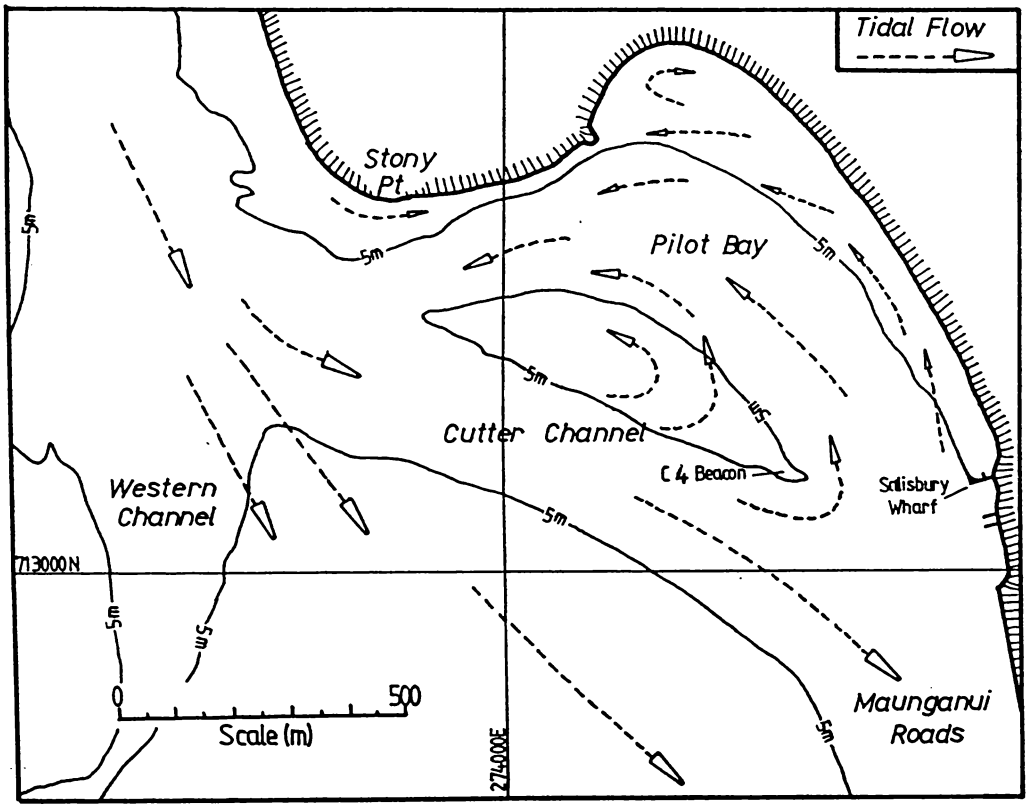

Figure 3.4 - Flood tide eddy in Pilot Bay defined by the directional data presented in Figure 3.3.

(2) The flood jet starts to develop during the first 1/4 of the flood tide and flood flow is established in Pilot Bay. The flood flow reaches the maximum flood velocity ($\simeq 0.30 ms^{-1}$) within Pilot Bay but continues to increase in Cutter Channel and elsewhere.

(3) At about 1/4 flood tide the flood jet is established. Flow velocities start to drop throughout Pilot Bay and flow directions start to change as the eddy starts to form. The time at which this occurs varies, both with location in Pilot Bay, and from cycle to cycle. The onset of the eddy controls the duration of ebb flow and reflects the size and strength of the eddy.

(4) By 1/2-3/4 flood tide the flood jet attains maximum strength and ebb flows within Pilot Bay reach peak velocity ($0.40-0.80 ms^{-1}$). The velocities reached usually exceed those achieved by the flood flow earlier in the cycle and may exceed those reached during the

succeeding ebb tide.

(5) At high tide the flood jet has disappeared and flow velocities in Pilot Bay drop to a minimum ($\leq 0.10 ms^{-1}$). The velocities are still higher than those recorded during the preceding low tide slack water and the change from flood to ebb flow ($\leq 0.05 ms^{-1}$).

(6) Ebb tide begins and the eddy disappears.

The presence of the eddy is responsible for the increased duration of ebb flows observed within Pilot Bay and also affects the timing and duration of peak flows. The strong tidal asymmetry implied by the increased duration of ebb flow would induce a net ebb sediment transport flux for any sediment already entrained. The entrainment of sediment will depend on the duration of flows exceeding the appropriate threshold velocity for the available sediment. Although the formation of a flood tide eddy does extend the duration of ebb flow, it does not alter the duration of peak flows during an ebb tide. Hence, the eddy does not enhance the sediment transport potential of the ebb tide. However, if the eddy is sufficiently strong the eddy velocities during the flood tide may also exceed threshold velocities, thereby increasing the net transport in the ebb direction, excluding any wave effects.

Close to the junction of the Pilot Bay channel and Maunganui Roads (site 1), the difference between peak flood and peak ebb velocities is negligible. However ebb velocities close to threshold are maintained for much longer than similar flood velocities. On 22% of the 67 tidal cycles sampled, the peak ebb velocity was associated with the eddy and on the remaining occasions the ebb tide peak velocity was within $0.05 ms^{-1}$ of the peak eddy velocity during the preceding flood tide. Consequently this region displays two periods of peak ebb velocity for every period of peak flood velocity.

In central Pilot Bay and the nearshore zone (6B1, site 2), the peak velocities are maintained for short periods of about 5-15min during the tidal cycle, with the duration of peak velocity varying in proportion to the tidal range. The velocities associated with the eddy are low so that there are only two periods of peak flow, with the highest peak velocities associated with ebb tides. The flood peak velocities are also of shorter duration than comparable ebb velocities.

Closer to the harbour entrance, near Stony Point, peak flood velocities ($\leq 0.30 ms^{-1}$) are reached early in a flood tide, before the

flood jet is fully developed, and are of very short duration. Subsequently the velocities drop and are relatively low (<0.15ms^{-1}) for the rest of the flood tide. The flow velocities then increase rapidly to a peak value 200-400% higher than the flood value, which is maintained for 1-2h. Therefore this region effectively experiences only one period of significant peak flow per cycle. On the opposite side of the channel, adjacent to No.1 Beacon, there are two periods of peak flow which display a slight flood dominance.

3.3 - Sublittoral sediment facies

Healy (1985) analysed and presented the bottom sediment facies for the southern basin of Tauranga Harbour and the ebb-tidal delta. These were derived from a side scan sonar survey, aerial photographs, bottom sediment samples, and observations and photographs made by SCUBA divers. Subsequent to the renourishment of Pilot Bay Beach, the author repeated the sampling of sediment sites located within Pilot Bay and Cutter Channel. These observations were combined with those reported by Healy (1985) to produce a sublittoral sediment facies distribution map (Fig. 3.5). Seven main facies have been identified, and these are defined below on the basis of the author's observations:

1 Rock outcrop. More than 75% of the sea bed is covered with rock, either *in situ* or as cobbles and boulders;

2 Shell lag. In these regions more than 80% of the sea bed is covered in shell (Plate 3.1). The proportion of live shellfish increases with depth and towards the harbour entrance;

3 Very shelly sands. 50-80% of the sea bed is covered in shells or shell fragments (Plate 3.2). Very few live shellfish are observed on the surface;

4 Shelly sands. 20-50% of the sea bed is covered in shell fragments or live shell (Plate 3.3). Ripples, if present, are dominantly asymmetric current bedforms;

5 Clean sands, generally lightly rippled. These usually contain <20% shell cover and the ripples are dominantly oscillatory wave formed types, not current ripples;

6 Silty sands. These sediments are finer in texture than the other sandy facies (Plate 3.4) and they are not associated with any

Plate 3.1 - Shell lag facies in 8.5m of water, consisting mainly of fresh pipi (*Paphies australis*) with small quantities of turret shell (*Maōricolpus roseus*) and white rock shell (*Thais orbita*). The marker is 0.3m long with a 10mm spacing between bars.

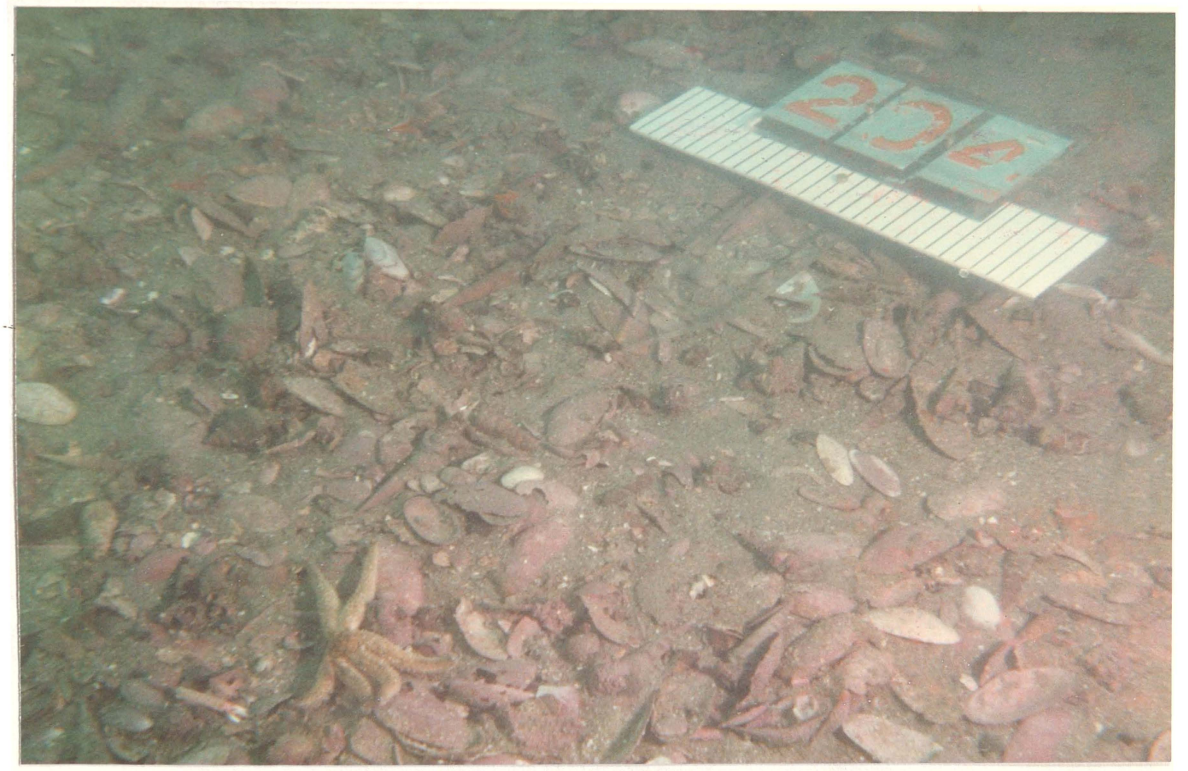

Plate 3.2 - Very shelly sand facies in 7.5m of water. 50-80% of the seabed is covered in shell, mainly old pipi (*Paphies australis*) and turret shell (*Maoricolpus roseus*).

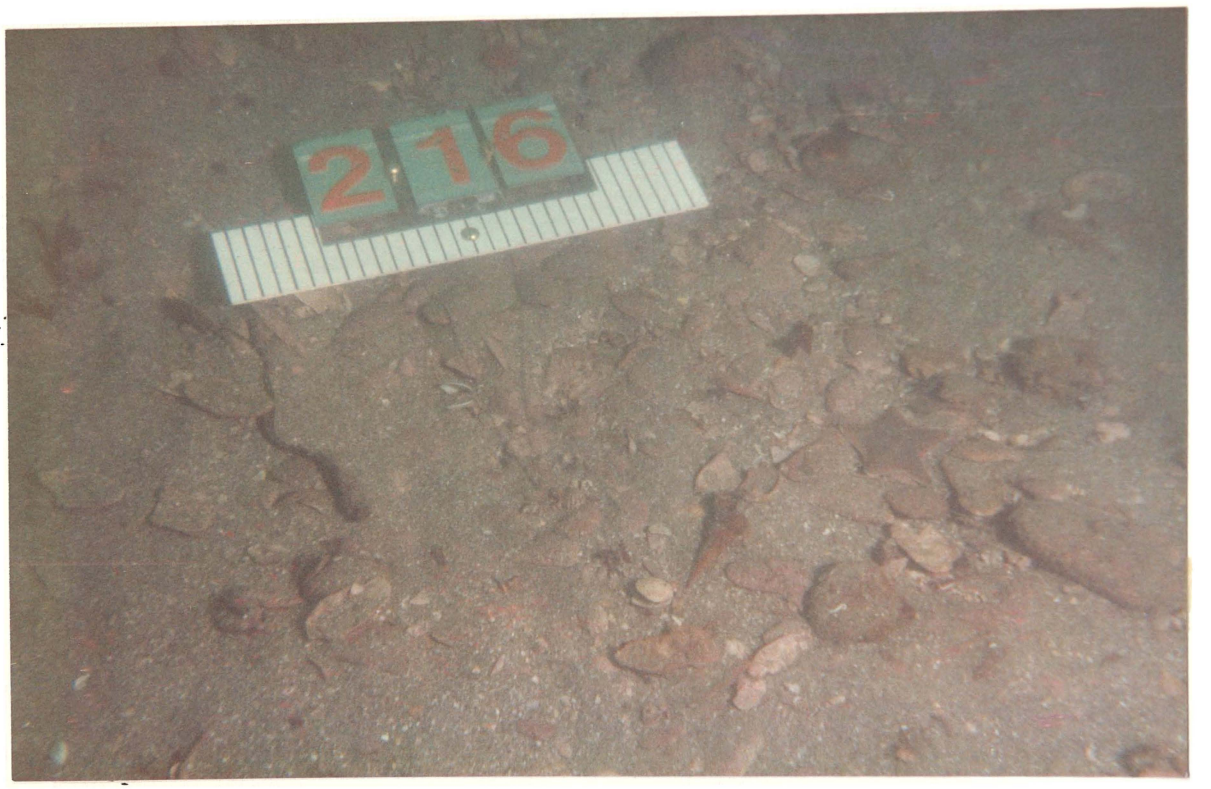

Plate 3.3 - Shelly sand facies in 13.7m of water. 20-50% of the seabed is covered in old shell fragments. Occasional live shellfish present include horse mussel (*Atrina zelandica*) and scallop (*Pecten novaezelandiae*).

Plate 3.4 - Silty sand facies in 9.4m of water. The sand is finer in texture than the other facies and, apart from the surficial 1-2mm, it is not easily disturbed. The main shell present is cockle (*Chione stutchburyi*) with occasional horse mussel (*Atrina zelandica*) clumps.

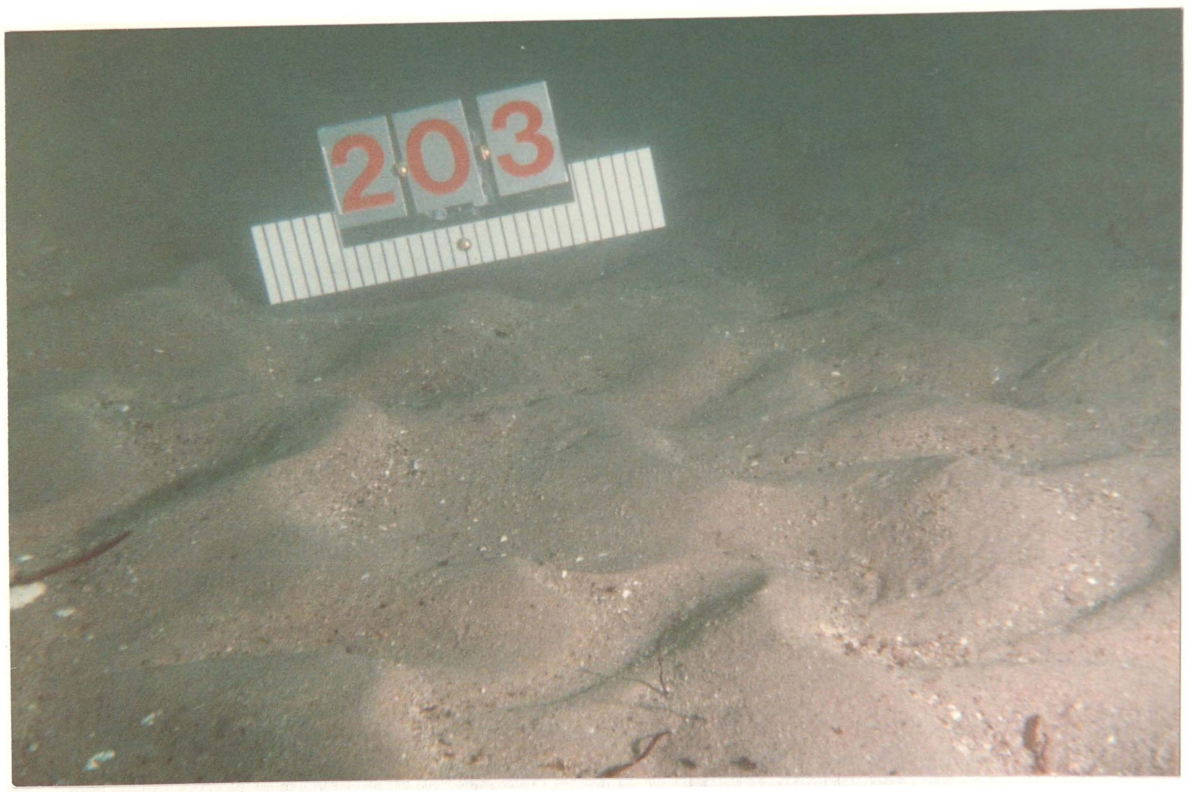

Plate 3.5 - Sand wave and megaripple facies in 11.5m of water. This plate shows the smaller ripples present on the stoss slope of a larger sand wave. Very little shell material is present except in the troughs.

bedforms. There are high concentrations of horse mussels (*Atrina zelandica*) and cockles (*Chione stutchburyi*); and

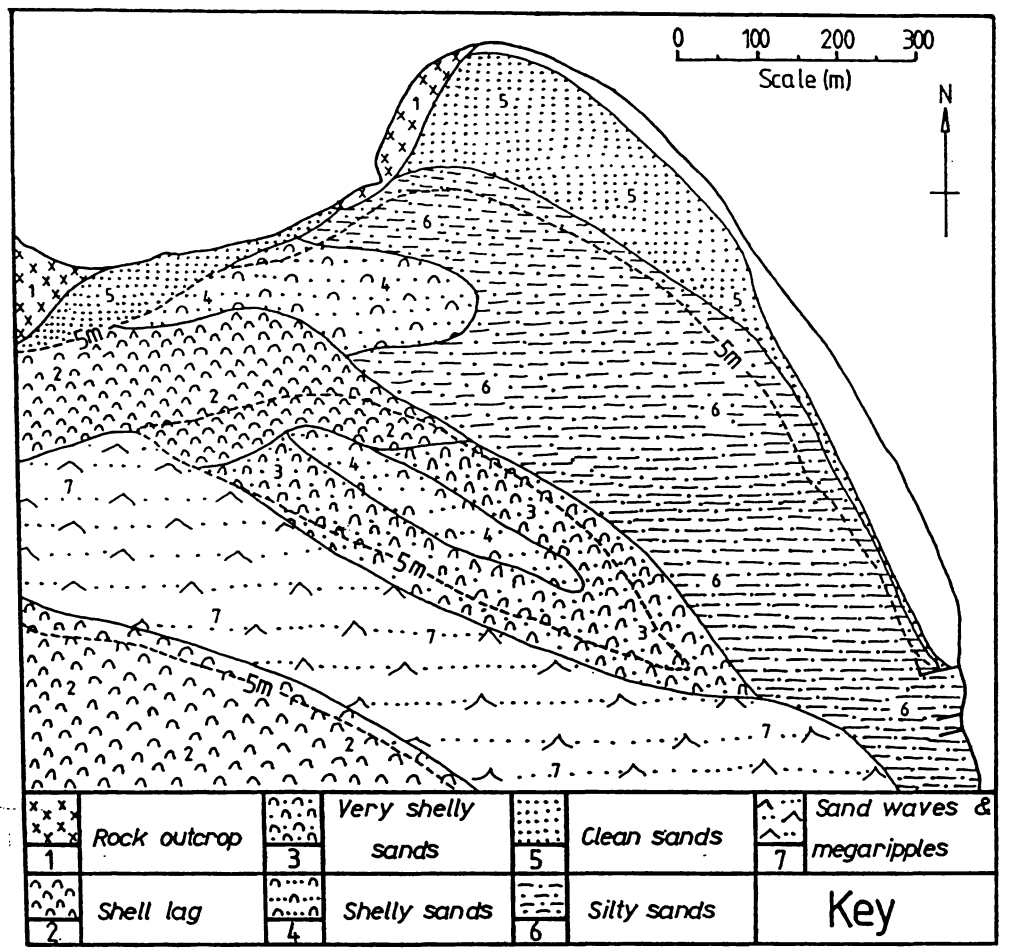

Figure 3.5 - Bottom sediment distribution for the Pilot Bay region. After Healy (1985), with additional data from this study.

7 Sand waves and megaripples. The troughs tend to contain high concentrations of shell fragments and the occasional shellfish, whereas the rest of the bedform consists of loosely packed sand. The troughs may represent an underlying shell lag, but shallow digging at the sites visited uncovered only thin veneers of coarse material of limited extent. The stoss sides of the bedforms are covered in current ripples (Plate 3.5).

3.3.1 - Relationship between facies and tidal currents

The strongest flows occur during ebb tides in Pilot Bay channel close to Stony Point (sites 5, 6), where the seabed is covered in a shell lag.

The shell comprising this lag consists mainly of dead shell fragments with the occasional live scallop (*Pecten novaezelandiae*). Passing into the harbour, away from the entrance, the shell material is fouled with an increasing quantity of algal growth, in contrast to the clean shell found in the entrance throat. Although diver visibility was limited, the lag surface appeared to represent subdued megaripples, and digging into the lag revealed >0.4m thickness of predominantly shelly material.

The peak velocities recorded in this vicinity ($\approx 0.80 ms^{-1}$) are sufficiently high to remove sand-sized material and maintain a lagged surface. However, it is unlikely that they are sufficient to develop bedforms in the thickness of shell observed since the presence of biological fouling indicates a relatively stable surface. Similar, apparently mobile, shell bedforms, consisting of a mixture of clean dead shell and live pipi (*Paphies australis*), were observed closer to the entrance throat where peak velocities are 200-300% higher. Therefore the shell lag bedforms are inferred to have formed under a higher flow regime, prior to the formation of the Cutter Channel.

Towards the centre of Pilot Bay the sediment becomes increasingly sandy and asymmetric current ripple bedforms are evident. These become smaller as the water shallows on entering Pilot Bay and disappear by about the 10m contour. Applying the sediment threshold velocity of $u_1 = 0.3 ms^{-1}$ for sand-sized sediment, employed by Black (1984) for sediment transport modelling of Tauranga Harbour, it is evident that none of the measured flood velocities within Pilot Bay are capable of initiating sediment motion. Depending on the location, peak ebb flows are capable of moving sediment, although these flows are not sustained for long - perhaps 30min per tidal cycle.

The seabed within the central Pilot Bay Channel is coated with a fine muddy or silty sand and shows no bedform development, except for minor depressions around individual horse mussels. The surficial 1-2mm consists of fine silty sediment which is easily disturbed by divers, but deeper layers are firm and cohesive, becoming increasingly anaerobic towards the Maunganui Roads. Given the cohesive nature of the sediment and the presence of fine, easily disturbed sediment on the surface, the brief periods of peak velocity appear insufficient to induce bedload sediment transport.

Closer to shore, the sediment is similar to the middle of the channel, region, but it is contaminated with medium sands derived from the adjacent renourished beach. These medium sands display beach parallel oscillatory ripples in shallow water and in deeper water appear to be gravity flow deposits (from the sublittoral beach face) with slight laminar bedding. The shell material present on the surface consists primarily of fragments of cockle (*Chione stutchburyi*) derived from the extensive beds present within the bay.

On the bank separating Pilot Bay channel from Cutter Channel, the sediment displays high concentrations of dead shell material in shallow water and on the margin of Cutter Channel. On the Pilot Bay side, high concentrations of living large and small turret shells (*Maoricolpus roseus* and *Zeacolpus fulminatus*) occur. The sediment becomes increasingly bedformed towards Cutter Channel with a higher proportion of current ripples on the flank of the Channel. In the shallow regions the bedforms are due primarily to wave action, while in deeper water the bedforms are current-induced.

In Cutter Channel the sediment is coarser (ϕ_{50}=0.8) than the central region of Pilot Bay (ϕ_{50}=1.5) and occurs as current induced megaripples. The orientation of these features adjacent to site 6B2 is indicative of flood dominance in Cutter Channel. This is in agreement with the flood dominated current data, although both ebb and flood flows are capable of moving sediment.

The sediment within the troughs of the megaripples consists primarily of dead pipi shells, probably derived from the extensive pipi beds located in the entrance and the smaller concentrations of pipi within the Cutter Channel. The shelly sediment is of limited extent and occurs as very thin layers within the troughs only. Therefore, the bedforms in Cutter Channel do not represent a thin veneer of sand traversing a shell lag.

Flood-orientated megaripples continue along Cutter Channel towards the Maunganui Roads until the neutral point bar near No.9 Beacon (Healy, 1985). South of this point the megaripples are ebb orientated. The neutral bar consists of a ridge of coarse sand and shell fragments crossing the channel margin bank and extending across the channel floor towards No.1 Berth. The ridge is approximately 2m high at the western margin of the channel and decreases in size towards the east. From

personal diver observations, the sediment is very loosely consolidated and the feature can be easily disturbed by the passage of large vessels within the channel. This suggests that the sediment may be reworked every tidal cycle, although its location, as indicated by depth soundings in the vicinity, did not vary much over 18 months.

The presence of such a feature is consistent with a change from flood-dominated conditions in Cutter Channel to ebb-dominated flows in the Maunganui Roads and Pilot Bay Channel. This region may be expected to accrete, the ridge discussed being one manifestation of accretion. This has been the case, resulting in maintenance dredging during 1984-1985.

Overall, the observed sublittoral sediment facies are consistent with the measured currents and, in terms of bedload transport, suggest high sediment fluxes through Cutter Channel and negligible fluxes through Pilot Bay. In terms of suspended sediment transport, most of Pilot Bay probably experiences little, due to low velocities in the central region and low sediment availabilities in the lagged regions. Cutter Channel can contribute suspended sediment which may be carried into Pilot Bay by the flood eddy. Some bedload may also be moved by the eddy towards the Pilot Bay channel from Cutter Channel, but the rapid loss of competence due to the reduction in tidal velocities should result in accretion offshore from Salisbury Wharf, and ultimately accretion on the Pilot Bay bank.

3.4 - Comparison with model predictions

On the basis of the evidence presented it is clear the tidal currents are flood-dominated in Cutter Channel and ebb-dominated in Pilot Bay. This is in agreement with the findings of the HRS and THS model studies, although the flood flow is stronger than predicted by HRS (1968). The presence of a flood tide eddy was predicted by HRS and adequately modelled by 2DD (Black, 1984). However, S21 indicated only a slight eddy, late in the flood, which affected a small area adjacent to Salisbury Wharf. Further, S21 indicates significant flood flow into Pilot Bay for most of the flood tide. These are not consistent with the currents measured by this study (Table 3.2).

Applying the measured current flow patterns and a sediment threshold criteria of $u_1 > 0.3 ms^{-1}$, sediment transport will be flood-dominated in

Cutter Channel and ebb-dominated in Pilot Bay. However, due to the short duration of peak flow, the transport flux in Pilot Bay should be quite low. This is consistent with the observed sediment facies distribution, but differs from the findings of Davies-Colley (1976) and, more significantly, from the THS results (Black, 1984).

The sediment transport fluxes reported by Davies-Colley (1976) were part of the first study into the sediment dynamics of Tauranga, and as such represent a broad scale analysis. The reported fluxes were based on bedload sediment traps and extrapolated current velocities. They did not consider sediment availabilities and suspended sediment loads were not measured. For Pilot Bay, the current velocities used by Davies-Colley were measured at one station located close to Aanderaa site 5, and the sediment trap results used appear to be from the same site. From Table 3.2 it is clear that this site is not representative of the currents in Pilot Bay. Davies-Colley (1976) noted that the sediment trap results indicated virtually no bedload transport at this station, but suggested that considerable fine sediment may move as suspended load.

The THS results are derived from the numerical model, 2SS, and incorporate both bedload and suspended load. The model considered the availability of sediment for transport and derived sediment transport fluxes from S21 velocity predictions. The final sediment flux through Pilot Bay predicted by the sediment transport model 2SS (9,000-27,000m^3yr^{-1}) was strongly influenced by large residual flows above sediment threshold predicted by S21. The bedload contribution to the total sediment flux was estimated to be 100-1,000m^3yr^{-1} (Black, 1984), so the bulk of the predicted sediment flux involved suspended load.

The residual flows measured by this study (Fig. 3.2) are due to the long duration of ebb flow, not to a significant difference between peak ebb and flood velocities, which is the case with the S21 residuals. If only current velocities exceeding the THS threshold criteria are considered, the measured residuals are smaller than those predicted by S21 and indicate that the contribution of Pilot Bay sediment to tidally-induced sediment transport is negligible. The large sediment flux predicted by 2SS may represent advection of sand-sized sediment entrained on Centre Bank or in the entrance (K.P. Black, pers. comm., 1985).

Given a mean settling velocity of $0.025ms^{-1}$ for suspended sand-sized sediment in Tauranga Harbour (Black, 1984) and an average water depth of 10m, more than 50% of sediment could be deposited within 10min once velocities drop below the critical value required to maintain suspension. The critical velocity is approximately equal to the settling velocity (Beer, 1983), which gives a critical velocity of 0.02-$0.03ms^{-1}$ (Beer, 1983). This velocity is exceeded for most of the tidal cycle within Pilot Bay, so sand-sized suspended sediment can advect through the bay. Finer sediment may also advect through the bay, but suspended sediment sampling undertaken by the THS indicated that sediments <4ϕ represented a very small proportion of the suspended sediment load close to the harbour entrance (Black, 1984). Therefore, the sediment fluxes calculated by 2SS were based on sand-sized sediment and ignored finer materials.

Considering long term sedimentation patterns, the HRS physical model indicated accretion within Cutter Channel until the completion of the eastern retaining wall at Sulphur Point (HRS, 1968). After that time, increased ebb tidal flows would remove the additional sediment and maintain a stable channel. Long term trends based on S21 flows indicate accretion within Cutter Channel and erosion in the Maunganui Roads. Black (1984) also reports predictions based on 2DD flows which suggest the same trends except the rates are higher and accretion within the southeastern end of Pilot Bay is indicated.

The major zone of accretion, as evidenced by the presence of a 2m high ridge of loose sediment, is the junction of Cutter Channel, Pilot Bay Channel and Maunganui Roads. The THS numerical models do indicate accretion in this area, although the extent of the accretion based on S21 is too limited and the rate based on 2DD is probably too high. The limited predictions made by the physical model best fit the observed sediment facies distribution.

3.5 - Summary

The tidal flow patterns within Pilot Bay are dominated by an eddy which operates for most of the flood tide. This eddy produces long duration ebb flows (8-11h) within the bay and controls the distribution and duration of velocities exceeding sediment threshold. The peak

velocities within Pilot Bay do not show a clear relationship with tidal range, unlike other locations within Tauranga Harbour. This suggests that the tidal flow velocities within Pilot Bay may be affected by factors other than tidal forcing.

The overall distribution of flows in the vicinity of Pilot Bay results in a strong flood-dominance in Cutter Channel and an ebb-dominance in Pilot Bay Channel. The observed flow velocities and sublittoral sediment facies distribution indicate that sediment fluxes through Pilot Bay are very low relative to other areas within the inner harbour.

Both the HRS physical model and the THS numerical models predicted the distribution of ebb-flow dominance in the Pilot Bay region and the long term sedimentation trends correctly. However, the numerical model results based on S21 velocity predictions suggest that the sediment flux through Pilot Bay is controlled by entrainment of sediment elsewhere. No model predicted the observed extent of the flood tide eddy well, with the S21 results being significantly worse than either the 2DD or HRS model results.

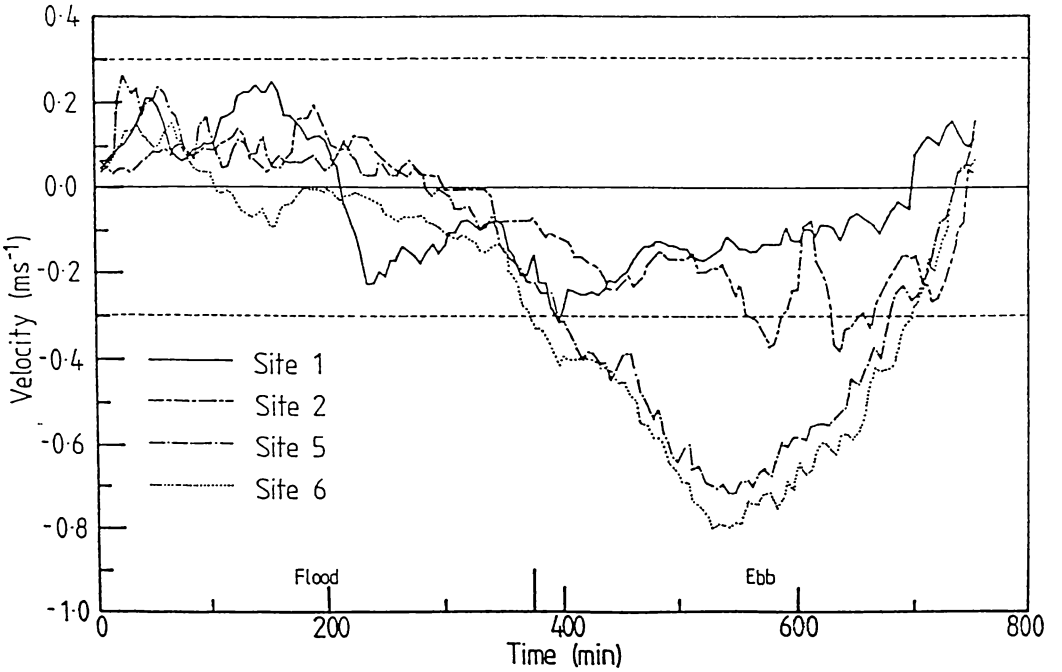

Figure 3.6 - Time-velocity graphs for Aanderaa sites with Pilot Bay (Table 3.1). The tidal cycles displayed were used to derive the residual current vectors in Figure 3.2. Currents in the flood direction (Table 3.2) are taken as positive, and ebb directed currents are negative.

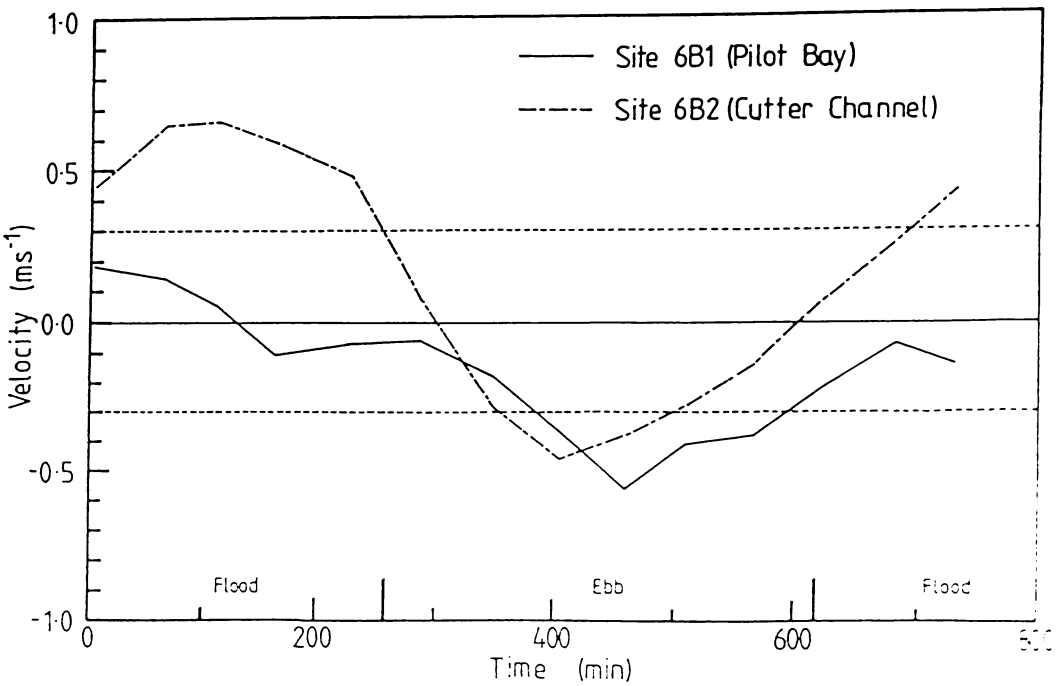

Figure 3.7 - Time-velocity graphs for THS Braystoke sites in Pilot Bay and Cutter Channel. The tidal cycles displayed were used to derive the residual current vectors in Figure 3.2. The conventions are the same as Figure 3.6.

Chapter 4 - Wind and Pressure Climatology of Pilot Bay

This chapter presents the results of wind and pressure measurements made during the course of this study. These have been recorded to enable an assessment of atmospheric predictors for non-tidal energy inputs affecting sediment transport within Pilot Bay.

The measured climatic parameters for the study period are compared to the long term record. To permit the use of wave prediction schemes for wave forecasting, a relationship between the Mt Drury anemometer and the 10m wind speed over the harbour is derived.

The temporal behaviour of wind and pressure are examined to determine whether any periodicity, which may be related to the variations in the extent and strength of the flood tide eddy in Pilot Bay, is evident.

4.1 - Climatology of the Tauranga region

Quayle (1984) discusses 5 main groups of weather systems affecting the Bay of Plenty region. These are:

1) north to northeast airstreams;
2) disturbed west to southwest airflows;
3) south to southeast airstreams;
4) west to northwest flows; and
5) tropical cyclones travelling towards the southeast across the Bay of Plenty.

The first two groups account for most of the wind at Tauranga, but the strongest winds are associated with the tropical cyclones. North to northeast airstreams entering the Bay of Plenty region contain very humid air due to long trajectories over warm ocean north of New Zealand (Quayle, 1984). Consequently they tend to produce widespread rain but generally only moderate northeasterly winds, with wind speeds $<8.5ms^{-1}$.

The disturbed west to southwest flows are more common and are associated with cold fronts which travel rapidly eastnortheast over New Zealand. In the Bay of Plenty the passage of the front may be associated with short duration light showers and moderate to strong southwesterly winds, with wind speeds $>8.5ms^{-1}$. Tropical cyclones are rare and occur during the summer months of November through April. They originate over the warm tropical oceans north of New Zealand and as they

move south their structure is modified extensively. They can produce heavy rain and very strong winds in the Bay of Plenty region (Quayle, 1984).

There are two climate stations maintained by the New Zealand Meteorological Service (NZMS) and located close to Pilot Bay. These are station B76611 at Tauranga and station B76621 located at Tauranga Airport. The Tauranga station has been operating since 1970 and does not record wind data. The airport station records all parameters and has been at its present site since 1942, although records are available back to 1898 for some parameters such as rainfall (NZMS, 1983c). The BOPHB has also operated an anemometer since 1961 (NZMS, 1983d) A summary of selected parameters is given in Table 4.1 for the Tauranga Airport station.

The rainfall values show a fairly uniform distribution throughout the year. There are marked variations in the summer months (e.g. January) due to thunderstorms which produce intense, short duration rainfall with relatively low return periods (Fig. 4.1). One event of April 17, 1948, holds the New Zealand record for maximum rainfall during 10, 20 and 30min with amounts of 34, 51 and 68mm respectively (NZMS, 1983a). The distribution of thunderstorms at Tauranga indicates a major peak during December-January with a secondary peak during April-May (Revell, 1984). Most occur during late afternoon, although a significant number occur late at night, and are caused by atmospheric destabilisation associated with daytime heating and 'sea-breeze' circulation (Revell, 1984), especially in the Kaimai Ranges to the west of Tauranga (NZMS, 1982).

The extremes in pressure recorded at Tauranga Airport span 59hPa. Given a sea level variation of $0.0001mPa^{-1}$, or 10mm/mbar (Beer, 1983), this could produce maximum water level changes of 0.59m, although the water surface does not respond immediately to pressure changes and the response is determined by the average change over a large area. The Bay of Plenty region also shows cyclic variations in pressure associated with atmospheric tides (Trenberth, 1977; NZMS, 1983b), resulting in fluctuations of <0.25hPa. Most marked is a diurnal cycle with two pressure maxima and minima a day. The maxima tend to occur at about 0900 and 2100 with the minima about 6 hours out of phase (NZMS, 1983b).

Table 4.1 - Summary of some climatological parameters for Tauranga Airport (Station B76621) to 1983.

	Jan	Feb	Mar	Apr	May	Jun	Jul	Aug	Sep	Oct	Nov	Dec	Year
Rainfall (mm) for 1898-1983.													
Maximum	532	343	504	383	311	381	348	253	274	357	285	447	2049
Mean	90	92	113	120	127	136	135	123	108	118	86	99	1341
Minimum	1	7	5	10	13	19	2	14	16	11	14	4	772
Pressure (hPa) for 1961-1983.[a]													
Maximum	1027	1029	1032	1032	1033	1036	1037	1036	1034	1034	1030	1031	1037
Mean	1015	1016	1017	1016	1016	1015	1015	1016	1016	1017	1016	1014	1016
Minimum	990	998	995	991	992	990	978	984	992	989	983	996	978
Wind for 1959-1980.[b]													
>17.5ms^{-1}	1.8	1.1	1.9	2.5	3.3	3.5	3.6	3.3	3.8	4.0	3.1	2.1	34.0
>26.7ms^{-1}	-	0.1	0.1	0.2	0.1	0.1	0.1	-	-	0.3	0.1	-	1.1
Wind (ms^{-1}) for 1970-1979.													
Mean	4.7	4.7	4.4	4.4	4.2	3.9	4.4	4.4	5.0	5.8	5.3	5.3	4.7
Wind (ms^{-1}) for 1981-1983.													
Maximum Gust	21.6	20.6	18.0	25.8	23.2	22.7	25.8	25.2	29.9	21.6	20.6	23.2	29.9
Direction (°)	240	120	270	210	300	240	260	250	270	270	260	270	210

Data are from various sources (NZMS, 1983b,c,e, 1984, 1985).

[a]Pressure readings taken at 0900 and corrected to mean sea level.

[b]Due to variations in the data available, the wind parameters are presented separately as: average days with gusts exceeding the limits specified, mean hourly wind speed, and maximum gust speed and direction.

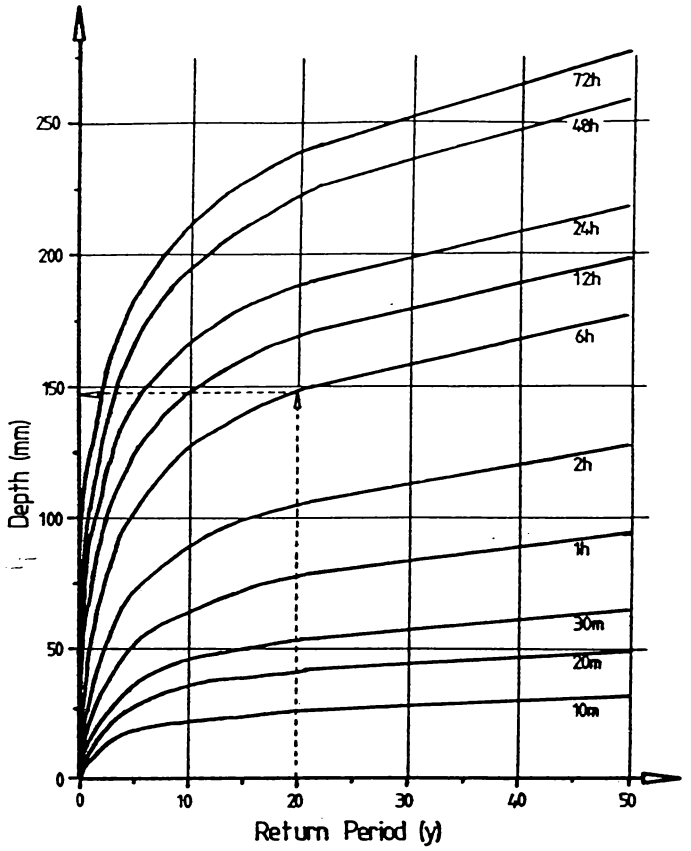

Figure 4.1 - Depth-Duration-Frequency graph for Tauranga Airport (B76621), after Quayle (1984). This diagram indicates the maximum amount of rainfall which can be expected, within the specified time interval, for any given return period. For example, given a return period of 20y, the maximum amount of rainfall expected during a 6h interval is 145mm.

In general the morning maxima and the afternoon minima are more pronounced due to local heating and cooling, although this does depend on local orographic factors (Trenberth, 1977). The seasonal variations involve major maxima in November and minima in June, and minor maxima in August, but these changes are slight as indicated by the mean pressure (Table 4.1). These pressure variations may not generate waves directly, but they do influence wave propagation within the estuary by affecting water depths.

This effect is usually of minor importance compared to normal tidal variations, but extreme pressure fluctuations alter the tidal range significantly. For example, the Wahine storm of 1969 induced extremely high tides due to the low pressures and onshore wind stresses. The

exact height of the tides is not known since the chart went off-scale at 3.0m (cf. MHWS=1.9m).

The winds in the Tauranga region are modified by the local topography (Quayle, 1984), primarily by the Kaimai Ranges to the west. As a result, less wind >17.5ms^{-1} is experienced than in other parts of New Zealand. Gales occur infrequently, have low maximum wind speeds compared to other regions, and are mainly from either the northeast or the southwest. The maximum gust recorded at Tauranga Airport for the period 1959-1980, was 33ms^{-1} during a southwesterly gale in April 1969. The mean wind speed (Table 4.1) reflects the presence of sea breezes and shows little seasonal variation, the maximum change between summer and winter being only about 33% (de Lisle and Kerr, 1963; Quayle, 1984).

Tauranga shows a diurnal variation in wind speed and direction associated with differential heating of sea and land, which results in sea breezes occurring mainly in early afternoon and tending to be slightly stronger during summer. The mean annual frequency of wind speed and direction (Fig. 4.2) shows opposing dominant wind directions; west to southwest (36%), and north to east (23%) (NZMS, 1982).

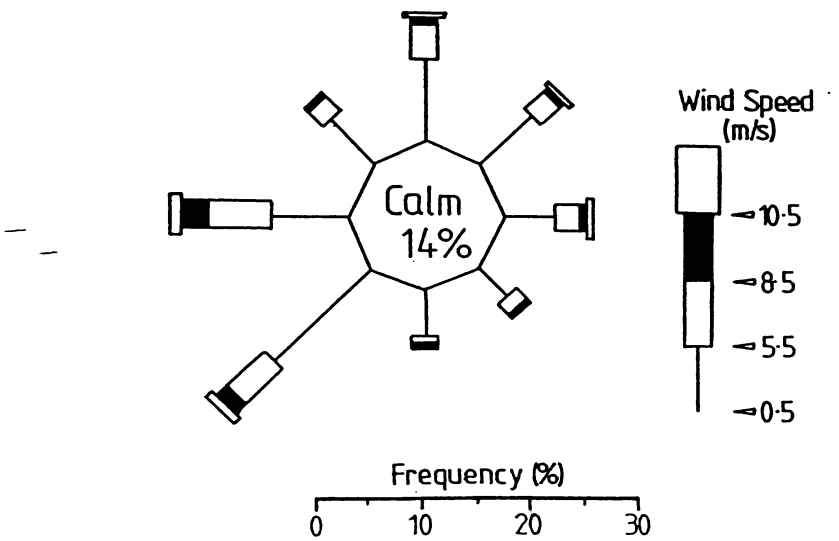

Figure 4.2 - Mean annual frequency of wind speed and direction for Tauranga Airport (B76621) over the period 1970-79. After Quayle (1984).

4.2 - Wind observations for the study period 1984-1985

Three anemometer sites were used to obtain wind data (Table 4.2), two of which were pre-existing long term sites at Tauranga Airport and the

Mt Maunganui wharves. Specifically for this study, a third anemometer was installed on the newest BOPHB tug berth (Plate 4.1). Airport anemometer records for June, July and August 1984 were obtained from the NZMS. However, these observations were made only while the Control Tower was manned and the records were unsuitable for subsequent analysis.

Table 4.2 - Anemometer sites used by this study. The grid references refer to NZMS 260 U14. Although the chart recorder for the BOPHB anemometer is located at Mt Drury, the actual rotor and vane assembly is mounted on a light pole half-way along the BOPHB wharves. However, this recorder will be referred to as Mt Drury in keeping with BOPHB practice.

	Tauranga Airport	Mt Drury Signal Station	Tug Berth
Grid ref.	924873	001898	899908
Type	Munro Anemometer	Munro Anemograph	Woelfle Anemometer
Height above ground level	10m	27m	8.5m
Height above mean sea level	14m	30m	10m
Period of record	1/6/84 -31/8/84	1/1/84 -31/12/85	7/7/84 -26/3/85
Number of observations	1093	16048	6311

The mean frequency and direction data for the Mt Drury and Tug Berth anemometers are summarised in Figure 4.3. Both recorders deviate from the average pattern for Tauranga Airport determined for the period 1970-79 (Fig. 4.2). The obvious anomaly is the percentage calm recorded at each of the three sites, which is attributed to differences in the recorders used as well as real variation in wind exposure between the sites. The Woelfle anemometer used at the Tug Berth site records wind run (Appendix 4). The mean hourly windspeed can be derived from the slope of the accumulated wind run (Lambrecht, 1983). This method of analysis results in a minimum measured mean windspeed of $0.5ms^{-1}$, and consequently no calm hours were recorded.

The Munro anemograph records instantaneous windspeed as an analogue trace. The mean windspeed was derived by a visual best fit as the record was digitised. Due to the poor resolution of the trace there was significant scatter about $0.5ms^{-1}$ and some readings recorded as $>0.5ms^{-1}$

Plate 4.1 - Woelfle Anemometer installation on the southern BOPHB Tug Berth. A fork lift provided access to the anemometer for servicing.

may represent calm periods. Hence the calm percentage may be closer to the Airport average than Figure 4.3 suggests. For the Mt Drury and Tug Berth records the reduction in the percentage calm is compensated for by an increase in the range 0.5-5.5ms^{-1}.

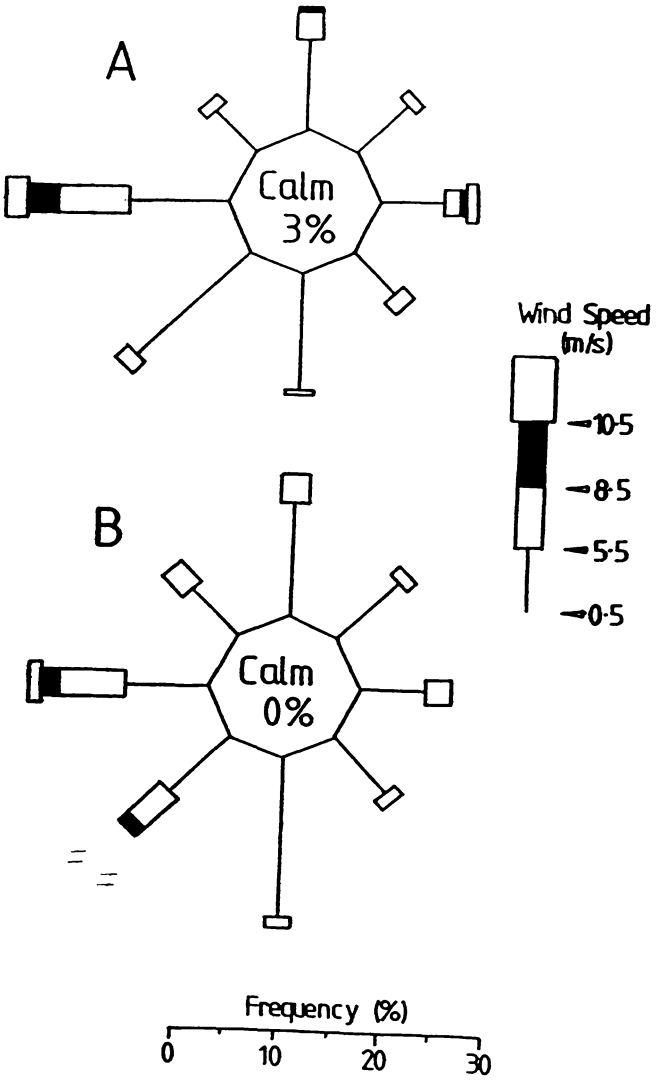

Figure 4.3 - Mean annual frequency of wind speed and direction for Mt Drury (A) and Tug Berth (B), over the period 1984-85. These represent the overall harbour and Pilot Bay wind conditions respectively.

The Mt Drury and Tug Berth records both show an increased southerly component in the wind field at low wind speeds compared to Tauranga Airport (Fig. 4.2), although the dominant wind directions are still west to southwest (45% and 31% respectively), and north to northeast (21% and 24% respectively). The incidence of winds >10.5ms^{-1} is similar to the

Airport site but these occurrences are now restricted to onshore-offshore (east-west) winds. No tropical cyclones were experienced during the study period.

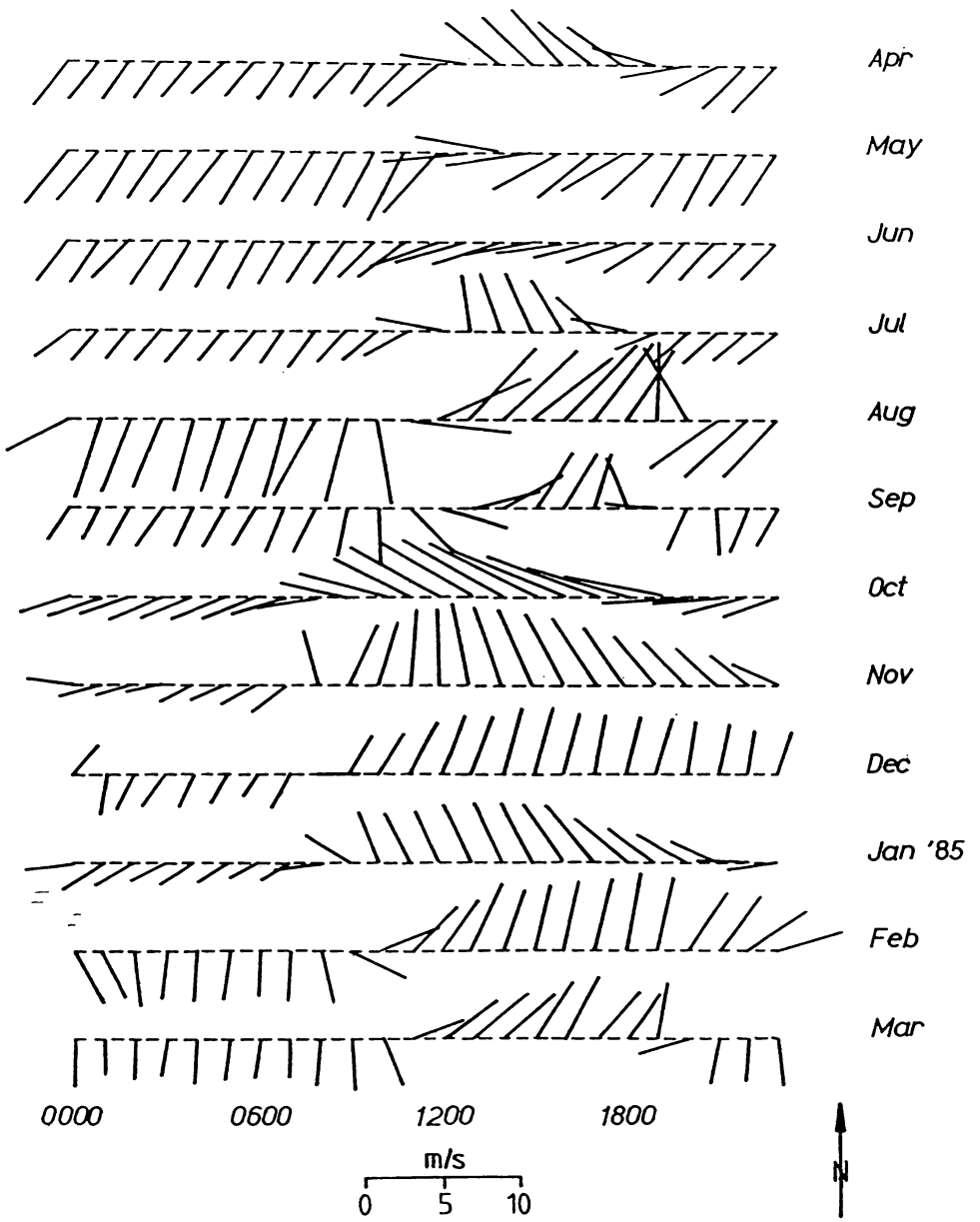

Figure 4.4 - Average hourly wind speed and direction for Mt Drury during the period 1/4/84 to 31/3/85. This diagram shows the daily sea breeze variation within Pilot Bay between mainly offshore winds in the morning and onshore during the afternoon.

A comparison between the Tug Berth and Mt Drury records shows that sheltering from the east and southeast by buildings at the Tug Berth

site results in lower wind speeds from these directions. The Tug Berth also shows a higher incidence of southerly winds along the wharf face, and stronger winds from the southwest. Despite these differences there is a strong correlation between the two sites for wind speed. Regression analysis on paired, ungrouped, wind speed data from Mt Drury and the Tug Berth gives equation 4.1 with r^2=0.75 (cf. Table 4.4).

$$Y = 1.775 + 0.639X \quad \ldots 4.1$$

where X = Mt Drury windspeed (ms^{-1}),
and Y = predicted Tug Berth windspeed (ms^{-1}).

All the data show a diurnal variation in wind speed and direction, reflecting the influence of sea breezes in the afternoon. The monthly average hourly wind speed and direction measured at Mt Drury for the period 1/4/84 to 31/3/85 (Fig. 4.4) clearly shows this diurnal variation. A slight seasonal trend is obvious with August having the strongest winds during the study period.

4.2.1 - Spectral analysis of winds

In order to check that the response of the Woelfle was equivalent to the response of the Mt Drury anemometer, cross-spectral analysis between the Tug Berth and the Mt Drury records was undertaken using the standard BMDP P1T package (Dixon *et al*, 1981). This was necessary to assess the suitability of Mt Drury records for wave forecasting and hindcasting. A similar analysis was not possible for Airport records due to the large gaps in the data.

A total of 6311 pairs of hourly means was used. The univariate statistics of the data are summarised in Table 4.3. Both data sets show a slight decline in wind speed between the start of the record in July to the end in March, reflecting seasonal trends. This trend was not removed because linear or sinusoidal detrending were inappropriate and the data did not span an entire year, ruling out a seasonal detrend (Dixon *et al*, 1981).

The coherence (i.e. degree of correlation at a particular frequency) between the two sites shows a fairly steady decline with increasing

frequency (Fig. 4.5), consistent with the increasing influence of local site specific effects. There is no significant phase difference between the records at all frequencies below $1x10^{-4}$Hz (3h) and all phase differences indicate that the Mt Drury recorder lags behind the Tug Berth recorder, so that wind conditions tend to change at the Tug Berth first. The gain between Mt Drury and the Tug Berth site indicates that the Tug Berth record has about 30% of the spectral density of the Mt Drury record for all frequencies below $7x10^{-5}$Hz (4h) and it decreases rapidly for higher frequencies. This is consistent with its lower elevation and more sheltered location.

Table 4.3 - Summary of univariate statistics for wind speed at the Mt Drury and Tug Berth anemometer sites during the period 7/7/84-26/3/85.

	Mt Drury	Tug Berth
Mean (ms^{-1})	4.11	4.40
Standard Deviation	3.04	2.24
Coefficient of variation	74%	51%
Maximum (ms^{-1})	18.20	15.30
Date[a]	6/8/84	23/8/84
Minimum (ms^{-1})	0.00	0.50

[a]The date on which the maximum wind speed occurred

The main peak in both spectra (Fig. 4.6) occurs at a frequency of $1.186x10^{-5}$Hz, indicating a major cycle with a period of approximately 24h. This results from the diurnal cyclicity associated with sea breezes. Other major peaks occur at $2.375x10^{-5}$Hz (12h) and $4.630x10^{-5}$Hz (6h). These may be harmonics of the diurnal cycle. A significant amount of energy lies to the left of the main peak but it is irresolvable due to the short duration of the record. Since the coherence between the two sites is high at low frequencies (>0.80), it is possible to use the Mt Drury recorder to predict the average 10m windspeed at the Tug Berth over time periods longer than 6h.

In order to predict wave conditions at the Tug Berth, the average windspeed for periods <6h is required, so the coherence at high frequencies is of interest. Using a narrower bandwidth of 0.0008Hz, the coherence is 0.80 at $9.259x10^{-5}$Hz (3h). Due to the sampling interval of 1h, the cutoff or Nyquist frequency is $1.389x10^{-5}$Hz (or a period of 2h). Therefore it is not possible to determine the coherence at higher

frequencies.

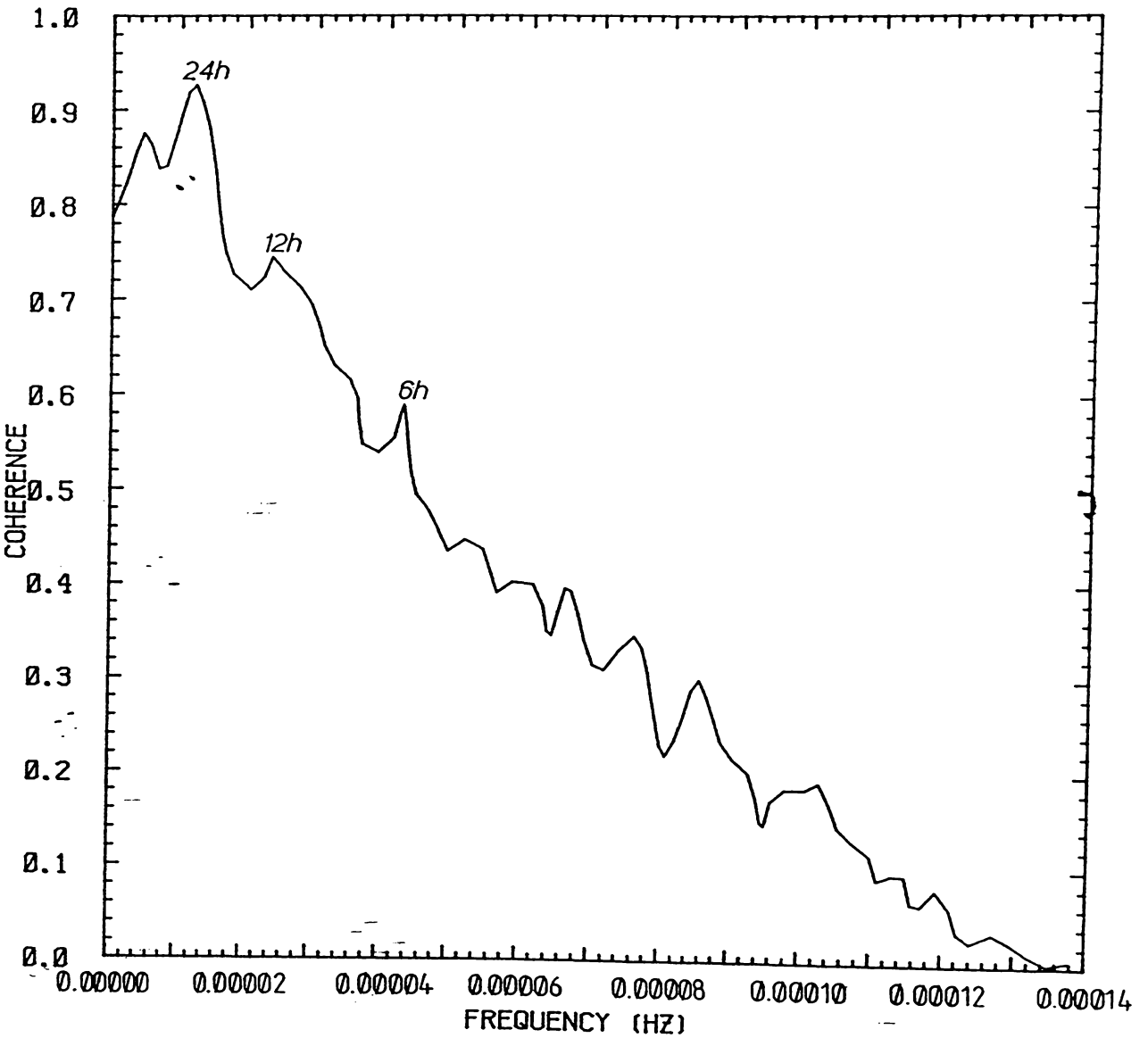

Figure 4.5 - Coherence between Mt Drury and Tug Berth wind speed spectra. The coherence has been averaged over intervals of 0.0271Hz (i.e. bandwidth=0.0271Hz). A coherence of 1 indicates perfect correspondence between the two spectra.

However, the coherence is high (>0.80) for all frequencies corresponding to integral multiples of the sampling interval between periods of 3-117h. Hence it is reasonable to assume that the coherence is also high for periods of 1 and 2h. Thus the Mt Drury wind speed record can be used to predict the wind speed at the Tug Berth for short time intervals.

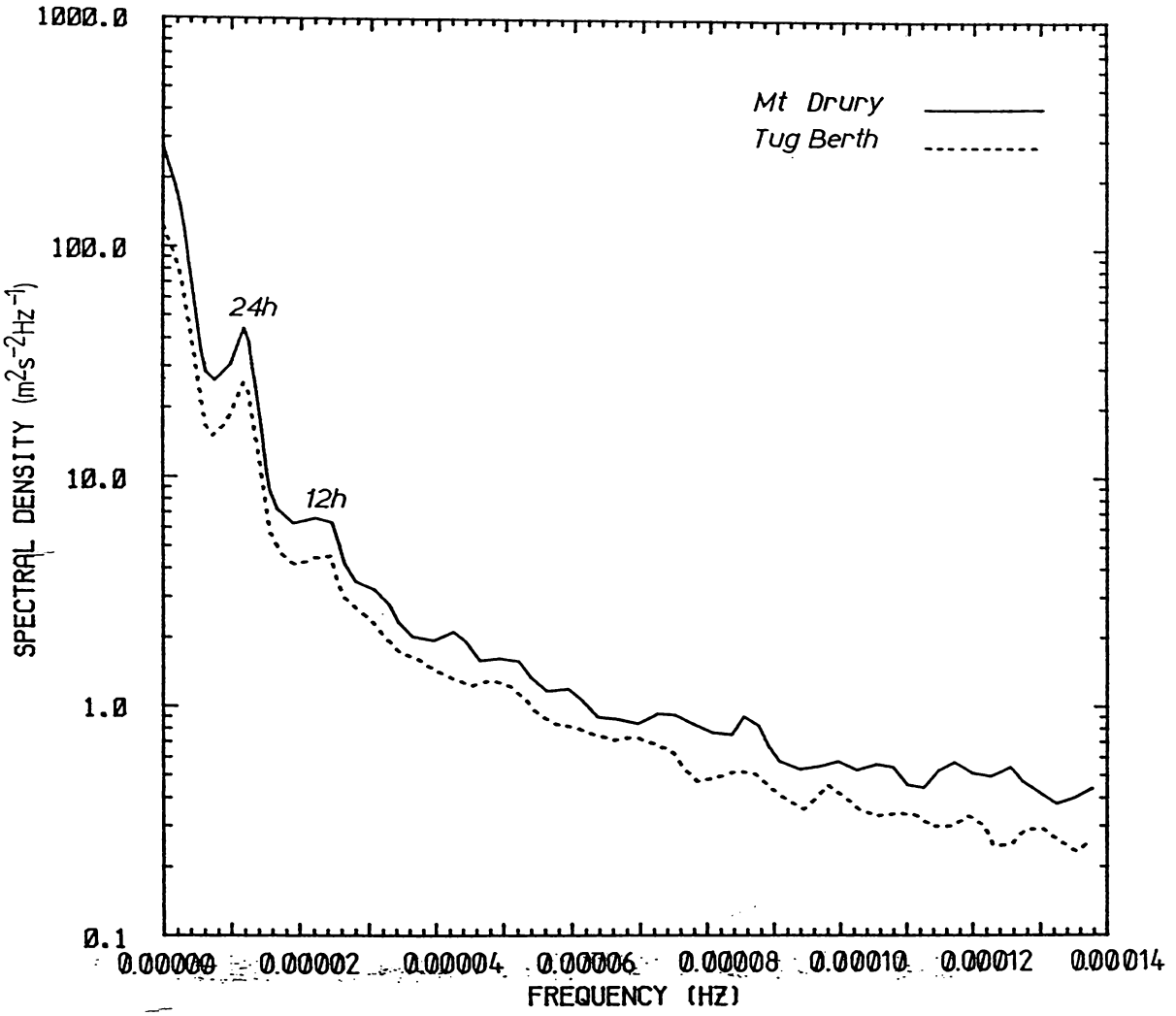

Figure 4.6 - Mt Drury and Tug Berth wind speed spectra. Bandwidth = 0.0271Hz.

4.2.2 - Wind parameter prediction

The sites used showed little seasonal variation in wind speed, but there were diurnal variations. However, from the spectral analysis results there is little temporal variation in wind speed between sites, with good coherence and insignificant phase lag at most frequencies. Hence it is not necessary to group data on the basis of either season or time of day. Examination of wind data revealed that, although the direction recorded at the Tug Berth was consistent with the direction at the Mt Drury recorder (within ±30° for >95% of the time), the wind speed at the Tug Berth showed evidence of sheltering for winds from the

easterly quarter. Therefore wind speed prediction was constrained by wind direction.

The data were grouped into the 8 sectors used for deriving wind rose frequencies (Fig. 4.3) depending on the wind direction determined by the Mt Drury recorder. Initially no assumptions about the wind speed distribution were made and a non-parametric Kruskall-Wallis test was used to examine the following null hypothesis:

> "that the means of the groups are not significantly different, i.e. the groups are samples of the same population."

The analysis was performed by the BMDP routine P3S with a separate analysis undertaken for each site. The tests gave χ^2 values of 1394 and 1133 with 7 degrees of freedom (df) for Mt Drury and the Tug Berth respectively. At the 0.001% significance level with 7df, χ^2=18, so in both cases the null hypothesis is rejected.

A further test of the null hypothesis was performed using a two-way ANOVA. In this case it was assumed that the two samples of the wind speed at Tauranga can be closely approximated by normal distributions having the same variance. In addition, this analysis also tested the variation between sites by treating the two sites as independent measurements of the same variable. The analysis was performed by the BMDP routine P2V, and resulting in an F value of 17823 (1 & 6303df) for between group interactions, and F=201 (7 & 6303df) for site variations. Therefore there is significant variation between the groups and between the sites.

Further analysis showed that none of the groups could be combined without increasing the variation significantly. The results could be improved slightly by further subdividing the 8 groups. However, this was not done so as to maintain groupings consistent with previous workers (e.g. Quayle, 1984).

To allow hindcasting of the Tug Berth wind speeds for wave prediction, linear regression was performed on the 8 groups and the total sample (Appendix 4). The results of these analyses are summarised in Table 4.4. The following null hypothesis was also tested by P1R;

> "that the slopes and/or intercepts of the linear regressions do not differ significantly between groups",

giving F=191 (14 & 6295df). Therefore the null hypothesis was rejected and wind speed prediction at the Tug Berth using Mt Drury data is best

performed by grouping data and using separate equations for each group.

Table 4.4 - Summary of regression equations and statistics for 8 directional groups of wind speed. For example, given a wind speed of Xms^{-1} from the north recorded at Mt Drury, the wind speed at the Tug Berth is given by 1.665+0.705X. SD is the standard deviation of the group and the correlation measures the degree of association between the two recorders.

Group	N	NE	E	SE	S	SW	W	NW	Total
Number	996	575	726	451	720	972	1338	533	6311
% of total	15.8	9.1	11.5	7.1	11.4	15.4	21.2	8.4	100.0
Mt Drury									
Mean ms^{-1}	4.13	3.12	5.48	3.99	1.99	2.74	6.12	3.72	4.11
SD ms^{-1}	2.26	1.89	3.81	2.30	1.96	2.05	3.46	2.36	3.04
Tug Berth									
Mean ms^{-1}	4.58	3.57	4.26	3.45	3.05	4.00	6.06	4.36	4.40
SD ms^{-1}	1.83	1.38	1.96	1.42	1.70	1.90	2.75	1.88	2.24
Correlation	0.87	0.86	0.86	0.81	0.82	0.90	0.92	0.84	0.87
Intercept	1.665	1.604	1.843	1.445	1.629	1.712	1.591	1.858	1.775
Slope	0.705	0.632	0.442	0.502	0.715	0.832	0.731	0.672	0.639

The statistics presented for the regression equations (Table 4.4) relate to the period during which the Tug Berth anemometer operated (7/7/84-26/3/85). This period may not have been representative of long term wind conditions for the Tug Berth site. Bardsley and Manly (1983) present a technique for regression-based estimation of the long-term mean and variance of wind speed for aerogenerator sites. This technique is applicable to this problem, although the record for the predictor site, Mt Drury, is not very long term.

Using all the available Mt Drury data the estimated long term wind speed at the Tug Berth is $4.43ms^{-1}$ with a variance of $4.49m^2s^{-2}$. The number of samples used was 16048, taken over 2 years (1984-85), which is sufficiently large for an unbiased estimate of the mean. The sampling error (or variance of the mean wind speed) due to the regression residuals alone was $0.84x10^{-4}$, and due to the residuals and the estimation errors for the slopes and intercepts was $0.74x10^{-3}m^2s^{-2}$. These are insignificant, although they indicate that the estimation errors for the slopes and intercepts are major contributors to the error in the predicted wind speed. The variance of the wind speed is a biased estimation, so the unbiased variance was determined to be $5.36m^2s^{-2}$.

From the above values the 95% confidence interval for the long term mean wind speed at the Tug Berth is $4.43 \pm 0.03 ms^{-1}$. The estimated values compare favourably with the measured values of 4.40 and 5.03 for the mean and variance at the Tug Berth. Compared with the long term mean wind speed at Tauranga Airport of $4.6 ms^{-1}$ (Table 4.1) the predicted value is lower, which is consistent with the sheltering at the Tug Berth. It can be concluded that the regression equations given in Table 4.4 are good predictors of the wind speed at the Tug Berth based on the Mt Drury data.

4.3 - Pressure observations for the study period 1984-1985

The BOPHB maintains a barograph in the Pilots Room at the Harbour Board offices. Data from this instrument were digitised manually at 3h intervals for the period 10 April 1984 to 1 July 1985. There was only one break of 12 readings, during 6-7 February 1985, over this period. The standard method for recording pressure data is to take the 0900 reading and correct it to sea level (NZMS, 1983b) based on the relationship between pressure and altitude (z) given in Equation 4.2.

$$p_z = p_o e^{-(gz/(RT))} \qquad \ldots 4.2$$

where T = temperature (°K),
R = $287 Jkg^{-1}K^{-1}$,
p_o = sea level pressure,
and p_z = pressure at altitude z.

This relationship assumes a negligible temperature gradient between sea level and the measurement altitude. If the temperature gradient is significant then it too must be compensated for. For the BOPHB barograph the altitude is <5m and the temperature gradient could be assumed to be negligible.

Therefore, taking a temperature range of -5.3-33.7°C (Table 4.1), the correction factor ranges from 0.99936 to 0.99944. For the mean pressure measured during this period (1016.5hPa) this amounts to a maximum change of 0.6hPa or 0.06%. The digitisation error is ±1hPa or 0.10% for the

mean pressure recorded. Since the maximum correction is less than the digitisation errors, the standard altitude correction was not applied to the data.

The mean, maximum and minimum monthly pressures based on the 0900 reading (Table 4.5) do not show any major deviations from the results for the period 1961-1983 (Table 4.1). The variation in pressure is at a minimum during November, December and January, reflecting a slight seasonal variation. These seasonal trends are not consistent with the expected trends (Section 4.1), where major maxima occur in November and minima in June. However both the expected seasonal variation and the observed trends are slight, so this apparent change is not significant.

Table 4.5 - Summary of uncorrected pressure readings recorded at 0900 for the BOPHB barometer during the period 10/4/84-1/7/85.

	Jan	Feb	Mar	Apr	May	Jun	Jul	Aug	Sep	Oct	Nov	Dec
Pressure (hPa) for 1984.												
Maximum				1027	1033	1034	1034	1034	1028	1028	1029	1020
Mean				1017	1019	1023	1017	1016	1015	1017	1019	1012
Coefficient of variation (%)				0.68	0.87	0.72	0.97	0.87	1.06	0.69	0.55	0.34
Minimum				999	1000	1004	996	1001	990	991	1007	1006
Pressure (hPa) for 1985.												
Maximum	1022	1029	1031	1034	1035	1025						
Mean	1013	1017	1016	1024	1021	1016						
Coefficient of variation (%)	0.46	0.68	0.66	0.74	1.01	0.77						
Minimum	1005	1003	1004	1004	997	992						

If all the available data are considered, the mean uncorrected pressure is 1017hPa with a coefficient of variation of 0.86%. The maximum recorded pressure was 1035hPa, which is within the upper limit of values given in Table 4.1. The minimum recorded was 885hPa, which lies more than 15σ from the mean and is well below the minimum recorded in Table 4.1. If the value is corrected for altitude, the resulting pressure is 886hPa. This reading occurred at 1030 on June 22, 1985 and was associated with a maximum gust of 31.9ms^{-1} at the Mt Drury recorder. Overall the pressure decreased from a maximum of 1018 at 0900 on June 20 to a low of 992 at 0900 on June 23. The minimum noted occurred as a result of a rapid decrease followed by an equally rapid increase lasting

less than 3h. This was the only such event noted during the sampling period.

4.3.1 - Spectral analysis of pressure data

As certain long period waves, such as seiches, may be generated by atmospheric forcing (Beer, 1983), spectral analysis was performed on the pressure data. To increase the size of the data set, the missing values for February 6-7, 1985, were estimated by linear interpolation. This gave a total of 3576 pressure readings, spanning 447 days.

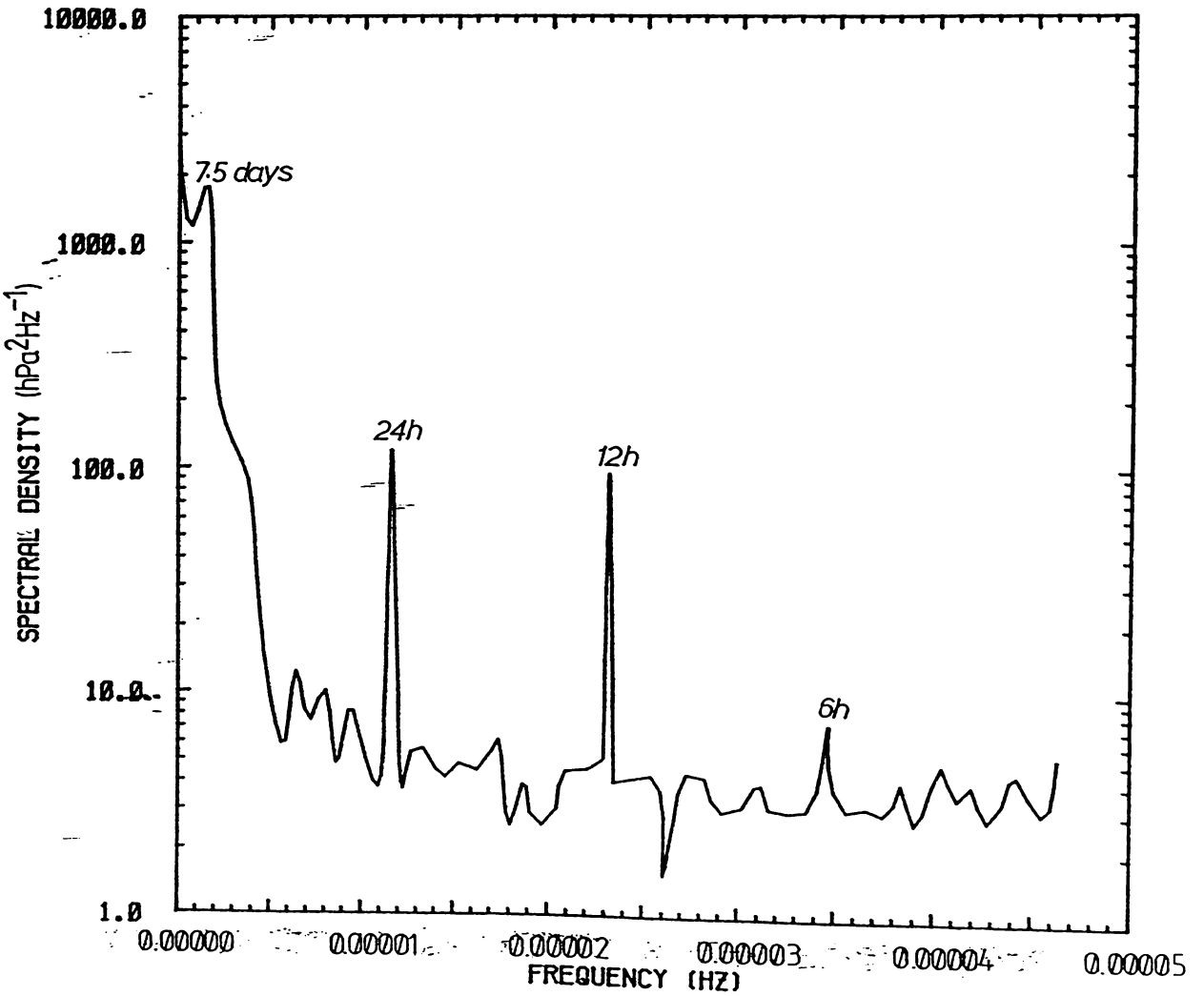

Figure 4.7 - Pressure spectrum for the barograph situated in the Pilots Room, BOPHB, for the period 10/4/84-1/7/85. Bandwidth = 0.0005Hz.

The analysis was carried out at bandwidths of 0.0005, 0.0021 and 0.0109Hz (8, 46, & 234df). Two major peaks were located (Fig. 4.7) at 2.315×10^{-5}Hz (12h) and 1.157×10^{-5}Hz (24h). These peaks coincide with the atmospheric tides (Trenberth, 1977). Minor peaks occur at 7.957×10^{-6}Hz (35h), 6.510×10^{-6}Hz (43h) and 1.447×10^{-6}Hz (7.5 days). It is not clear what these peaks represent.

Winds occur in response to pressure gradients (Barry and Chorley, 1982), therefore it is reasonable to expect some relationship between the pressure and the observed wind speed at Mt Maunganui. Cross-spectral analysis was undertaken between the pressure and wind speed as recorded at Mt Drury for the period 10/4/84 to 1/4/85. Since the pressure was recorded every 3h, the Mt Drury wind speed was reduced to 3h averages. Each pressure reading was then paired with the average wind speed for the succeeding 3h.

A total of 2899 pairs of data were obtained. The univariate statistics for the data used (Table 4.6) show no significant deviation from the total data sets discussed previously.

Table 4.6 - Summary of univariate statistics for pressure and the 3 hourly average wind speed at the Mt Drury site during the period 10/4/84-1/4/85.

	Pressure	Wind speed
Mean	1016hPa	$4.00ms^{-1}$
Standard deviation	8hPa	$2.90ms^{-1}$
Coeff. of variation	0.81%	72.50%
Maximum	1034hPa	$17.5ms^{-1}$
Minimum	987hPa	$0.0ms^{-1}$

The two data sets were detrended before spectral analysis and the analysis was not constrained by the pairing in the data set. This was necessary in case wind speed lagged pressure changes. From the spectra produced (Fig. 4.8) there are some consistent trends between pressure and wind speed. Two major peaks occur in the coherence (Fig. 4.9) at 1.148×10^{-5}Hz (24h) and 2.296×10^{-5}Hz (12h). Of these two peaks the 24h cycle dominates with a coherence of 0.60, compared to 0.25 for the 12h cycle. This peak can be attributed to atmospheric tides for the pressure spectrum and diurnal 'sea breezes' for the wind speed spectrum.

For a narrower bandwidth of 0.0005Hz, minor peaks with strong

coherences of 0.60 and 0.89 occur at frequencies of 1.530×10^{-6}Hz (7.5 days) and 9.183×10^{-5}Hz (30h). These peaks are not evident in Figure 4.9 due to averaging associated with a bandwidth of 0.0109Hz. It is uncertain what these minor peaks represent.

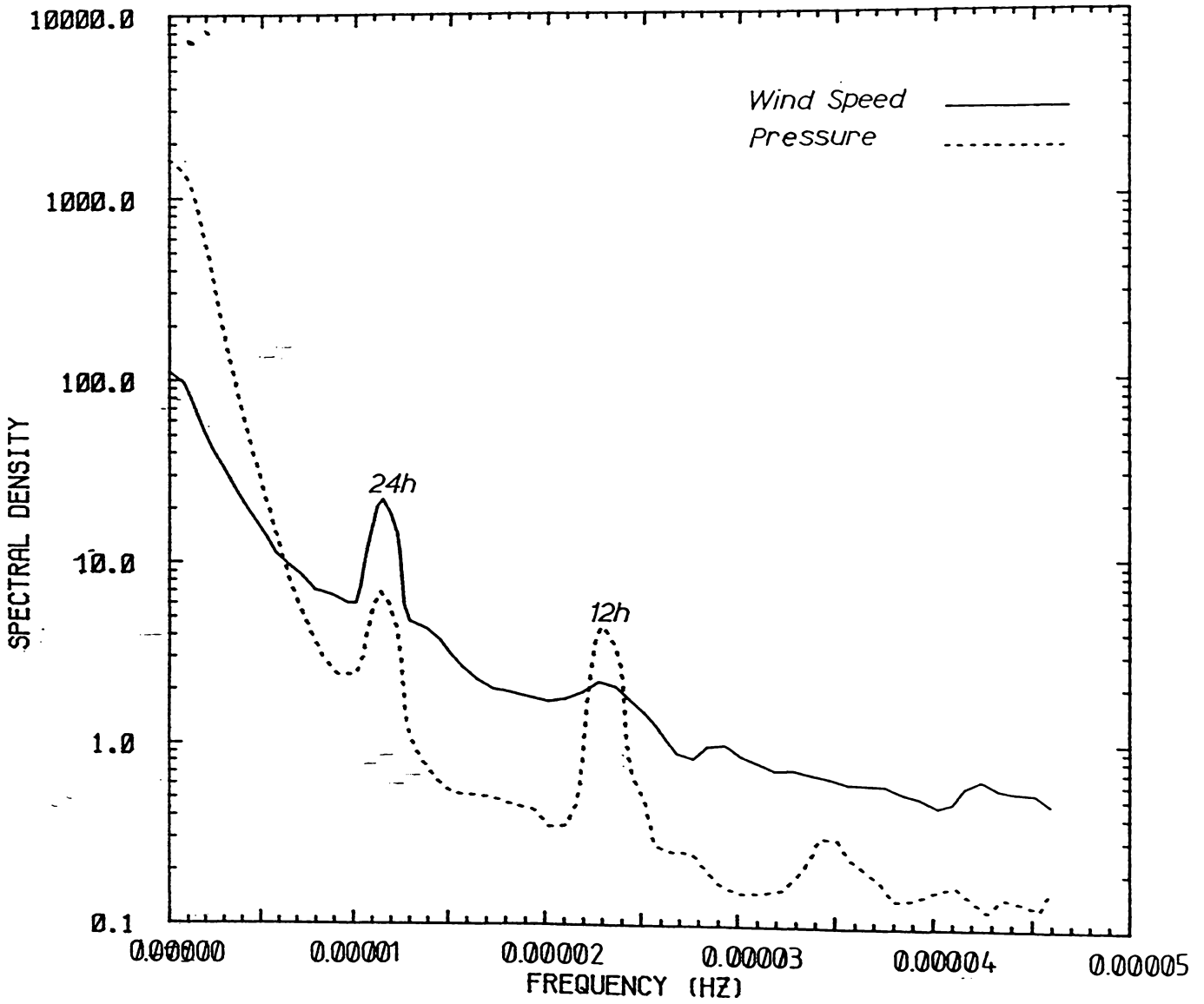

Figure 4.8 - Pressure spectrum and the 3h average wind speed spectrum, based on the BOPHB barograph and Mt Drury records respectively, for the period 10/4/84-1/4/85. Bandwidth = 0.0109Hz.

4.4 - Summary

The wind climate of Pilot Bay, based on observations made by this study, is dominated by a diurnal sea breeze cycle resulting in a

relatively high average wind speed compared to inland regions. The prevailing wind directions were determined by the onshore/offshore sea breezes. Despite the high average wind speed, very few strong wind events occurred during the study period. The strongest winds are expected from the southwest in association with tropical storms or disturbed south to southwest airflows.

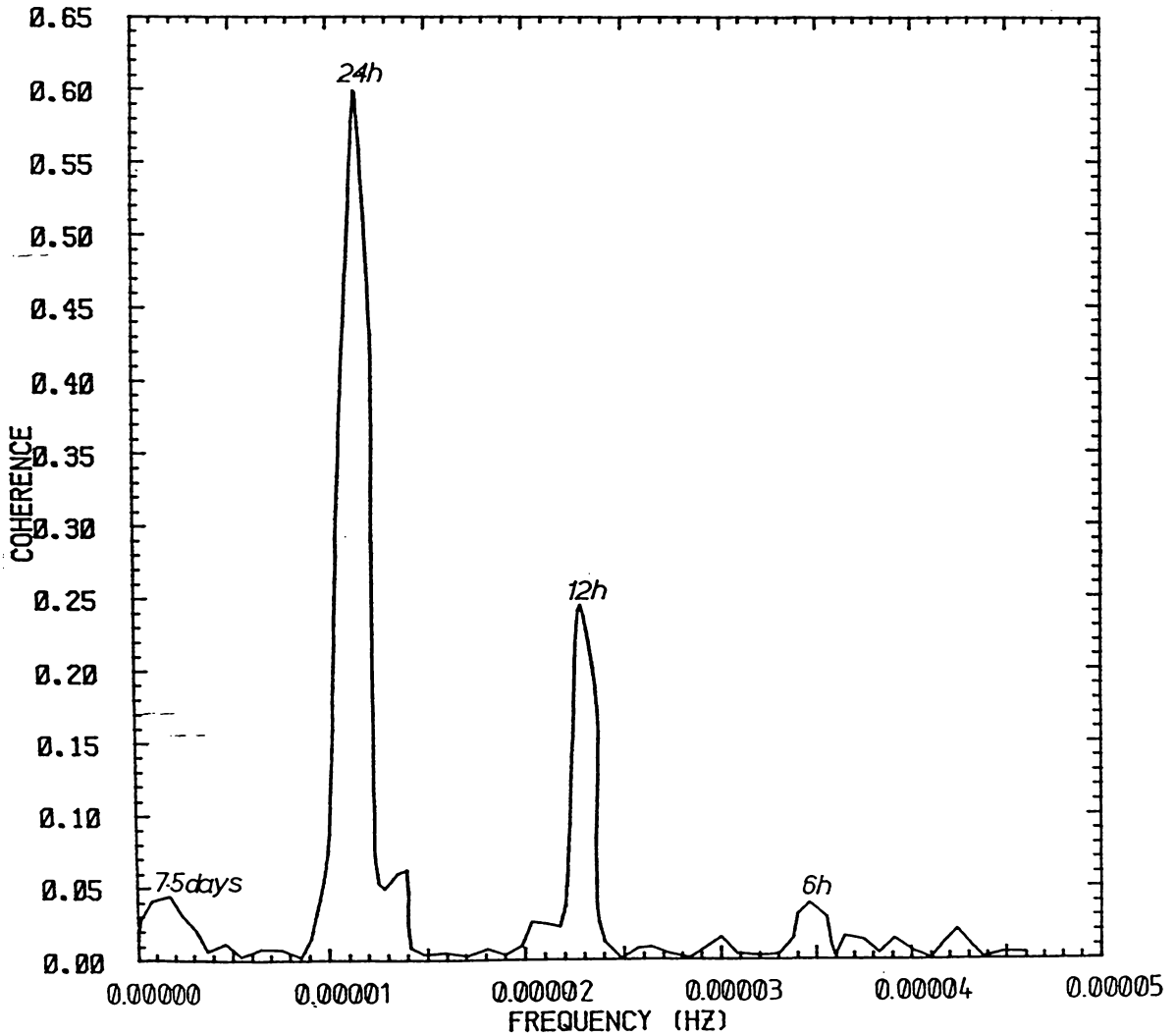

Figure 4.9 - Coherence between pressure and 3h average wind speed at Mt Drury. Bandwidth = 0.0109Hz.

The wind and pressure measurements made during the study period were not significantly different from climatic conditions prior to 1983. Therefore the study results can be considered as typical of the climate for Tauranga Harbour.

The Tug Berth anemometer provided a good record of the 10m wind speed (required for wave prediction) although the site was affected by sheltering from the east to southeast. The Tug Berth wind speed can be predicted from the 30m wind speed at the Mt Drury recorder, using separate regression equations corresponding to 8 groups of wind direction as determined by the Mt Drury recorder.

The wind speed spectrum has major peaks at periods of 24h and 12h. The 24h cycle is associated with sea breezes. The pressure spectrum also has major peaks at periods of approximately 24h and 12h associated with atmospheric tides. There is a reasonable coherence between the wind speed and pressure spectra at the major peaks. Both spectra have a minor peak at about 7.5 days. The origin of this latter cycle is not known.

Chapter 5 - Short Period Waves in Pilot Bay

This chapter reviews the literature concerning the generation of waves within estuaries, and considers the suitability of various predictive schemes for forecasting local wave conditions within Pilot Bay.

The existing wave climate is defined in terms of standard wave statistics and an average spectral shape, which is compared to several existing spectra used to predict wind generated waves.

5.1 - Potential sources of waves within Pilot Bay

The tidally-induced sediment transport flux within Pilot Bay is small, yet significant erosion has occurred within the nearshore and littoral regions of the bay. It is evident that, due to the ebb dominance of the tidal currents, the observed patterns of erosion could be explained by the tidal currents, if an additional source of energy for entraining sediment could be found. The most probable sources of non-tidal energy are wave-induced currents and turbulence.

The wave climate of an estuary represents a combination of wave fields from one or more sources. Seymour (1977b) identifies four major sources:

1) wakes of vessels;
2) seiches;
3) leakage of wave energy from the open ocean through the estuary entrance; and
4) locally generated wind waves.

The relative importance of these four main factors varies from estuary to estuary. For Pilot Bay all four sources are potentially present.

Obviously, due to its proximity to the Port of Tauranga, ship and boat wakes will contribute to the overall wave climate. Heath (1985) records a series of seiches with periods of 2, 1.1, and 0.3h which were excited in response to the 1960 Chilean tsunami. Hence seiches generated by tsunamis and storms are a probable component of the Pilot Bay wave climate, and these will be considered further in Chapter 6.

Refraction analysis on the basis of bathymetry alone (de Lange, 1984) indicated that the Tauranga Harbour entrance acts as a barrier to ocean wave energy due to its narrowness, depth, and the orientation of the Mt Maunganui tombolo and Matakana Island. However, that analysis ignored

both diffraction and the effects of tidal currents.

Diffraction will cause energy to migrate into the shadow zone behind Mt Maunganui. Southgate (1985) identifies two types of diffraction, internal diffraction in the vicinity of ray caustics and ray crossings as determined by refraction, and external diffraction where a surface obstacle produces a discontinuity in wave amplitude. Internal diffraction is difficult to predict since it requires the complete solution of wave refraction first.

Southgate (1985) discusses several techniques for solving external diffraction and concludes that ray plotting techniques offer the best approach. These techniques are restricted to very simple bathymetric configurations and do not consider diffraction effects in a general manner. Further, the analyses do not consider current effects. The Pilot Bay situation involves both complex bathymetry and currents.

In terms of tidal current interaction with ocean wave energy propagating through the entrance, there are two basic situations; an opposing current during the ebb tide, and a following current during the flood tide. A flood flow would tend to carry waves into the harbour, although the wavelength of the waves will increase and the spectral density decrease in the process (Gonzalez, 1984).

For a wave propagating on an opposing current, a velocity >0.25C (C = phase velocity) will cause the wave to break and dissipate (Peregrine and Jonsson, 1983). Ebb currents measured in the Tauranga Harbour Entrance by the THS achieved peak velocities close to $2ms^{-1}$. These could dissipate waves with a period less than 5s, but longer period waves would be transmitted with some energy loss and possibly a frequency shift.

Gonzalez (1984) reports a case study of the Columbia River Entrance, which is shallower and has slightly higher ebb velocities than Tauranga, and notes that significant wave energy is transmitted through the entrance, especially during flood tide, but also during ebb. Low amplitude swell waves were also observed propagating over Centre Bank in aerial photographs taken during the THS (Healy, 1985).

Once inside the harbour the wave energy approaching Pilot Bay would be affected by tidal currents in Cutter Channel and Pilot Bay. These currents filter the wave spectra by dissipating or reflecting some components and transmitting other components with some attenuation or

gain (Peregrine and Jonsson, 1983). It appears probable that ocean wave energy may be transmitted into Pilot Bay by diffraction and current induced processes.

Waves in oceans exhibit a wide range of frequencies and are created by a number of different processes (Fig. 5.1). Within an oceanic wave spectrum, most of the energy is associated with wind-generated waves which have a frequency greater than about 0.005Hz. Therefore a significant component of the wave energy in Pilot Bay may be due to locally generated wind waves.

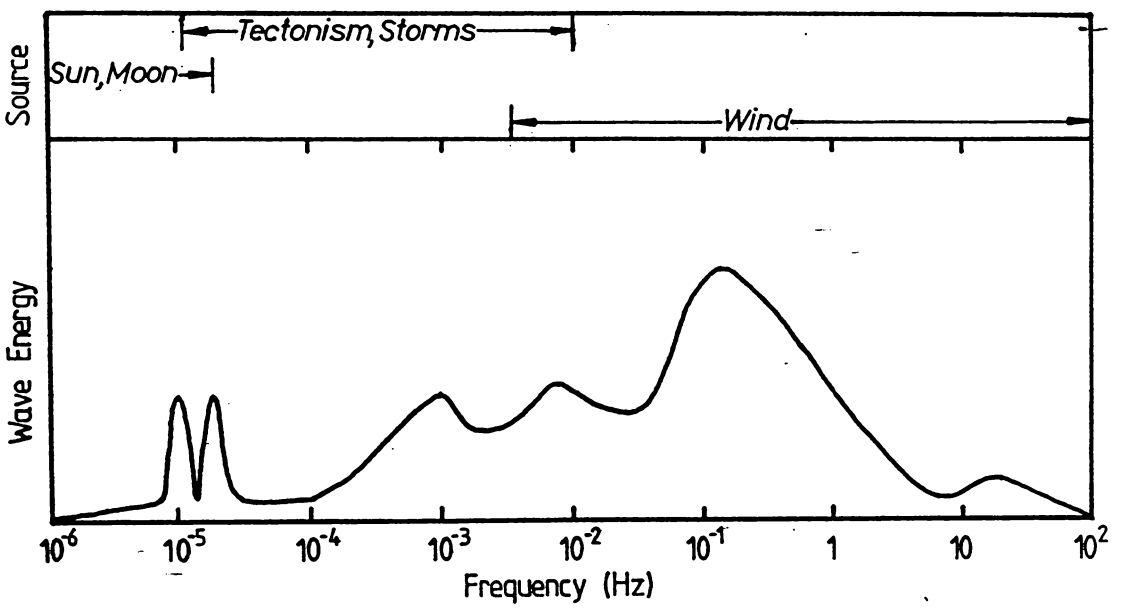

Figure 5.1 - Classification of wave types in terms of frequency and the relative distribution of wave energy across the available spectrum for a typical oceanic wave field. Also included are the principle sources of waves for each frequency. After Thurman (1985).

5.2 - Wave generation under limiting conditions

The process of wave generation by wind is essentially due to the transferal of wind energy to the water surface, and the mechanisms involved are reviewed in Appendix 1. Wave generation in a confined estuary is a more complex problem than wave generation in deep water due to factors which restrict the development of a wave field (Komar, 1976;

Knowles, 1982; Peregrine and Jonsson, 1983; Hughes, 1984), including:

a) wind velocity;

b) duration, or the length of time a given wind velocity persists;

c) fetch, the length of water over which the wind can blow;

d) water depth; and

e) currents.

The wind velocity determines the energy available for wave generation, with the magnitude of the generated waves being proportional to wind speed (Komar, 1976). There is a threshold wind velocity below which transfer of atmospheric energy to waves ceases and waves are not generated (Appendix 1). This threshold may be controlled by the potential phase velocities of the fluid at the sea/air interface (LeBlond and Mysak, 1978), which are determined by water depth. In addition, an upper limit to the wave field generated by winds may exist. A spectrum attaining this upper bound is said to be saturated and this condition is referred to as a fully developed sea (Komar, 1976).

Phillips (1958) quantified this concept for wind-generated gravity waves in deep water in terms of an upper bound on the spectral density, or distribution of wave energy, given by:

$$S(f) = \alpha g^2 f^{-5} (2\pi)^{-4} \qquad \ldots 5.1$$

where f = frequency,

g = gravitational acceleration,

$S(f)$ = energy density distribution,

and where α was assumed to be a universal constant with a value of approximately 0.008. The region of the spectrum defined by this upper bound is called the equilibrium range and occurs on the high frequency side of the spectral peak, or tail region (Fig. 5.2). Any spectra conforming to this upper bound will have a tail region proportional to f^{-5}. Most observations of deep water wave spectra correspond to tail region slopes between f^{-4} and f^{-5} (Bouws *et al*, 1985).

A saturated spectrum is achieved when any increase in spectral density is immediately compensated for by wave breaking. Therefore the equilibrium range is controlled by the process governing wave breaking. It was considered that some single variable, such as the local vertical

acceleration, would determine the onset of wave breaking. The variable involved was believed to be independent of wind stress or speed, so that the equilibrium range would also be independent of the wind speed. However, recent work has shown that wave breaking is not controlled by one variable and, more importantly, it is not independent of wind speed (Phillips, 1985).

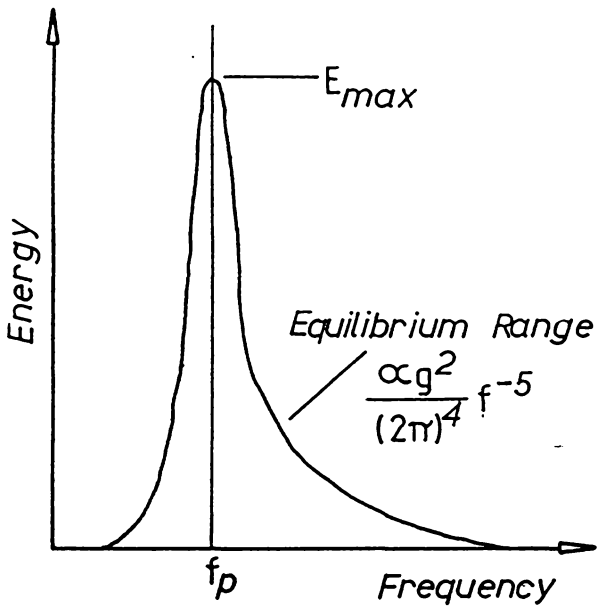

Figure 5.2 - Definition diagram for terms used in relation to a wave spectrum.

This implies that the equilibrium range is not a fixed upper limit independent of wind speed. Instead, as wave spectra develop with increasing fetch, duration and wind speed, the limits of the equilibrium range also increase. Therefore a fully developed sea cannot be achieved, since the equilibrium range will continue to grow, although at a very slow rate, for as long as generating conditions are maintained. However, despite predicting a fixed upper bound, the equilibrium range defined by Equation 5.1 is still a good approximation to the form of the equilibrium range and it is adequate for defining spectral shape.

The growth of waves in shallow water is not well understood (Bouws *et al*, 1985). As a result of the interaction of processes such as wave shoaling and refraction, and linear and non-linear bottom dissipation, the wave spectrum produced tends to have a higher peak frequency, f_p, and lower total energy than deep water spectra formed

under the same atmospheric conditions (Knowles, 1982).

As a wave shoals the wave becomes increasingly non-linear and wave/wave interactions become more important (Thornton, 1979). In response to these interactions, energy is transferred from low to high frequencies, the reverse situation to wave generation (Thornton, 1979; Knowles, 1982). The processes by which this transferal occurs, and their relative importance, are unknown (Knowles, 1982; Bouws and Komen, 1983; Bouws *et al*, 1985).

The processes which affect shoaling waves also restrict wave growth in shallow water, resulting in a change in the slope of the equilibrium range for the linear component of the spectra (Bouws *et al*, 1985). Kitaigorodskii *et al* (1975) derived an equilibrium range for shallow water conditions by transforming the upper bound as defined in Equation 5.1 into wave number space to produce a suitable similarity form. This gives the following equation (Hughes, 1984):

$$F(k) = \beta k^{-3} \qquad \ldots 5.2$$

where k = wave number ($2\pi/L$),
$F(k)$ = energy density in wave number space,
β = constant,
and L = wave length.

Following comparisons with field observations Kitaigorodskii *et al* (1975) concluded that this equation was a valid scaling relationship for both deep and shallow water equilibrium ranges. This finding was confirmed by other studies (Knowles, 1982; Vincent, 1982; Bouws *et al*, 1985). From Equation 5.2, and the shallow water limit of the linear wave dispersion relationship, it can be shown that the tail region of a saturated or nearly saturated spectrum transforms from f^{-5} to f^{-3} between deep and shallow water (Hughes, 1984). This relationship holds for the linear components of the spectrum only and does not consider the non-linear factors which become increasingly important as depth decreases (Vincent, 1985).

Vincent (1985) considers data for waves propagating from 36m to 2.7m depth and shows a progressive change from f^{-5} to approximately f^{-3} over a narrow band of the spectrum between f_p and $2f_p$. Knowles (1982)

discusses observations of wave spectra obtained in a finite depth, restricted fetch estuary and concludes that the data tend to approximate f^{-3} rather than f^{-5}. Sawaragi and Iwata in 1980 presented results for very shallow water which demonstrated a f^{-2} dependence for the tail region (Vincent, 1985). Thornton (1979) suggests that in the surf zone the equilibrium range has a $f^{-7/3}$ dependence due to a non-linear cross-spectral transfer of wave energy towards higher frequencies. Consequently the shallow-water spectrum has a different slope for the spectrum tail compared to a comparable deep-water spectrum, but the actual slope expected does not appear to be well predicted by theory.

Waves interact with currents within a water body (LeBlond and Mysak, 1978), resulting in a doppler shift of the wave spectrum which manifests itself as changes in wave height, wavelength and phase velocity (Kato and Tsuruya, 1978; Burrows and Hedges, 1985). For example, a current flowing in the direction of wave advance decreases wave height and increases wavelength, whereas an opposing current has the opposite effect, leading to a steeper, possibly breaking, wave. Currents can lead to marked refraction for propagating waves, independent of bathymetric changes (Peregrine and Jonsson, 1983). Peregrine *et al* (1983) have produced an annotated bibliography which summarises wave-current interaction, primarily for propagating waves.

There are three main effects that currents have on wave generation by winds (Kato and Tsuruya, 1978; Peregrine and Jonsson, 1983; Burrows and Hedges, 1985):

1) The relative velocity between air and water is either increased or decreased. Hence an opposing current produces a more energetic wave field due to enhanced wind velocities. This effect has been demonstrated by satellite imagery of the Gulf Stream (Peregrine and Jonsson, 1983);
2) The rate of wave energy propagation is altered producing an effective fetch for any given fetch which varies with current velocity. For an opposing current the rate of energy propagation is reduced, resulting in a longer time interval during which waves can be generated. This longer duration can be expressed in terms of an effective fetch. Kato and Tsuruya (1978) have determined effective fetches for a range of current velocities in laboratory flumes, but these are difficult to apply outside

flumes; and

3) The upper bound on the spectral density in the equilibrium range changes in the presence of a current, resulting in enhanced wave breaking for opposing currents.

In general, it can be concluded that an opposing current will produce larger, steeper waves for any given wind speed.

The expected changes to a wave spectrum, due to the actions of the factors discussed above, are summarised in Figure 5.3. These changes are qualitative only, since they are difficult to quantify, and give an indication of the expected shifts of f_p and the equilibrium range.

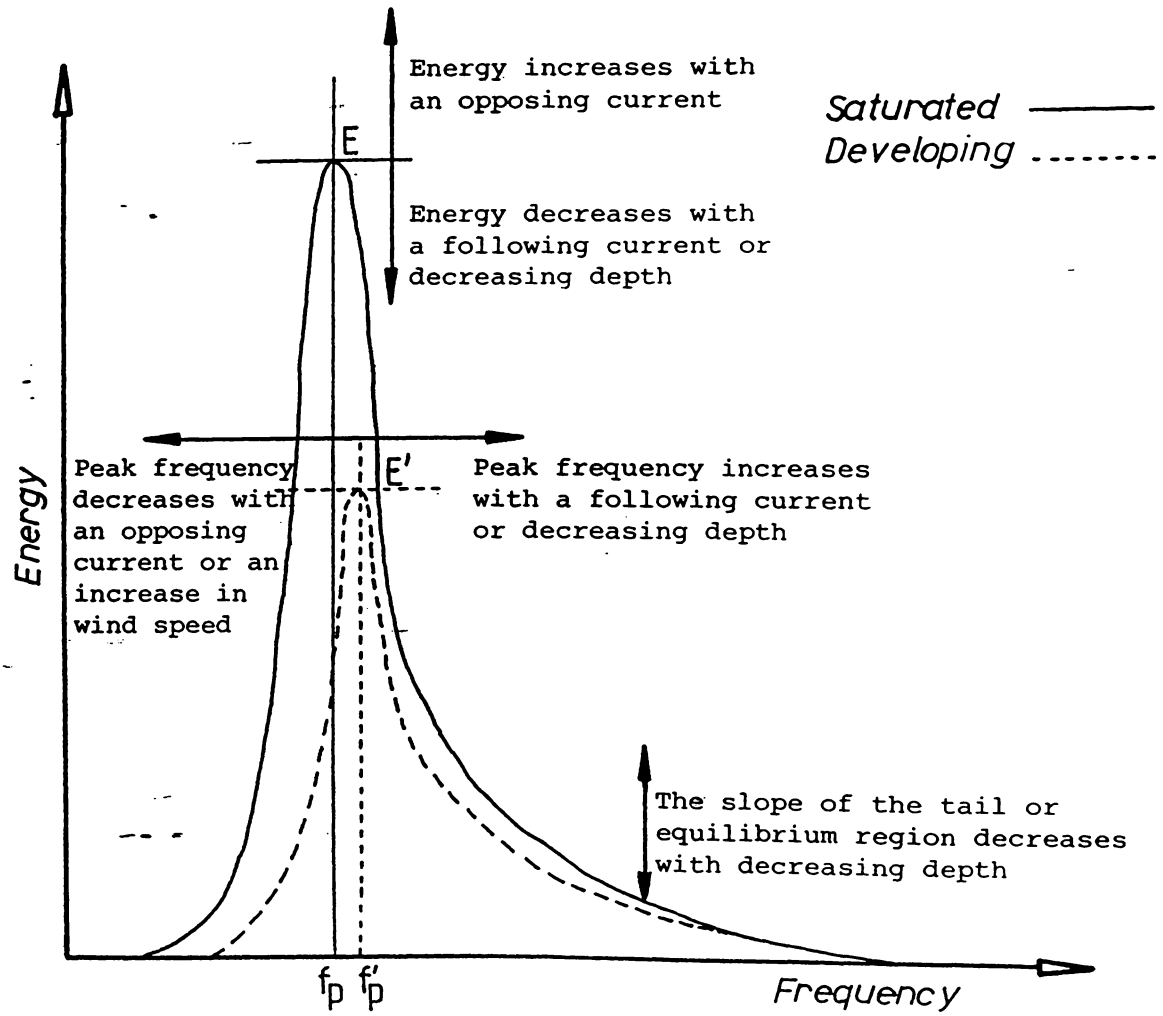

Figure 5.3 - Changes induced in a wave spectrum by limiting conditions.

5.3 - Wave prediction in estuaries

Local wind waves within Pilot Bay will be generated under restricted conditions. There is currently no ideal wave prediction scheme for these conditions. Therefore, to determine a suitable predictive technique for locally generated waves in Pilot Bay, it is necessary to compare various models against measured spectra.

Wave prediction models which may be applied to Pilot Bay and Tauranga Harbour have been reviewed in Appendix 2. Since none of the predictive schemes considered is directly applicable to estuarine conditions, it is necessary to consider those factors which may alter or affect wave prediction within estuaries.

A saturated spectrum is unlikely within estuaries, either due to the short duration of sufficiently steady wind, or due to a restricted fetch (Seymour, 1977b; Resio and Vincent, 1982). Hence the spectrum produced would be either duration limited, fetch limited, or both.

Estuaries represent shallow water conditions for most wave periods so that depth limited spectra are necessary. In addition, estuaries have a complex current regime which cannot be considered to be uniform in either space or time (Bowden, 1983). These last two factors may be more significant than either fetch or duration, although more work is required before their influence can be quantified.

5.3.1 - Fetch considerations

There are two ways in which a fetch can be construed as limited. Firstly, there is a limit imposed by the length of the fetch. This concept has been included in most numerical schemes from the Sverdrup-Munk-Bretschneider (SMB) method through to JONSWAP (Appendix 2). The second limit is imposed by restrictions in fetch width, since it is known that energy is also transferred by dispersion (i.e. tangentially to the wind direction). This concept has been investigated by Saville (1954) and Seymour (1977a).

The initial approach used was the effective fetch method proposed by Saville (1954) where an effective fetch is defined by:

$$F_{eff} = \frac{\Sigma x_i \cos\theta_i}{\Sigma \cos\theta_i} \qquad \ldots 5.3$$

where F = fetch,

x_i = radial distance to shoreline,

and θ_i = angle between wind axis and radii.

The effective fetch can be used to replace the actual fetch in models such as the SMB model (Appendix 2).

There are two assumptions inherent to Saville's effective fetch (Seymour, 1977a) which need further consideration. First, the wave energy is assumed to be distributed as the cosine of the angle relative to the wind axis, and the energy input ceases at some unspecified angle less than 90°, normally taken as 45°. However, more recent work suggests a $\cos^2$ dependence for the energy distribution (Seymour, 1977a; Resio and Vincent, 1982).

The second assumption made was that the wave field parameters are proportional to fetch length, but none of the predictive models considered use a linear assumption for the relationship between fetch and wave parameters. It is apparent that due to difficulties with the assumptions made by the Saville approach, this method may be invalid.

Seymour (1977a) derived an improved method based on the Pierson *et al* (1955) energy distribution function:

$$E_t = 2\int_0^{\pi/2} e_o \cos^2\theta d\theta \qquad \ldots 5.4$$

where e_o = energy contribution per radian.

By rearranging the terms and combining the resulting energy term with a one dimensional spectrum, Seymour (1977a) derived:

$$S_i(f,\theta_i,F_i) = 0.6336\Delta\theta S(f,F_i)\cos^2\theta_i \qquad \ldots 5.5$$

where $S(f,F_i)$ = one dimensional spectra,

and $\Delta\theta$ = angular width of segment.

This scheme indicates that the total energy spectrum is arrived at by summing scaled spectra for individual fetch components, so that each is

treated as a discrete entity. If wave growth is primarily due to wave/wave interaction (Hasselmann *et al*, 1976; Resio and Vincent, 1982) then this method is of dubious validity since the spectral components will not be independent.

Both Seymour's method and Saville's method tend to under-predict wave parameters for restricted fetches such as estuaries and lakes, although Seymour (1977a) claimed good agreement with test observations from several estuaries in Canada and the United States. Resio and Vincent (1982) state that the whole concept of effective fetch requires re-evaluation in terms of recent theory regarding wave growth.

5.3.2 - Duration considerations

There appears to be less documented work concerning the effect of duration on wave spectra (Resio and Vincent, 1982), although it is frequently stated that duration is very significant (Liu, 1971; Komar, 1976). In most cases the duration limited spectra are derived by assuming a constant wind speed and deriving a corresponding fetch (Carter, 1982). For some models, such as the SMB method, this is straightforward, but for others, such as the JONSWAP spectrum, there is no clear relationship between duration and fetch (Carter, 1982).

Liu (1971) suggests that duration limited spectral equations can be derived by applying the dynamic equivalence relation proposed by Phillips (1958), given by:

$$F = DCn \qquad \ldots 5.6$$

where D = duration,
and n = factor relating C to the group velocity.

The important feature here is that there is a linear relationship between fetch and duration. All the predictive models considered follow this relationship, so that spectral growth with time is very similar to growth with distance (Resio and Vincent, 1982). Recent studies (Resio and Vincent, 1982; Bouws and Komen, 1983) indicate that the wave/wave interaction as applied to fetch limited conditions may not be completely valid for other situations such as duration limited. It can be

concluded that the effect of duration on wave spectra development needs further investigation.

5.4 - Data analysis of measured short period waves

Wave data were obtained for Pilot Bay on several occasions during the period 1984-1987 (Table 5.1). A number of different wave recording systems was developed and deployed with varying success (Appendix 3). All the sensors used by the various systems were located in the vicinity of the BOPHB tug berths (Fig. 5.4), where additional data from tide gauges and the Woelfle anemometer were also being collected. The following discussion will consider the wave data collected from 12/2/85-26/3/85, and 15/10/86-31/12/86. Earlier data collection periods provided some useful data, but most records were disrupted by dropouts and a wide variety of component failures.

Table 5.1 - Deployment data for the wave recording systems deployed in the vicinity of Pilot Bay.

System	Deployment Period	Sampling Rate	Data Points	Sampling Interval	Number of Observations
SUBTLE	13/4/84-6/7/84	8Hz	2048	6h	267[a]
SUBTLE	27/6/84-14/8/84	2Hz	1024	6h	11[b]
SUBTLE	8/10/84-3/12/84	4Hz	1024	6h	165[a]
Apple 1	12/2/85-26/3/85	4.6Hz	2048	1h	509
Apple 2	15/10/86-4/11/86	4.3Hz	4096	1h	246
Apple 3	4/11/86-31/12/86	4Hz	256	15min	3644

[a]Data affected by numerous dropouts
[b]No time control due to failure of the timing unit

The wave time series records collected during the first sampling period considered (12/2/85-26/3/85) were pre-analysed using an Apple II+ computer. This analysis consisted of plotting the raw data to determine if anything unusual had occurred and a basic statistical analysis. The statistics determined included the mean, standard deviation, and maxima and minima for each record. Any unsuitable data records were rejected at this stage. Time series records obtained during 15/10/86-4/11/86 also underwent a zero up-crossing analysis as illustrated by Bowden (1983).

Suitable time series data records were subsequently transferred from

the Apple disks to the Vax 11/780. After error checking, cross-spectral analysis was performed between the wave probe and tide gauge data using the standard BMDP spectral analysis program P1T (Dixon *et al*, 1981). During this analysis the data were detrended to remove tidal components from the records. The parameters derived from the cross-spectral analysis were used to check the relative performance of the two transducers and to provide directional data for the observed waves. Further, the gain between the two transducers determined for the frequency band centred on 0.2857Hz was used to correct the wave probe data for the signal amplification produced by the transmitter (Appendix 3).

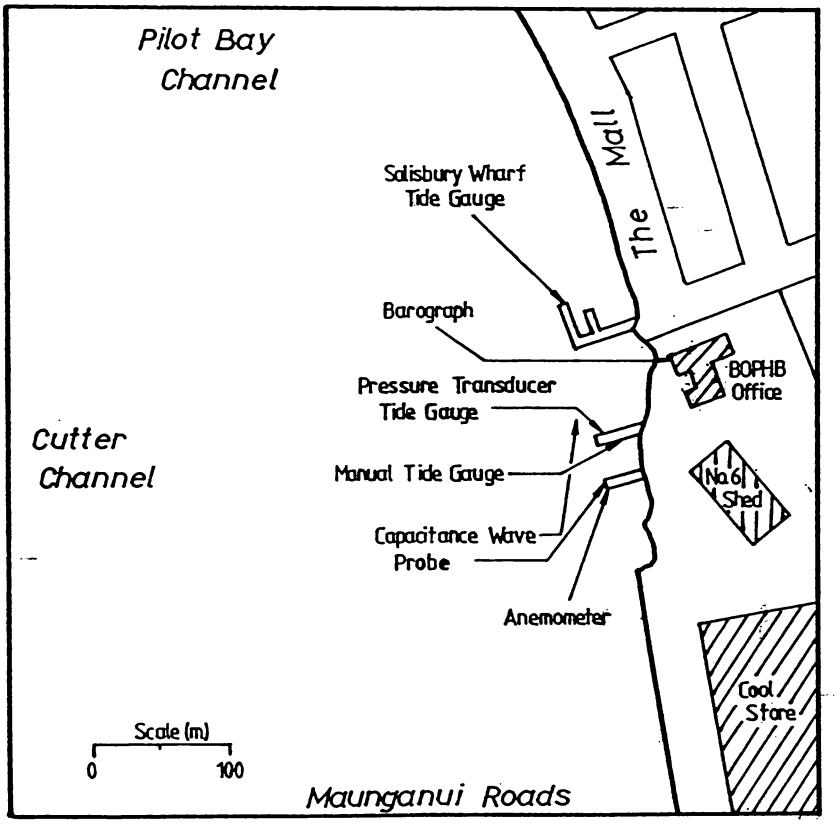

Figure 5.4 - Map of Pilot Bay showing location of wave sensors in relation to the Woelfle Anemometer and tide gauges. Appendix 3 gives a full description of the wave recorder systems employed.

Having adjusted the wave probe data, two sets of analyses were applied to all records transferred to the Vax. First, the data obtained by the wave recorder were analysed in terms of zero up-crossing waves (Bowden, 1983) and the parameters defined in Table 5.2 were determined.

They will be presented in accordance with the formats proposed by Draper (1966), and these statistics can be used to characterise the wave field (Baird and Thompson, 1977). In addition, the ratio of various height and period parameters to the significant values were determined to allow comparison with other published values (Komar, 1976; Lee and Black, 1978).

Table 5.2 - Summary statistics for wave data (Baird and Thompson, 1977; Bowden, 1983; Thompson and Vincent, 1985).

Statistic	Name	Definition
H_{rms}	Root mean square wave height	Square root of the average squared height of all waves
H_m	Mean wave height	Average height
H_s	Significant wave height	Average height of the highest 33%
H_σ	Significant wave height	4σ, σ^2 = variance of elevations
H_{10}		Average height of the highest 10%
H_{max}	Maximum wave height	Highest wave
T_z	Mean period	Duration / (number of waves)
T_c	Crest period	Duration / (number of crests)
T_s	Significant period	Average period of the longest 33%
T_{10}		Average period of the longest 10%
T_{max}	Maximum period	Longest period

Two parameter systems of wave description, such as the joint distribution of H_s and T_z, have several limitations (Baird and Thompson, 1977). The use of single parameters, which assume normal or Gaussian population distributions for wave height and wave period, does not adequately account for the actual distribution of waves within any given record. Further, most non-spectral parameterisations do not account for the presence of more than one distinct wave system (Baird and Thompson, 1977). This is true of parameters derived here from the zero up-crossing waves (Bowden, 1983).

Lee and Black (1978) compared measured wave height distributions against Rayleigh, truncated Rayleigh and Weibull distributions, and also measured wave period distributions against a symmetrical distribution proposed by Longuet-Higgins (1975) and the Weibull distribution. They found that the Weibull distribution produced the best fit for both wave height and wave period distributions in shallow water over a coral reef.

The Weibull probability density function can be defined as:

$$F(x) = \frac{\beta x^{\beta-1}}{\alpha} e^{-(x^{\beta}/\alpha)} \qquad \ldots 5.7$$

where α = is a location parameter similar to a mean,

β = is a shape parameter defining the peakedness, and

where x can be wave height or wave period (Johnson and Kotz, 1970; Lee and Black, 1978). The Rayleigh distribution applied to deep water waves (Komar, 1976) is a special case of the Weibull distribution, where $\beta=2$ and $\alpha=H_{rms}^2$. The Weibull distribution was fitted to the zero up-crossing wave heights and wave periods, using the curve fitting technique discussed by Black (1983).

The Weibull distribution parameters fully describe the distribution of waves within the record, providing a four parameter description of the wave field (α_H, β_H, α_T and β_T). If all four are known then the distribution of the original data can be recreated from the probability function for the Weibull distribution. Lee and Black (1978) present equations which allow several wave parameters to be predicted, given the total number of waves (N). These equations are given below (Equations 5.8-5.11):

$$H_m = 0.325(\ln(N)\alpha)^{1/\beta} \qquad \ldots 5.8$$

$$H_s = 0.395[(\ln(N)\alpha)^{1/\beta}+(\ln(3)\alpha)^{1/\beta}] \qquad \ldots 5.9$$

$$H_{10} = 0.435[(\ln(N)\alpha)^{1/\beta}+(\ln(10)\alpha)^{1/\beta}] \qquad \ldots 5.10$$

$$T_s = 0.385[(\ln(N)\alpha)^{1/\beta}+(\ln(3)\alpha)^{1/\beta}] \qquad \ldots 5.11$$

The second group of analyses considered the spectral analysis of the wave probe time series data. Snapshots and scatter plots of the data were produced to check for any unusual behaviour (Dixon *et al*, 1981). Spectral analysis was undertaken, after detrending to remove tidal components, at bandwidths of 0.0112 and 0.1808Hz (8 and 161df). The 0.0112Hz bandwidth spectral estimates were used to determine various spectral parameters as defined in Table 5.3.

Table 5.3 - Spectral parameters determined from the spectral analysis of wave time series data.

Parameter	Name	Definition
m_n	nth spectral moment	(n=0 gives total energy)
H_{m0}	Spectral wave height	$4(m_0)^{½}$ ($=H_\sigma$ in deep water)
H_e	Monochromatic wave height	$2^{3/2}(m_0)^{½}$
H_{max}	Maximum wave height	$K.H_{m0}$ (K=function of T_z)
f_p	Peak frequency	Frequency at the spectral peak
f_m	Mean frequency	m_1/m_0
$S(f_p)$	Peak energy density	Energy density at the peak
T_p	Peak period	$1/f_p$
T_z	Mean period	$(m_0/m_2)^{½}$
T_c	Crest period	$(m_2/m_4)^{½}$
Q_p	Godas peakedness parameter	$(2/m_0^2)\int fS^2(f)df$
ϵ_s	Spectral width	$(1-m_2^2/(m_0m_4))^{½}$

It also was possible to determine the direction of wave approach for the low frequency waves, using the cross-spectral analyses preformed to derive the gain functions. Given the phase lag between the wave probe and the tide gauge sensors, and the values for the constants defined in Figure 5.5, the direction of wave approach is given by (Walton and Dean, 1982):

$$\theta = \beta \pm \cos^{-1}(\phi/(kl)) \qquad \ldots 5.12$$

where ϕ = phase lag.

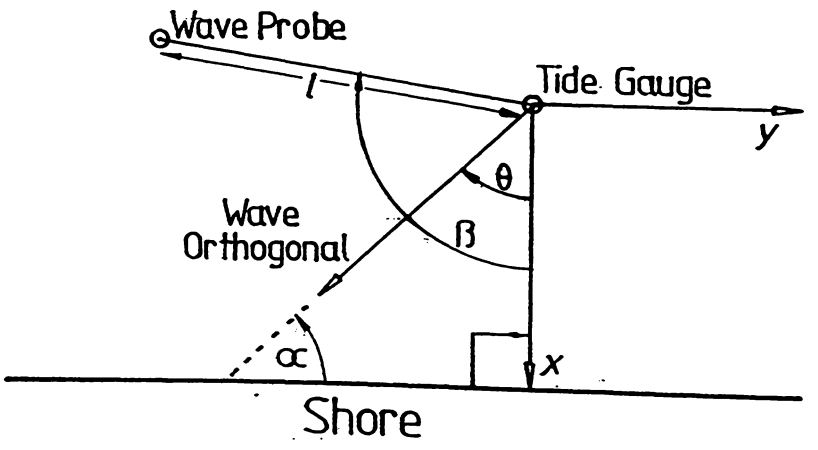

Figure 5.5 - Definition diagram of coordinate system and variables used to determine direction of wave propagation from cross-spectral analysis results. For the wave recorders employed at Pilot Bay, l=40.80m and β=70.25°, and the actual direction of wave advance is given by 357.5°-θ.

Finally, by assuming that the mean squared variance of a sinusoidal waveform is equal to half the wave amplitude squared, it is possible to convert the spectral density for each frequency band to an equivalent component wave height. The component wave height is given by:

$$H_c = (8S(f)\Delta f)^{\frac{1}{2}} \qquad \ldots 5.13$$

where Δf=frequency interval.

This enables presentation of frequency energy spectra as wave height versus period histograms if desired. Summation of the individual H_c values present does not give a measure of the total wave height expected. However, these values may give a clearer picture of the wave trains which may be contributing to the observed wave field.

5.5 - Results

5.5.1 - Zero up-crossing wave parameters

The univariate zero up-crossing wave statistics for all the available wave data recorded by the wave probe are summarised in Table 5.4. These data show that the average wave heights in Pilot Bay are less than those reported by Davies-Colley (1976) on the basis of visual estimates (H_s=0.30m and H_{max}=0.60m). This can partly be attributed to the lack of extreme meteorological conditions during the sampling periods, and partly to a tendency to over-estimate wave height by visual techniques.

Table 5.4 - Summary of the univariate statistics for the wave probe zero up-crossing parameters. No mode is given if the data were polymodal.

	H_{rms}	H_m	H_s	H_σ	H_{10}	H_{max}	T_z	T_s	T_{10}	T_{max}
Observations	4003	4003	4003	3644	4003	4003	4003	359	359	359
Maximum	0.31	0.23	0.31	0.32	0.68	0.69	6.92	5.05	5.80	9.02
Minimum	0.01	0.01	0.02	0.03	0.02	0.03	1.03	1.44	1.68	2.88
Median	0.06	0.05	0.08	0.09	0.11	0.15	2.91	3.57	3.85	4.35
Mode	0.05	0.05	0.08	0.09	0.10	0.11	3.61	3.59		3.87
Mean	0.073	0.054	0.090	0.102	0.132	0.250	3.198	3.459	3.905	4.582
SD	0.041	0.025	0.038	0.042	0.075	0.171	1.115	0.555	0.456	0.860

The univariate statistics do not give as good an indication of the distribution of wave heights as the percentage exceedance for any given wave height (Fig. 5.6). If the temporal distribution of wave heights followed either Gaussian or Rayleigh distributions, the exceedances would appear as S-shaped curves. Although H_s and H_σ do follow such a trend, the remaining wave height parameters show increasingly marked deviations with increasing wave height. These deviations are not expected if the wave field is completely wind induced. Further, the correlation between H_{max} and wind speed was found to be low (r=0.13).

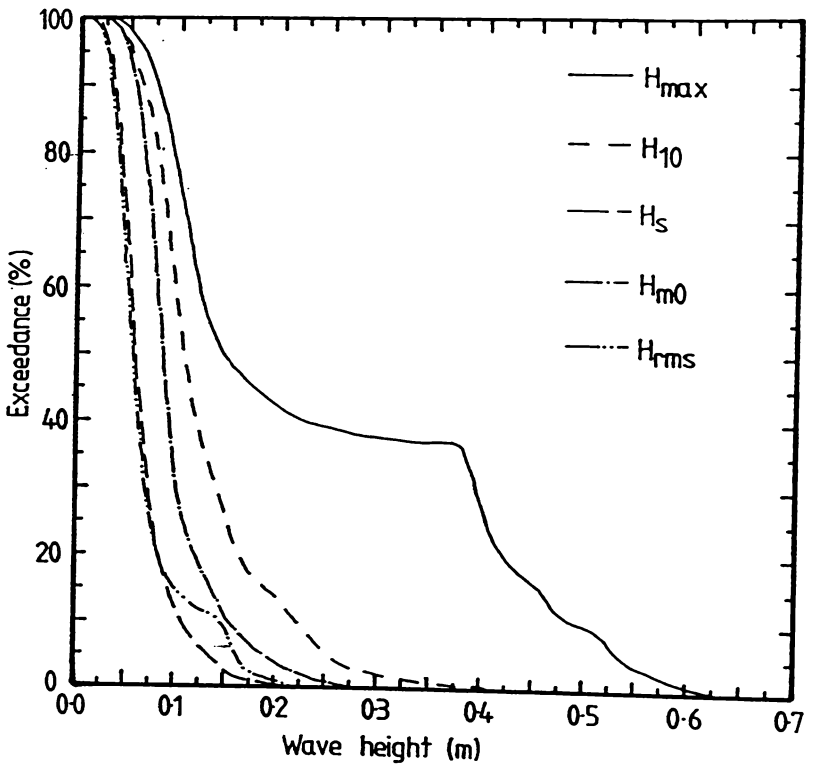

Figure 5.6 - Percentage exceedance for wave height parameters derived from wave probe data for the periods 13/2/85-26/3/85 and 15/10/86-31/12/86.

The wave data were sorted on the basis of the time at which each wave record was collected and the time of known shipping movements (i.e. tug, ferry, Pilot Launch, and large vessel movements) in the vicinity of the wave probe. By considering only those data associated with shipping movements, it was found that H_{max} ranged from 0.25-0.69m. This corresponds to the range of the major deviation in Figure 5.6. However, not all of the data within this region could be attributed to known

shipping movements. It is probable that most of the remaining data within this region may be associated with the transit of small vessels, such as fishing boats and pleasure craft. These movements were not recorded by the BOPHB, but could occur during the sampling periods.

It is clear from the data that vessel wakes significantly affect the observed wave field in Pilot Bay. The wakes tend to dominate the other waves present for short intervals as the vessel passes and the wake decays. Consequently vessel wakes may be expected to have the greatest impact on the extreme wave parameters such as H_{max}. As more averaging is involved in the derivation of the parameter, the influence of vessel wakes should diminish. H_{rms}, despite averaging all the data, is based on the squared deviations from still water level, and therefore is biased towards the largest deviations. The observed pattern of deviations from the expected curves is consistent with vessel wakes superimposed on a wind-induced wave field.

The distribution of zero up-crossing periods (T_z) is strongly positively skewed (Fig. 5.7). For a zero up-crossing analysis, at least two consecutive points are required to define a wave. Therefore, given the sampling frequency of 4Hz used for the majority of the observations included in the analysis, the zero up-crossing analysis cannot resolve periods less than 0.5s. This suggests that the steep rise for the short period region of the graph may be due to resolution limitations in the analysis. However, data collected at 8Hz did not reveal any periods below 1s, so the distribution of wave periods is inferred to be real.

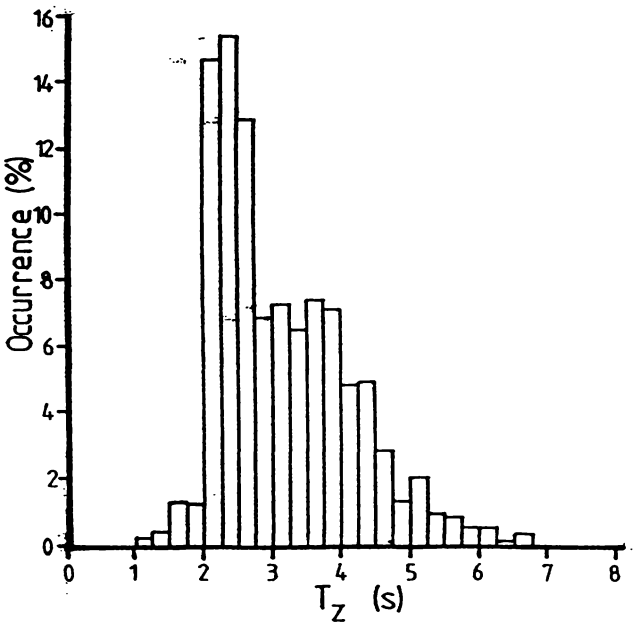

Figure 5.7 - Zero up-crossing period (T_z) percentage occurrence.

The period distribution displays a slight bimodality, with a major peak from 2.0-2.75s and a minor peak from 3.5-4.0s. Due to the change in class size from 0.01s to 0.25s, the modal period is different from that given in Table 5.4. Two populations of wave period may exist; one broad population centred between 2.25 and 2.50s and a narrow population centred between 3.50 and 3.75s. The second population may represent the influence of vessel wakes. However, T_z represents the average period over the duration of a wave record (Table 5.2) so will not be greatly affected by the short persistence of a vessel wake.

The joint H_s and T_z occurrence distribution is shown in Figure 5.8, along with curves of constant wave steepness. These curves were determined from the wave height using the Airy Theory general expression for wavelength, given by:

$$L = \frac{gT^2}{2\pi}\tanh\frac{2\pi h}{L} \qquad \ldots 5.14$$

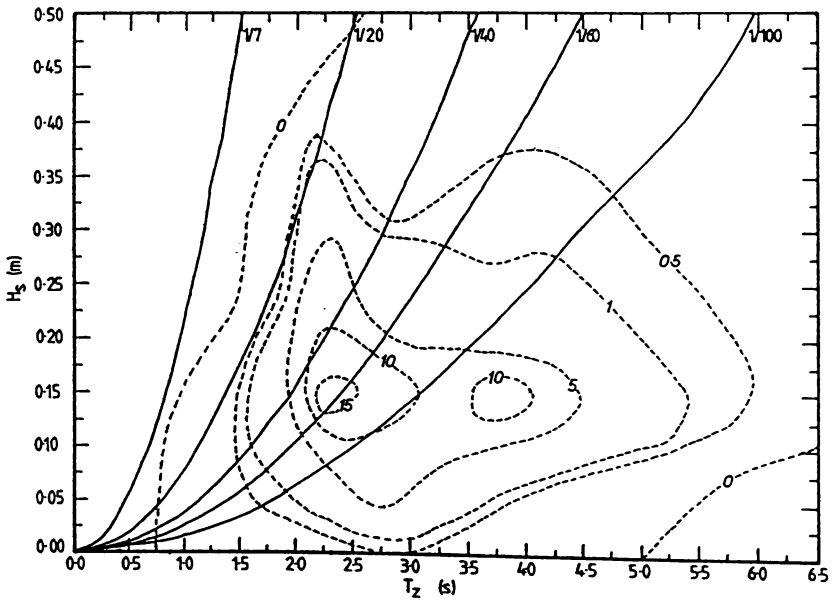

Figure 5.8 - Joint occurrence distribution of H_s and T_z. The values plotted are the percentage occurrences based on 4004 pairs of data. Curves represent constant wave steepness assuming a water depth of 11m, with 1/7 representing the limiting steepness of breaking waves.

No data exceed the limiting wave steepness of 1/7 corresponding to breaking waves (Komar, 1976), with virtually all the data confined to wave steepnesses less than 1/20. This is expected, especially since the data represent the average conditions, not individual waves. The only

breaking waves observed in the vicinity of the transducers during calibration were associated with vessel wakes. The joint distribution indicates a major cluster around H_s=0.05-0.10m, T_z=2.5-3.0s with a second cluster involving the same wave heights and T_z=4.0-4.5s. There does not appear to be any clustering associated with longer period and larger wave heights, as could be produced by vessel wakes. Therefore, the two populations indicated by the T_z distribution are not the result of vessel wakes.

The distribution of wave heights may be described by a Rayleigh distribution which allows the prediction of wave parameters if one parameter such as H_s is known (Komar, 1976). The average ratios between H_s and other wave height parameters are presented in Table 5.5, along with average values reported by various other studies. Two sets of wave probe data are presented; the first includes all data points available, and the second omits those data associated with known shipping movements. Comparing the wave probe data with the theoretical values for a Rayleigh Distribution (Longuet-Higgins, 1952), the influence of vessel wakes is apparent for most ratios and the deviations are consistent with those indicated in Figure 5.6.

Table 5.5 - Ratios between H_s and other wave height parameters.

Data source	H_m/H_s	H_{rms}/H_s	H_{10}/H_s	H_{max}/H_s
Longuet-Higgins (1952)[a]	0.64	0.71	1.27	1.53-1.85[b]
Wiegel (1949)			1.29	1.87
Putz (1952)	0.62		1.29	
Goodknight & Russell (1963)	0.60	0.69	1.25	1.57
Goda (1978)	0.62		1.28	1.66
Barthel (1982)	0.62			1.88
Black (1983)			1.30	1.56
Hastie (1985)	0.62	0.70	1.22	1.56
Wave probe[c]	0.60	0.80	1.45	2.81
Wave probe[d]	0.60	0.75	1.38	1.75

[a]Theoretical values predicted for a narrow spectrum wave field.
[b]This value varies with the wave period and the length of record.
[c]Total data set
[d]Omitting records affected by known shipping movements

Considering the second set of wave probe results, the ratios measured are in reasonable agreement with those of other workers. although they do tend to be slightly higher. This may be due to the presence of

vessel wakes in other data records which have not been omitted from the data set. These will tend to increase the value of the ratio slightly. Further, the assumptions of a narrow spectrum source for the waves may not hold for estuarine conditions (Barthel, 1982).

The data presented by Black (1983) were measured by the same wave probe used in this study under similar conditions, although a different data logging system was utilised. These results were based on 5 records, selected by Black using unspecified criteria. The standard deviations for Black's data are 0.08 for H_{10}/H_s and 0.30 for H_{max}/H_s, compared with 0.30 and 1.88 respectively, for the wave probe as used in this study. Therefore the two distributions do overlap, despite the difference in the average values. Insufficient data are presented by Black (1983) to permit a suitable statistical test for the significance of this difference.

Black (1983) suggests that ratios based on period parameters are more stable than wave height parameter ratios. The average ratios between T_s and other wave period parameters are presented in Table 5.6 along with the corresponding results reported by other studies. These results show less agreement than the wave height ratios, which would not be the case if wave period parameter ratios were more stable.

Table 5.6 - Relationship between T_s and other wave period parameters.

Data Source	T_z/T_s	T_{10}/T_s	T_{max}/T_s
Goda (1978)	0.87	- 1.01	1.00
Black (1983)	0.56		2.88
Wave probe	0.70	1.14	1.35

A Weibull distribution was fitted to a subset of the data. The univariate statistics of the Weibull parameters derived are summarised in Table 5.7. All the Weibull parameter distributions are positively skewed due to the presence of vessel wakes. Therefore no great significance should be placed on the maximum values.

The α results are also affected by the skewness of the distribution of individual waves within each wave record. Consequently they are not very stable and these values are not reported in the literature. The wave period β values tend to be slightly higher than the wave height values, although this trend is very slight. Black (1983) notes that the

wave period distributions at Whangarei tend to be less peaked than the wave heights. This is the opposite from the tabulated Pilot Bay results.

Table 5.7 - Summary of the Weibull distribution parameters for the period 12/2/85-26/3/85. The parameters were derived from the zero up-crossing waves using the curve-fitting technique of Black (1978).

	Location (α)		Peakedness (β)		r^2	
	H	T	H	T	H	T
Maximum	0.524	804.20	10.53	24.68	1.00	0.99
Minimum	0.000	0.89	1.24	1.11	0.50	0.37
Median	0.004	6.20	2.09	1.98	0.97	0.91
Mode	0.001		1.75	1.99	0.99	0.95
Mean	0.009	21.48	2.34	2.46	0.94	0.87
SD	0.029	68.61	1.17	2.50	0.07	0.12

The β results deviate slightly from a theoretical Rayleigh distribution (β=2), and the α values vary considerably from the measured H^2_{rms} values. Black (1983) quotes wave height β values of 1.67 for a coral reef and 1.58 for Whangarei Harbour. The coral reef values are for shoaling waves in shallow water, so the comparison with Pilot Bay is inappropriate. The Whangarei Harbour value is for similar conditions to those encountered in this study. Black's results indicate that the wave height distribution within Whangarei Harbour is less peaked than predicted by a Rayleigh distribution, whereas the wave probe results indicate that the Pilot Bay distribution is more peaked. This may be partially due to differences in shipping movements, with the Pilot Bay site being exposed to more vessel wakes.

Based on the average number of zero up-crossing waves per record, Table 5.8 compares the wave parameters predicted by equations 5.8-5.11, against the measured mean values. There is good agreement between the predicted and measured values, indicating that these equations can be applied to the Pilot Bay data. Further, the Weibull distribution parameters are better predictors of the wave field than the theoretical ratios based on a Rayleigh distribution.

Table 5.8 - Wave parameters predicted by Equations 5.8-5.11 (N=182) compared to measured parameters for the period 12/2/85-26/3/85.

	H_m (m)	H_s (m)	H_{10} (m)	T_s (s)
Predicted	0.049	0.088	0.110	3.26
Measured	0.058	0.089	0.106	3.54

5.5.2 - Spectral wave parameters

A total of 360 spectral analyses was performed on data collected by the first Apple II+ wave recording system (Appendix 3) between 12/2/85 and 26/3/85. From this data set, 95 records were subsequently rejected due to contamination by vessel wakes, noisy signals or suspect data. The remaining 265 spectra were combined into an average spectrum by determining average densities for each frequency in the range 0.00-1.25Hz (Fig. 5.9). The spectral estimates used were originally determined at a bandwidth of 0.0112Hz, giving 2119df for the average spectrum.

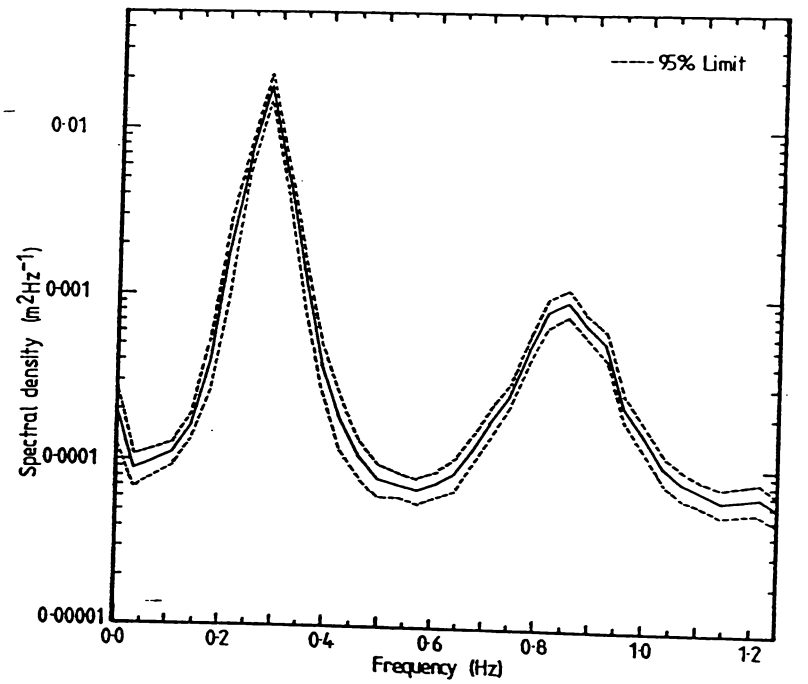

Figure 5.9 - Average spectrum for Pilot Bay derived by averaging 265 spectra collected between 12/2/85 and 26/3/85. The dashed lines represent the 95% confidence limits (Table 5.9).

The average spectrum displays two major peaks; one at 0.2857Hz (3.5s) and the other at 0.8571Hz (1.2s). The first of these peaks is fairly steep and dominates the spectrum with ~75% of the energy lying within a frequency band ±0.0357Hz either side of it (Table 5.9). The second peak is fairly broad and accounts for ~9% of the total energy. The sum of the average spectral densities is $3.9707 \times 10^{-2} m^2 Hz^{-1}$ which corresponds to H_c=0.107m as determined by Equation 5.13. This estimate compares favourably with the mean energy-based significant wave height,

H_o=0.102m, given in Table 5.4.

Table 5.9 - Spectral densities for the average Pilot Bay spectrum derived by averaging 265 spectra collected between 12/2/85 and 26/3/85.

Frequency (Hz)	Period (s)	Spectral density (m^2Hz^{-1})	Lower 95% bound	Upper 95% bound	% of total	H_c (m)
0.0000		0.0002026	0.0001284	0.0002768	0.51	0.0076
0.0357	28.01	0.0000868	0.0000678	0.0001057	0.22	0.0050
0.0714	14.01	0.0000959	0.0000783	0.0001136	0.24	0.0052
0.1071	9.34	0.0001083	0.0000906	0.0001260	0.27	0.0056
0.1429	7.00	0.0001564	0.0001289	0.0001839	0.39	0.0067
0.1786	5.60	0.0003963	0.0002504	0.0005422	1.00	0.0106
0.2143	4.67	0.0018502	0.0009430	0.0027575	4.66	0.0230
0.2500	4.00	0.0067175	0.0053887	0.0080463	16.92	0.0438
0.2857	3.50	0.0177508	0.0145065	0.0209950	44.70	0.0712
0.3214	3.11	0.0052550	0.0040757	0.0064343	13.23	0.0387
0.3571	2.80	0.0012578	0.0008547	0.0016610	3.17	0.0190
0.3929	2.55	0.0003709	0.0002527	0.0004892	0.93	0.0103
0.4286	2.33	0.0001734	0.0001118	0.0002349	0.44	0.0070
0.4643	2.15	0.0001035	0.0000771	0.0001298	0.26	0.0054
0.5000	2.00	0.0000778	0.0000597	0.0000958	0.20	0.0047
0.5357	1.87	0.0000722	0.0000598	0.0000846	0.18	0.0045
0.5714	1.75	0.0000672	0.0000552	0.0000793	0.17	0.0044
0.6071	1.65	0.0000729	0.0000600	0.0000858	0.18	0.0046
0.6429	1.56	0.0000843	0.0000661	0.0001026	0.21	0.0049
0.6786	1.47	0.0001191	0.0000962	0.0001420	0.30	0.0058
0.7143	1.40	0.0001777	0.0001406	0.0002148	0.45	0.0071
0.7500	1.33	0.0002519	0.0002112	0.0002926	0.63	0.0085
0.7857	1.27	0.0004775	0.0003932	0.0005618	1.20	0.0117
0.8214	1.22	0.0008102	0.0006499	0.0009706	2.04	0.0152
0.8571	1.17	0.0009298	0.0007543	0.0011053	2.34	0.0163
0.8929	1.12	0.0006705	0.0005634	0.0007777	1.69	0.0138
0.9286	1.08	0.0005253	0.0004220	0.0006287	1.32	0.0122
0.9643	1.04	0.0002135	0.0001755	0.0002515	0.54	0.0078
1.0000	1.00	0.0001448	0.0001180	0.0001716	0.36	0.0064
1.0357	0.97	0.0000950	0.0000767	0.0001133	0.24	0.0052
1.0714	0.93	0.0000768	0.0000619	0.0000918	0.19	0.0047
1.1071	0.90	0.0000683	0.0000566	0.0000799	0.17	0.0044
1.1429	0.87	0.0000614	0.0000497	0.0000730	0.15	0.0042
1.1786	0.85	0.0000637	0.0000513	0.0000760	0.16	0.0043
1.2143	0.82	0.0000655	0.0000518	0.0000793	0.16	0.0043
1.2500	0.80	0.0000559	0.0000448	0.0000671	0.14	0.0040

The average spectra was restricted to 0.00-1.25Hz to avoid harmonics associated with non-linear effects in shallow water. These effects are also present within the range chosen, since wave spectra can only be treated as linear within the range f_p to $2f_p$ (0.2857-0.5714Hz). This cut-off would have rejected all wave periods <1.75s, which ignores

locally generated wind waves. Therefore the cut-off was extended to 1.25Hz, beyond which harmonics made it difficult to interpret all the spectra.

The second peak may represent a harmonic of the first. However, the temporal responses of the second peak did not always follow those of the first. For example, the second peak could grow while the first decayed, usually in conjunction with strong offshore winds. On other occasions the first peak grew while the second was absent or declined. Therefore the second peak was considered to represent a different source of wave energy from the first peak.

The average spectrum was non-dimensionalised using the method proposed by Mitsuyasu in 1968 (Hasselmann *et al*, 1976; Harris *et al*, 1983), where a scaled energy density, Sn(f), is derived from:

$$Sn(f) = \frac{S(f).f_p}{\int S(f)df} \qquad \ldots 5.15$$

Figures 5.10 and 5.11 plot Sn(f) versus the non-dimensional frequency (f/f_p) for the first and second peaks respectively. Also plotted are non-dimensional JONSWAP and TMA spectra, these being considered the most appropriate for wave prediction in Pilot Bay (Appendix 2).

Considering the first peak, it is clear that the JONSWAP spectrum provides a reasonable fit for $f \leq f_p$ close to the peak, but the equilibrium range is considerably steeper than predicted by either spectra. The TMA spectrum deviates most from the average spectrum, despite the fact that it should give a better fit in shallow water. The second peak shows a better fit to both spectra, although it appears to contain more energy than predicted by either and there are still significant deviations within the equilibrium range.

The value of α, defining the equilibrium range (Equation 5.1), may be derived using the method of Hasselmann *et al* (1976), where α is equal to the mean of:

$$S(f)f^5g^{-2}\Lambda^{-1} \qquad \ldots 5.16$$

$$\text{where } \Lambda = \exp\left(-1.25\left(\frac{f_p}{f}\right)^4 + \ln\gamma . \exp\left[\frac{-(f-f_p)^2}{2\sigma^2 f_p^2}\right]\right)$$

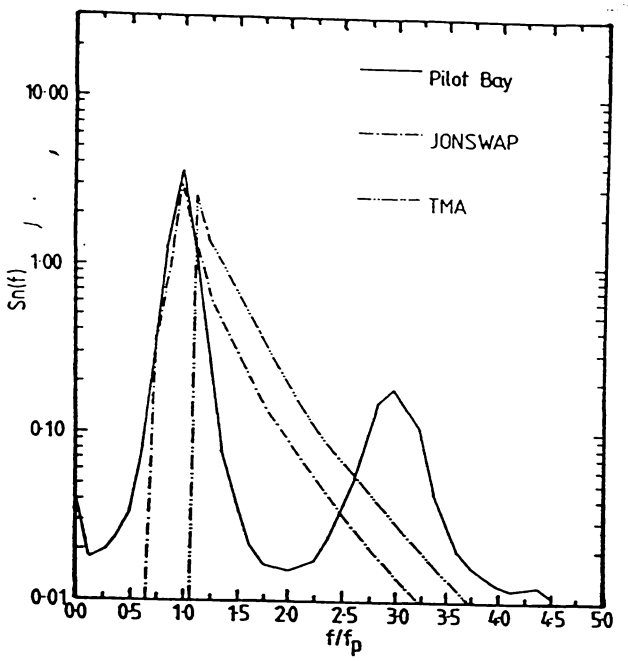

Figure 5.10 - Sn(f) versus f/f_p for the average Pilot Bay spectrum. Also plotted are non-dimensionalised JONSWAP and TMA spectra. All spectra were calculated using f_p=0.2857Hz.

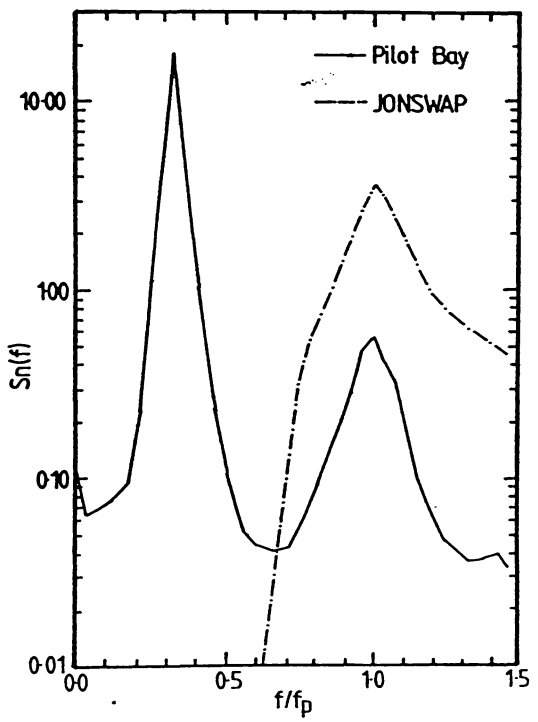

Figure 5.11 - Sn(f) versus f/f_p for the average Pilot Bay and JONSWAP spectra. For the peak frequency used to calculate the non-dimensional spectra (f_p=0.8751Hz) the TMA spectrum is identical to the JONSWAP spectrum.

over the range $1.35f_p<f<2f_p$. Considering the average spectrum, the first peak predicts $\alpha=3.6x10^{-8}$ and the second peak $\alpha=2.3x10^{-6}$. These results are considerably less than the mean value ($\alpha=5.1x10^{-3}$) reported by studies in the North Sea and Baltic Sea (Kahma, 1981), and the value for waves off East Cape ($\alpha=1.7x10^{-3}$) measured by Harris *et al* (1983). Kitaigorodskii *et al* (1975) suggest that two main factors may cause significant deviations within the equilibrium range resulting in variations in α from that predicted by Equation 5.1.

As discussed previously (Section 5.2), shallow water conditions alter the equilibrium range so that it shows a f^{-3} dependence instead of the f^{-5} relationship predicted by Phillips (1958). However, the tail region of the average spectra is considerably steeper than this and for the first peak it shows an f^{-8} relationship. Therefore the shape of the first peak does not display the characteristics expected of a shallow water, wind-generated spectra. Due to the presence of harmonics, it was not possible to reliably determine the tail slope for the second peak.

The second major factor to consider is the presence of currents. Kitaigorodskii *et al* (1975) indicate that currents have a strong influence on spectra, particularly when the spectrum has a narrow angular distribution. This would be the case for waves propagating into the harbour through the entrance. Aerial photographs taken during the THS (Plate 5.1) clearly show waves propagating through the entrance and diffracting into Pilot Bay. The first peak is considered to represent external wave energy propagating through the entrance, where the shape of the peak reflects the doppler shifts and filtering caused by strong currents in the vicinity of the entrance.

The total wave energy prior to propagation through the entrance is determined by the wave climate outside the harbour. Hence poor correlation between wave parameters and local windspeed is reasonable given that the first peak accounts for 75% of the wave energy. The second peak shows a reasonable correlation between peak energy density and wind speed (r=0.90). Therefore, the second peak is considered to be due to locally generated wind waves.

To define the second peak better, the energy associated with this peak was extracted from the average spectra by assuming a linear response for the external wave field component for 0.5714-1.1429Hz and subtracting this energy from the average spectrum. The resulting spectrum (Table

Plate 5.1 - Aerial photo of the Tauranga Harbour entrance taken in THS, August 1984. Waves (L=~120m) are propagating across Central Bank with some diffraction occurring in the vicinity of Pilot Bay.

5.10) represents the average local wind-generated component. The sum of the average spectral densities was $3.7537 \times 10^{-3} m^2 Hz^{-1}$ which corresponds to H_c=0.033m. Thus the wind component represents 31% of the wave height and 9% of the total spectral energy.

Table 5.10 - Spectral densities for the local wind-generated component of the average Pilot Bay spectrum. The densities were derived by assuming a linear response for background wave energies betweeen 0.5714 and 1.1429Hz.

Frequency (Hz)	Period (s)	Spectral density (m^2Hz^{-1})	% of total	H_c (m)
0.6071	1.65	0.0000061	0.16	0.0013
0.6429	1.56	0.0000179	0.48	0.0023
0.6786	1.47	0.0000530	1.41	0.0039
0.7143	1.40	0.0001120	2.98	0.0057
0.7500	1.33	0.0001866	4.97	0.0073
0.7857	1.27	0.0004125	10.99	0.0109
0.8214	1.22	0.0007456	19.86	0.0146
0.8571	1.17	0.0008655	23.06	0.0157
0.8929	1.12	0.0006066	16.16	0.0132
0.9286	1.08	0.0004618	12.30	0.0115
0.9643	1.04	0.0001503	4.00	0.0066
1.0000	1.00	0.0000820	2.18	0.0048
1.0357	0.97	0.0000326	0.87	0.0030
1.0714	0.93	0.0000147	0.39	0.0021
1.1071	0.90	0.0000066	0.18	0.0014

This spectral component was non-dimensionalised and plotted against f/f_p (Fig. 5.12). Within the frequency range and depth (11m) considered, the TMA and JONSWAP spectral forms are identical (Φ=1) so only the non-dimensional JONSWAP spectrum is included for comparison. The shape of the two curves is similar away from the peak, but the observed spectrum is more peaked and the tail region close to f_p is steeper than the JONSWAP form. The third curve plotted represents an empirical curve derived from the JONSWAP form by adjusting values of γ and σ until the best fit, as determined by least squares, was achieved. Table 5.11 summarises the shape constants derived and compares these with others available in the literature.

The shape parameter which defines the width of the spectral peak (σ) is generally fairly stable (Hasselmann et al, 1976), and this is borne out by the values determined by this study. The peakedness parameter

(γ) is considerably more variable. Hasselmann et al (1976) summarise the findings of 9 studies with mean values for γ of 0.92-5.06. In general the value of γ is thought to vary from 1 for very long fetches, where the JONSWAP spectrum is equivalent to the Pierson-Moskowitz spectrum, towards infinity for extremely short fetches. Hence, given that the fetches for the other studies in Table 5.11 are at least an order of magnitude larger than the maximum fetch for Pilot Bay (11km), the value determined for γ is not unreasonable.

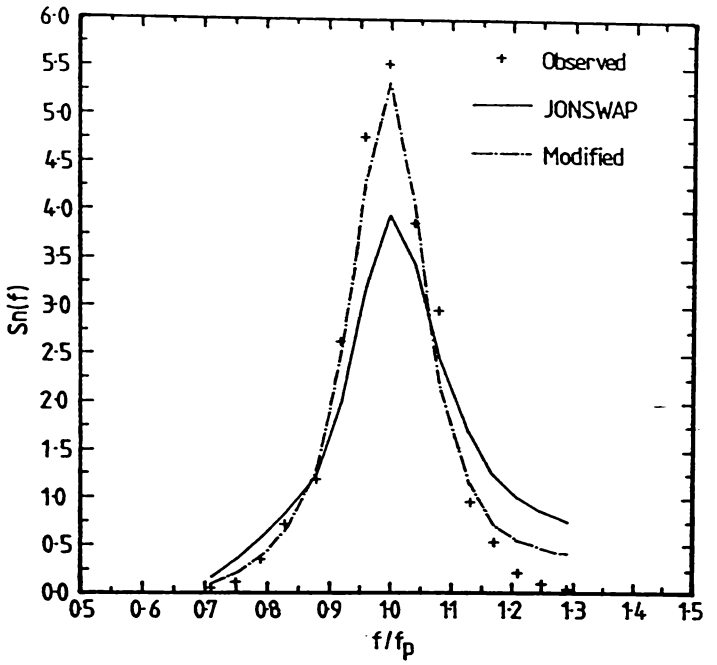

Figure 5.12 - Sn(f) versus f/f_p for the local wind generated component of the average Pilot Bay spectrum. Also plotted are non-dimensionalised spectra representing the JONSWAP spectrum and a modified JONSWAP spectrum with new shape constants (Table 5.11).

Table 5.11 - Comparison of shape statistics for the JONSWAP spectral form. The values quoted represent mean values.

Source	γ	σ ($f \leq f_p$)	σ ($f > f_p$)
Hasselmann *et al*, 1973	3.3	0.07	0.09
Hasselmann *et al*, 1976	2.65	0.085	0.098
Chiswell and Kibblewhite, 1981	1.55	0.09	0.09
Knowles, 1982	1.5		
Bouws and Komen, 1983	2.0	0.08	0.08
Bouws *et al*, 1985	3.68	0.102	0.122
This study	8.13	0.094	0.083

Therefore the local wind-generated component of the Pilot Bay wave field can be given by:

$$S(f) = \frac{\alpha g^2}{(2\pi)^4} f^{-5} e^{-(1.25(f/f_p)^{-4})} \gamma^q \qquad \ldots 5.17$$

where $\alpha = 2.3 \times 10^{-6}$

$\gamma = 8.13$,

f_p = spectral peak frequency,

and $q = e^{-(f-f_p)^2/(2\sigma^2 f_p^2)}$

where $\sigma = \begin{cases} 0.094 & f \leq f_p \\ 0.083 & f > f_p \end{cases}$

For the average spectrum, f_p=0.8571Hz. Hasselmann *et al* (1976) present equations relating f_p to wind speed and fetch length. These may be rearranged to calculate the fetch required to produce the observed f_p. For the average wind speed associated with the spectra analysed ($4.37 ms^{-1}$), the required fetch is 1.6km. This fetch is realistic for Pilot Bay.

The derived equation does not consider depth which, although not important adjacent to the wave recorder site, will restrict wave growth throughout most of Tauranga Harbour. However, depth could be accounted for by incorporating the TMA scaling factor (Φ). The major problem with this equation is that it presupposes the presence of wave energy due to an external wave field. This would restrict the applicability of this equation to the regions where this extra energy input does exist.

All 360 spectra available were analysed in terms of the parameters listed in Table 5.3 and results are summarised in Table 5.12. Comparing the zero up-crossing parameters estimated from the wave spectra (H_{m0} and T_z) with those derived by zero up-crossing analysis for the same data sets suggests that the spectral technique overestimates the wave height, but appears to estimate the period reasonably well.

To investigate this further, the spectral estimates were regressed against the corresponding zero up-crossing parameters for all 265 cases using BMDP P6D. Table 5.13 summarises the regression statistics derived. All the regressions were significant at the 99.9% confidence level and bivariate plots showed a random scatter for the period data, and a tendency for increased scatter at higher wave heights for the wave height data. The regression statistics confirm that the average

spectral estimate of T_z is a good predictor of the average zero up-crossing parameter. However, due to the scatter in the data, the spectral estimate is not a particularly good estimate of individual T_z values.

Table 5.12 - Summary of the univariate statistics for the wave probe spectral parameters (Table 5.3). These statistics were derived from 360 spectra obtained between 12/2/85 and 26/3/85. Also included for comparison are corresponding zero up-crossing parameters (^{z}).

	Maximum	Minimum	Median	Mode	Mean	SD
m_0	0.0107100	0.0000569	0.0008533		0.0014129	0.0014989
f_p	0.8571	0.0000	0.2857	0.2857	0.2844	0.0001
f_m	0.6879	0.2521	0.3583	0.3299	0.3781	0.0767
$S(f_p)$	0.218600	0.0005264	0.0110700		0.0205531	0.0275620
ϵ_s	0.79	0.26	0.64	0.65	0.62	0.09
Q_p	15.06	1.09	4.56	3.46	5.41	2.87
T_z	3.78	1.35	2.40	2.64	2.43	0.52
T_c	2.88	1.07	1.38		1.49	0.33
H_e	0.29	0.02	0.08	0.07	0.10	0.05
H_{m0}	0.41	0.03	0.12	0.11	0.13	0.07
H_{max}	0.52	0.04	0.18	0.13	0.19	0.09
T_z^z	4.40	1.03	2.33		2.43	0.72
H_s^z	0.26	0.02	0.08	0.07	0.09	0.04
H_{max}^z	0.37	0.03	0.12	0.11	0.13	0.06

However, spectral estimates for wave height overestimate the zero up-crossing parameters by a considerable amount, except for H_e. These results are comparable to those reported by Thompson and Vincent (1984) for measurements of monochromatic waves in a flume. Their data indicated that H_s was ~70% of H_{m0} in deep water (~6H) and that the difference decreased as the waves approached their limiting steepness. The Pilot Bay data show that H_s is ~60% H_{m0} in deep water (~100H).

Table 5.13 - Regression statistics for zero up-crossing parameters versus spectral estimates determined from wave records obtained between 12/2/85-26/3/85.

Spectral estimate	Zero up-crossing parameter	Constant	Slope	Correlation
T_z	T_z	0.01121	0.99684	0.712
H_{m0}	H_s	0.00812	0.60133	0.895
H_e	H_s	0.00817	0.85174	0.896
H_{max}	H_{max}	0.01695	0.57582	0.865

H_{m0} is an energy based parameter, whereas H_s is derived directly from measurements of the actual wave heights in the wave record. Most engineering applications use H_s (Thompson and Vincent, 1985). However, since most wave records are now obtained digitally, energy based parameters (H_{m0} and H_σ) have been used as a substitute under the assumption that they are equivalent to H_s in deep water. Similarly, most empirical or semi-empirical wave prediction schemes are energy based and derive either H_{m0} or H_σ, although they are commonly presented as H_s (Thompson and Vincent, 1985). From the observed relationship between H_{m0} and H_s within Pilot Bay, it is necessary to distinguish carefully between these two parameters.

5.6 - Comparison with the external wave climate

About 70% of the average Pilot Bay spectrum is derived from the external wave field. It is therefore useful to compare the internal spectrum with the external spectrum in order to determine the nature of any transformations which may have occurred during propagation through the harbour entrance.

There is very little wave data available for the Tauranga region. The two main studies available are those of Davies-Colley (1976) for the harbour entrance and Harray (1976) for Waihi Beach at the northern end of Matakana Island. Most of these data were obtained by visual estimates of H_s and T_s, although short instrumental records were obtained by Harray (1976), and none involved spectral analysis of time series data. Two studies involving spectral analysis have been undertaken adjacent to the Bay of Plenty. These considered waverider buoys deployed at Hicks Bay to the south (Harris *et al*, 1983), and offshore from Great Barrier Island to the north (Ewans and Coup, 1982a & b).

The Bay of Plenty wave climate is dominated by waves arriving from the north-east (Pickrill and Mitchell, 1979). These waves are typically associated with relatively fast moving mid-latitude or Tasman depressions travelling west to east (Harris *et al*, 1983; Heath, 1985)). Due to the speed at which the generating systems travel, the generated wave field is usually duration-limited and rarely achieves a fully saturated state. Therefore, the average wave spectrum could be

expected to be more peaked than the Pierson-Moskowitz spectrum and should approximate a JONSWAP spectral form. The wave spectra for Great Barrier (Ewans and Coup, 1982a & b) show two main spectral peaks; one dominant peak at 0.1215±0.0026Hz, and a second, highly variable peak which occurs between 0.3 and 0.5Hz. The first of these represents distant swell wave energy and the second is the locally generated wave field.

Figure 5.13 plots the average wave spectra obtained at Pilot Bay and Hicks Bay as energy density (S(f)) versus frequency (f). It can be seen that the peak density obtained at Pilot Bay is lower and occurs at a higher frequency than the Hicks Bay spectrum. The Hicks Bay spectrum is considered to be representative of deep water conditions (Harris, 1985). Therefore, it would not be typical of wave spectra immediately adjacent to Tauranga Harbour. The data from Great Barrier are also considered to represent deep water, although they are from shallower, more sheltered waters than the Hicks Bay data.

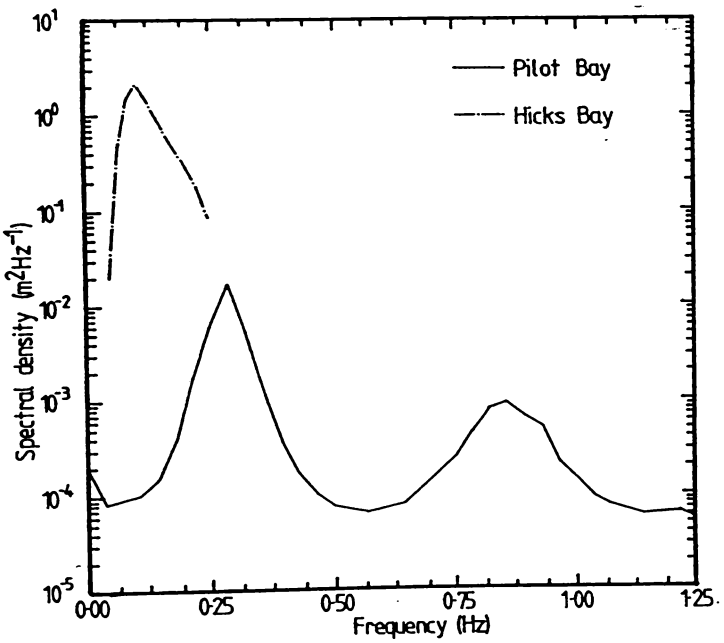

Figure 5.13 - Average wave spectra obtained at Hicks Bay (Harris *et al*, 1983) and Pilot Bay.

Ewans and Coup (1982a&b) do not present an average spectral form for their Great Barrier data. Examination of their data indicates that the wave field measured is a combination of background swell (0.07-0.15Hz) and locally generated seas (0.3-0.5Hz) and that the energy present is

lower than observed at Hicks Bay. The combination of these two dominant sources will produce apparent periods of 4-8s. Harris (1985) has analysed the H_{m0} and T_z parameters derived from the Great Barrier data. The T_z parameters have a mode of 6-7s and >80% of all observed waves lay between 4 and 8s. The Great Barrier data also included more short period waves than the Hicks Bay data, which is consistent with the higher frequency swell component (f_p=0.1215Hz cf. f_p=0.1067Hz).

Harris (1985) compared the H_{m0}, H_σ and H_s exceedance curves for several sites including Hicks Bay, Great Barrier and Tauranga (Fig. 5.14). Allowing for the fact that these three parameters are not strictly equivalent, the Tauranga and Great Barrier data are similar, although the wave field at Tauranga has slightly lower wave heights overall. The Tauranga data also has a greater incidence of small waves as indicated by the steeper gradient of the curve. These changes can be attributed to shoaling.

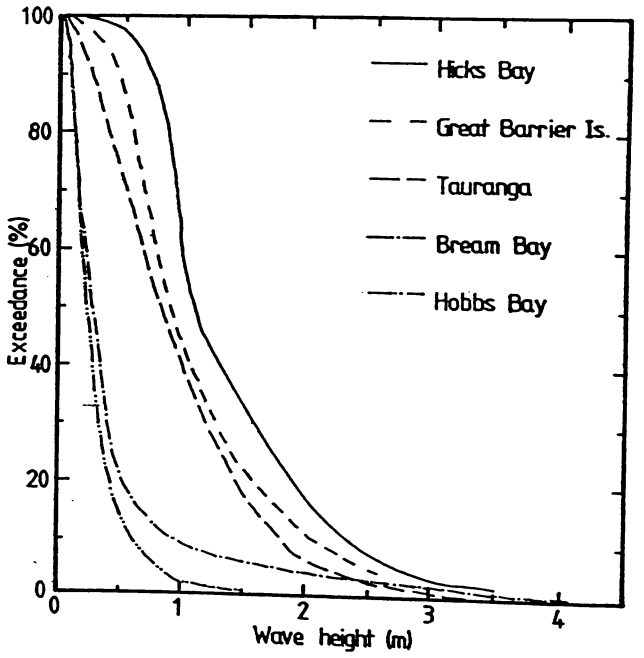

Figure 5.14 - Significant wave height exceedance curves for Hicks Bay (H_{m0}), Great Barrier Island (H_{m0}), Tauranga Harbour (H_s), Bream Bay (H_σ) and Hobbs Bay (H_σ). After Harris (1985).

As indicated in Figure 5.3, shoaling of deep water spectra results in several changes to the spectral form. The main changes observed are:

a) a decrease in the total energy within the spectrum due to energy losses associated with shoaling,

b) the peak frequency shifts to higher frequencies due to non-linear

interactions,

and c) the slope of the equilibrium range decreases.

These changes are evident in Figure 5.13 and may also be inferred from comparisons between the Hicks Bay and Great Barrier data sets. However, allowing for the distortions induced by a logarithmic axis, the peak of the Pilot Bay spectrum is also slightly broader than the deep water spectra.

The broadening of the spectral peak is not a response to shoaling transformations. This may be due to the averaging of several spectra. The spectra considered involve both ebb and flood tidal conditions. Therefore, in addition to shoaling transformations of the deep water wave spectra, it is necessary to include the effects of following and opposing currents. The tidal currents experienced in the Tauranga Harbour entrance will cause slight shifts in the peak frequency between ebb and flood tide.

5.7 - Summary

No existing method of predicting waves is adequate for the conditions which exist within Tauranga Harbour. First, the region involves fetches which are restricted in terms of both length and width. At present no method adequately considers the effect of such restricted fetches on a growing wave field. Second, the winds within the harbour display diurnal variations in both wind speed and wind direction associated with sea breeze cycles. Therefore, except under storm conditions, wave growth is likely to be duration-limited. Although the JONSWAP spectral form has been adapted for duration-limited applications, the assumptions under which this was done may not be valid.

The conditions within much of the area of interest are classed as depth-limited. Recent work on shallow water wave spectra indicates that the slope of the equilibrium range changes from f^{-5} towards f^{-3} and possibly f^{-2} as the depth decreases. The TMA spectrum accounts for shallow water conditions by introducing a frequency dependent scaling factor. Therefore, a fetch limited form of the TMA spectra would be the most appropriate form for shallow water within the harbour.

The effect of currents on wave generation is poorly understood and has been quantified for simple conditions. Within Tauranga Harbour there

are extreme temporal and spatial variations in current speed and direction. No existing predictive scheme can account for these current variations.

The average wave conditions have been quantified for the period of observation. Although the observations do not include any extreme events, they are representative of the local climatic conditions during the study.

Comparison of wave height parameter ratios between this study and previous work indicates that the measured wave field at Pilot Bay is more peaked than expected for a Rayleigh distribution. This is reasonable if the wave field is derived from more than one source.

The Weibull distribution provided a good fit to the zero up-crossing wave height and period distributions.

Marked deviations between energy based and zero up-crossing wave height parameters were noted. In particular, H_s is approximately 60% of H_{m0} and H_σ in the vicinity of the Tug Berth. Given that most wave recording systems derive energy based statistics, the use of significant wave height in engineering applications should be viewed with caution.

An average spectrum was derived from the available data. It is clear that two major sources of wave energy are present in the short period region of the spectrum. The wave field outside the harbour entrance contributes ~70% of the spectral energy and local-wind generated waves ~9%. The remainder of the energy is due to dissipation of longer period waves and vessel wakes. The shape of the short period region of the spectrum is consistent with shoaling and current induced transformations of the deep water wave field present off the northeast coast of New Zealand.

An empirical spectrum was derived to fit the wind-generated component of the average spectrum. This spectrum assumes an external source of additional wave energy and has a JONSWAP form with shape factors of γ=8.13, σ_a=0.094 and σ_b=0.083.

Chapter 6 - Non-tidal Low Frequency Waves in Pilot Bay

This chapter defines several types of low frequency waves that may occur in estuaries, and also reviews the potential source mechanisms for such waves within Tauranga Harbour. Measurements of seiches and tsunamis recorded at Salisbury Wharf are presented and these results are related to the behaviour of low frequency waves within Pilot Bay.

The sampling frequencies and record lengths of the wave recorder systems (Table 5.1) did not provide good resolution of the wave spectra at frequencies <0.0714Hz (T>14s). From Salisbury Wharf tide gauge chart records, it is apparent that waves with a frequency <0.0714Hz may be a significant component of the wave field, although comparison between plots of the recorded sea elevations (Fig. 6.1) and concurrent tide gauge records suggests that some of the apparent oscillations in the Salisbury Wharf record may be attributed to short-duration fluctuations associated with the interference of two or more wave trains having similar frequencies (surf beat).

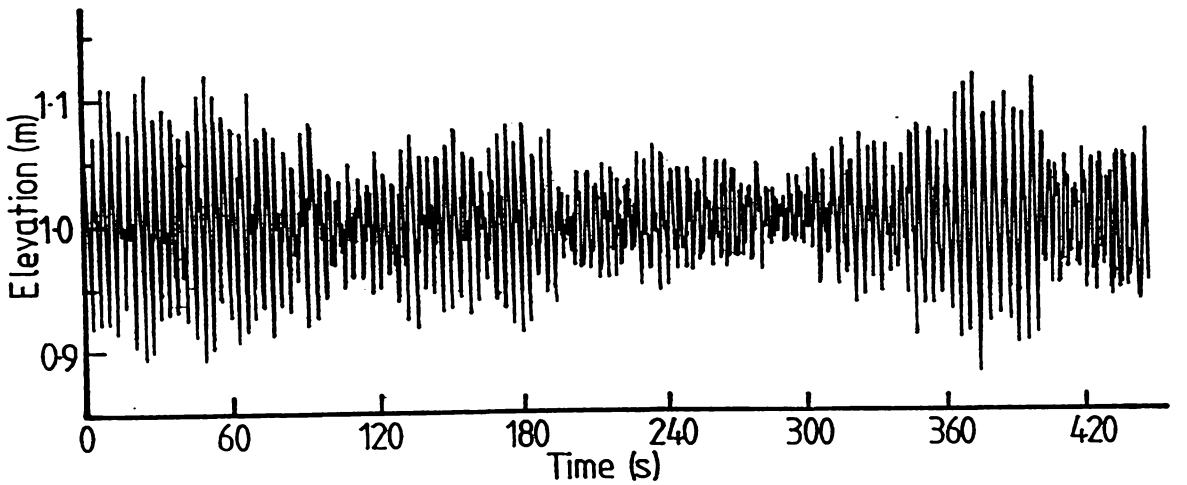

Figure 6.1 - Water elevation time history recorded by the wave probe at 1700, 20 February 1985. The corresponding wave parameters determined by a zero up-crossing wave analysis were H_s=0.11m and T_z=2.87s.

6.1 - Potential low frequency waves in Pilot Bay

Within an estuary, there are a number of possible sources for oscillations with an apparent frequency <0.0714Hz. These can be broadly classified as (Komar, 1976; Csanady, 1982; Bowden, 1983; SPM, 1984):

1) Tsunamis, long period waves generated by tectonic processes;

2) Seiches, long period standing waves induced by external forcing by atmospheric processes, or long period waves on the continental shelf adjacent to the estuary;
3) Surf beat, localised superelevation of the water surface due to interference between several wave trains;
4) Storm surges or meteorological tides, changes in water elevation caused by atmospheric pressure variations and wind stress;
5) Climatological variations, very low frequency variations due to variations in climate over a period of 1y or longer, e.g. El Niño; and
6) Secular variations, extremely low frequency variations associated with perturbations in the Earth's orbit and long term variations in the energy output of the sun.

The first four source mechanisms generate frequencies of 0.40×10^{-6} to 0.15×10^{-1} Hz (1min to 28 days), whereas the last two involve considerably lower frequencies (>1 month). The very long term changes involved with climatological and secular variations are not considered to be important in relation to the observed day to day changes in Tauranga Harbour. However, long term changes in sea level are of some importance for medium to long term planning, so the effects of the last two mechanisms will be considered briefly.

6.1.1 - Tsunamis

Tsunamis may directly affect water surface elevations by their propagation through the estuary, in the same manner as normal tidal waves. In general, the progressive components of a tsunami are transmitted more readily than those of a tidal wave, and these often manifest themselves as bores within the shallow reaches of estuaries in the Bay of Plenty (de Lange and Healy, 1986b). These processes continue as long as the tsunami waves continue to arrive at the harbour entrance.

A tsunami may also induce oscillations, or seiches, within the harbour. By considering the behaviour of the estuary and entrance as analogous to a Helmholtz resonator (Seelig, 1977), it is possible to predict the response to tsunami forcing. This was done for Tauranga Harbour by de Lange (1983). The analysis was limited to the immediate vicinity of the harbour entrance, but does hold for the Pilot Bay

region. It was found that tsunami forcing would induce seiching, and this activity would continue for some time after the forcing ceased.

Although two tsunamis were generated within the South Pacific region during the study period, neither produced a detectable wave at Salisbury Wharf. Earlier tsunamis have produced seiches and bores in Tauranga Harbour (de Lange and Healy, 1986a). All available tide gauge records from Salisbury Wharf involving appreciable tsunami-induced responses were obtained (Table 6.1) and digitised for spectral analysis (Section 6.2).

Table 6.1 - Summary of tsunami events used for spectral analysis for the period 1960-1987. The source refers to the approximate geographic region of origin.

Date	Source	Number of data points
23-25/5/60	Chile	1536
29-30/3/64	Alaska	1473
15/2/76	Kermadec Is.	1020

Heath (1985) measured at least 3 distinct seiche periods induced by the 1960 Chilean tsunami; 2, 1.1, and 0.3h. He suggested that the seiches produced were harmonics of the tsunami frequencies and that, since the amplitudes involved were considerably less than the tsunami amplitude, the forcing tsunami frequencies did not correspond to natural oscillation frequencies within Tauranga Harbour.

Unless an extreme locally generated tsunami occurs, the main effect of a tsunami on Pilot Bay will be due to the formation of seiches within the harbour (de Lange, 1983; de Lange and Healy, 1986b).

6.1.2 - Seiches

Seiches are usually low frequency, small amplitude standing waves caused by resonance within an estuary. They can be generated by local variations in atmospheric pressure and wind stress, or by oscillations transmitted into an estuary from the open ocean. If the forcing mechanism is periodic and in phase with a natural free oscillating frequency of the estuary, the seiches are amplified with time and may develop into large amplitude waveforms (Seymour, 1977b; Beer, 1983;

Shore Protection Manual, 1984).

An estuary can develop a series of seiches, which are usually considered as existing independently, each having its own amplitude and wavelength distributions (Csanady, 1982). As a first approximation, a simple rectangular basin of uniform depth may be considered. Possible free oscillation frequencies are then given by (Csanady, 1982):

$$f_n = \frac{(1+2n)(gh)^{1/2}}{4B} \qquad \ldots 6.1$$

where n = mode of oscillation,
h = water depth,
and B = length of the basin.

The modes of oscillation which appear as seiches depend on the forcing mechanism, and do not always correspond to free oscillations. For example, wind stress only generates odd numbered modes, whereas external oscillations generate modes which are harmonics of the driving frequency and they are not controlled by the possible free oscillation modes. If a forced oscillation corresponds to a free oscillation mode it will be amplified, otherwise it will be attenuated.

One important derivation from Equation 6.1 is Merian's formula (Csanady, 1982; SPM, 1984) which defines the minimum or fundamental frequency for a basin. This is associated with n=0 and is given by:

$$f_0 = \frac{(gh)^{1/2}}{4B} \qquad \ldots 6.2$$

6.1.2.1 - Seiche generation by local atmospheric effects

Two local processes may generate seiches within an estuary, namely atmospheric pressure changes and wind stress. If the phase velocity of the atmospheric pressure wave corresponds to the phase velocity of a free oscillation in the harbour, resonance will occur. The maximum pressure changes experienced at Tauranga may cause water level variations of up to 0.59m (Section 4.1).

Wind stress within the harbour will move water in the direction of wind propagation, resulting in a wind-induced super-elevation, or setup, at one end of the basin. If the applied wind stress is removed

suddenly, the resulting hydraulic adjustment of water levels may generate a seiche, as has been recorded in Lakes Whakatipu and Taupo (Gilmour and Butcher, 1987a, 1987b). Further, wind stress may result in resonance at some free oscillation modes.

6.1.2.2 - External seiche generating mechanisms

Seiches within Tauranga Harbour may be induced by a number of processes, including:

1) Longshore currents. These can induce seiching within an estuary, in a manner analogous to the resonance caused by blowing across the top of a milk bottle (Beer, 1983);
2) Onshore currents. The onshore components of coastal Eckman transport and other wind-induced currents may result in water level variations within estuaries (Garvine, 1985; Walters and Gartner, 1985). Since the origin of these currents may be distant from the estuary, remote responses to meteorological conditions may be more significant than local ones;
3) Low frequency trapped waves. These are waves which are confined to the continental shelf by reflection at the shelf boundaries, or propagate parallel to the shore; and
4) Tsunamis.

The seiches induced by these processes tend to be very low frequency (T>1 day).

With respect to Pilot Bay, the first two processes are mainly related to meteorological forcing within the Bay of Plenty, since the major geostrophic current present, the East Auckland Current, does not penetrate sufficiently close inshore to be an important factor (Harris, 1985). Measurements of currents offshore from the harbour entrance and in the vicinity of Karewa Island (HRS, 1963,1968; Barnett, 1985) indicate the presence of a shore-parallel current beyond the nearshore zone. The behaviour of this current has been attributed to offshore wind stresses (HRS, 1968), but this has yet to be substantiated.

Low frequency trapped waves can be classified by their frequency and wave number (Fig. 6.2). The major distinction between the wave types is their relationship to the inertial frequency given by:

$f_i = \sin\phi/43200$ ... 6.3

where ϕ = latitude of the point of interest.

Waves with a frequency $<f_i$ are strongly affected by the Earth's rotation and their phase velocity is not necessarily controlled by water depth. These waves may be collectively referred to as planetary or Rossby waves (Beer, 1983). Otherwise the waves behave in the same way as shallow water high frequency waves.

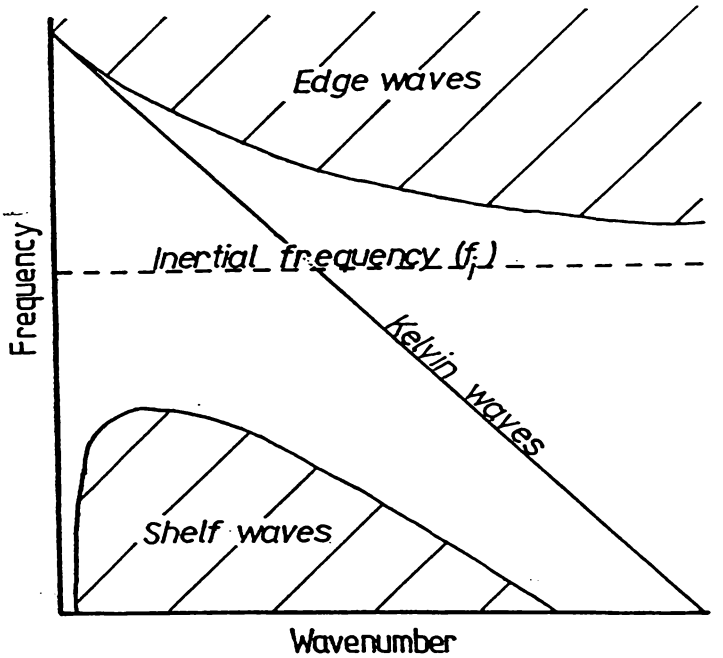

Figure 6.2 - Dispersion diagram showing definition of major classes of trapped waves in terms of frequency and wave number. For Tauranga Harbour (ϕ=37°38'), f_i=1.413x10^{-5}Hz (Equation 6.3).

Kelvin waves can occur along basin boundaries and they are associated with discontinuities in the water column due to density or bathymetric changes. They span the entire frequency range and propagate as shallow water waves, the phase velocity in coastal waters being determined by the depth in the adjacent ocean basin. They are the dominant coastal response to any major disturbance (Beer, 1983).

Shelf waves are strongly controlled by the Earth's rotation. The way in which these waves are excited is not known, but they are associated with the passage of storms (Beer, 1983). Edge waves can be considered as the trapped longshore component of incoming waves, and may be maintained for some time after the initial wave disturbance has

dissipated.

Continental shelf edge waves have been recorded for the east coast of New Zealand between Banks Peninsula and East Cape (Heath, 1979), but they did not extend into the Bay of Plenty. Harris (1985) calculated possible storm-induced shelf and edge wave periods of 1.3 and 0.3h, respectively, for the continental shelf in the vicinity of Tauranga Harbour.

6.1.3 - Surf beat

When two or more wave trains arrive at a location from different sources they interact to produce a systematic variation in wave heights and associated water levels (Fig. 6.3). When the interacting wave trains are in phase, the wave heights reach a maximum, and when out of phase, the wave heights are a minimum. This systematic variation is known as surf beat (Komar, 1976), and usually has a period of 2-3min.

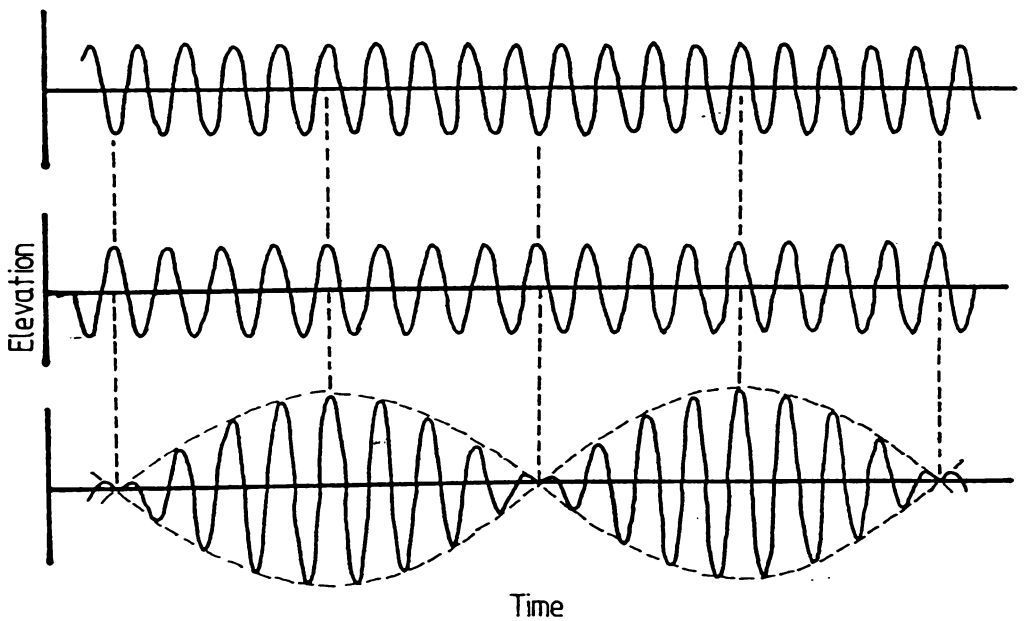

Figure 6.3 - The summation of two or more wave trains from different sources produces a systematic variation in wave height known as surf beat. After Stowe (1979).

Associated with surf beat is a systematic variation in water elevation, possibly due to changes in wave setup (Komar, 1976; Barthel, 1982). These variations in water level have been called bounded long waves and they occur whenever short-period waves become grouped into

large and small amplitudes. At present the mechanism by which they are generated is not understood.

The wave records obtained during this study do exhibit grouping on some occasions (Fig. 6.1), coinciding with small amplitude oscillations on the Salisbury Wharf tide recorder. These oscillations are too small to digitise effectively, but visually the period was estimated to be in the range 30-220s. This range is consistent with measurements of bounded long waves made off Newfoundland, Canada, which had a mean period of 61s and a range of 36-183s (Barthel, 1982).

6.1.4 - Storm surges

There is a number of factors which contribute to non-tidal changes in sea level during storm conditions (Beer, 1983; SPM, 1984; Harris, 1985). The most important of these are atmospheric pressure and wind stress, although significant variations can be produced by various types of waves associated with the storm. Therefore a storm surge represents an extreme combination of most of the processes discussed above.

Several large storm surges have been experienced within Tauranga Harbour, including during the Wahine Storm (9-10 April, 1968) when the tide record went off scale, indicating a storm surge >0.78m. During 17-20 July, 1978, a storm produced a surge which resulted in significant deviations from the predicted tidal curve at Salisbury Wharf (Harris, 1985). The maximum deviation experienced was 0.56m, of which the pressure drop (34hPa) contributed 0.34m. Analysis of the residual deviations revealed an oscillatory component with an amplitude of 0.10m and an apparent period matching the tidal period (Harris, 1985), but with the maximum occurring at low tide.

Harris (1985) suggested that this oscillation is due to wind setup reinforcing the tidal wave. Alternatively, it may be associated with the onshore component of Eckman transport.

6.1.5 - Long term sea level variations

The daily mean sea level measured at any locality varies in response to local weather conditions and the combined effects of the low frequency waves discussed above (Komar, 1976; Thurman, 1985). Daily

mean sea level fluctuations >0.50m have been generated within Tauranga Harbour by tsunamis and storm surges. The largest of these events recorded at Salisbury Wharf were the 1960 Chilean Tsunami (maximum amplitude 1.2m) and the storm surge associated with the 1968 Wahine Storm (>0.78m). Despite the greater amplitude of a tsunami, a storm surge has a greater impact on mean sea level due to its longer apparent period. For example, the mean sea level deviation associated with 1960 Chilean Tsunami was only 0.05-0.10m.

Short term fluctuations may be removed by averaging over longer time intervals, such as a month or year. The monthly mean sea level at Salisbury Wharf can vary by ~0.1m from month to month during the year (Fig. 6.4). The monthly variations show a slight seasonal trend with the highest levels during later summer and autumn (April to June) and the lowest during spring (August to October). This trend is consistent with monthly variations determined for 400 locations around the world by Pattullo *et al* (1955). However, the variation is quite small at Tauranga compared to most comparable locations near 40° latitude, due to the absence of strong seasonal variations in the climate (Chapter 4). Hence the monthly variation of sea level can be considered relatively insignificant compared to daily variations which are influenced by very occasional tropical depressions.

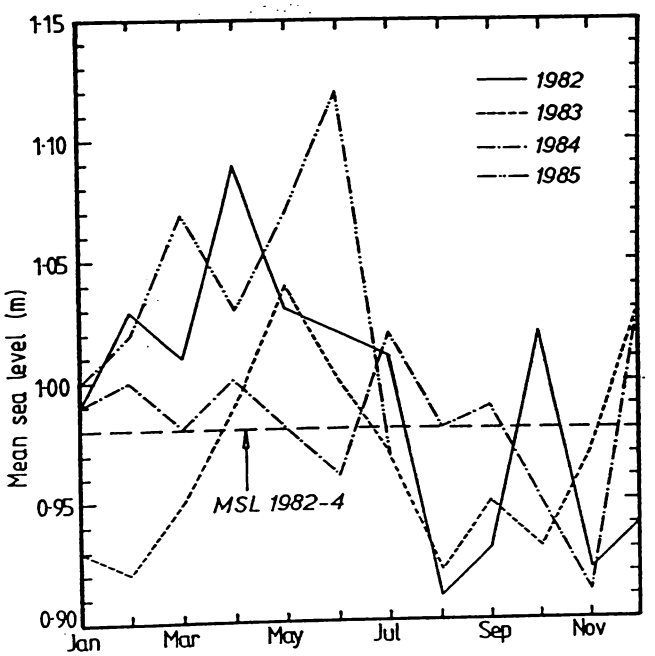

Figure 6.4 - Monthly mean sea level measured at Salisbury Wharf during the period 1982-1985.

Longer term mean sea level values reflect global variations in sea level (Komar, 1976; Gibb and Aburn, 1986) and regional tectonic movements. This study did not undertake the necessary tide level analyses and geodetic surveys to determine the long term sea level variations at Tauranga. Analysis of Auckland tide levels for the period 1903-1977 using 10y running means (Gibb and Aburn, 1986) recorded a net sea level rise of $1.6mmy^{-1}$. This value is consistent with the average global rise of $1.51\pm0.15mmy^{-1}$ determined for tectonically stable areas around the world for the period 1900-1980 (Gibb and Aburn, 1986). Therefore a similar net sea level rise could be expected for Tauranga for this period.

There is some evidence that the rate of sea level rise is accelerating due to increased melting of northern hemisphere ice caps (60%) and thermal expansion of the oceans (40%). These changes are due to an increase in global temperatures attributed to the 'greenhouse effect' (Hoffman *et al*, 1983). During the past few decades there has been an accumulation of various compounds in the atmosphere which trap re-radiated heat, or destroy the ozone layer allowing more heat in. The analysis of tide levels in Auckland suggests that for the later part of the period analysed (1945-1977) sea level rise reached $2.59mmy^{-1}$ (Gibb and Aburn, 1986), whereas for the earlier part of this century it was almost zero.

A number of simulations have been performed to predict the likely sea level rise over the next 100-120y (Hoffman *et al*, 1983; Gibb and Aburn, 1986). Assuming no or little change in the current rates of emission of carbon dioxide, methane, nitrous oxide and chloro-fluorocarbons the likely sea level rise by 2100 is 1.4-2.2m (Hoffman *et al*, 1983). If the emission rates were to be reduced or increased, the predicted rises are 0.6-3.5m. These predictions assume that the increased melting is essentially confined to the northern hemisphere (mainly Greenland). If the West Antarctic ice sheet, which is essentially marine and not land based, were to be affected by global warming an additional sea level rise of 5-7m is expected during the next several hundred years (Gibb and Aburn, 1986).

These predictions are speculative in that very little is known about the way in which the atmosphere and global climate will respond to the observed global warming. However, it is apparent that the rate of sea

level rise is increasing and a rate of >7mmy^{-1} within the next 100y is considered probable.

6.2 - Measurement and data analysis

Low frequency waves were obtained from the Salisbury Wharf tide gauge records by digitising the chart trace for selected events (Tables 6.1 and 6.2). The digitiser used had a spatial resolution of 0.1mm which corresponds to a time interval of 14.2s and an elevation interval of 1.2mm. The major source of error during digitisation was associated with tracking the trace, which varied in width from 0.4-0.6mm. Hence the minimum practical time and elevation interval are 60s and 5mm respectively. Therefore only events producing waves with a period greater than 120s could be considered for spectral analysis.

Table 6.2 - Summary of the seiche events used for spectral analysis for the period 1983-1984. The wind data refer to the mean conditions recorded at Mt. Drury during the sampling period.

Date	Number of data points	Wind speed (ms^{-1})	Wind direction (°)
10/ 7/83	250		
7- 8/12/83	1895		
11/ 2/84	760	9.7	29
24-25/ 5/84	2575	9.5	155
28/ 6/84	1433	1.5	156
30/ 6/84	1120	6.8	11
11-18/ 8/84	8626	11.3[a]	104[a]

[a]Mean for the period 11-15/8/84 only. The wind conditions were relatively uniform during this period, subsequently they became highly variable in both direction and wind speed.

The digitised data were transferred to the Vax 11/780, where the data were cleaned to remove spurious values and corrected to a standard time interval using linear interpolation. The data were then processed by BMDP P1T.

Over the record lengths considered (24-96h) seiches are not stable waveforms since their amplitude increases and then decays, although the frequency appears to be constant. As a result, it is not possible to accurately determine the amplitude, and hence the spectral density. Further, tidal components cannot be removed by simple detrending.

Consequently, to provide a better definition of the spectral peaks, low- and high-pass filters were employed. The data were not recoloured after filtering.

Spectral analyses were subsequently performed at the default BMDP settings. This resulted in slight variations in the actual frequencies considered due to the different record lengths. Although there were differences in the frequencies considered, all data sets were analysed at a bandwidth of ~0.0001Hz.

6.3 - Results

Within the limits imposed by different sample sizes, all the data produced a consistent sequence of peaks (Table 6.3). The significance of each spectral peak is expressed in terms of the normalised energy density relative to the largest peak. The distribution of energy between the observed peaks is quite variable, although one peak clearly dominates each record. The dominant peak occurs at either 0.0038Hz or 0.0045Hz. To test if the spectra determined by BMDP were valid, the Chilean Tsunami and February 1984 data were run through another spectral analysis routine from the NAG subroutine library. The results were in complete agreement with the BMDP spectra.

Equation 6.1 can be rearranged to give the basin length (B) as follows:

$$B = \frac{(1+2n)(gh)^{\frac{1}{2}}}{4f} \qquad \ldots 6.4$$

Given the measured seiche frequencies, idealised basin lengths capable of generating the observed seiches can be derived. At Pilot Bay, seiching may be associated with oscillations involving the whole harbour, or dominated by oscillations trapped in the deeper harbour channels. In the latter case, the basin formed by the Maunganui Roads is likely to be significant, given its uniform depth and rectangular shape (Fig. 6.5).

From Equations 6.1 and 6.4 it can be seen that the free oscillation frequencies are a function of the water depth. Therefore, as the tide rises and falls, the changing water depth will alter the seiche frequencies. Further, within an estuary the changing tide level will

also alter the effective basin length. Therefore, if the observed seiches are associated with oscillation of the entire harbour or the southern basin, the seiches should change progressively during a tidal cycle. These changes will be superimposed on any changes resulting from variations in the driving oscillations.

Table 6.3 - Summary of spectral peaks obtained from the digitised seiches (Tables 6.1 and 6.2). The size refers to the normalised energy density relative to the largest peak.

Chilean Tsunami					
Frequency (Hz)	0.0030	0.0038	0.0046	0.0061	0.0076
Period (s)	334	265	219	163	132
Size (%)	6.3	19.6	100.0	1.3	4.9
Alaskan Tsunami					
Frequency (Hz)	0.0030	0.0038	0.0045	0.0061	0.0076
Period (s)	329	260	221	165	132
Size (%)	48.9	19.2	100.0	47.0	2.8
Kermadecs Tsunami					
Frequency (Hz)	0.0030	0.0038	0.0045	0.0061	0.0075
Period (s)	329	262	222	165	133
Size (%)	12.7	100.0	14.8	10.3	4.5
10/ 7/83					
Frequency (Hz)	0.0031	0.0039	0.0045	0.0060	0.0076
Period (s)	326	259	221	167	132
Size (%)	2.2	8.0	100.0	1.1	5.1
7- 8/12/83					
Frequency (Hz)	0.0030	0.0038	0.0046	0.0061	0.0075
Period (s)	334	260	219	163	133
Size (%)	1.5	42.8	100.0	4.5	4.6
11/ 2/84					
Frequency (Hz)	0.0031	0.0038	0.0045	0.0060	0.0076
Period (s)	326	261	222	166	132
Size (%)	14.5	100.0	15.6	2.6	2.9
24-25/ 5/84					
Frequency (Hz)	0.0031	0.0038	0.0045	0.0060	0.0076
Period (s)	326	263	221	167	132
Size (%)	6.1	100.0	3.2	2.8	15.4
28/ 6/84					
Frequency (Hz)	0.0030	0.0038	0.0045	0.0061	0.0075
Period (s)	329	261	222	164	133
Size (%)	24.4	100.0	17.0	17.4	7.2
30/ 6/84					
Frequency (Hz)	0.0030	0.0038	0.0045	0.0060	0.0076
Period (s)	329	262	220	166	132
Size (%)	6.9	100.0	72.5	4.6	10.5
11-18/ 8/84					
Frequency (Hz)	0.0030	0.0038	0.0046	0.0060	0.0076
Period (s)	331	260	218	166	132
Size (%)	74.0	100.0	49.0	46.6	20.2

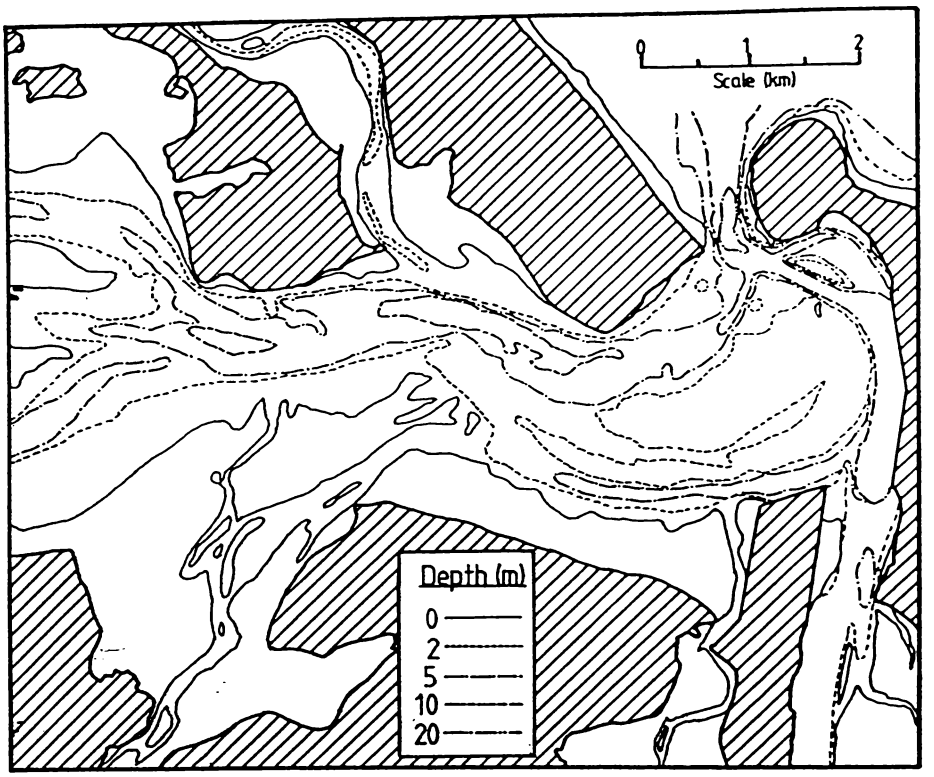

Figure 6.5 - Bathymetry of the southern basin, Tauranga Harbour.

For Pilot Bay the seiche amplitudes are largest at high tide and the behaviour of seiches differs between ebb and flood tide conditions. These changes may account for the apparent changes in the dominant spectral frequency between the various seiche events (Table 6.3), since each record analysed involved different sequences of tidal cycles. For example, in shallow water the tidal range is sufficient to produce a frequency shift of 0.0006-0.0008Hz. This would account for a change between the two main frequencies observed.

Seiche amplitude is inversely proportional to the water depth, and proportional to the basin length (Csanady, 1982). This suggests that, for Tauranga Harbour, the observed seiche amplitudes are controlled by the changes in basin length more than the water depth. If this is the case, the seiches must involve the shallower tidal flats, since the basin length in deeper channels will not change during a tidal cycle. Deep channels would also involve a smaller frequency shift than shallow tidal flats. For example, given B=1km, a depth change of 12m to 13m involves a frequency shift of 0.0001Hz whereas a change of 2m to 3m changes the frequency by 0.0003Hz.

Using equation 6.4, the simplest combination of depth and basin length

required to account for the observed frequencies requires h=2-4m and B=3.5-4.5km. Under these conditions seiches with frequencies of 0.0038Hz and 0.0045Hz require the same basin length (±10m) and the remaining observed frequencies need lengths within ±200m. The depth range rules out a dominant input from seiches trapped in the Manganui Roads.

In the vicinity of Pilot Bay, the appropriate conditions are provided by Centre Bank and the Otumoetai foreshore. The water depths and available basin lengths closely approximate the conditions discussed above. Further, the observed variations in seiche amplitude and frequency may be accounted for by the changes in water depth and current velocities across Centre Bank due to tides.

6.3.1 - Cusps on Pilot Bay beach

On one occasion during the study period, cusps formed along the renourished portion of Pilot Bay beach. Two distinct sets of cusps formed, corresponding to high and low water. The cusps were surveyed the day after they formed (S. Fox, 1984, pers. comm.), and the mean wavelengths were 122.7m and 77.4m for the high and low water cusps respectively (Fig. 6.6). Beach cusps may form in response to edge waves generated by incoming waves (Bowen and Inman, 1969), in this case sieches, with the cusp spacing being equal to the wave length of the edge waves (L_e). From Linear Wave Theory it can be shown that L_e is given by:

$$L_e = g.\sin[(2n+1)s]/(2\pi f^2) \quad \ldots 6.5$$

It is possible to rearrange Equation 6.5 in order to calculate frequencies capable of generating the observed cusps given that the mean beach slope was 0.06 when the beach was surveyed. By applying Equation 6.4 to the first 20 edge wave harmonics, the required basin lengths and water depths could be calculated. The observed cusps could form under the same conditions as the seiches discussed above (B=3.5-4.5km, h=2-4m) for the fundamental edge wave mode (n=0). This mode involves waves seiches with a frequency range of 0.03478-0.02762Hz (28-36s) between low and high water conditions. Waves within this frequency range were

detected in aerial photographs taken during the THS (Plate 5.1).

If the water depth and current velocities remained constant, standing waves could be generated between Pilot Bay and the Otumoetai foreshore and the cusps would be more regular than observed (Fig. 6.6). However, changing tidal conditions result in a continual shift in both the seiche frequency and the number of modes required to form the edge waves associated with the cusps. Only at high and low water would conditions be sufficiently stable to allow the development of rhythmic shoreline features.

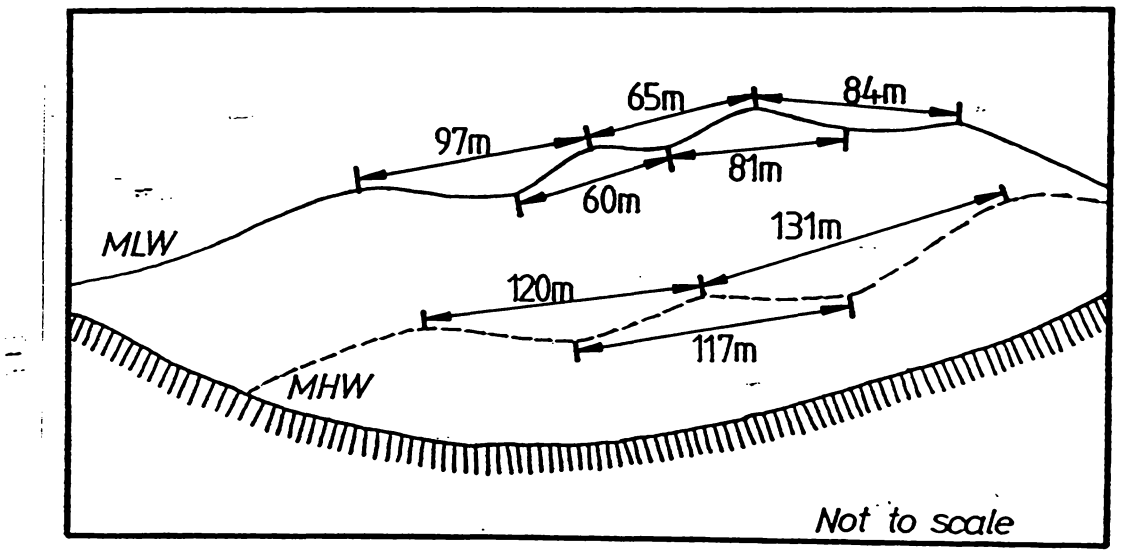

Figure 6.6 - Cuspate features developed on the renourished portion of Pilot Bay beach following a northeasterly storm, 1-2/5/84. Surveyed by S. Fox (pers. comm., 1984).

6.4 - Summary

Three main types of non-tidal low frequency waves have been recorded within Tauranga Harbour; tsunamis, storm surges and seiches. This study has concentrated on seiches produced by external forcing. Two main forcing mechanisms have been considered; tsunamis and meteorological processes.

Spectral analysis of tide gauge records reveals the presence of a consistent series of seiche frequencies. These are attributed to oscillations trapped over Centre Bank, between Pilot Bay and the Otumoetai foreshore. The dominant frequency fluctuates between 0.0039-

0.0045Hz (220-265s) during the tidal cycle. The formation of cusps on Pilot Bay Beach indicate the presence of another important wave component associated with northeasterly storms, with a frequency range of 0.0276-0.0348Hz (28-36s).

Chapter 7 - Sedimentological Observations Within Pilot Bay

This chapter presents the results of a beach monitoring programme and assesses the medium term (10-20y) impact of beach renourishment for Pilot Bay. Textural changes in the surficial sediments along Pilot Bay Beach are evaluated for an 18 month period following renourishment, and the net sediment flux for the beach determined.

7.1 - Beach nourishment and monitoring programme

During 1984-1985, the BOPHB undertook maintenance dredging of the shipping channels and turning bay at the junction of the Cutter Channel, Maunganui Roads and Pilot Bay channel (Fig. 7.1). The initial phase of dredging, during February and March 1984, involved a cutter suction dredge which discharged the spoil onto the southeastern end of Pilot Bay beach. A total of 20,000m^3 of sediment was dumped and redistributed on the beach from Salisbury Wharf to Pacific Ave, a linear distance of ~350m.

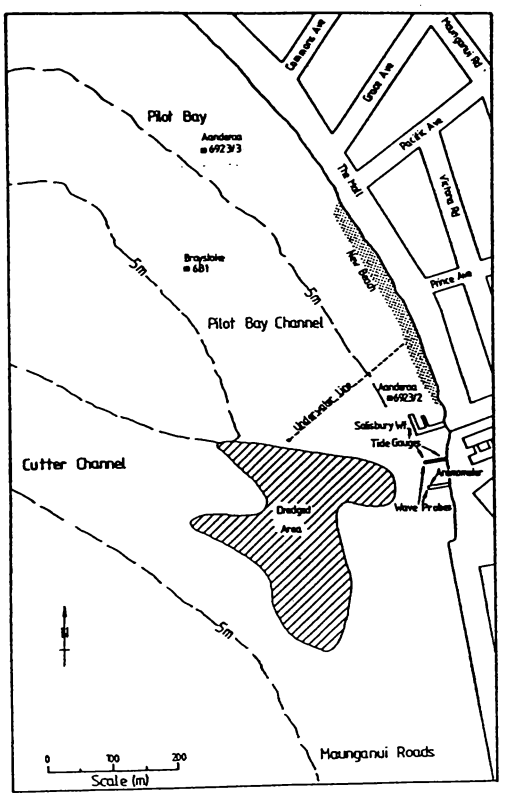

Figure 7.1 - Location diagram of the dredged region and the restored section of Pilot Bay beach (stippled area).

7.1.1 - Profile measurements

The BOPHB installed several survey lines across the proposed beach nourishment area and the adjacent beach to the north prior to the commencement of dredging (Fig. 7.2). These were used to plan the contours of the new beach. Subsequent to the dredging these lines were periodically resurveyed (Table 7.1) and, while each land survey was in progress, the bathymetry of Pilot Bay adjacent to the new beach was usually resounded.

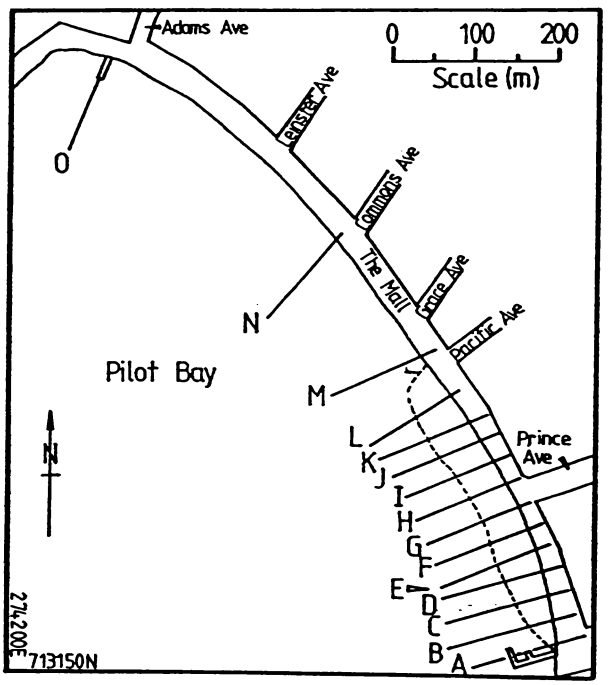

Figure 7.2 - Location diagram for beach profile survey transects. After BOPHB plan 113.

The surveyed profiles and sounding data were digitised from BOPHB plans and analysed to determine changes between successive profiles. Variations between profiles can be quantified as volumetric differences (Healy, 1978), expressed as m^3/m or m^3/m^2, or as the distance to a given beach contour (Holland and Kirk, 1985). To allow comparisons between surveys, the following parameters were determined for the longest profile section common to all surveys along any given transect:

a) the distance to specified elevations;

b) the beach slope at specified elevations;

c) the elevation at specified distances;

d) the unit volume (m^3/m) above and below chart datum; and

e) the unit volume (m^3/m) above specified elevations.

Table 7.1 - Survey dates and the transects covered by the BOPHB along Pilot Bay Beach. The days elapsed are determined as from 16/12/83.

Date	Days elapsed	Transects surveyed
30 Mar 83	-261	A B C D E F G H I
16 Dec 83	0	A B C D E F G H I J K L M N
4 Apr 84	111	A B C D E F G H I J K L M N
18 Jun 84	186	A B C D E F G H I J K L M N
17 Aug 84	246	A B C D E F G H I J K L M N
30 Nov 84	351	A B C D E F G H I J K L M N
13 Feb 85	422	A B C D E F G H I J K L M N
13 Aug 85	603	A B C D E F G H I J K L M N O
2 Dec 86	1080	B C D E F G H I J K L M N O
17 Jul 87[a]	1308	B C D E F G H I J K L M N O
7 Oct 87	1390	A B C D E F G H I J K L M

[a]Soundings only

The beach profile data were adjusted so that the horizontal datum corresponded to the top of the gabion basket sea wall. Standard elevations corresponding to mean sea level (0.98m), mean high water (1.69m) and mean low water (0.28m), were chosen for distance calculations (Fig. 7.3). The beach slopes and unit volumes were also determined for these elevations, so that possible differences between high and low tide sediment transport regimes could be examined. Finally, elevations were determined at distances of 2, 22 and 42m from the sea wall, which corresponded to surficial sediment sampling sites.

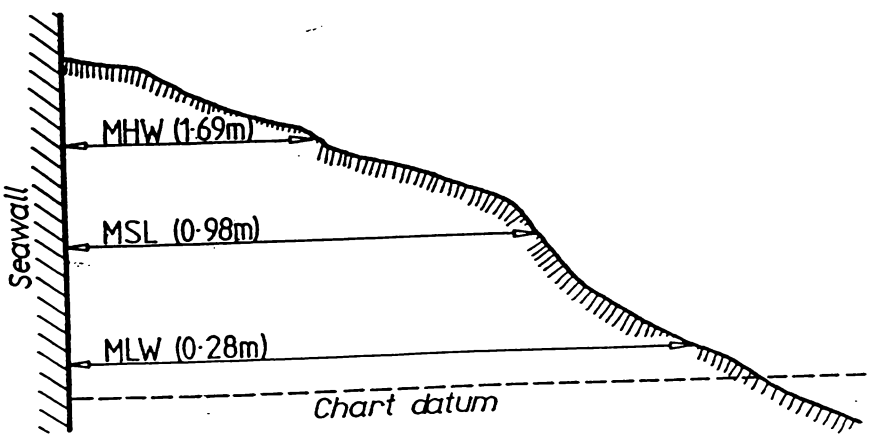

Figure 7.3 - Definition diagram of the distances determined for Pilot Bay beach profiles.

7.1.2 - Surficial sediment sampling

To monitor the short term changes in beach texture, surficial sediment samples were taken from Pilot Bay beach at approximately regular intervals for the first 12 months during and following the completion of dredging and irregularly subsequent to that period (Table 7.2). The samples were taken from 11 transects spaced every 100m along Pilot Bay beach (Fig. 7.4). Along each transect, samples were collected at 2, 22 and 42m from the top of the gabion basket seawall unless the water was too deep.

Table 7.2 - Surficial sediment sampling dates for the Pilot Bay beach monitoring programme. The days elapsed are after 16/12/83.

Date	Days elapsed	Number of samples
9 Mar 84	85	13
13 Apr 84	120	25
16 May 84	152	25
12 Jun 84	180	27
13 Jul 84	211	28
15 Aug 84	244	27
11 Sep 84	271	30
8 Oct 84	298	32
6 Nov 84	327	32
18 Dec 84	369	32
17 Jan 85	399	32
19 Feb 85	432	32
3 Jul 85	567	32

Each sample was collected with a square-mouthed coal shovel from the top 10-20mm of the beach profile and a total sample weight of 200-400g was taken. The samples were dried (75°C) immediately after collection to facilitate storage. For textural analysis, 50-100g splits were washed over a 4ϕ seive to remove salt and sediment finer than 4ϕ in size (silt and clay); any clasts coarser than -3ϕ (pebble) were picked out by hand. The prepared samples were then analysed in the University of Waikato Rapid Sediment Analyser (RSA) to determine size and settling velocity parameters (Appendix 4). This study used the settling velocity results for subsequent analyses.

At least two samples from each collection period were analysed twice to check the reproducibility of results. All parameters determined in

the repeated analyses deviated by <1%, except for Passega's C statistic. This parameter corresponds to the size of the coarsest 1% of the sediment, which for Pilot Bay sediment samples represented whole shells. Different falling modes (Appendix 4) and variable numbers of shells present in the sub-samples account for the differences.

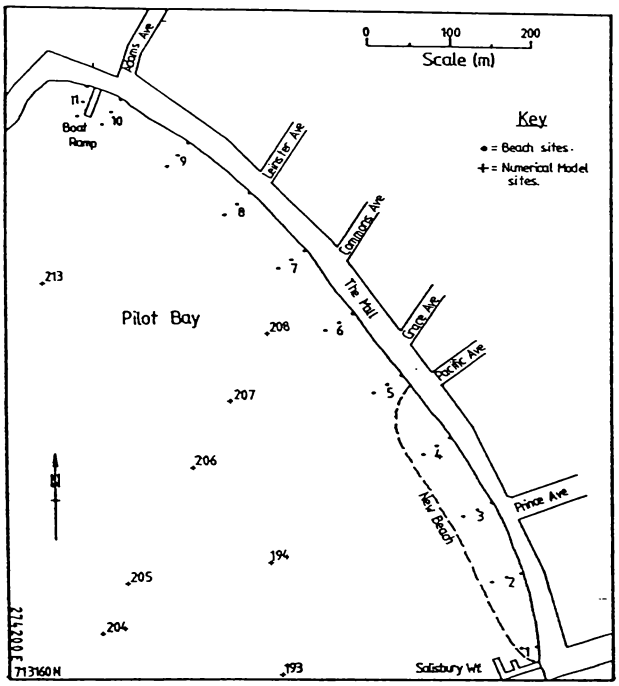

Figure 7.4 - Location of surficial sediment collection sites used during this study. Three digit site numbers are THS seabed sample sites.

In addition to surficial sediment samples from the beach, THS seabed sample sites within the bay were re-examined periodically and resampled on 27 July 1984.

7.1.3 - Sediment transport measurements

Bedload sediment fluxes within the intertidal regions of Pilot Bay beach were measured using VUV sediment traps based on plans presented by Graf (1971). These sediment traps are reported to have a ~70% sampling efficiency (Graf, 1971), although this varies considerably depending on the sediment grain size and the transport flux. Comparative studies under controlled conditions suggest that the VUV traps are the best samplers available for unidirectional flow in open channels having sediment sizes of -3ϕ to 3ϕ (Graf, 1971; Hubbell *et al*, 1987).

Black (1983) compared the responses of VUV traps to pit traps for intertidal flats within Whangarei Harbour. His findings indicated that the VUV traps were more efficient, although partitioned pit traps gave a good indication of the direction of net sediment transport. Tests of the same traps carried out in this study confirmed Black's findings.

Accordingly, for determination of the net sediment flux along Pilot Bay beach, 4 VUV samplers were deployed in a cross-formation (Fig. 7.5) at various locations. From diver observations it was apparent that virtually no bedload transport occurred in the deeper regions of Pilot Bay, so bedload measurements were confined to the shallow platform adjacent to the beach, slightly below low tide.

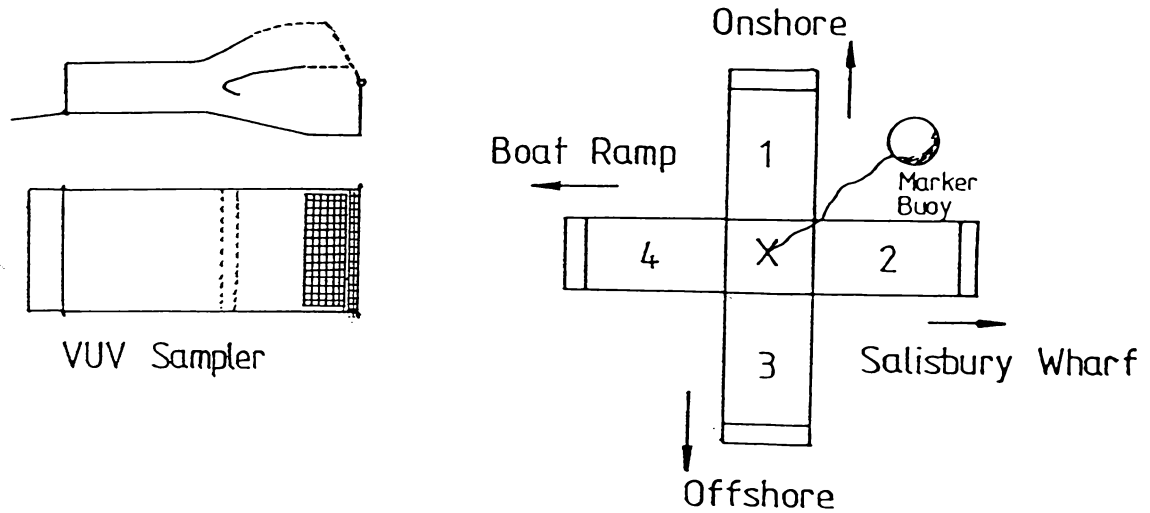

Figure 7.5 - Schematic diagram showing the VUV sampler as deployed and the arrangement of 4 samplers used to get an indication of net sediment transport directions.

Unfortunately, the deployment of these particular sediment traps suffered in two respects:

a) The high flat sides offered considerable resistance to the passage of waves and tidal currents, causing localised scouring around the traps. The eroded material may have contributed to the measured sediment fluxes and the scouring displaced the traps from their initial positions; and

b) The traps were frequently interferred with by other beach users.

Due to these problems, the traps were not used extensively.

Suspended sediment samples were obtained with a Mannings S-4050 water sampler (Plate 7.1) connected to a tripod which fixed the sampling depth at 1m above the bottom and directed the sampler orifice into any

currents present. The pumping system used in the Manning S-4050 was capable of pumping to a 10m head and was found to cope with >45m of hose below water level. The sampler collected 24 samples of 500ml at either 30 or 60min intervals.

The water samples were then sieved through preweighed 1.2μm micropore glass-fibre filters. After oven drying for 24h, the filters were reweighed and the weight of sediment determined by difference. Selected filters were examined under a binocular microscope to check the nature of the accumulated material.

Only two minor problems were experienced: the batteries used to power the system discharged faster than expected; and the pre-sampling purge cycle caused the sampler hoses to float, resulting in a minor navigation hazard. These problems posed a few difficulties for locating and servicing the system. Consequently the system was only deployed from the BOPHB Tug Berths and Salisbury Wharf.

7.2 - Survey changes 1983-1987

The analyses performed were based on segments of survey lines common to all the surveys considered. Therefore the data represented only a limited portion of the total renourished beach. The total volumetric change calculated for the region common to all surveys (IS.A to IS.L), during the period between 16 December 1983 and 4 April 1984, was 13,000m^3.

Records kept by the dredge operators indicated that a maximum volume of 20,000m^3 had been pumped onto the beach. The region from which the sediment had been extracted was resounded after the dredging and the volume removed was determined to be ~18,000m^3 (J.C. Stephenson, Pers. comm., 1984). Thus the surveys considered by this study account for ~65% of the material transferred to the beach during renourishment.

7.2.1 - Pilot Bay beach profiles

Since one of the aims of the renourishment was to enable better public utilisation of the beach, it is useful to consider the observed changes above MLW separately. The addition of dredge spoil to the beach at the southeastern end of Pilot Bay provided ~5 times more beach area at MLW

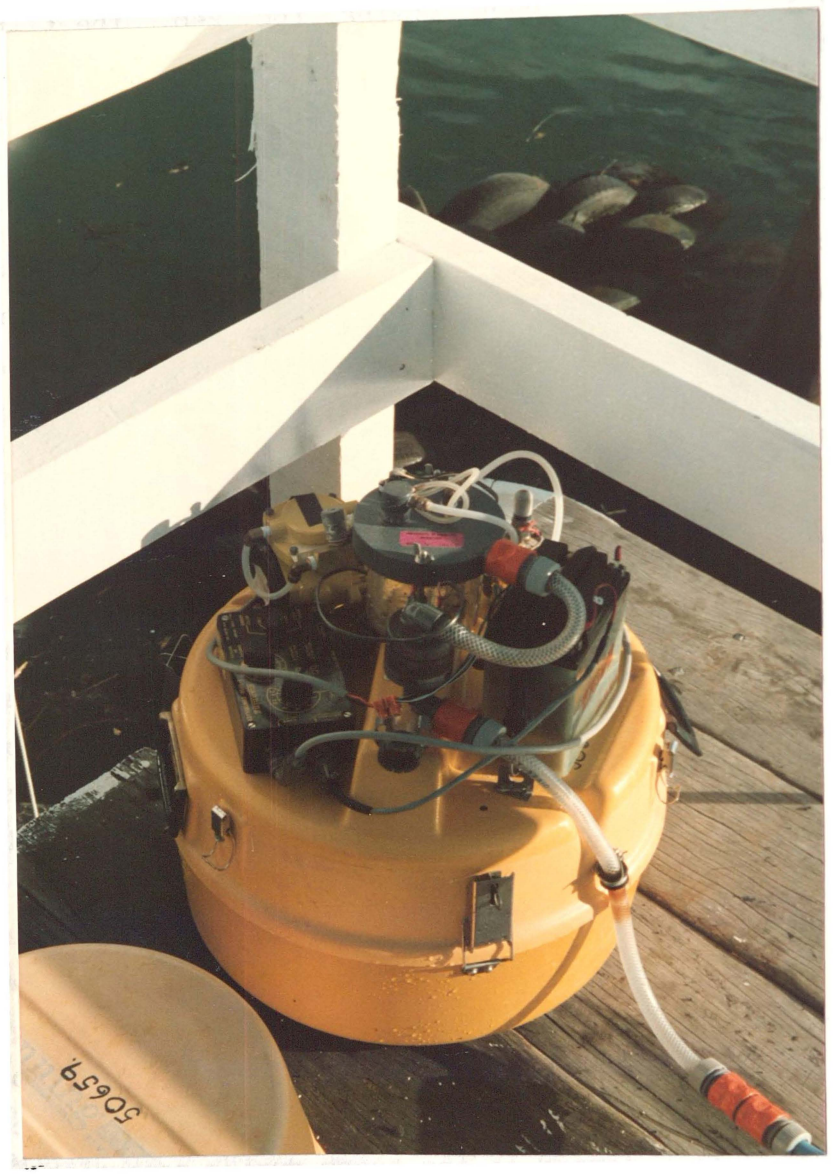

Plate 7.1 - Manning S-4050 water sampler used to collect suspended sediment samples within Pilot Bay.

(Fig. 7.6).

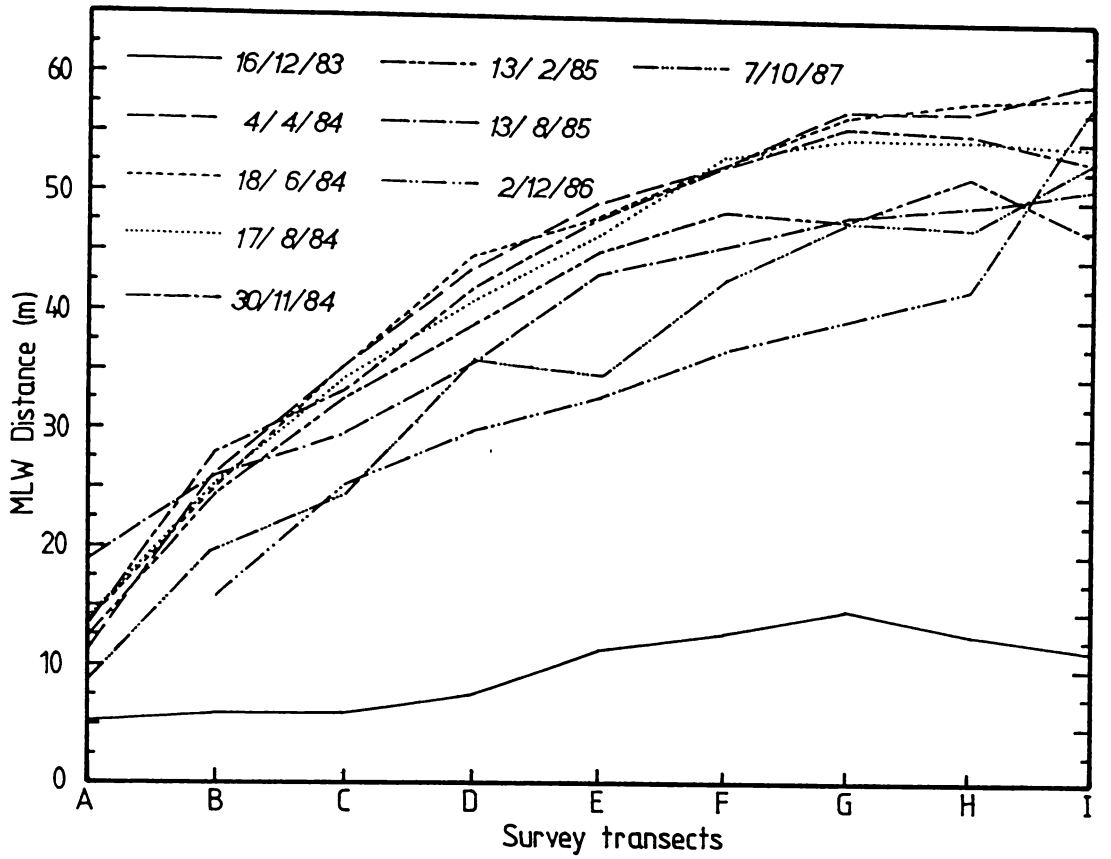

Figure 7.6 - Distance to MLW for sites IS.A to IS.I during the period December 1983 to October 1987.

The artificial beach face was steeper (s=4°30') than the pre-existing beach (s=1°40') so that the seaward movements of higher elevations of the beach profile were greater than observed at MLW. MHW was immediately adjacent to the seawall for most of the southeastern end of Pilot Bay (Sites IS.A-IS.I) prior to renourishment. After dredging and landscaping of the spoil was complete, MHW lay 10-30m seaward of the seawall.

The distances measured during the period December 1983 to October 1987 are summarised for MLW and MHW in Tables 7.3 and 7.4 respectively. Most of the beach has experienced continual erosion since the completion of dredging with an ~30% reduction in beach area in $2\frac{1}{2}$y. However, some localised zones of accretion are apparent, mainly at the ends of the original renourishment zone (e.g. IS.A).

Table 7.3 - Distances from the seawall to MLW (m) for Pilot Bay beach during the period December 1983 to October 1987 (Table 7.1).

Days elapsed	Transects								
	IS.A	IS.B	IS.C	IS.D	IS.E	IS.F	IS.G	IS.H	IS.I
0	5.2	6.0	6.0	7.6	11.4	12.9	14.9	12.8	11.4
111	11.0	26.2	35.3	43.7	49.2	52.8	57.5	57.6	60.2
186	13.5	25.0	35.4	44.7	48.2	52.8	57.0	58.4	59.0
246	13.7	25.3	34.3	40.9	46.6	53.4	55.1	55.1	54.5
351	13.2	27.9	33.3	42.0	48.0	52.5	56.0	55.5	53.2
422	12.2	24.5	32.7	38.9	45.2	48.8	48.0	51.8	47.0
602	18.8	26.0	29.7	35.7	43.4	45.9	48.4	49.4	51.0
1080		15.9	25.3	30.0	32.9	37.6	40.9	42.3	38.8
1390	8.8	19.7	24.5	36.0	35.2	43.0	48.0	47.3	53.7

Table 7.4 - Distances from the seawall to MHW (m) for Pilot Bay Beach during the period December 1983 to October 1987 (Table 7.1).

Days elapsed	Transects							
	IS.B	IS.C	IS.D	IS.E	IS.F	IS.G	IS.H	IS.I
0	0.0	0.0	0.0	0.0	0.0	1.8	0.0	0.0
111	9.1	18.3	20.6	22.6	22.8	29.6	28.4	20.0
186	7.4	15.1	21.1	22.7	26.2	29.3	28.4	27.8
246	6.9	12.8	17.2	18.2	25.7	24.4	27.7	26.5
351	6.7	12.6	16.9	20.5	25.5	27.1	26.0	25.6
422	8.0	13.9	18.5	22.8	27.7	30.1	32.0	26.2
602	7.3	13.4	18.6	24.0	28.4	30.3	29.9	28.5
1080	3.4	12.2	15.9	19.9	24.4	26.1	26.6	27.3
1390	3.4	8.3	12.4	15.5	18.6	20.1	20.0	17.3

The slope determined by regressing distance against time elapsed provides an indication of long term trends and rates of change (Holland and Kirk, 1985). Regressions were performed for MLW, MSL and MHW distances from the seawall. Given the limited number of data points used in the analyses, the results of these regressions should be treated with caution, especially with respect to predicted rates of advance or retreat. The regression results (Table 7.5) indicate that all the transects are retreating shoreward at average rates of 3-16mm/day. The rate of erosion varies within each profile, the highest rates tending to occur at MLW and the lowest at MHW (Fig. 7.7).

Table 7.5 - Summary of MLW, MSL and MHW distance regressions. The slope represents the average rate of accretion (+) or erosion (-) for the period April 1984 to October 1987, and life refers to the time required to erode back to the December 1983 position.

	IS.A	IS.B	IS.C	IS.D	IS.E	IS.F	IS.G	IS.H	IS.I
MLW									
Intercept	13.9	26.9	35.8	42.8	49.2	53.2	50.3	56.8	55.8
Slope $\times 10^{-3}$	-2.3	-7.1	-9.4	-8.7	-12.9	-11.2	-6.1	-10.7	-8.2
r^2	0.11	0.66	0.97	0.66	0.91	0.78	0.07	0.77	0.31
Life (y)	6.9	7.8	8.5	11.4	8.0	9.8	19.1	11.5	16.3
MSL									
Intercept	5.2	17.4	24.3	30.5	34.2	39.0	42.6	42.8	44.8
Slope $\times 10^{-3}$	-1.8	-6.2	-5.6	-7.6	-7.7	-8.8	-10.7	-11.1	-15.6
r^2	0.22	0.80	0.87	0.96	0.89	0.85	0.84	0.93	0.81
Life (y)	7.2	7.3	12.5	10.7	10.5	9.9	9.2	9.4	7.4
MHW									
Intercept		8.3	15.5	19.9	22.5	26.6	29.4	29.7	26.3
Slope $\times 10^{-3}$		-4.1	-5.1	-5.2	-3.9	-3.9	-5.3	-5.3	-3.2
r^2		0.83	0.68	0.75	0.38	0.32	0.46	0.47	0.13
Life (y)		6.1	9.8	10.9	15.9	16.1	14.4	14.7	17.1

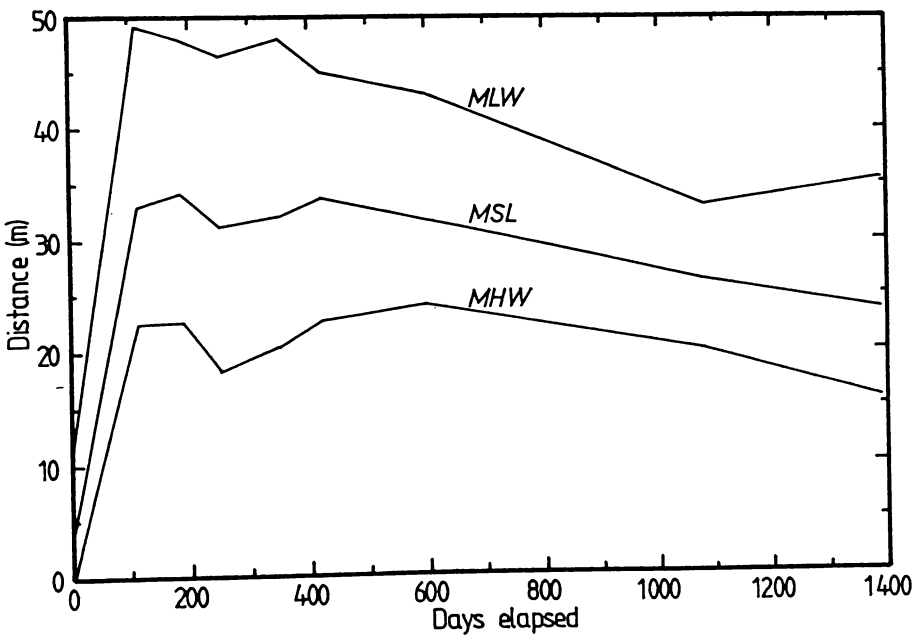

Figure 7.7 - MHW, MSL, and MLW distances for site IS.E, Pilot Bay. Although all show an erosive trend, the rate (slope) decreases with increased height above datum (see Table 7.5).

The approximate life of the renourished beach can be determined by dividing the distance gained through renourishment by the loss rate predicted by the regression analyses (Table 7.5). Although there is some scatter in the results, the expected life of the renourished beach

is ~7-16y, assuming that the long term rates remain more or less constant.

The behaviour of the renourished beach may also be considered in terms of volumetric changes. Unit volume data obtained for sites IS.A-IS.I (Table 7.6) have been used to calculate the sediment volume present in the central region of the nourished beach (IS.B-IS.E) during the period December 1983 to October 1987 (Fig. 7.8). This region originally contained ~50% of the sediment added during renourishment. It is evident that the beach volume has also been decreasing in conjunction with the shoreward retreat of MLW.

Table 7.6 - Unit volumes (m^3/m) above MLW for Pilot Bay beach transects.

Days elapsed	Transects								
	IS.A	IS.B	IS.C	IS.D	IS.E	IS.F	IS.G	IS.H	IS.I
0	0.4	0.6	0.8	0.7	2.2	4.3	9.8	4.7	1.9
111	2.6	25.1	44.1	44.6	44.9	50.5	60.5	65.8	59.7
186	4.2	23.9	42.1	47.3	47.8	57.5	61.3	66.1	66.0
246	5.5	22.2	37.1	41.7	41.6	56.7	51.5	67.1	63.6
351	4.9	22.1	37.0	40.9	43.8	55.0	61.3	63.6	55.9
422	5.3	22.7	37.4	42.6	47.2	56.7	64.9	70.5	54.5
602	8.5	21.4	34.8	41.5	47.3	57.4	66.6	66.0	54.9
1080		11.7	28.1	32.5	38.5	49.4	68.5	60.0	61.2
1390	1.8	13.8	24.1	31.1	33.1	40.7	50.1	49.5	32.9

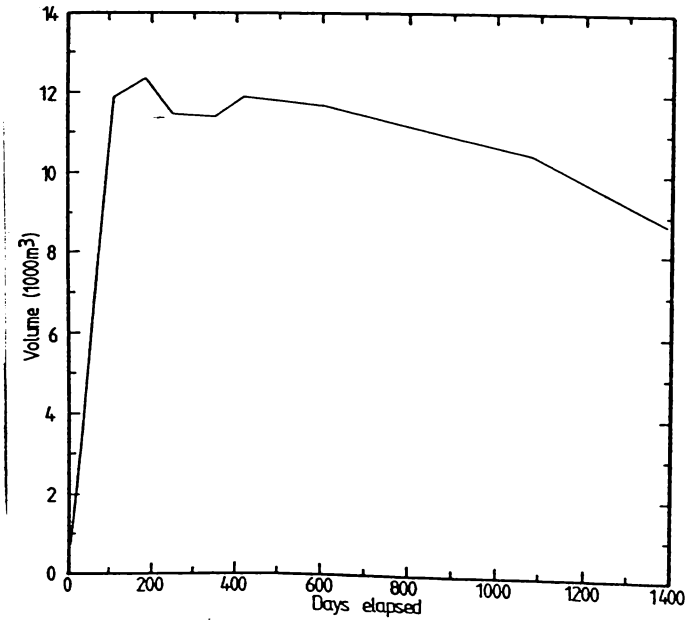

Figure 7.8 - Beach volume above MLW versus time elapsed for the region of Pilot Bay beach between sites IS.B and IS.I common to all surveys.

By regressing beach volume against days elapsed after completion of renourishment it is possible to predict the life of the renourished beach. Linear regression predicts an average erosion rate of $2.52m^3$/day for the period April 1984 to October 1987, which would remove the volume added during renourishment within 13y. Although the regression line is a reasonable fit (r^2=0.81), it probably represents an upper limit on the life of the beach since the rate of volume loss is increasing with time (Fig. 7.8).

7.2.2 - Discussion

Although the above analysis of trends considers uniform rates of erosion or accretion, the changes observed occurred episodically. A number of factors contributed to the measured beach profile changes, including: stormwater discharge from outfalls; maintenance work along the shorefront reserve, the Salisbury Wharf slip and the boat ramp; and storm wave activity. These factors and their effects will be considered briefly.

7.2.2.1 - Stormwater outfalls

Stormwater outfalls discharge across Pilot Bay beach at ~500m intervals between Salisbury Wharf and the boat ramp. During renourishment, no provision was made for extending outfalls through the new beach and several were completely blocked by sediment. Mt Maunganui City experiences many high intensity, short duration rain storms (Chapter 4). These result in large discharges from the outfalls along Pilot Bay.

One of these outfalls is located adjacent to Salisbury Wharf, coincident with site IS.A. During intense rainfall events, the discharge from the stormwater outfall entrained sediment from the beach and carried it offshore, building a small delta towards the wharf and reducing water depth on the shoreward side. To prevent further erosion and growth of the delta, the outfall was extended by 5m. The extension was undermined by continued erosion, requiring the placement of rock rubble to underpin the pipe (Plate 7.2).

Two major periods of delta advance associated with a series of high

Plate 7.2 - Southeastern end of Pilot Bay beach on 15 August 1984 showing stormwater discharge eroding the beach and remedial work underway to prevent further collapse of the extended outfall.

intensity rain squalls were observed; one in August 1984 and the other in September 1986. These two events account for the observed accretion of sediment at site IS.A (Tables 7.3 and 7.6).

The remaining outfalls within the renourished region were completely buried by sediment, preventing surface discharge. The rainfall event of August 1984 resulted in an accumulation of water in the stormwater system and minor street flooding eventuated. To relieve the build-up of water the blocked outfalls were cleared by excavating holes in the beach. The water was then discharged in these holes, ponding in the back beach area. Over successive rainstorms these ponding areas breached the berm and established embayments in the renourished beach.

Site IS.G coincided with one of the buried outfalls and shows a 16% reduction in beach volume between the June and August surveys in 1984 (186 and 246 days elapsed). The volume lost was due to the clearance of the outfall. Subsequent to the August survey, the transect line was shifted slightly to avoid the outfall, accounting for most of the sediment accumulation recorded.

7.2.2.2 - Maintenance work

Polypropylene break fences were erected by the Mt Maunganui City Council in May 1984 to prevent fine sand blowing inland from the renourished beach (Plate 7.3). This was followed up by spraying the partially stabilised back beach area with grass seed. The fence was erected along the approximate position of the buried seawall and grass planting extended 5-10m seaward of the fence. These measures stopped fine sand movement landward of the fence and severely limited it over the grassed area seaward of the fence. This situation was maintained until the summer period of 1984-85, when the turf established during the winter was disrupted by beach users. Since then the grassed area has retreated.

The region directly affected by these works was outside the area covered by the profile analyses. However, the disruption of the grass turf by beach users did affect the data obtained. The removal of the grass occurred during a period of predominant offshore wind within Pilot Bay. This caused in an influx of fine sand to the upper regions of the beach resulting in the measured accretion. The disturbed turf re-

Plate 7.3 - Polypropylene break fencing constructed adjacent to the renourished beach, May 1984. This fence effectively stopped the onshore movement of fine sand from the back beach area. The immediate area surrounding the fence was subsequently sprayed with grass seed, producing a reasonably continuous turf out to the position of the aluminium dinghy.

established itself by April/May 1985.

The grass turf was progressively undermined by continued erosion and by October 1987 little remained seaward of the seawall. The break fence was removed, except for the portions that had been completely buried. This permitted further onshore movement of sand during the winter of 1987.

The BOPHB maintain a small boat slip adjacent to Salisbury Wharf. The renourished beach initially did not extend as far as the slip. However, accretion in the vicinity of site IS.A buried the slip with 0.2-0.3m of sediment within 2-3 weeks of the completion of dredging. Subsequently, the slip was periodically cleared of sediment to permit access by boats at low tide, with the excavated sediment being deposited at MSL 20-30m westwards of the slip. Within 7-10 days of exhumation the slip was buried again. Therefore, the changes caused by slip clearance near Salisbury Wharf resulted in very temporary changes to beach profiles at Site IS.A, adjacent to the slip. None of the surveys were carried out immediately after removal of sediment from the slip.

The remaining major work carried out along Pilot Bay beach involved removal of sediment from the boat ramp at the northwestern end. After the completion of renourishment, sediment accumulated on the boat ramp, particularly within the intertidal zone, at a vertical rate of ~1mm/day. When the thickness of sediment became a problem for ramp users, the sediment was removed and piled on either side of the ramp above MHW. Large piles of sediment built up either side of the boat ramp during the period 1984 to 1987. Although a sounding transect was located along the centreline of the boat ramp, the sediment accumulation was not included in any surveys undertaken.

7.2.2.3 - Wave activity

Local wind-generated waves were observed to cause major changes in the renourished beach profiles on several occasions during the period 1984 to 1985. Westerly to northwesterly (270-290°) winds with speeds of 10-15ms^{-1} and 6-12h durations, generated a steep chop (H_s=0.3m, T=2s) which cut into the higher regions of the beach, particularly near MHW, leaving a steep berm (Plate 7.4) and liberating pumice which choked the swash zone. Several wind events were associated with measurable changes to

Plate 7.4 - Erosion at the southeastern end of Pilot Bay beach on 13 April 1984, shortly after completion of landscaping of the renourished beach.

the beach profile during the period 1984-1985 (Table 7.7). The events listed represented 70% of the total number of intervals longer than 3h in which wind speeds >10ms^{-1} were recorded.

The first windy period after completion of dredging cut the greatest depth at MHW, probably since the sediment had not been greatly compacted or modified after deposition. The height of the cut face diminished rapidly after this initial period of erosion. The events of May 1984 and February 1985 are notable in that both were associated with the formation of beach cusps (Section 6.3.1). These two events had higher mean wind speeds than the others considered, but one involved onshore and the other offshore winds.

Table 7.7 - Major wind events observed during the period 1984-1985 and the height of the associated vertical cut at MHW on the renourished portion of Pilot Bay beach. The wind speed and direction data represent average conditions during the duration specified.

Date	Days elapsed	Wind speed (ms^{-1})	Wind direction (°)	Wind duration (h)	Berm height (m)
7- 8 Apr 84	114-115	12.4	287	14	0.45
1- 2 May 84	137-138	14.6	264	23	0.25
9-10 Jun 84	168-169	10.4	277	33	0.20
10-15 Aug 84	239-244	10.8	105	123	0.05
28 Sep 84	288	11.0	261	17	0.10
21-22 Oct 84	311-312	12.0	267	29	0.05
16-17 Feb 85	429-430	13.9	104	14	0.10
14-15 Jun 85	547-548	10.6	67	30	<0.05
16-18 Sep 85	637-639	11.0	92	65	0.05

Although the long period of strong winds during August 1984 did not result in a large cut face in the beach profile, the intense rain associated with this storm did cause considerable erosion in the vicinity of storm outfalls, as discussed above.

7.3 - Textural changes 1984-1985

The prenourishment beach sediment was quite coarse (Plate 7.5), mainly due to the concentration of shells and pebbles on the surface. At both ends of the beach, significant quantities of cobbles and boulders were present: the northwestern region being supplied from the rhyolite dome

of Mt Maunganui; and the southeastern end from the gabion basket seawall and fill used in wharf construction. These larger clasts showed no evidence of wave or tidally induced transport at any stage during the period January 1982 to July 1987, except for some settling due to scouring of underlying sediment.

The dredged sediment used to renourish the beach was taken from a megarippled sand facies region (Plate 3.5). This material differed from the original beach sediment, mainly due to a lack of staining on the clasts. Samples of the sediment discharged by the dredge were collected from the dredge outfall in April 1984, as well as a limited number of samples of the original beach sediment. The dredge spoil samples (χ_{50}=3.97χ) are similar to the original beach sediment (χ_{50}=4.12χ) on the basis of mean settling velocity.

However, the dredge spoil is positively skewed (Sk=0.58), whereas the original sediment is negatively skewed (Sk=-0.50). The overall χ distributions do differ (Fig. 7.9), with the original sediment being slightly bimodal with one peak at 2.25-2.5χ and the other at 4.25χ, whereas the dredge spoil is unimodal at 3.5-3.75χ. The two sediments were distinguished in the field by visual characteristics (Table 7.8), which mainly reflected compositional variations and staining (Plates 7.5 and 7.6).

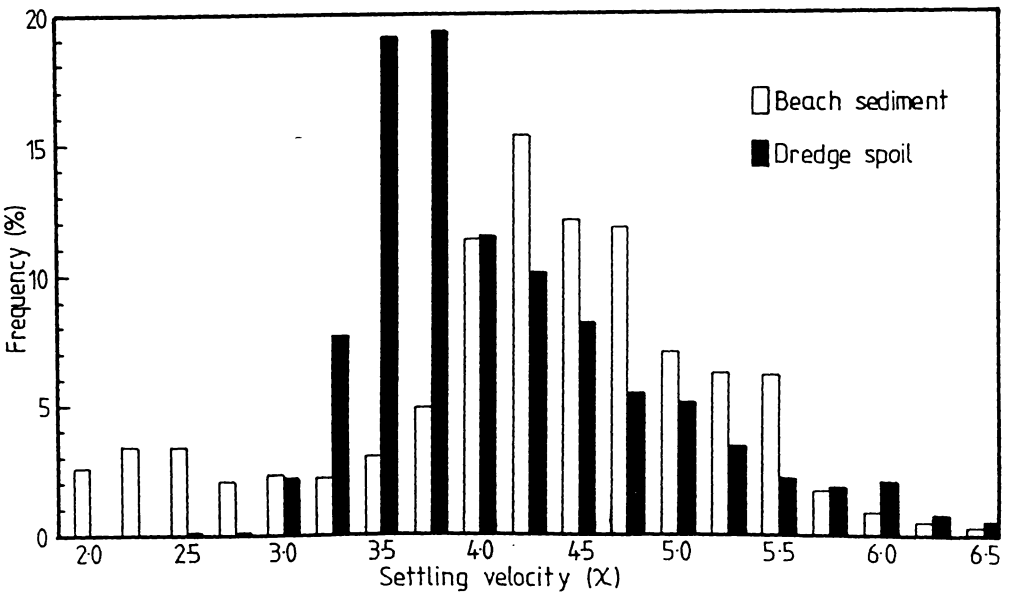

Figure 7.9 - Percentage frequency versus settling velocity (χ) for the original beach sediment and dredge spoil. These distributions represent the average of 5 beach samples and 3 dredge spoil samples.

Plate 7.5 - Surficial sediments on Pilot Bay beach at site IS.D near MSL prior to renourishment (July 1983). The sediments exposed consist of a mixture of pebbles and shell fragments, mainly of *Chione stutchburyi*. The lens cap is 49mm in diameter.

Plate 7.6 - Surficial sediments near MSL at site IS.D, 6 months after renourishment. The dominant shell present is pipi (*Paphies australis*) and some pebbles are exposed. The lens cap is 49mm in diameter.

Table 7.8 - Summary of the visual characteristics used to distinguish dredge spoil from original beach sediment in the field.

	Original sediment	Dredge spoil
Dominant shell	*Chione stutchburyi*	*Paphies australis*
Staining	Present	Absent
Pumice	Absent	Present
Titanomagnetite	Common	Rare
Pebbles	Common	Rare

The texture of the surficial sediments was monitored to examine the changes which occurred as dredge spoil was eroded and mixed with original beach sediment *in situ* and further downdrift.

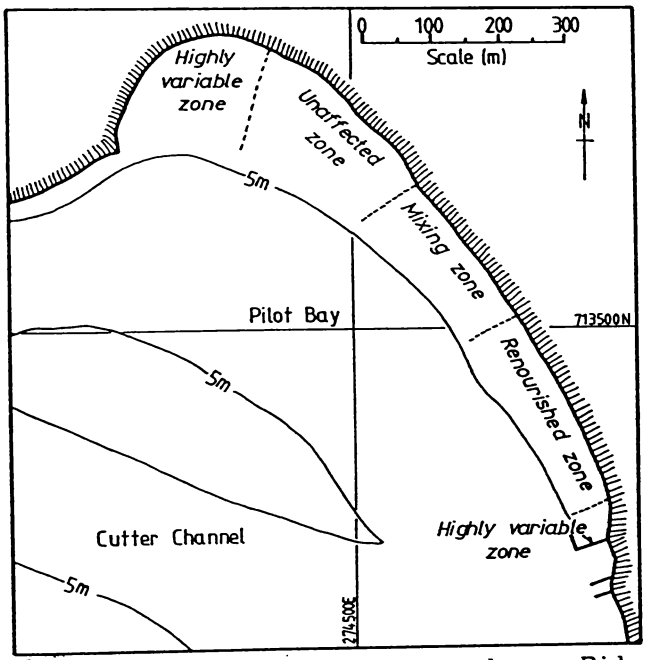

Figure 7.10 - Textural zones determined along Pilot Bay Beach from temporal variations of mean settling velocity (χ_{50}) and sorting (σ).

From the observed temporal variations in the textural parameters, several zones could be distinguished along Pilot Bay (Fig. 7.10):

1) Renourished zone. Initially this contained dredge spoil which was progressively eroded and reworked as time elapsed. In the upper and middle reaches of the beach mean settling velocity (χ_{50}) and sorting (σ) remained fairly constant (Fig. 7.11). The lowest part of the beach sampled became coarser and more poorly sorted with time, mainly due to the accumulation of a shell and pebble lag (Plate 7.6);

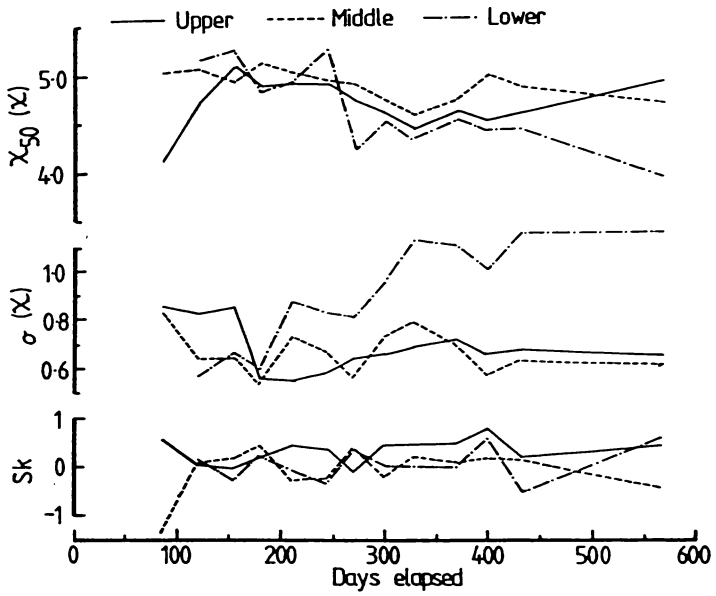

Figure 7.11 - Mean settling velocity (χ_{50}), sorting (σ) and skewness (Sk) for sampling site 3. The temporal variations shown are typical of a renourishment zone.

2) Mixing zone. Initially this contained original beach sediment which was progressively buried by, and mixed with, dredge spoil. The lower and upper parts of the beach remained fairly constant (Fig. 7.12), whereas the intertidal region became progressively coarser and switched from negatively skewed to positively skewed;

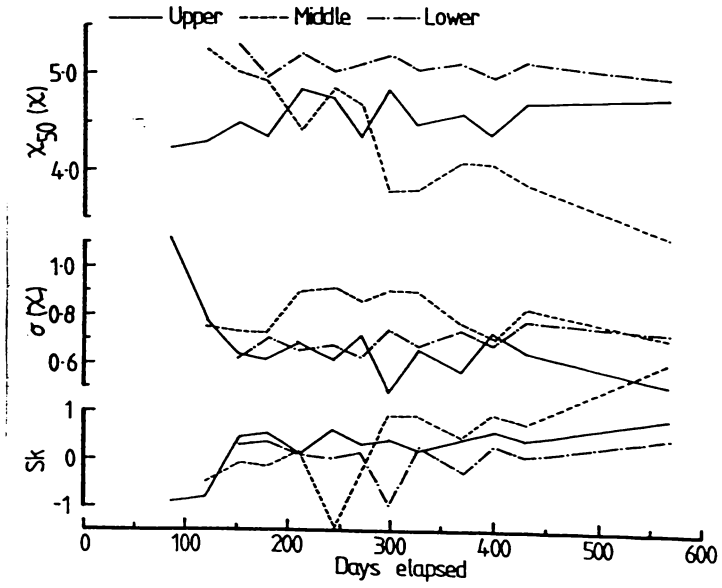

Figure 7.12 - Mean settling velocity (χ_{50}), sorting (σ) and skewness (Sk) for sampling site 5. The temporal variations shown are typical of a mixing zone.

3) Unaffected zone. No major changes occurred during the sampling period; and

4) Highly variable zone. The values of χ_{50} and σ changed markedly with time.

The patterns observed in the renourished and mixing zones can be attributed to the removal of fine to medium sand from the surficial sediment within the renourished beach and subsequent deposition and mixing with the beach sediments downdrift. The unaffected zone showed little or no indication of addition of sediment derived from dredge spoil during the sampling programme. The highly variable zone located at the southeastern end of the beach is adjacent to the stormwater outfall and slip discussed earlier and the 22m-distant samples were obtained from the delta constructed by discharge from the outfall.

The other highly variable zone at the opposite end of the beach shows quasi-periodic variations in mean settling velocity (Fig. 7.13). The finer samples (largest χ values) contain low density clasts, mainly pumice, bark and granulated plastics, which are absent in the coarser samples. The presence of pumice within sediment samples collected at site 11, was usually preceded by accumulations of pumice within the swash zone along the length of the beach, particularly the western end. The observed textural variations at site 11 are therefore attributed to influxes of low density sediment causing an increase in χ_{50}.

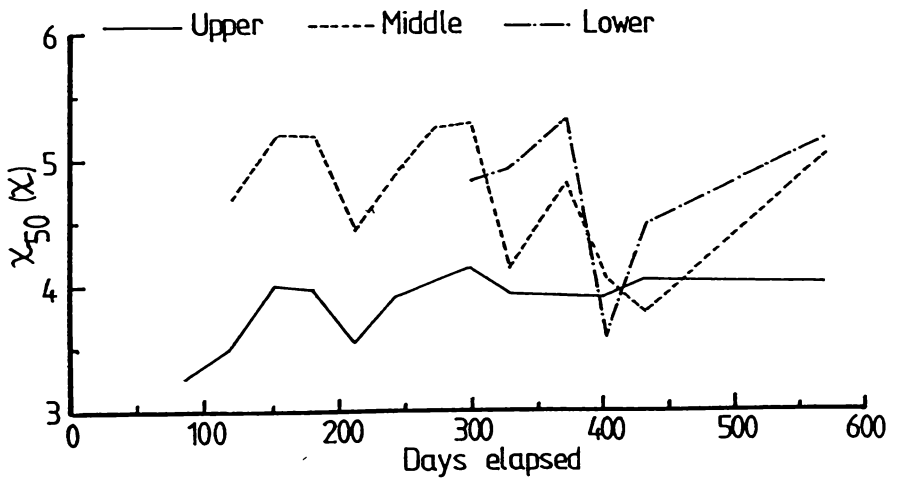

Figure 7.13 - Temporal variations of mean settling velocity (χ_{50}) for sampling site 11.

The main source of low density sediment is pumice eroded from the renourished beach, although some material is produced by bulk cargo

loading and unloading, particularly of wood chips, raw logs, shredded paper, granulated plastics and sulfur. This sediment is easily transported along the length of beach, but is held up at the northwestern end of the beach by tidal eddies and very low currents (Chapter 3). Eventually, most of the low density sediment is lost, either by degradation in the case of pumice and other weak materials, or by transport out of the bay.

7.3.1 - Texturally determined transport directions

Textural parameters have been used as indicators of sediment transport direction (Leeder, 1982). One model which has been applied in New Zealand at Mangatawhiri Spit with some success (Bridgwater, 1986), is the model proposed by Sunamura and Horikawa (1972). This model relates the spatial variations of mean grain size (ϕ_{50}) and sorting (σ) to sediment sources. The transport direction may be inferred if one of four patterns of variation is found (Fig. 7.14). Any other pattern is considered inconclusive.

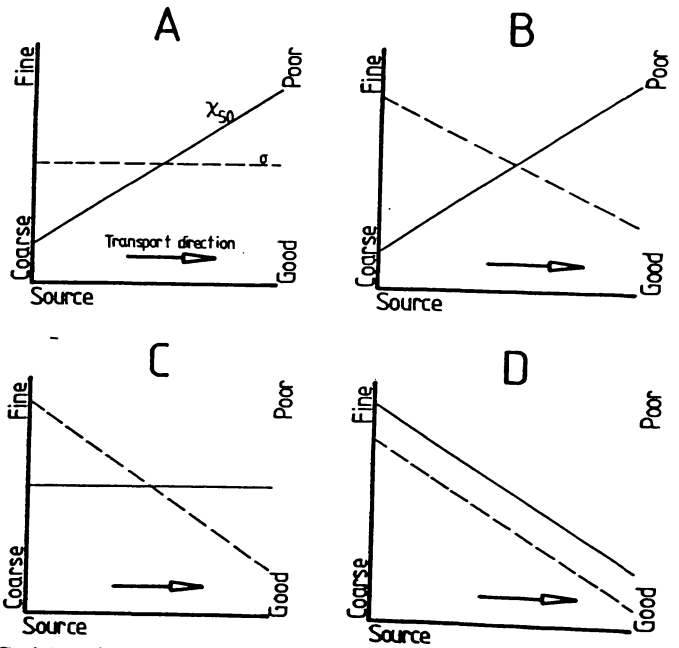

Figure 7.14 - Criteria for the inference of sediment transport direction from mean settling velocity (χ_{50}) and sorting (σ). Modified from Sunamura and Horikawa (1972).

In the original model the textural parameters are derived by the moment method from sieved data (Sunamura and Horikawa, 1972), whereas Bridgwater (1986) derived the parameters from sieve data using graphical

methods. Both approaches gave sensible results for the beaches analysed. In this study, χ parameters derived by the moment method are substituted for the ϕ parameters in the original model. Since the model is based on the relative trends of size and sorting, and not quantitative values, this modification should not affect the validity of the approach.

Transport directions were determined for each of the surficial sediment sampling periods (Fig. 7.15). The dominant transport direction is from site 1 toward site 11, or from the southeastern end of the beach towards the northwest. This is consistent with the residual tidal flows discussed in Chapter 3.

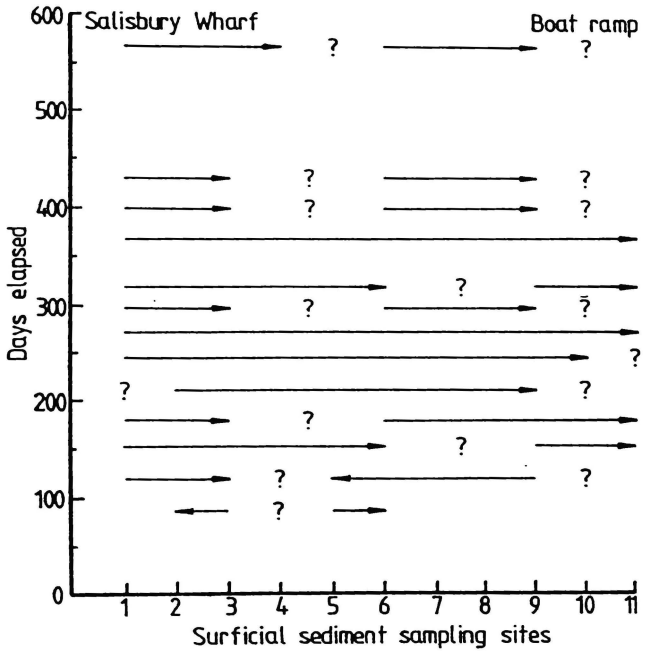

Figure 7.15 - Sediment transport directions, inferred from textural characteristics of sediment samples collected 22m from the seawall, for Pilot Bay beach during the period April 1984 to July 1985.

7.4 - Measured sediment fluxes

7.4.1 - Bedload

The traps were deployed on beach survey section IS.E for 5 tidal cycles during the period 14-16 August 1984 (Table 7.7). For most of the sampling period, small (H_s<0.10m) short period (T=1.5-3s) waves were experienced along Pilot Bay beach.

The average weight of sediment accumulated in each trap (Table 7.9) was converted to a mass flux by assuming a sampling duration of ½ tidal cycle (22350s). To enable comparison with the annual sediment fluxes predicted by the sediment transport model 2SS, the mass fluxes have been converted to approximate annual volume fluxes by further assuming a sediment grain density of 2650kgm^{-3} and a packing factor of 0.6 (Komar, 1976). No corrections were made for the efficiency of the VUV trap since all available correction factors are based on unidirectional channel flow (Hubbell *et al*, 1987) and not oscillatory flow in an intertidal zone.

Table 7.9 - Bedload sediment fluxes for Pilot Bay beach during the period 14-16 August 1984. The directions and numbers correspond to Figure 7.5.

	Offshore (1)	Onshore (3)	Northwest (2)	Southeast (4)
MSL				
Average weight (g)	1854	1924	2327	630
Mass flux ($\times10^{-6}$kgm^{-1}s^{-1})	166	172	208	56
Volume flux (m^{3}m^{-1}y^{-1})	3.29	3.42	4.13	1.12
MLW				
Average weight (g)	1526	1410	1982	1047
Mass flux ($\times10^{-6}$kgm^{-1}s^{-1})	137	126	177	94
Volume flux (m^{3}m^{-1}y^{-1})	2.71	2.50	3.52	1.86

The sediment fluxes indicate that the dominant sediment transport direction during the sampling period was towards the northwest at both MSL (~3m^{3}m^{-1}y^{-1}) and MLW (~2m^{3}m^{-1}y^{-1}). The onshore/offshore sediment flux was an order of magnitude smaller, with a tendency for sediment to move offshore near MLW and onshore near MSL. The net longshore volume sediment flux agrees with the 2DD prediction (~3m^{3}m^{-1}y^{-1}) for the annual bedload sediment flux within Pilot Bay Channel (Black, 1984).

7.4.2 - Suspended load

Suspended load measurements were made in conjunction with current

velocity measurements (Table 7.10). All the current measurements were made at 1m above the bottom as close as possible to the sampler intake. Two different current meters were used, an Ono and an Aanderaa. The Ono current meter was extremely unreliable and failed to work on the second deployment (12/6/84), so it was replaced by an Aanderaa.

Table 7.10 - Deployment data for the Manning S-4050 water sampler and current meters used to determine suspended sediment fluxes at the southeastern end of Pilot Bay.

Period deployed	Location of intake	Number of observations	Current meter	Current meter location
16-18/5/84	713110N 274820E	34	Ono	713102N 274824E
12/6/84	713105N 274824E	14	Ono	713102N 274824E
14-17/8/84	713194N 274797E	47	Aanderaa	713231N 274776E
3-4/9/84	713190N 274793E	24	Aanderaa	713231N 274776E

The suspended load entering Pilot Bay contained small mineral grains and pumice clasts, some clays and variable amounts of organic matter, such as plankton, small fish and algae. All the material collected by the sampler was included in the suspended sediment load results. Therefore the measurements are slightly different from those conducted during the THS which ignored material finer than 4ϕ (Black, 1984). A few samples obtained by this study which appeared to have large quantities of fine material were passed through a 4ϕ seive. The material retained accounted for >95% of the sediment weight. Therefore the contribution of finer material to the mass sediment fluxes was considered to be negligible.

The suspended sediment concentrations varied throughout the tidal cycle, which can be attributed either to different sources of water or changing velocities in the source region for the suspended sediment. Treating samples with H_2O_2 revealed that organic matter comprised ~30% by weight for samples obtained within 2h of low tide and ~15% for samples within 2h of high tide. This possibly represents variations between estuarine and oceanic waters, although no data were available to test this.

One factor which significantly affected suspended sediment loads was stormwater discharge during rain events. The sampling period in August 1984 coincided with one such event. Each large peak in the suspended

sediment flux (Fig. 7.16) occurred shortly after a rain squall which produced high discharges from the outfall at the southeastern end of Pilot Bay Beach. The sampler intake was positioned immediately offshore from the outfall, ~7m below chart datum.

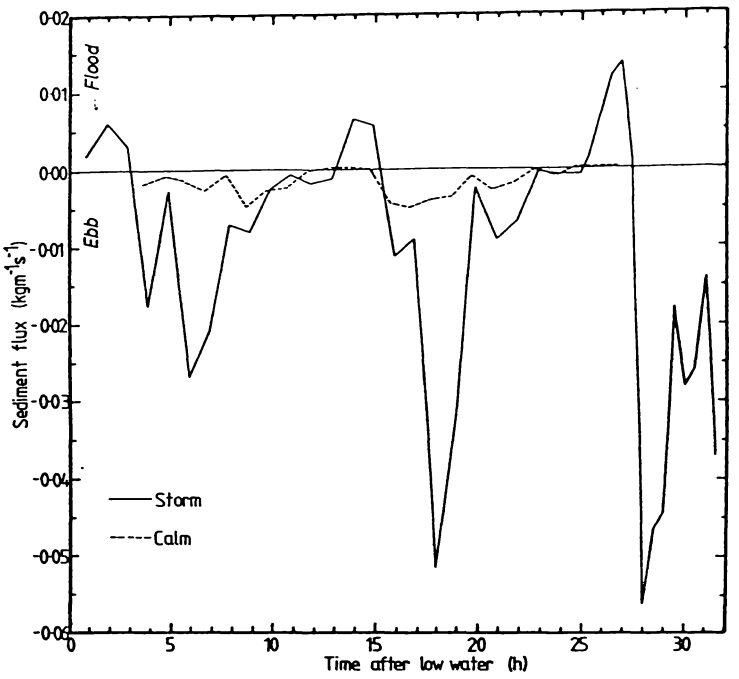

Figure 7.16 - Suspended sediment fluxes near Salisbury Wharf measured for storm and calm conditions during August and September 1984. The time elapsed is expressed as hours after the most recent low tide prior to sampling.

The sediment concentrations obtained were converted to sediment fluxes by multiplying each concentration with the corresponding velocity obtained at the nearby current meter. Ebb directed velocities (Chapter 3) were defined to be negative. Due to equipment malfunctions with the Ono current meter, only data obtained in conjuction with Aanderaa deployments could be converted to fluxes. Once sediment fluxes were determined, the net sediment flux at 1m was obtained by integrating the measured fluxes over time. The integrations were only performed for data sets which spanned complete tidal cycles.

The net 1m sediment flux obtained for Salisbury Wharf, excluding the tidal cycle affected by the stormwater discharge, was $670 \times 10^{-6} kgm^{-2}s^{-1}$ in the ebb direction (~330°). This is an order of magnitude lower than the net flux affected by stormwater discharge ($3780 \times 10^{-6} kgm^{-2}s^{-1}$). For normal tidal cycles the peak sediment fluxes were in the range $1500-1800 \times 10^{-6} kgm^{-2}s^{-1}$ during both ebb and flood tides, whereas the maximum

storm affected flux was $20590 \times 10^{-6} kgm^{-2}s^{-1}$.

Suspended sediment sample measurements were made by the THS within Pilot Bay (SS10), with each measurement consisting of one vertical profile taken as close to peak flow as possible (Healy, 1985). Using these data, Black (1984) derived suspended sediment fluxes of 2100 and $400 \times 10^{-6} kgm^{-1}s^{-1}$ for ebb and flood tides respectively. The THS results represent vertically integrated sediment fluxes, whereas this study only measured the 1m flux.

The 1m flux can be converted to a vertically integrated flux if the suspended sediment and velocity profiles are known. These can be approximated by using standard formulae derived for open channel flow. The distribution of suspended sediment in a water column is given by (Raudkivi, 1976; Fredsøe *et al*, 1985):

$$\frac{c}{c_a} = \left(\frac{h-y}{y} \cdot \frac{a}{h-a}\right)^z \qquad \ldots 7.1$$

where c = concentration,
c_a = concentration at reference height a,
y = distance above the sea bed,
and z = the Rouse number defined by:

$$z = \frac{s}{\beta \kappa u_*} \qquad \ldots 7.2$$

where s = settling velocity of the sediment,
β = correction factor (3.27),
κ = von Kármán constant (≈ 0.4),
and u_* = skin friction velocity.

The velocity profile for the lower 10-20% of the water column can be represented by the Kármán-Prandtl velocity law (Leeder, 1982; Black, 1983; Moon, 1983). This may be expressed as:

$$u = 5.75 u_* \log_{10}(y/k) \qquad \ldots 7.3$$

where k = roughness length.

The total suspended sediment flux, q_s can be derived by integrating

the product of equations 7.1 and 7.3 through the total water column. Raudkivi (1976) presents the following solution to this integral:

$$q_s = 11.6u_* c_a a[2.303\log_{10}(y/k)I_1+I_2] \quad \ldots 7.4$$

$$\text{where } I_1 = [0.216A^{z-1}/(1-A)^z]\int[(1-y')/y']^z dy \quad \ldots 7.5$$

$$\text{and } I_2 = [0.216A^{z-1}/(1-A)^z]\int[(1-y')/y']\ln y dy \quad \ldots 7.6$$

where $A = a/h$,
and $y' = y/h$.

For Pilot Bay, assuming that the ratio y/k in equation 7.3 can be replaced by $30.2/2D_{65}$ (Raudkivi, 1976; Black, 1983), the values of u_* varied between 0.0015 and 0.0107ms^{-1}. The mean settling velocity of a sample of the sediment collected by the Manning water sampler was 0.0065ms^{-1}, producing Rouse numbers from 0.4-2.3.

Equation 7.4 was used to estimate the suspended sediment flux and gave peak ebb and flood sediment fluxes from 3000-4000$\times10^{-6}kgm^{-1}s^{-1}$ for normal conditions, and 20000-50000$\times10^{-6}kgm^{-1}s^{-1}$ for storm conditions. The net suspended sediment flux was $1680\times10^{-6}kgm^{-1}s^{-1}$ in the ebb direction. These values are similar to the sediment fluxes reported by Black (1984).

7.4.3 - Total sediment flux

The total sediment flux through Pilot Bay is the sum of the suspended sediment flux and the bedload flux. The measurements taken by this study can be combined to give an indication of the net sediment flux in the vicinity of the renourished beach. Considering the longshore components of the bedload sediment flux only (Table 7.9), the net flux is $150\times10^{-6}kgm^{-1}s^{-1}$ in the ebb direction (northwest). Combined with the suspended sediment flux, the total sediment flux is $1830\times10^{-6}kgm^{-1}s^{-1}$ in the ebb direction.

The average erosion rate predicted by regression of the beach volumes ($2.52m^3$/day), can be converted to a sediment flux given an average beach width of 41.25m, a porosity of 40%, and grain density of $2650kgm^{-3}$. These values predict a sediment flux of $1120\times10^{-6}kgm^{-1}s^{-1}$. Given that the average erosion rate predicted by the regression, and the sediment

flux derived from measured fluxes, involve a number of gross approximations, the observed agreement may not be very significant.

7.5 - Pilot Bay beach sediment pathways

The erosion and transport of the renourished region of Pilot Bay beach is due primarily to the interaction of waves and tidal currents, and, to a lesser extent, stormwater discharges from outfalls along Pilot Bay. The tidal currents are generally below sediment threshold, but are capable of moving sediment entrained by either waves or stormwater discharge. However, in addition to tidal currents, sediment will move in response to currents induced by stormwater discharge and waves. The currents associated with stormwater discharge dissipate rapidly away from the outfall, so that their influence is localised.

Wave-induced currents may be present throughout the bay and may oppose or reinforce tidal currents. The mean velocity of a wave-induced longshore current may be predicted in a number of ways (Komar, 1976), with the two dominant methods involving either the continuity of water mass or radiation stress. The two approaches give consistent results (Galvin, 1987), although the continuity approach is independent of wave height and the radiation stress method is not (Komar, 1976).

Since the breaking wave height distribution along Pilot Bay beach was not measured, the continuity equation for longshore current (Galvin, 1987) will be used to estimate the influence of wave-induced currents. The mean velocity is given by:

$$v = kgT\tan(s)\sin(\alpha_b) \qquad \ldots 7.7$$

where k = constant.

The value of k depends on the geometry of the wave (Galvin, 1987), and varies between 0.6 and 0.9 for Pilot Bay.

Observed breaker angles within Pilot Bay are $\leq 5°$, except for vessel wakes which may impinge at greater angles. Taking values of k=0.75 and T=3.5s, the mean velocity can be calculated for the original (s=1°40′) and renourished (s=4°30′) regions of Pilot Bay beach (Table 7.11). For $\alpha_b > 1°$, the wave-induced currents along the renourished beach are similar

to the tidal currents measured immediately offshore from the breaker zone. The wave-induced currents are considerably weaker for the remainder of the beach.

Table 7.11 - Mean longshore current produced by a range of breaker angles (α_b) for the dominant spectral component of the average Pilot Bay spectrum. The renourished region of the beach (v_r) has a slope of 4°30', and the remainder of the beach (v_o) has a slope of 1°40'.

α_b	(°)	0.25	0.50	0.75	1.00	1.50	2.00	2.50	3.00	3.50	4.00	4.50	5.00
v_r	(ms^{-1})	0.02	0.04	0.06	0.08	0.11	0.15	0.19	0.23	0.27	0.30	0.34	0.38
v_o	(ms^{-1})	0.01	0.01	0.02	0.03	0.04	0.06	0.07	0.08	0.10	0.11	0.13	0.14

No detailed measurements were taken of breaker angles within Pilot Bay. However, wave approach directions derived from the wave recorder system indicated that most waves approached the tug berths from 240±15°. The bathymetry between the tug berths and the renourished zone would not cause significant refraction in the absence of tidal currents. The resultant breaker angles would induce a northwestwards current along the renourished zone.

The rest of the beach is fronted by a wide shallow platform and most observed wave crests are shore parallel by the breaker zone. The resulting value of α_b and the lower slope produces weaker wave-induced currents compared to the renourished zone. Therefore, the effect of wave-induced currents is likely to be more significant within the renourished zone.

The net movement of sediment from the renourished portion of Pilot Bay beach is summarised in Figure 7.17. Most of the sediment eroded from the beach travels northwestward along the intertidal zone, with lesser quantities travelling offshore into the channel, onshore onto the coastal reserve, and southeastwards under Salisbury Wharf.

Some sediment accumulates as a shore-parallel sub-tidal spit attached to the western end of the renourished region. The rest initially mixes with original beach sediment further northwest, partially restoring the beach in this area. From the observed changes in the beach profile immediately adjacent to the renourished region it appears that only small quantities of dredge spoil are retained within this mixing zone, with most, particularly pumiceous material, continuing to be transported northwestward. Therefore the eroded sediment effectively bypasses the

central region of Pilot Bay beach.

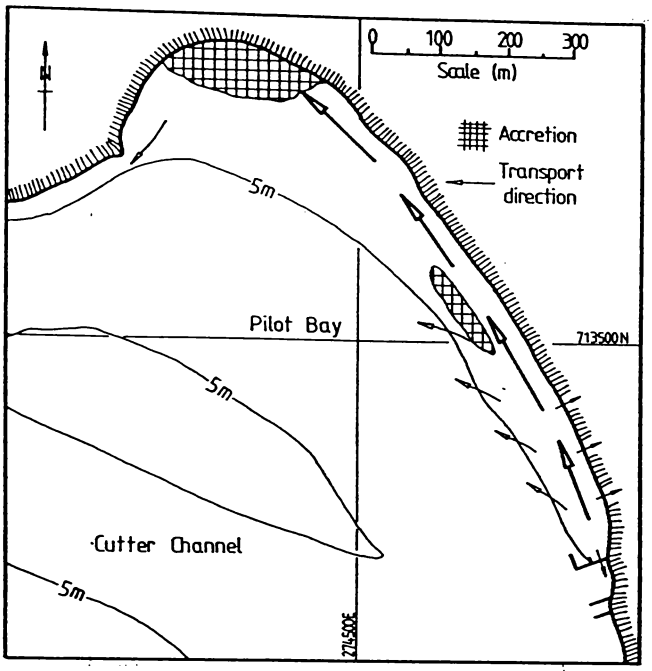

Figure 7.17 - Summary of the sediment transport pathways followed by sediment from the renourished region of Pilot Bay beach, and the major zones of sediment accumulation during the period 1984-1987.

The bypassing sediment accumulates within the intertidal zone at the northwestern end of the beach, near the boat ramp. Shortly after the completion of dredging the boat ramp required clearing once a month. During 1987, the sediment accumulation was removed weekly. This region of Pilot Bay beach acts as a sediment trap due to low current velocities, and a wide shallow offshore platform which dissipates waves. Therefore most of the dredge spoil material will accumulate in the vicinity of the boat ramp within the medium term (10-20y).

Sediment can only be transported from this area if it can be moved into the strong tidal currents adjacent to Mt Maunganui. This appears to occur fairly readily for low density materials, such as pumice, but not for large shell fragments and titanomagnetite, since the accumulation of sediment on the boat ramp consists primarily of high density or large clasts.

7.6 - Summary

The renourished beach has undergone continual erosion since the completion of dredging and landscaping. The expected life of the

artificial section of beach is between 7 and 16y, based on the observed shoreward retreat of MLW, or <13y, based on the observed volumetric changes in a representative section of the beach.

Most of the eroded sediment moves along the intertidal zone towards the northern end of the beach. This has not significantly changed the textural characteristics of the beach, but has changed the appearance of the surficial sediments.

The Sunamura and Horikawa (1972) criteria for predicting sediment transport directions may also be applied to settling velocity parameters derived from the RSA. These criteria predicted sediment transport directions for Pilot Bay beach which were consistent with directions derived by other methods.

The measured sediment fluxes of were consistent with the predictions of the sediment transport model 2DD. The net sediment flux determined from measured sediment fluxes was $1830 \times 10^{-6} kgm^{-1}s^{-1}$ in the ebb direction, compared to a net flux of $1120 \times 10^{-6} kgm^{-1}s^{-1}$, also in the ebb direction, predicted by volumetric changes within Pilot Bay beach.

The primary medium-term destination of sediment lost from the renourished portion of Pilot Bay beach is the northwestern end of the bay in the vicinity of the boat ramp. By October 1987, the rate of sediment accumulation was sufficient to require constant maintenance.

Chapter 8 - Wave-induced Sediment Transport Within Tauranga Harbour

Initiation of sediment transport by wave-induced oscillatory motion is the main consideration of this chapter. The observed wave climate is used to predict the depth of wave stirring in relation to the maximum grain size which can be moved. These data are related to the sediment facies within the southern Tauranga Basin to identify regions where wave-induced sediment transport may be significant.

Wave-induced suspended sediment loads are compared to the THS numerical model predictions to assess the potential contribution of wave-induced sediment transport to total sediment fluxes within the area considered.

8.1 - Initiation of sediment transport under waves

The initiation of sediment transport under waves differs in one important respect from the initiation of transport in fluvial channels or under unidirectional currents. Prior to breaking, waves induce oscillatory currents. For unidirectional steady flow, the conditions required for the initiation of sediment transport may be defined by the Shields criterion (Madsen and Grant, 1976a, 1976b; Allen, 1977; Leeder, 1982). This determines the critical value for the ratio of the entraining to stabilising forces acting on a grain at the sediment/fluid boundary.

The Shields criterion has also been applied to oscillatory flows and found to be reasonably successful (Madsen and Grant, 1976a, 1976b; Vincent *et al*, 1981; Nielsen, 1986). As given by Madsen and Grant (1976a) the Shields parameter for oscillatory flow is:

$$\psi = \frac{\tau}{(\rho_s-\rho)gD} = \frac{f_w \rho u_{max}^2}{2(\rho_s-\rho)gD} \qquad \ldots 8.1$$

where τ = bed shear stress,

D = grain diameter,

f_w = wave friction factor, and

u_{max} = maximum wave orbital velocity.

This parameter (ψ) is usually related to a dimensionless parameter

representing the ratio between the inertial and viscous forces existing in the fluid medium (Reynolds number). However other parameters, such as the parameter S_* defined below (Madsen and Grant, 1976a, 1976b), have also been used.

$$S_* = \frac{D((\rho_s-\rho)gD)^{1/2}}{4\nu} \qquad \ldots 8.2$$

where ν = kinematic viscosity.

An empirically derived relationship (Fig. 8.1) between Shields parameter and the other parameter chosen can then be applied to determine the critical shear stress (τ_c), which must be exceeded before sediment transport will begin. This approach assumes that the near-bed current can be completely defined by the shear velocity $(\tau/\rho)^{1/2}$ when the fluid density and bottom roughness are known (Rigler and Collins, 1984).

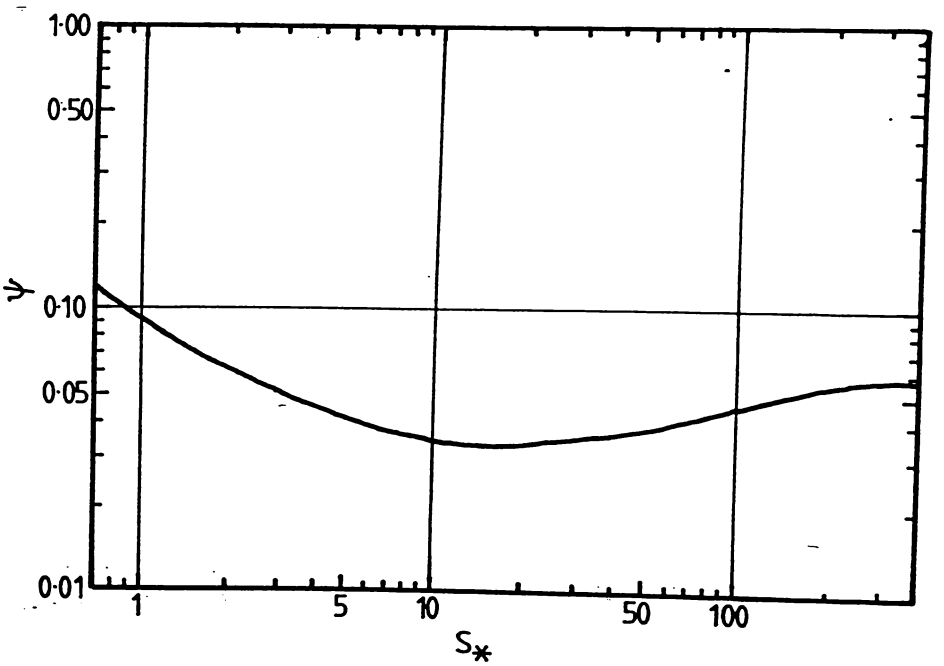

Figure 8.1 - Relationship between Shields parameter and S_* (Equation 8.2). After Madsen and Grant (1976b).

Under oscillatory flow, the shear velocity is constantly changing at a rate determined by the wave frequency. The application of Shields parameter to oscillatory flows assumes that τ_c can be approximated by:

$$\tau_{max} = \tfrac{1}{2} f_w \rho u_{max}^2 \qquad \ldots 8.3$$

Measurements of τ_c, for a variety of grain sizes and densities, under oscillatory flows (Komar and Miller, 1975; Hallermeier, 1980; Rigler and Collins, 1984) indicate that τ_{max} does not account for all variations due to wave frequency and amplitude.

Komar and Miller (1973, 1975) reviewed and developed empirical criteria, relating u_{max} to grain size, for sediment threshold. Relationships were produced for two ranges of grain size. For D<0.5mm:

$$\frac{\rho u_{max}^2}{(\rho_s-\rho)gD} = k\left(\frac{d_0}{D}\right)^{1/2} \qquad \ldots 8.4$$

where k = 0.21 (Komar, 1976),
and d_0 = orbital diameter.

For D>0.5mm, the influence of the wave frequency on τ_c is significant and must be accounted for. The relationship is:

$$\frac{\rho u_{max}}{(\rho_s-\rho)gT} = k\left(\frac{d_0}{D}\right) \qquad \ldots 8.5$$

where k = constant.

An alternative form of Equation 8.5, which does not include the wave frequency explicitly and resembles Equation 8.4 more closely, was developed by Rance and Warren (1969). This relationship is:

$$\frac{\rho u_{max}^2}{(\rho_s-\rho)gD} = 0.46\pi\left(\frac{d_0}{D}\right)^{1/4} \qquad \ldots 8.6$$

Hallermeier (1980) presents an alternative relationship for grains $\leq$0.7mm, restricted to ρ_s=2650kgm^{-3} and $u_{max} \leq 0.35$ms^{-1}, given by:

$$d_0 u_{max} = \frac{0.35D^{1/4}(\gamma' g)^{3/4}}{\omega^2} \qquad \ldots 8.7$$

where $\gamma' = (\rho_s-\rho)/\rho$.

Rigler and Collins (1984) reviewed the applicability of several criteria for the threshold of grain motion under oscillatory flows, including all those discussed above except Equation 8.6. They concluded that Equation 8.4 was the most appropriate criterion to use for

estimating critical wave conditions, providing the constant (k) was changed from 0.21 to 0.32. Therefore this study used Equation 8.4 with k=0.32 for sediments finer than 0.5mm (1ϕ) and, in the absence of better formulations for coarser sediments, Equation 8.6 for D>0.5mm.

8.2 - Depth of wave stirring in southern Tauranga Harbour

Assuming Linear Theory, u_{max} and d_0 are related to the water depth and other wave parameters (Komar, 1976) by:

$$u_{max} = f\pi d_0 = f\pi H/\sinh(2\pi h/L) \qquad \ldots 8.8$$

For the peak spectral frequencies of 0.2857Hz and 0.8571Hz measured within Tauranga Harbour the waves are not always shallow-water waves. Therefore the wavelength must be computed using the general Linear Theory expression for wavelength (Equation 5.14).

To determine the depths at which waves are just capable of stirring sediment within Tauranga Harbour, u_{max} was calculated for frequencies between 0.00 and 1.25Hz, and depths from 0-10m (Fig. 8.2). To make u_{max} independent of wave height, u_{max} was normalised by dividing by H (Harris *et al*, 1983). Considering the peak frequencies for the average Pilot Bay spectrum (Table 5.9), u_{max}/H approaches zero at 7.4 and 0.9m respectively.

The threshold velocity for sand-sized sediment (-1 to 4ϕ) was determined for frequencies in the range 0.00-1.25Hz (Fig. 8.3). This required a slight rearrangement of the formulae discussed in the previous section to give:

$$u_{max}^{3/2} = 0.32\gamma' g\left(\frac{D}{\pi f}\right)^{1/2} \qquad \ldots 8.9$$

for D≤0.5mm, and

$$u_{max}^{7/4} = \frac{0.46\gamma' g(\pi D)^{3/4}}{f^{1/4}} \qquad \ldots 8.10$$

for D>0.5mm.

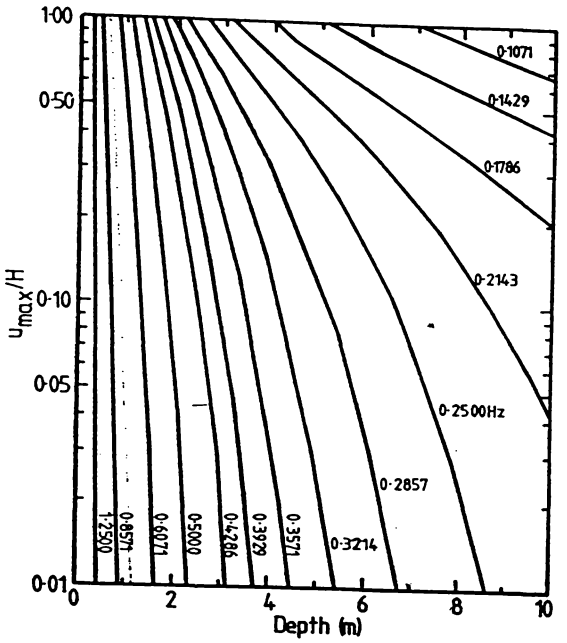

Figure 8.2 - Maximum orbital velocity per unit wave height (u_{max}/H) versus depth for selected frequencies from 0.0-1.2Hz.

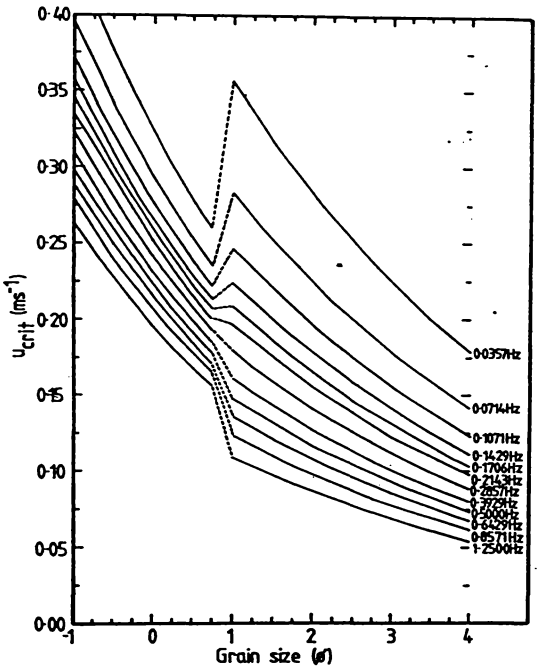

Figure 8.3 - Near-bottom orbital velocity (u_{max}) at sediment threshold for various frequencies between 0.0 and 1.2Hz.

The component wave heights for the average Pilot Bay spectrum (Table 5.9) were used to determine the depth at which threshold would be exceeded for sand-sized sediment under waves of various frequencies (Fig. 8.4). For the wave heights used, none of the wave components are capable of moving sand-sized sediment deeper than 2m. This analysis assumes that wave components act independently, which may not be valid

since some wave components may be in phase.

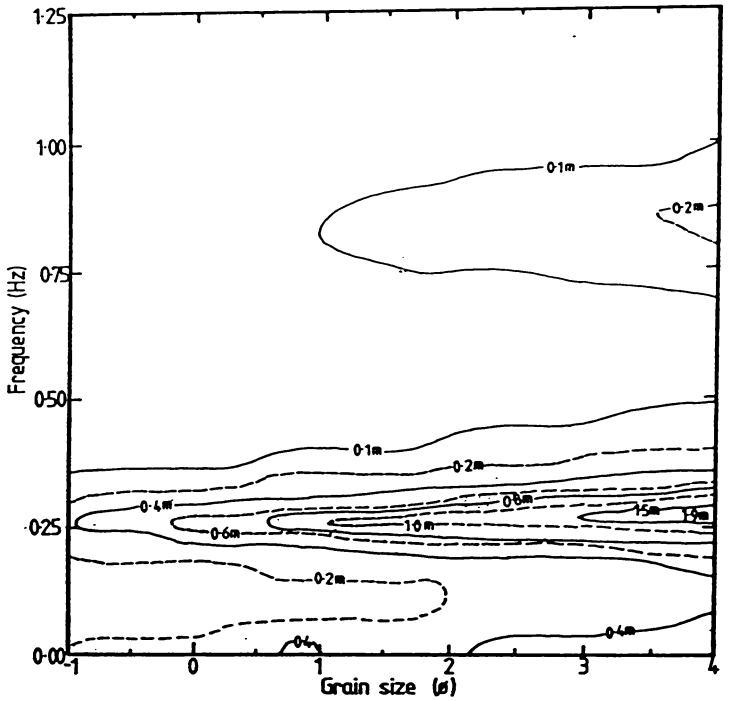

Figure 8.4 - The depth to sediment threshold as a function of grain size and wave frequency determined from Equations 8.8-8.10 for the average wave conditions in Tauranga Harbour.

If all the components are assumed to be in phase, which is unlikely, the maximum value of u_{max} is equal to the sum of the component orbital velocities. For example, at 2m depth $\sum u_{max}=0.34ms^{-1}$, which can entrain sand-sized sediment. However, by 5m $\sum u_{max}<0.05ms^{-1}$ and no sand-sized material will be affected.

Since the phase relationships between the various wave components are not known, the threshold depths for individual component waves have been used to investigate the significance of wave-induced motion within the southern Tauranga Basin. The THS collected 296 seabed sediment samples, mainly from the southern basin, which were analysed by the University of Waikato RSA (Healy, 1985). The mean particle size (ϕ_{50}) data were contoured to provide the grain-size distribution within Tauranga Harbour by Black (1984). Almost all of the shallow-water sediments are finer than 1ϕ (<0.5mm), except for an area of shell lag on Centre Bank where ϕ_{50} ranges between 0 and 1ϕ (1.0-0.5mm).

By combining the threshold depth data (Fig. 8.4) with the grain-size data obtained by the THS, it is possible to map the extent of wave stirring within the southern basin (Fig. 8.5). Wave stirring is restricted to shallow (<2m) inter-tidal regions within the harbour,

although under extreme conditions it can persist to a maximum depth of ~5m.

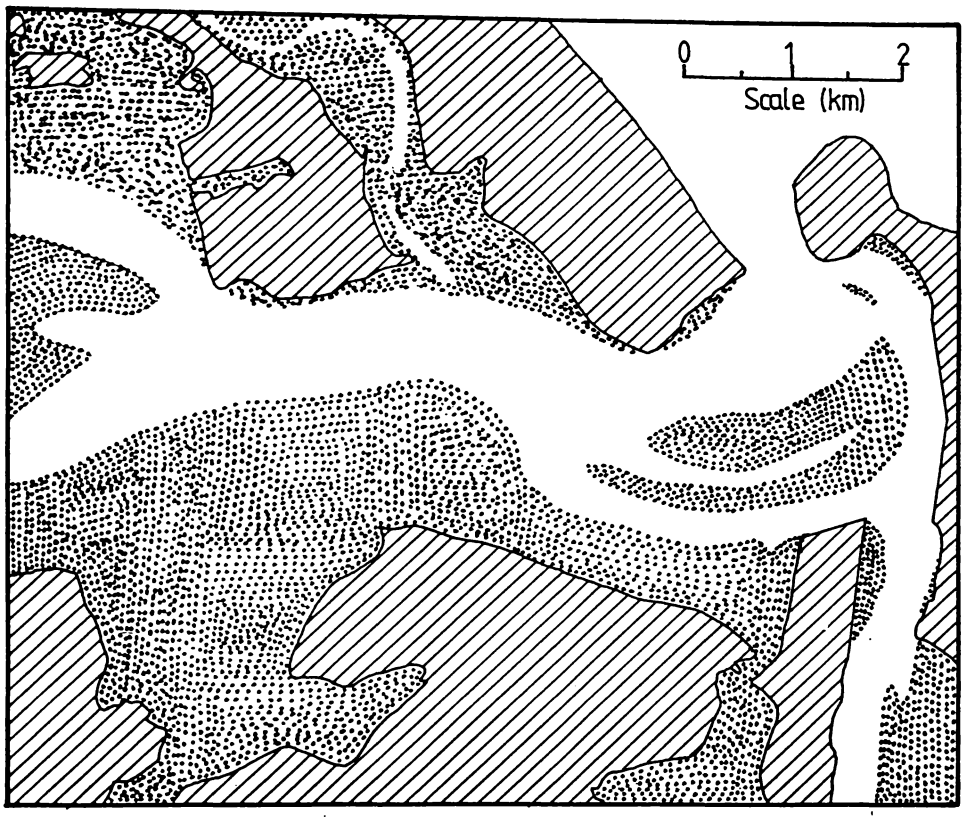

Figure 8.5 - Distribution of wave-induced stirring of surficial sediments within the southern basin of Tauranga Harbour (stippled areas), determined for the median grain-size distribution (Healy, 1985) and average wave conditions.

Within Tauranga Harbour, most current-induced sediment transport occurs in the tidal channels at depths >2m (Black, 1984). In shallower regions, tidal currents generally have low velocities and persist for only short periods during a tidal cycle, particularly within the inter-tidal zone. One major exception to this is Centre Bank. On Centre Bank, the tidal currents are sufficiently strong to entrain sand-sized sediment throughout most of the tidal cycle, particularly close to the harbour entrance (Black, 1984; Barnett, 1985). The sediment facies map produced by the THS (Healy, 1985) classifies ~50% of the Centre Bank as either shell lag or very shelly sand. The shell material produces a lag surface which armours the sediment, increasing the threshold velocity.

SCUBA observations by the author indicate that the shells comprising the shell lag are imbricated sub-parallel to the dominant tidal flow. In this position the threshold velocity is considerably greater than for

other orientations (Moon, 1983). Based on observations at Whangarei and Tauranga, Black (1984) considered that <20% of the sediment present in the lagged regions of Centre Bank could be entrained by tidal flows.

Oscillatory flows due to wave action, particularly those at an angle to the tidal flow, may disturb an imbricated lag surface (Moon, 1983). This reduces the threshold velocity and exposes finer sediment to the current, thereby producing greater sediment availabilities than assessed on the basis of tidal currents alone.

The remainder of Centre Bank consists of clean to shelly sands (~40%) with a narrow band of sandwaves and megaripples. These sediments are susceptible to wave stirring and diver observations during the THS noted that the clean sands were slightly rippled. Most of the ripples observed close to major channels were current ripples, but those occurring away from channels tended toward oscillatory ripples. The sandwave and megaripple field is highly mobile and wave-induced stirring is likely to have a negligible impact.

The inter-tidal flats were not usually sampled by the THS, except in the vicinity of the bridge development in Waipu Bay. A survey in this study of Duck Bay, Waipu Bay and the Otumoetai inter-tidal zones classified their sediments as silty sand facies. All these areas displayed small-amplitude (≤0.05m), oscillatory ripples, except where the surface was covered with eel grass (*Zostera* sp.) or stabilised by algal mats. By assessing the movement of ripples relative to a fixed stake, it was evident that the ripples were mobile. The ripple crests were sub-parallel to the shoreline and generally the direction of propagation was onshore.

8.3 - Wave-induced sediment fluxes

The mean suspended sediment load under random waves can be approximated by:

$$s_s = c_0 . \ell \qquad \ldots 8.11$$

where c_0 = the sediment concentration at the seabed,
and ℓ = the relative concentration gradient.

The complete concentration gradient has been described by various mathematical relationships, such as parabolic (Fredsøe *et al*, 1985) or exponential (Nielsen, 1986). However, most of the suspended sediment load is concentrated in a near-bottom layer (Stive and Battjes, 1985), which can be described by a linear relationship of the form:

$$\ell = \epsilon/s \qquad \ldots 8.12$$

where ϵ = turbulent viscosity,
and s = sediment settling velocity.

Stive and Battjes (1985) present a semi-empirical relationship for deriving ϵ when $2\pi d_0/w>20$, which may be expressed as:

$$\epsilon = 0.35\times10^{-3}(\Xi+0.4\delta)gT\left(\frac{2\pi d_0}{Tw}\right)^{0.68} \qquad \ldots 8.13$$

where

$$\Xi = \frac{\rho u_{rms}^{\ 2}}{(\rho_s-\rho)gD} \qquad \ldots 8.14$$

and

$$\delta = 0.072d_0(2.5D/d_0)^{1/4} \qquad \ldots 8.15$$

The parameter δ defines the boundary layer thickness and determines the nature of the concentration gradient in the absence of ripples. The other parameter (Ξ) dominates when ripples are present and is related to the ripple height (ζ) by:

$$\zeta = 21d_0\Xi^{-1.85} \qquad \Xi>10$$

$$\zeta = 0.3d_0 \qquad \Xi\leqslant10 \qquad \ldots 8.16$$

If $2\pi d_0/(Tw)<20$, ϵ may be approximated by (Ikeda and Nishimura, 1986):

$$\epsilon = 0.077(\tau/\rho)^{½}h \qquad \ldots 8.17$$

For a rippled bed, the near-bed concentration is given by (Nielsen, 1986):

$$c_0 = 0.005\psi_r^3 \qquad \ldots 8.18$$

where ψ_r is Shields parameter adjusted for flow distortions over ripples as given by:

$$\psi_r = \psi/(1-\pi\zeta/\lambda)^2 \qquad \ldots 8.19$$

where λ = ripple length.

Alternatively, if the dimensions of the ripples are not completely known, the near bottom suspended sediment concentration may be obtained from (Stive and Battjes, 1985):

$$c_0 = (2k/\pi)(\psi-\psi_c)\cos^{-1}(\psi_c/\psi)^{1/2} \qquad \ldots 8.20$$

where k = 0.028
and ψ_c = critical value of ψ (0.05).

The $\cos^{-1}$ term accounts for the fraction of time that Shields parameter (ψ) exceeds the critical stress (ψ_c). If $\psi<\psi_c$ this relationship is not applicable, and the relationship also does not hold when ripples are absent (Losada et al, 1987).

Equations 8.12-8.20 were solved for the dominant wave component of the average Pilot Bay spectrum (H_c=0.07m, T=3.5s), and average sediment for the clean sand facies (D≈1ϕ or 0.5mm). The dominant spectral wave component closely approximates the average wave conditions determined by zero up-crossing analysis (Table 5.4). Under these conditions, Equation 8.20 is applicable to water depths between 0.2 and 0.8m. Outside this range either $\psi<\psi_c$, or ψ exceeds the upper limit for rippled beds, 0.8-1.0 (Deigaard et al, 1986). Measurements of ripples within Pilot Bay produced ripple indices (λ/ζ) of 6-9, which are consistent with the findings of Nielsen (1984). Therefore a constant ripple index of 7.5 was assumed for all analyses. This reduces the denominator of Equation 8.19 to 0.3377.

The ripple heights predicted (Table 8.1) are in reasonable agreement with the observed oscillatory ripples within Pilot Bay. The two formulae for near-bed sediment concentration (Equations 8.18 and 8.20) produce different results, with the relationship of Stive and Battjes (1985) predicting larger concentrations than the Nielsen (1986) equation for depths between 0.3 and 0.8m. At a depth of ~0.3m the value of ψ_r exceeds the upper limit for rippled beds, therefore Equation 8.18 is probably not applicable.

Table 8.1 - Summary of parameters predicted by Equations 8.12-8.20 for the dominant wave component of the Pilot Bay spectrum and clean sand facies sediment.

Depth (m)	u_{max} (ms^{-1})	ψ	ζ (m)	c_0 ($10^{-3}m^3m^{-3}$) a	b	s_s ($10^{-6}kgm^{-2}$) a	b
0.1	1.945	1.942	0.001	854.150		17960.0	
0.2	0.971	0.577	0.003	22.367	11.941	512.6	273.7
0.3	0.647	0.286	0.010	2.740	4.805	66.4	116.3
0.4	0.483	0.175	0.021	0.622	2.237	15.7	56.4
0.5	0.386	0.120	0.038	0.199	1.076	5.2	28.1
0.6	0.320	0.087	0.064	0.078	0.474	2.1	12.7
0.7	0.273	0.067	0.091	0.035	0.161	1.0	4.4
0.8	0.238	0.054	0.078	0.018	0.016	0.5	0.5
0.9	0.210	0.044	0.070	0.010		0.3	
1.0	0.187	0.036	0.063	0.006		0.2	

[a]Calculated with Equation 18
[b]Calculated with Equation 20

8.4 - Implications for Tauranga Harbour Study results

The sediment transport model 2SS, used in the THS, considered bedload and suspended sediment load independently. The calculated loads were then combined to produce the total sediment flux (Black, 1984). Bedload was derived from the 1m current velocity by following a procedure developed by Black (1983) in Whangarei Harbour. Equation 7.3 can be rearranged to give:

$$u_* = u_1/[5.75\log_{10}(30.2/2D_{65})] \qquad \ldots 8.21$$

where D_{65} = 65% of the grains present are finer than this size.

The calculated skin friction velocity is then used in the Yalin bedload equation given by:

$$q_b = 0.635\rho_s D u_* [\tau_* - (1/a)\ln(1+\tau_* a)] \quad \ldots 8.22$$

where

$$\tau_* = u_*^2/u_{*cr}^2 - 1 \quad \ldots 8.23$$

and

$$a = 2.45\psi_c^{1/2}/(\rho_s/\rho)^{0.4} \quad \ldots 8.24$$

where u_{*cr} = threshold friction velocity.

Suspended sediment loads were calculated using the Engelund and Fredsøe (1976) method. This approach determines the near-bed sediment concentration by:

$$c_b = 0.65/(1+1/\lambda_b)^3 \quad \ldots 8.25$$

where

$$\lambda_b = ((\psi' - \psi_c - \pi p.\tan\xi/6)/(0.027\rho_s\psi'))^{1/2} \quad \ldots 8.26$$

where ψ' = Shields parameter for rippled or duned beds,
p = probability of transport,
and ξ = dynamic friction angle.

The numerical model 2SS calculates p, the probability that any particular surficial grain will be transported, from the product of two parameters called the erodibility and the availability (Black, 1983). These parameters characterise bed cohesion and the amount of sand present, respectively.

The parameters derived from the numerical model calibrations and used for the final THS production simulations are summarised in Table 8.2. These parameters differ slightly from those used in the derivation of

Table 8.1. In particular, ψ_c=0.064 (c.f. 0.05) and D_{50}=0.40mm (c.f. 0.50). The THS production parameters were used to calculate the bedload and near-bed suspended sediment concentration for a range of 1m current velocities (Table 8.3). The numerical model 2SS only calculated suspended sediment loads for 1m current velocities exceeding 0.47ms^{-1}, whereas bedload was determined for all velocities greater than the 1m threshold velocity given by (Black, 1983):

$$u_{1cr} = 5.75u_{*cr}\log_{10}(1/k) \qquad \ldots 8.27$$

Table 8.2 - Mean sediment transport parameters used in 2SS numerical simulations of Tauranga Harbour. After Table 3.1 (Black, 1984).

D_{50} (mm)	D_{65} (mm)	U_{*cr} (ms^{-1})	s (ms^{-1})	ρ_s (kgm^{-3})	ρ (kgm^{-3})	ξ (°)	β	k (m)
0.40	0.45	0.016	0.022	2650	1025	24	3.0	0.008

Table 8.3 - Summary of parameters predicted by Equations 8.21-8.26 for u_1=0.4-1.0ms^{-1}.

u_1 (ms^{-1})	u_* (ms^{-1})	q_b (10^{-6}kgm^{-1}s^{-1})	ψ'	c_b (10^{-3}m^{3}m^{-3})
0.40	0.0154	11	-0.01	
0.45	0.0173	54	0.03	
0.50	0.0192	391	0.07	
0.55	0.0211	1151	0.12	
0.60	0.0231	2470	0.17	0.017
0.65	0.0250	4487	0.23	0.146
0.70	0.0269	7345	0.29	0.257
0.75	0.0288	11184	0.35	0.342
0.80	0.0307	16147	0.42	0.407
0.85	0.0327	22323	0.50	0.458
0.90	0.0346	30002	0.58	0.498
0.95	0.0365	39171	0.66	0.531
1.00	0.0384	50016	0.75	0.558

For Tauranga Harbour, the mean roughness length was taken to be 0.008m, although there was considerable scatter (Black, 1984). This length corresponds to a 1m threshold velocity of 0.19ms^{-1} for non-cohesive sand-sized sediment. However, the presence of shell material increases the 1m threshold velocity to between 0.44 and 1.05ms^{-1} (Moon, 1983; Black, 1983). Therefore, the results in Table 8.3 (u_{1cr}≈0.42ms^{-1})

are appropriate for the southern basin of Tauranga Harbour, which does contain a significant quantity of shelly sediment (Healy, 1984). It is also evident from the calculated shear stresses that the Engelund and Fredsøe (1976) method is only applicable to 1m velocities >0.55ms^{-1} for the parameters chosen (Table 8.2).

Assuming that the total suspended sediment concentration due to a combination of tidal currents and waves may be approximated by the sum of c_b and c_0, it is possible to determine the percentage increase in the near-bed concentration, caused by wave-induced stirring, as:

$$\% \text{ increase} = ((c_b+c_0)/c_b*100)-100 \quad \ldots 8.28$$

Table 8.4 summarises the percentage increase for depths between 0.2 and 0.7m, and current velocities of 0.6-1.0ms^{-1}, where c_0 is derived from Equation 8.18. Outside the range of conditions specified, either c_b=0, or c_0 is less than 1% of the smallest value of c_b. It is evident that the wave-induced component of the near-bed suspended sediment concentration becomes more significant with decreasing depth and decreasing current velocity. From these results, the numerical model 2SS underestimates the near-bed suspended sediment concentration by <10% across Centre Bank (h>0.4m) for current velocities >0.6ms^{-1}.

Table 8.4 - Percentage increase (Equation 8.28) in the near-bed suspended sediment concentration due to wave-induced stirring.

Velocity (ms^{-1})	Depth (m)					
	0.2	0.3	0.4	0.5	0.6	0.7
0.60	2876	372	88	29	12	5
0.65	335	43	10	3	1	1
0.70	190	25	6	2	1	0
0.75	143	19	4	1	1	0
0.80	120	16	4	1	0	0
0.85	107	14	3	1	0	0
0.90	98	13	3	1	0	0
0.95	92	12	3	1	0	0
1.00	88	11	3	1	0	0

However, the final numerical model results are based on the total sediment flux, not the near-bed suspended sediment concentration. Therefore it is useful to consider the extra suspended sediment flux due

to wave-induced stirring. The sediment flux can be derived from the near-bed concentration by applying Equation 7.4 (Table 8.5), assuming $c_a=c_0$ and $a=2D_{50}$ (Englelund and Fredsøe, 1976).

Table 8.5 - Extra suspended sediment flux ($10^{-6}kgm^{-1}s^{-1}$) due to wave-induced stirring for different current velocities and depths observed within the southern basin of Tauranga Harbour.

Velocity (ms^{-1})	Depth (m)					
	0.2	0.3	0.4	0.5	0.6	0.7
0.10	1239	84	16	5	2	1
0.20		421	102	31	11	5
0.30			324	87	32	13
0.40				370	134	55
0.50					344	172
0.60						381

Additional wave-induced fluxes were only determined for the range of water depths and tidal velocity measured within the southern basin of Tauranga Harbour by the THS and this study (Chapter 3). The wave-induced sediment flux decreases rapidly with increasing water depth and below 0.8m it is either $<10kgm^{-1}s^{-1}$, or <10% of the current-induced suspended sediment flux. For depths ≤0.2m, the sediment fluxes become quite large. However, for the average wave conditions experienced within the harbour (Chapter 5), the waves are shoaling rapidly at these depths. The approach used is for conditions under non-breaking waves, so the predictions may no longer be valid.

When the wave-induced sediment flux is combined into the total sediment flux, the additional contribution may be insignificant (<10%). Assuming that the total sediment flux is given by the sum of q_b and q_s, where q_s is determined by Equation 7.4 with $c_a=c_b+c_0$, it is possible to calculate the percentage contribution made by wave-induced suspended sediment (Table 8.6). These percentages confirm that wave-induced suspension of sediment is most significant for low current velocities and/or shallow water depths. As water depth or current velocity increase, the effect of wave activity diminishes rapidly.

8.4.1 - Discussion

The influence of wave-induced suspension of sediment is most

pronounced in shallow water, particularly for depths <0.8m. From the hypsometric curve for the southern basin of Tauranga Harbour (Fig. 8.6), it is evident that a large proportion of the harbour lies above wave base (60-70%), depending on the state of the tide. Although the wave-induced sediment flux may be small, given the area affected, the annual wave-induced sediment flux for the harbour may be quite large.

Table 8.6 - Percentage of the total sediment flux contributed by wave-induced suspension of sediment. The total flux represents the sum of q_b (Table 8.3) and q_s (Equation 7.4), where the reference concentration (c_a) is taken as c_b+c_0.

Velocity (ms^{-1})	Depth (m)					
	0.2	0.3	0.4	0.5	0.6	0.7
0.10	100	100	100	100	100	100
0.20		100	100	100	100	100
0.30			100	100	100	100
0.40				97	92	83
0.50					47	31
0.60						13

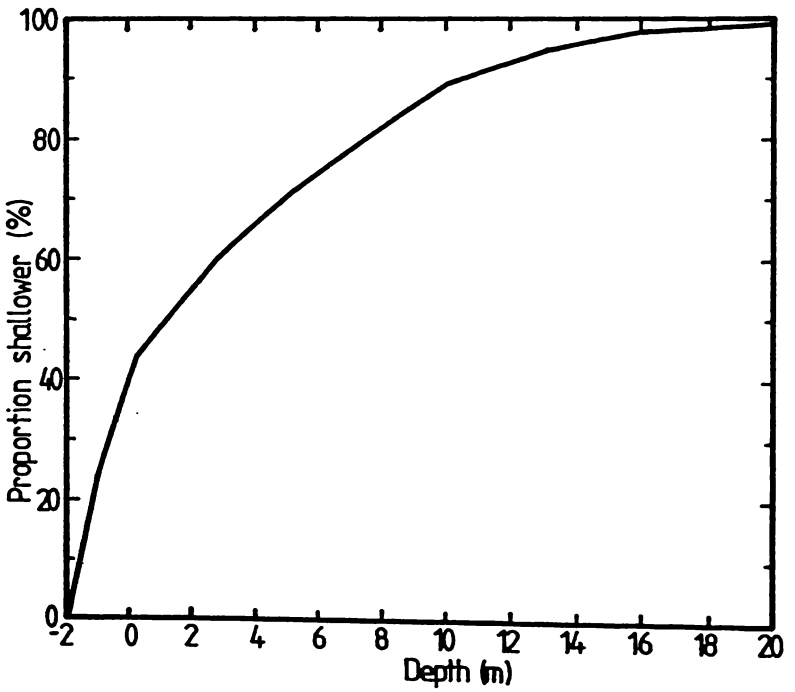

Figure 8.6 - Hypsometric curve for the southern basin of Tauranga Harbour. The data were obtained from Chart NZ 5412, 1983 edition.

Aanderaa current meter recordings taken adjacent to the inter-tidal region of Pilot Bay beach indicate a mean velocity <0.1ms^{-1}. Due to the close proximity of a major tidal channel, the mean velocity recorded may

be slightly high compared to the more extensive inter-tidal flats further from tidal channels. However, in order to estimate the annual wave-induced flux for the harbour, a mean tidal velocity of $0.1ms^{-1}$ will be assumed.

As the tide rises and falls, the area affected by wave-induced stirring within the harbour changes (Fig. 8.6). To allow for these changes, a tidal range of 1.4m was assumed with a tidal duration of 12h 25min. These conditions correspond to the mean tidal conditions at Salisbury Wharf (Davies-Colley, 1976; Black, 1984). Given that the tidal curve near the entrance is closely approximated by a sinusoidal curve (Barnett, 1985), it is possible to calculate the percentage of tidal cycle spent at each tidal elevation. This was determined for 0.05m intervals between MLW and MHW.

Combining the sediment fluxes for $0.1ms^{-1}$ current speeds (Table 8.5) with the hypsometric curve, and weighting the results with the tidal height data, it is possible to derive the approximate suspended sediment flux for one tidal cycle ($61 \times 10^{-6} kgm^{-2}$). Assuming an average width of 250m for the shallow regions within the southern harbour, and 705 tidal cycles per annum, the gross annual sediment flux is $\sim 60000 m^3 y^{-1}$. This is 1-2 orders of magnitude smaller than the tidally-induced fluxes determined by the numerical model 2SS for the major channels and similar to the fluxes in minor channels (Table 8.7).

Table 8.7 - Gross annual sediment fluxes for parts of the southern basin of Tauranga Harbour, as determined by the numerical model 2SS. Data from Figure 4.6 (Black, 1984).

Region	Gross annual sediment flux ($m^3 y^{-1}$)
Entrance	368000
Lower Western Channel	2239000
Middle Western Channel	205000
Upper Western Channel	150000
Lower Otumoetai Channel	70000
Upper Otumoetai Channel	35000
Western Centre Bank	1102000
Eastern Centre Bank	8000
Maunganui Roads	27000
Cutter Channel/Pilot Bay	24000

This comparison is very approximate, since the wave-induced flux is based on an average load taken over the entire harbour area within the appropriate depth range, whereas the 2SS values are based on fluxes through representative cross-sections. Given that the gross annual sediment flux for the harbour will be dominated by the fluxes within the major channels, particularly the entrance and Western Channel, the numerical model may be underestimating the sediment fluxes by ~10-20%.

In reality, the error in the THS results is probably less, since the calibration of the numerical model 2SS implicitly included wave-induced suspended sediment. All of the suspended sediment sampling for calibration, at sites other than the harbour entrance, occurred during periods of wave activity (Healy, 1985).

During calibration, model parameters were adjusted to recreate the observed suspended sediment fluxes (Black, 1984). Hence the modelled fluxes would include some wave-induced suspended sediment, even though it has not been calculated by 2SS. Further, at velocities below sediment threshold for current-induced transport, the model incorporated an advection scheme to enable continued sediment transport (Black, 1984). This approach was found to be necessary to enable the model to correctly predict observed sediment fluxes in some areas, such as Pilot Bay. Advection of suspended sediment from adjacent regions would compensate for the omission of wave-induced suspension within an area.

8.5 - Summary

The observed waves within Tauranga Harbour are capable of stirring sediment down to a maximum depth of ~2m below the still water level. For the distribution of sediment facies and water depths within the southern basin of the harbour, wave-induced stirring is mainly confined to the fringing shallow inter-tidal areas. However, wave-induced stirring may also occur on Centre Bank, particularly where shell lags are absent. The areas of likely stirring based on theoretical evaluations coincide with the distribution of oscillatory wave ripples observed during the THS and this study.

In shallow water, the sediment fluxes resulting from wave-induced suspension of sediment may significantly increase the total sediment flux. This is particularly true for depths <0.5m and currents $<0.5 ms^{-1}$.

The absence of an explicit determination of wave-induced sediment fluxes for the region modelled by the THS within the harbour may have resulted in an underestimate of sediment fluxes by 10-20%. However some wave-induced suspended sediment loads were implicitly included as a result of the calibration procedures followed by Black (1984).

Wave-induced sediment fluxes are significant in the areas not modelled by the THS, particularly the very shallow inter-tidal fringes and beaches within the southern basin. However, the annual flux for these areas is small compared to the fluxes in the major tidal channels.

Chapter 9 - Summary and Conclusions

9.1 - Summary of findings

9.1.1 - Wave climate

This study investigated two main components of the wave climate within Tauranga Harbour: high-frequency (short-period) waves, including wind-generated waves; and low-frequency (long-period) non-tidal waves, including seiches and tsunamis.

Using wave records obtained within the harbour at Pilot Bay, three main sources of high-frequency wave energy were identified:

a) vessel wakes;
b) wind stresses within the harbour; and
c) energy transmitted through the entrance from the external wave field.

Vessel wakes were transient features within the wave records, with individual wakes involving <10 consecutive wave crests with diminishing amplitudes. Wakes affected the distribution of recorded extreme zero up-crossing wave parameters (e.g. H_{max}), but contributed little energy to the average wave spectrum. The remaining sources of wave energy accounted for most of the wave spectrum between 0.00 and 1.25Hz.

Wind-induced waves within the harbour form under extreme limiting conditions. Factors limiting wave development within the harbour included:

a) fetches which are restricted in terms of both width and length;
b) shallow water, with ~60% of the study area being <2m in depth; and
c) interactions between waves and tidal currents.

Hence, the amount of energy which can be transferred from the wind to the internal wave field is much less than would occur in deep water.

Spectral analysis of Pilot Bay wave records indicates that locally generated wind waves account for ~9% of the energy present in the average wave field. This energy is concentrated within a small region of the spectrum and accounts for >30% of the wave height. Propagation of external wave energy through the harbour entrance contributes ~70% of the energy of the average wave spectrum. When wave energy enters the

harbour the spectral distribution is modified by interactions with strong tidal currents in the vicinity of the entrance. For the average spectral form, the external wave field component is less peaked than the probable offshore spectrum, and the peak frequency is Doppler shifted to higher frequencies.

An empirical relationship, based on the JONSWAP spectral form, was derived to account for the local wind-generated wave spectral component and is given by:

$$S(f) = \frac{\alpha g^2}{(2\pi)^4} f^{-5} e^{-(1.25(f/f_p)^{-4})} \gamma^q \qquad \ldots 9.1$$

where $\alpha = 2.3 \times 10^{-6}$

$\gamma = 8.13$,

f_p = spectral peak frequency,

and $q = e^{-(f-f_p)^2/(2\sigma^2 f_p^2)}$

where $\sigma = \begin{cases} 0.094 & f \leq f_p \\ 0.083 & f > f_p. \end{cases}$

For the average spectrum, f_p=0.8571Hz.

This relationship has a narrower peak than the original JONSWAP form due to a larger peak enhancement factor. The remaining shape constants are consistent with those determined for similar conditions by other studies. Defining the full wave field from the local wind conditions is difficult, because energy is derived from the external wave field. This study did not derive a relationship to predict the contributions to the internal wave climate from outside the harbour.

The modal zero up-crossing wave conditions (H_s=0.08m, T_z=3.6s) agreed well with the predicted waves associated with the average spectral peak (H_c=0.07m, T_p=3.5s). The maximum wave height observed during the study (0.69m) was a vessel wake. Generally, waves not associated with the passage of vessels attained maximum heights of 0.10-0.15m. The average wave heights measured by this study are smaller than those reported by Davies-Colley (1976).

Three types of non-tidal low-frequency waves are recorded in Tauranga Harbour: tsunamis; storm surges; and seiches. Seiches occur most frequently, usually developing when local wind speeds exceed 9.5ms^{-1}. They also form in response to forcing by swell wave activity outside the harbour or storm surges and tsunamis within the harbour. Tsunamis and

storm surges produce larger amplitude oscillations within the harbour than seiches, but they occur less often. Within historical times, the highest water elevation recorded (>2.75m) was due to the storm surge associated with the 1968 Wahine Storm, and the greatest amplitude (1.2m) was due to the 1960 Chilean Tsunami.

Spectral analysis of seiches for frequencies between 0.6×10^{-5} and 0.02Hz reveal a dominant oscillation occurring across Centre Bank, between the harbour entrance and the Otumoetai foreshore. This region is associated with seiches having frequencies of 0.0039 and 0.0045Hz (220-265s), depending on the tidal height. The maximum seiche amplitude occurs at high tide and generally is in the range 0.1-0.2m, unless associated with tsunami forcing, when it may reach 0.5m.

9.1.2 - Wave-induced sediment transport

High-frequency waves within Tauranga Harbour are capable of moving sand-sized sediment down to a maximum depth of ~2m below the still water surface. Therefore, wave-induced sediment transport is confined to shallow intertidal regions around the harbour, although some stirring also occurs on the shallower parts of the flood delta (Centre Bank) where shell lags are absent.

Wave-induced sediment fluxes in the absence of tidal currents are small, due to the low orbital velocities produced by the small short-period waves found within the harbour. However, when tidal currents are present, additional energy is available to move sediment entrained by wave action. By combining tidal currents and waves, the average sediment flux for the intertidal region within the southern basin of Tauranga Harbour is $\sim 60 \times 10^{-6} kgm^{-2}$ per tidal cycle. Although this is not large compared to current-induced sediment fluxes within the harbour, the large area affected by wave stirring results in an annual sediment flux of $\sim 60000 m^3 yr^{-1}$. This is 1-2 orders of magnitude smaller than current-induced fluxes close to the harbour entrance, and similar to sediment fluxes elsewhere in the harbour.

9.1.3 - Tauranga Harbour model studies

The physical modelling undertaken by the Hydraulic Research Station

(HRS) and the numerical models used by the Tauranga Harbour Study (THS) produced results consistent with the overall circulation patterns observed within the southern basin of Tauranga Harbour. Overall, the numerical model results were closer to the measured situation, reflecting the more intensive field programme undertaken to calibrate the model and advances in modelling techniques since the completion of the HRS study.

However, small discrepancies were evident when considering details of the tidal circulation, such as within the Pilot Bay region. Both the physical model and the numerical models identified an ebb dominance within Pilot Bay. However, neither produced long duration ebb flows comparable to the measured current data. Further, the peak current velocities predicted by the models were 50-75% higher than those observed, and persisted for 300-500% longer than observed. Despite this, the numerical model predicted net sediment fluxes through Pilot Bay which closely matched the measured fluxes along Pilot Bay beach.

9.1.4 - Pilot Bay beach renourishment

The renourished region of Pilot Bay beach has experienced continual erosion since the completion of dredging and landscaping. The estimated life of the beach varies between 7 and 16y, depending on the method used and the section of the beach considered. A reasonable time limit for planning purposes would be ~10y, assuming that the original state of the beach represented a somewhat less than desirable condition.

Most of the sediment travels within the wave zone along the beach towards the northwestern (boat ramp) end of the beach. Two major zones of accretion were observed during the study: a low bar or spit, running parallel to the shore adjacent to the northern end of the renourished zone; and adjacent to the boat ramp. Sediment deposition was highest in the latter region, necessitating frequent removal.

Some sediment blew onshore during windy periods. This effectively ceased when break fences were erected, but these were not permanent features during the study period. A minor quantity of sediment was observed by SCUBA to move offshore into the channel. However, less than 0.10m vertical accretion was noted within the channel during the period 1984-1988. Finally, a small amount of sediment travelled southeast

under Salisbury Wharf.

Due to low velocities ($V=0.40-0.80ms^{-1}$) within the bay, the sediment can not be readily moved by tidal currents. However, wave action may provide sufficient additional energy to enable some material to be carried into stronger currents closer to the harbour entrance. This mechanism may have been responsible for the removal of low density sediments from the vicinity of the boat ramp.

9.2 - Implications for the Bay of Plenty Harbour Board

It is evident that the external wave climate does affect conditions within the harbour in two ways: first, by the direct propagation of wave energy through the entrance; and second, by inducing seiching across Centre Bank. However, although these two processes do contribute almost 90% of the observed wave energy within the harbour, this energy is spread over a wide frequency range resulting in small-amplitude wave forms. Therefore, the external wave climate does not appear to induce large waves within the harbour which may affect engineering structures or ship operations, unless all the components of the wave spectrum happen to be in phase. Even if this occurs, the maximum wave height is probably <0.5m.

The local wind-generated waves represent about 1/3 of the observed wave height. Due to the presence of background wave energy, this portion of the wave field component may grow very rapidly. This results in the development of a steep chop within the harbour soon after an increase in wind speed, as may be observed in conjunction with afternoon sea breezes. However, the local waves are restricted by fetch, water depth and interactions with tidal current. Therefore, although they can grow rapidly, they soon reach an upper limit, at which point they break.

The waves present within the harbour are capable of entraining sand-sized sediment on the shallow intertidal flats. This sediment may then be transported by tidal currents at velocities below sediment threshold ($<0.35ms^{-1}$). Given the extent of the intertidal regions within the harbour, wave action is a major source of suspended sediment in Tauranga Harbour. Although the numerical models employed by the THS did not explicitly consider wave activity, the calibration procedure employed partially compensated for the additional suspended sediment. The model

results underestimate sediment fluxes by 10 to 20%, with the greatest errors occurring in intertidal regions and the least in tidal channels.

The dominant seiche frequencies determined by this study are associated with Centre Bank, and not the major shipping channels. No change was noted in seiche frequencies between 1960-64 and 1983-85. Consequently the extension of dredging into Stella Passage has not resulted in additional seiching within the frequency range considered. It seems probable that further dredging will also not greatly affect seiching.

The renourishment of Pilot Bay beach has resulted in a sandy beach which may be expected to persist for about 10y. At the end of this period, the region dredged to provide the sediment is likely to require further dredging based on the THS predictions. Renourishment at this time would not affect any of the shipping channels, or the mooring area in Pilot Bay Channel.

However, renourishment has had an adverse effect on the boat ramp at the northwestern end of the beach. This area was accreting prior to 1984, but the rate of accretion has accelerated with the additional input of dredge spoil. If further renourishment were not undertaken, the rate of accretion could be expected to decline in 5-10y, but it will continue to accrete. Given that the boat ramp is considered desirable, it will require shifting or continual maintenance. In addition to accretion on the boat ramp itself, it appears that sediment is accumulating on the shallow platform offshore, although insufficient survey data are available to be certain.

Appendix 1 - Wave Generation Under Ideal Conditions

Ursell (1956), in a review of wind-wave generation theories, suggested that early wave theories were inadequate to account for observations of wave generation. However, the ideas expressed in a number of these theories are still considered to be valid (LeBlond and Mysak, 1978).

The first of these early theories was that of Lord Kelvin (1871), which in combination with the work of Helmholtz in 1888 has become known as the Kelvin-Helmholtz Instability Mechanism (Chandrasekar, 1961). This approach is based on the formation of a stratified shear flow in a two layer model which, for the purpose of wave generation in the ocean, assigns the lower layer a density of sea water and the upper layer a density of air. This approach has also been used for the generation and propagation of internal waves along boundaries in stratified layers of the ocean (Chandrasekar, 1961).

In a stable situation, and ignoring surface tension effects, waves propagate along the air/water interface or any other zone with a sharp density contrast. In a non-stable situation it is possible for energy to be transferred from the higher velocity layer to the lower velocity layer, which for wave generation requires that the wind is travelling faster than the sea surface. If the opposite occurs then the wave will dissipate due to energy losses to the air.

By including surface tension effects it is found that for wind speeds $<6.5ms^{-1}$ the surface tension suppresses the Kelvin-Helmholtz instability (Ursell, 1956). Therefore this theory can only account for the generation of waves at wind speeds $\geq 6.5ms^{-1}$, whereas observations show that waves can be generated at lower wind speeds (Chandrasekar, 1961; Komar, 1976). However, in 1947, Munk (Chandrasekar, 1961; Komar, 1976) noted that a change in the pattern of air flow over waves occurs at a wind speed of $6.5ms^{-1}$, manifesting itself as a marked increase in the irregularity and turbulence of the water surface.

Jeffreys (1925, 1926) proposed that wave growth occurred due to boundary layer flow separation on the leeward side of existing wave crests. The separated eddy results in a low pressure region at a location in the wave profile where particle velocities are upward (Fig. A1.1), producing a momentum transfer, $-\langle p\eta_t \rangle$, from the low pressure area to the existing wave field. For a sinusoidal, monochromatic wave field

the rate of energy transfer is given by:

$$-\langle p\eta_t \rangle = \pm\frac{s\rho_a}{g\rho_w}k^2C(U-C)^2\frac{\rho_w g H^2}{2} \qquad \ldots \text{A1.1}$$

where s = sheltering coefficient,

ρ_a = density of air,

ρ_w = density of water,

and U = wind speed.

Wave growth can only occur if the wind speed exceeds the wave velocity, with wave damping occurring in the opposite case. Jeffreys (1924) deduced a range of values from 0.23 to 0.32 for the sheltering coefficient, but model studies (Ursell, 1956; LeBlond and Mysak, 1978) produced a much lower range of values, indicating that the pressure forces produced by the Jeffreys mechanism would be too low for wave generation. Further, flow separation requires a stagnation point on the interface, which for the wind/wave situation only occurs at the onset of wave breaking (Banner and Melville, 1976). Thus the Jeffreys mechanism cannot lead to growth of non-breaking waves, due to the lack of flow separation, but may operate in the presence of breaking waves.

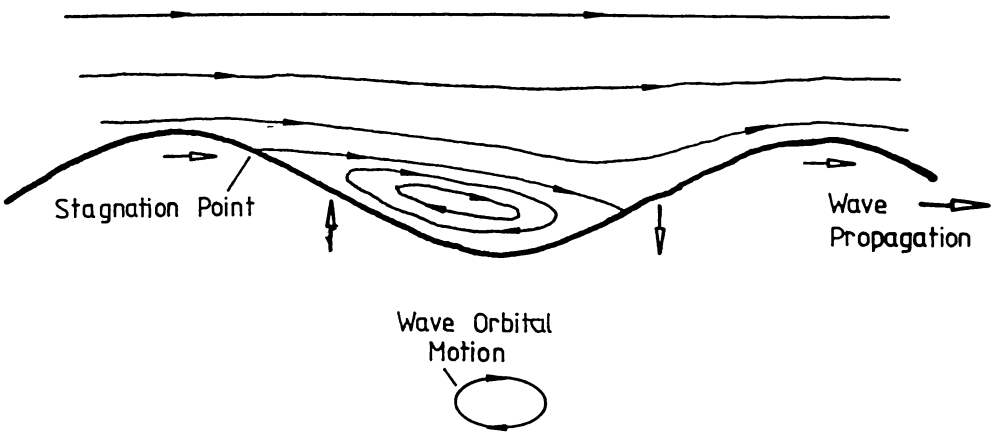

Figure A1.1 - Schematic of the sheltering theory for wave generation as proposed by Jeffreys (1925).

Banner and Melville (1976) found that a sharp increase in the rate of momentum transfer from air to sea occurs over breaking waves. Since in a fully developed sea the high frequency component of the spectrum is dominated by wave breaking, it is possible that the wave separation

produced by the breaking of these waves would contribute to the growth of lower frequency waves (LeBlond and Mysak, 1978). Komar (1976) states that the lowest wind speed at which energy is effectively transferred to a wave is $4.8ms^{-1}$. However, Banner and Melville (1976) found that energy was transferred effectively at $4.3ms^{-1}$. This suggests that, for breaking waves, the minimum wind speed at which energy transferal begins is $<4.3ms^{-1}$.

Wuest in 1949 and Lock in 1954 (Ursell, 1956; LeBlond and Mysak, 1978) extended the Kelvin-Helmholtz Instability theory to explain the growth of small oscillations from an almost still surface. Lock assumed that laminar boundary layers form above and below the interface. The boundary layers start at a definite point on the interface with no boundary layers occurring upwind. A slight oscillation with a wave height much smaller than the distance from the origin of the boundary layers propagates down wind (Fig. A1.2). This leads to perturbations in the flow which in some conditions lead to amplification of the waveform and decay in others. The conditions leading to decay or amplification can be quantified in terms of the wind speed, distance from the origin of the boundary layers, and the wavelength of the original oscillation.

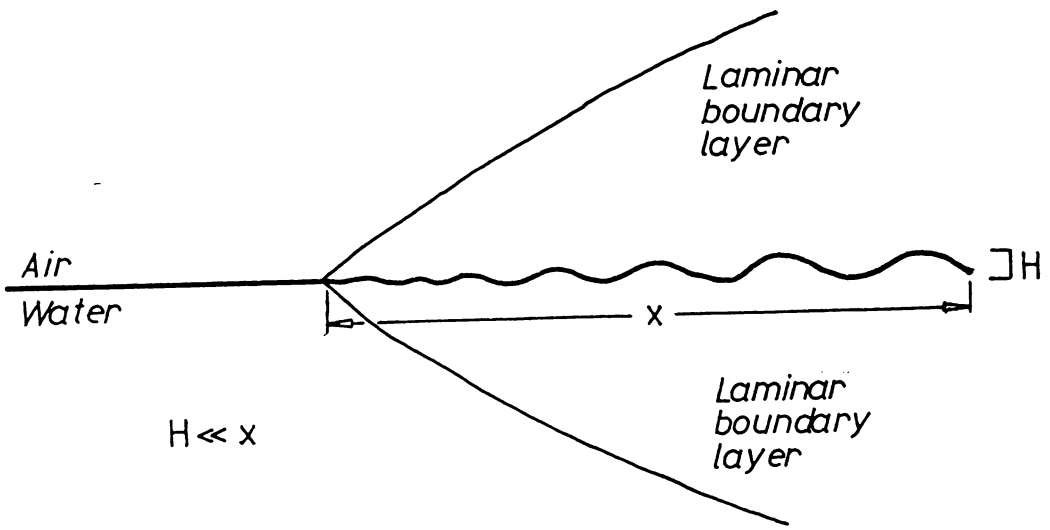

Figure A1.2 - Schematic of the instability mechanism for wave generation proposed by Lock in 1954.

The model developed by Wuest is similar except that hypothetical steady velocity profiles are used instead of laminar boundary layers. These approaches provide for the generation of waves by wind speeds down

to 1.0ms^{-1}. However, there are reservations about the applicability of these theories (Ursell, 1956). The model developed by Wuest uses several physically inconsistent assumptions about the boundary layer structure, resulting in an infinite shear stress on the interface. Ursell (1956) also notes that several of Wuest's computations contain errors, so the results may be invalid. The Lock model requires a persistent laminar boundary layer with a sharp leading edge. This is difficult to achieve experimentally and may not occur at all during wave generation.

All the mechanisms considered above require a pre-existing wave field, or some initial oscillation, which initiates and contributes to wave generation. It is evident that wave generation does occur more readily when the interface is not still (Chandrasekar, 1961; Chiswell and Kibblewhite, 1981). However, it is also evident that waves can be generated from an initially still surface, when the above mechanisms do not operate. Eckart (1953) proposed that wave growth from an initially still surface was due to a random distribution of pressure gusts and the tangential stresses exerted by these gusts on the water surface. However he concluded that this mechanism does not completely account for observed wave spectra produced by a given wind speed.

Phillips' (1957) theory explains initial wave formation and is essentially an extension of the mechanism proposed by Eckart (1953). Turbulent pressure gusts advect over the water surface at a velocity determined by the wind speed. Resonance is possible when the wave phase velocity matches the rate of advection of the pressure cells. This mechanism accounts for the formation of waves on an initially still surface but it is too weak to account for the continued growth of wind waves.

Additional growth can be accounted for by a momentum transfer mechanism, such as that proposed by Miles (1957). Once the waves are large enough to affect the airflow behaviour over them, Miles (1957) showed that any waves on the sea surface must be matched by waves on the bottom of the air layer resulting in small perturbations in the mean shear flow across the air/water boundary. These perturbations lead to a transfer of momentum from the wind to the wave field with the magnitude of this transfer at any frequency being proportional to any wave energy already present. The rate of energy increase for a particular wave is

given by:

$$\delta E/\delta t = C\tau_0 \qquad \ldots \text{A1.2}$$

where τ_0 = shear stress at the water surface.

A combination of the Phillips and Miles theories provides a mechanism for generating waves from an initially still surface. There are however serious discrepancies between the values for the rate of energy transfer and wave growth predicted by the Miles-Phillips approach and the values actually observed, especially in the presence of an existing wave field (Komar, 1976; Riley *et al*, 1982). In general the Miles-Phillips approach underestimates the rate of energy transfer (Riley *et al*, 1982).

Two additional mechanisms for wave generation proposed by Stewart in 1967 and developed by Longuet-Higgins in 1969 are discussed by Komar (1976). The first of these suggests that the boundary layer induced by wind stress on the surface is thickest on the upwind slope of an existing wave, permitting energy transfer to the wave. The second mechanism, known as the Maser Mechanism, suggests that energy is absorbed by long period waves from the breaking and steepening of smaller short period waves as they coincide (Banner and Melville, 1976). The short period waves are then regenerated by the wind through some other mechanism.

Recent studies, such as JONSWAP (Hasselmann *et al*, 1973; Hasselmann *et al*, 1976), have highlighted the importance of non-linear wave/wave interactions in the generation of longer period waves once an initial wave field has developed. Hasselmann *et al* (1973) have determined an energy balance equation for the development of a wave field. This relationship is based on three energy terms and can be expressed as:

$$S = S_{in} + S_{nl} + S_{ds} \qquad \ldots \text{A1.3}$$

These energy terms represent the energy input from the atmosphere via momentum transfer (S_{in}), the non-linear energy transfer due to conservative wave/wave interactions (S_{nl}), and the energy dissipated by

wave/wave interactions and non-linear processes such as white-capping (S_{ds}). The combination of these three terms, across the range of frequencies present, leads to the development of a characteristic spectral shape (Fig. A1.3), assuming no energy losses due to other processes such as shoaling. Once a dynamic equilibrium is achieved between the energy factors, no further changes should occur to the energy spectrum, and the spectrum is said to be saturated (Phillips, 1985).

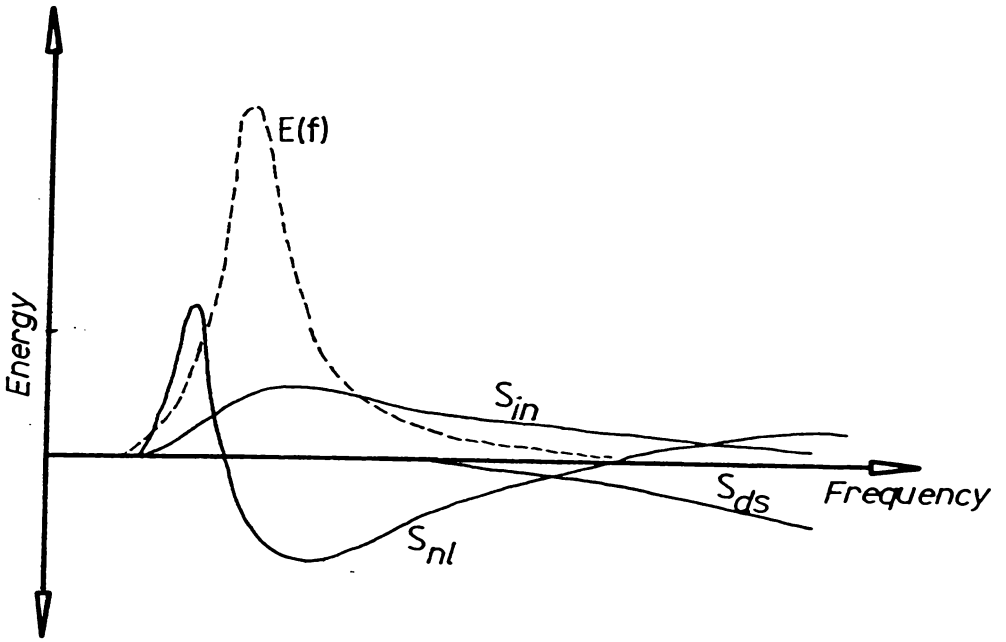

Figure A1.3 - Schematic diagram showing the three energy terms in Equation A1.3 and their relationship to the energy spectrum. After Hasselmann *et al* (1973).

Appendix 2 - Wave Prediction Models

In the absence of accurate theoretical formulations, empirical relationships have been derived to allow a wave spectrum to be predicted from a few parameters defining the wind field. A large number of numerical schemes are discussed in the literature but only a few appear to be widely used. Of these, even fewer may be applicable to estuarine conditions, since most are derived for near ideal conditions, i.e. deep water with unlimited fetches. The models which may be suitable for wave prediction in Pilot Bay, and Tauranga Harbour, are discussed below.

A2.1 - Sverdrup-Munk-Bretschneider (SMB) method

The SMB method is based on a series of predictive curves developed by Sverdrup and Munk (1947) and later modified by Bretschneider (1977) using additional empirical data. These curves have been converted to a series of equations which predict the spectral wave height (which is less than the significant wave height in shallow water) and the peak spectral period (Shore Protection Manual (SPM), 1984). The spectral parameters are preferable for shallow water wave prediction, since they are based on the wave energy, whereas other wave parameters are not (Vincent, 1985a). The predictive equations are based on the fetch and an adjusted windspeed given by:

$$U_A = 0.71U^{1.23} \qquad \ldots \text{A2.1}$$

where U = the wind speed at 10m.

These parameters are then used in the following set of predictive equations:

$$\frac{gH_\sigma}{U_A^2} = 0.0016(gF/U_A^2)^{1/2} \qquad \ldots \text{A2.2}$$

$$\frac{gT_p}{U_A} = 0.2857(gF/U_A^2)^{1/3} \qquad \ldots \text{A2.3}$$

where g = gravitational acceleration,

H_σ = spectral wave height,

and T_p = spectral peak period.

A relationship is also available (SPM, 1984) which defines the minimum time the wind must blow to ensure the waves are fetch limited and not duration limited. This is given by:

$$\frac{g\bar{\bar{D}}}{U_A} = 0.688(gF/U_A^2)^{2/3} \qquad \ldots \text{A2.4}$$

The SMB method produces only the spectral wave height and period and no other data about the spectral density.

A2.2 - Liu method

Liu (1971) derived an empirical spectrum for fetch-limited deep-water waves using wind and wave data collected from Lake Michigan in 1967. The wind speed was recorded at 4m, 8m, 12m and 14m above the mean water surface. The hourly averaged wind speeds were then fitted to a logarithmic curve to derive the wind speed at 10m above the surface. The friction velocity U* is derived from the 10m speed by

$$U_* = U(U^2/(gF))^{1/3} \qquad \ldots \text{A2.5}$$

A total of 62 sets of wind data and their corresponding wave records were normalised and used to derive a best-fit curve utilising a different similarity analysis to that used by Pierson and Moskowitz (1964). The records covered a range of wind speeds of 5-15ms^{-1} and included both decaying and growing wave fields. The fetch limits considered are not given by Liu (1971). Defining a dimensionless fetch parameter $\bar{F}_o$ as

$$F_o = gF/U_*^2 \qquad \ldots \text{A2.6}$$

the spectrum is given by:

$$S(f) = \frac{0.4g}{(2\pi)^4 F_o^{1/4}} f^{-5} e^{(-0.0055(g/(2\pi U_* F_o^{1/3}))^4 f^{-4})} \qquad \ldots \text{A2.7}$$

Essentially the equation tends to the same form as the spectrum proposed by Pierson and Moskowitz (1964), especially at longer fetch values (Komar, 1976). Liu (1971) suggests that this spectrum is applicable to deep-water wind waves which are fetch limited and not fully developed. Komar (1976) notes that this spectrum will never reach an equilibrium state for low frequency waves, indicating that a fully developed sea cannot be attained. The spectrum as developed does not include the wind duration. Liu (1971) indicates that the applicability of this spectrum is restricted to cases of sufficient duration, but no definition of the minimum duration required is given.

A2.3 - JONSWAP method

In 1969 the Joint North Sea Wave Project (JONSWAP) was carried out in the North Sea west of Denmark (Hasselmann *et al*, 1973). This project measured wave energy spectra at distances up to 160km from the shore during periods of wave growth. The results of this study were used to calculate a spectrum for a developing sea. This spectrum, the JONSWAP spectrum, is given by:

$$S(f) = \frac{\alpha g^2}{(2\pi)^4} f^{-5} e^{-(1.25(f/f_p)^{-4})} \gamma^q \quad \ldots \text{A2.8}$$

where α = constant (defined in Table A2.1),

γ = constant,

f_p = spectral peak frequency,

and $q = e^{-(f-f_p)^2/(2\sigma^2 f_p^2)}$

where $\sigma = \begin{cases} 0.07 & f<f_p \\ 0.09 & f>f_p \end{cases}$

For the mean JONSWAP spectrum γ=3.3 while the other constants and definitions are given in Table A2.1. This table summarises the original (Hasselmann *et al*, 1973) and revised values (Hasselmann *et al*, 1976). The JONSWAP spectrum is essentially the Pierson-Moskowitz spectrum with the addition of a peak enhancement factor. The JONSWAP spectrum has been used widely for a range of conditions (Kahma, 1981; Knowles, 1982; Bouws and Komen, 1983) resulting in a number of revised constants for particular situations.

Table A2.1 - JONSWAP non-dimensional parameters. After Carter (1982).

Parameter	Symbol	Values		
		Jonswap 1973	Fetch limited	Duration limited
Peak frequency	υ	$3.5\zeta^{-0.33}$	$2.84\zeta^{-0.3}$	$16.8\delta^{-3/7}$
Surface variance	ϵ	$9.91\times10^{-4}\alpha\upsilon^{-4}$	$1.63\times10^{-7}\zeta$	$4.08\times10^{-10}\delta^{10/7}$
Spectral shape	λ	1.96×10^{-4}	1.6×10^{-4}	1.6×10^{-4}
=	α	$0.076\zeta^{-0.22}$	$0.0662\zeta^{-0.2}$	$0.203\delta^{-2/7}$

Where ζ = non-dimensional fetch (gF/U^2) and δ = non-dimensional duration (gD/U).

A2.4 - TMA method

Kitaigorodskii *et al* (1975) derived a frequency dependent depth scaling factor, based on their transformed equilibrium range upper bound relationship (Equation 5.3). The scale factor is given by:

$$\Phi(2\pi f,h) = \frac{k^{-3}(\omega,h)(\partial k(\omega,h)/\partial\omega)}{k^{-3}(\omega,\infty)(\partial k(\omega,\infty)/\partial\omega)} \quad \ldots \text{ A2.9}$$

where h = water depth,

and $\omega = 2\pi f$

This factor can be used to transform the deep water equilibrium range to a finite depth form. Bouws *et al* (1985) substituted the finite depth form of the equilibrium range into the basic JONSWAP equation to derive the TMA spectra, given by:

$$S(f) = \frac{\alpha g^2}{(2\pi)^4} f^{-5}\Phi(2\pi f,h)e^{-(1.25(f/f_p)^{-4})}\gamma^q \quad \ldots \text{ A2.10}$$

Vincent (1985a,b) and Hughes (1984) present equations, derived from this spectral form, for determining H_s and f_p at various depths.

The TMA spectrum assumes that saturation is achieved, so it is not available in fetch or duration limited forms. It also assumes a gently varying bathymetry with a slope less than 0.01, since it does not account for shoaling transformations. This spectrum shows good agreement with previous empirical relationships for shallow water spectra and with observed surf zone spectra between f_p and $2f_p$.

A2.5 - Discussion

All the models considered are based on only two parameters, fetch and wind speed. An accurate definition of the fetch and wind speed for the region and time of interest is necessary to provide accurate predictions. The 10m wind speed is the primary parameter used to define the wind field, although it is modified to produce an adjusted wind speed for the SMB model and a friction velocity for the Liu model. Therefore the definition of the 10m wind speed is of paramount importance.

Despite the different approaches utilised, all the models produce comparable results for fully developed conditions (Resio and Vincent, 1982; Hughes; 1984). There are major discrepancies between the various models for limited conditions, with no model intended to predict waves given a combination of restricted depth, fetch and duration.

Only the JONSWAP spectrum is available in a duration limited form (Carter, 1982), although both the Liu and SMB models do have criteria for assessing the influence of duration. All the models have strictly fetch limited forms, except for the TMA spectra. The TMA spectra represents a scaled form of the JONSWAP spectra, so although the scaling does not consider fetch directly, by selecting the appropriate JONSWAP spectrum fetch may be compensated for (Hughes, 1984).

The SMB and TMA spectra are the only ones which consider depth restrictions. However, the SMB model does not predict the spectral density or form, only the spectral wave height and period. These should be adequate for design considerations, but the full energy distribution is more useful when considering the hydrodynamics and sediment transport processes within the estuary.

Overall, if the conditions are not duration limited and only two parameters are required, the SMB model is the most applicable. Otherwise, a combination of the appropriate JONSWAP spectral form with the TMA scaling factor is more suitable.

Appendix 3 - Wave Recording Systems

Initial data collection was by the SUBTLE wave recording system developed by Black (1983) for Whangarei Harbour. This system used a Tasman Data Logger with a specially built timing unit connected to a Robertshaw Capacitance Transmitter, Model 167-A-1, with a 6m long capacitance probe (Model 740-B1-A236) and a stainless steel earth rod (Plate A3.1). A voltage regulator was developed by Black (1983) to provide a constant 18V supply and to convert the 4-20mA output to a voltage range of 0.51-2.51V (Plate A3.2). The transmitter and probe used has a response time of 0.1s (Robertshaw, 1980) and a resolution of 0.024m in the configuration employed by Black (1983) and the initial data collection for this study.

The capacitance probe is covered with a Teflon insulator and the water height is determined by measuring the capacitance of the immersed coating (Bacchetti and Schuler, 1985). With the transmitter operating at radio frequencies, the probe should not be affected by changes in the conductivity of the fluid surrounding the probe. Black (1983) reports an 8% change in response between freshwater and seawater, but states that differences in salinity during a normal tidal cycle will have a negligible effect. Bacchetti and Schuler (1985) state that the configuration used will have a linear response for the purposes of level measurement in process control and this is supported by the calibration undertaken by Black (1983).

Black (1983) noted that radio frequency interference produced a slight ripple in the probe output voltage. This was compensated for by the addition of capacitors in parallel with the probe. Two configurations were tried at Whangarei, corresponding to extra capacitances of 69.8mF and 22.4mF. Black (1983) determined that these configurations reduced the wave amplitudes by 50% and 20% respectively. However, at Tauranga the majority of observed wave amplitudes were so small that the amplitude reductions due to additional capacitors was considered less desirable than the radio frequency interference ripple. Therefore, the additional capacitors were not used.

Once installed and calibrated by the procedure employed by Black (1983), data collection commenced. The probe was sampled at 8Hz for a total of 1024 data points every 6 hours, which allowed the device to run for up to 7.75 days before requiring attention. During calibration it

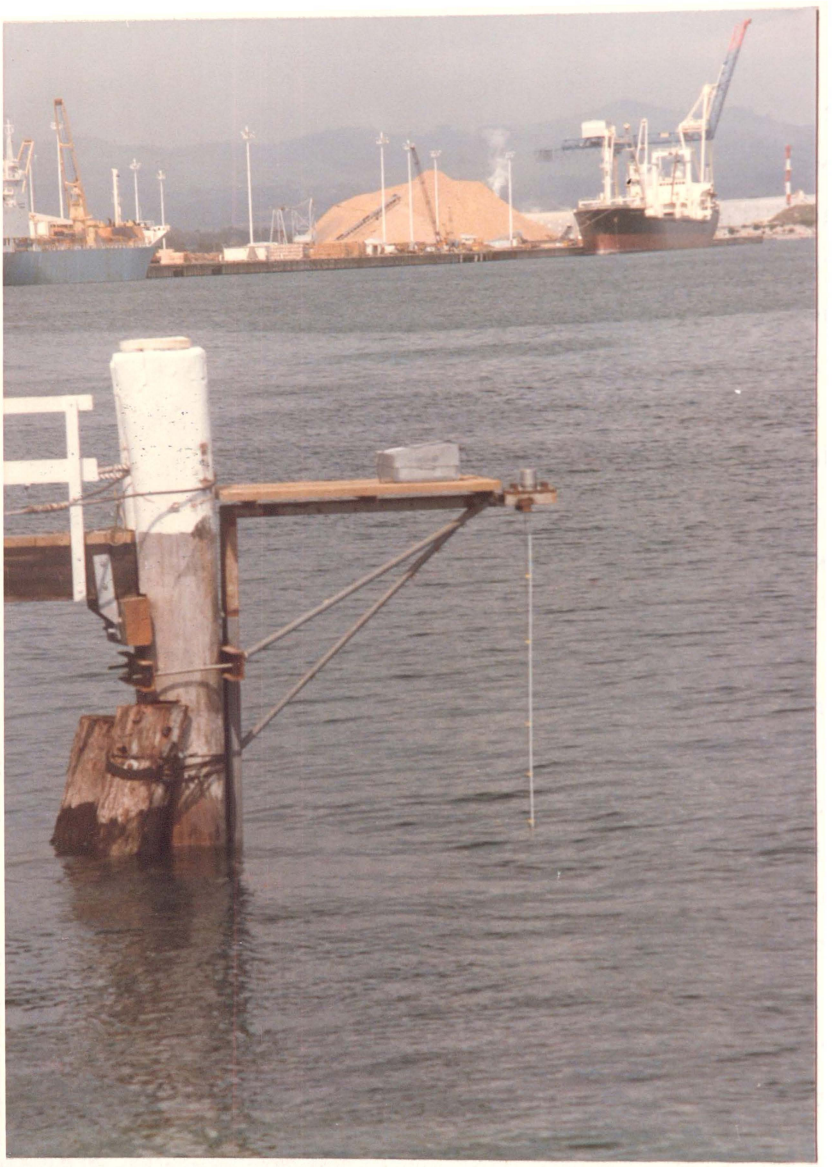

Plate A3.1 - The SUBTLE recording system as deployed on the southern BOPHB Tug Berth, Tauranga Harbour.

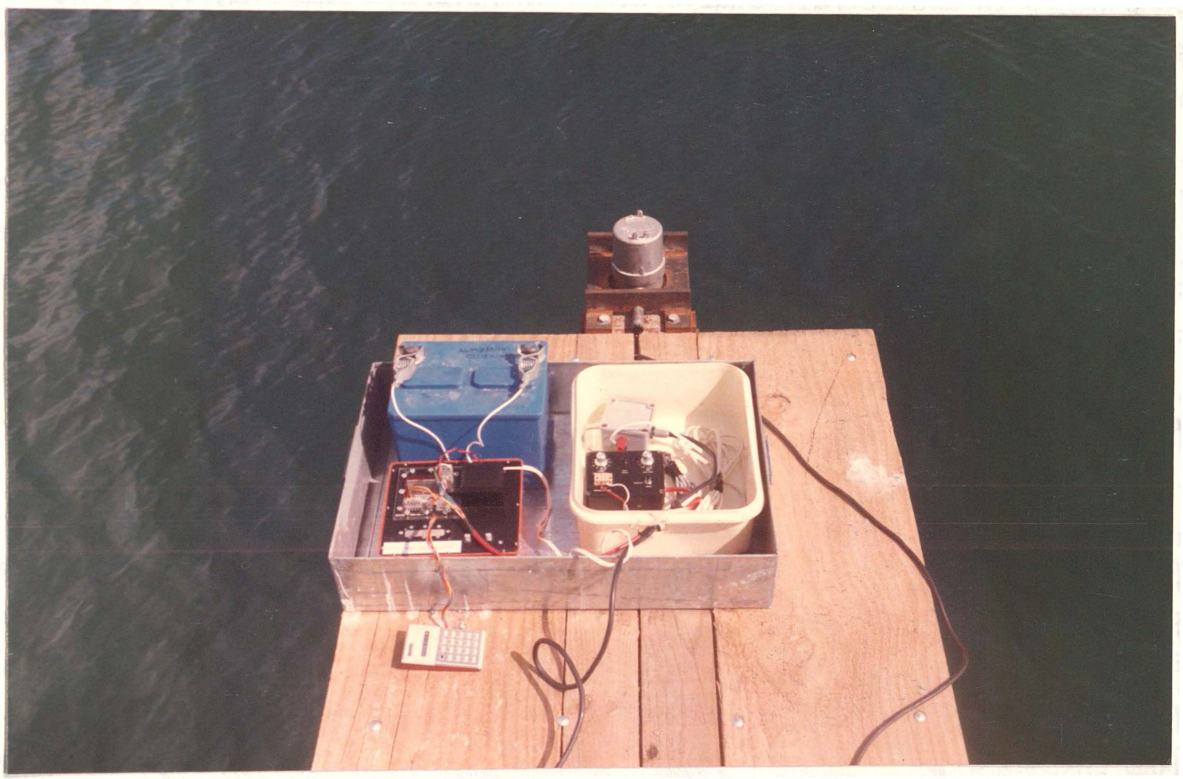

Plate A3.2 - Close up of the original electronics used to operate the capacitance probe and log the data.

was noted that the average water level, as determined by the mean of all probe values for a given sampling event, showed a linear response although the wave amplitudes were slightly amplified. Due to repeated component failures, most records obtained contained >10% dropouts, so very little usable data were collected. Eventually data collection had to be abandoned during Harbour Board dredging operations.

Examination of the data obtained showed that the resolution was insufficient to adequately detect small high frequency waves. The sampling rate of 8Hz defined the peaks of the waveforms well within the limits of the resolution, although some noise due to radio frequency interference did clutter the records. Further, given the short length of the record, 8Hz was too fast to detect and define swell wave components in a spectral analysis. Therefore a sampling frequency of 4Hz and a longer sampling period of 2048 data points were considered more desirable.

At the end of 1984 the data logger and associated hardware were returned to the Northland Harbour Board, leaving only the capacitance probe, transmitter and the voltage regulator. Subsequently a new data collection system was developed during January 1985 and installed at the completion of dredging.

A3.1 - The first Apple II+ wave recording system

The system developed in January 1985, consisted of two sensors and an Apple II+ computer. The first sensor consisted of the remaining components of the SUBTLE system. The second was provided by the Harbour Board pressure transducer tide gauge. To distinguish these sensors they will be referred to as the wave probe and the tide gauge respectively. The tide gauge is a Philips P9404/215/60161 pressure transducer with a settling time of 0.5s and a resolution of 0.005m. This transducer produces a 4-20mA signal which is converted by a chart recorder to a 0-1V signal. It was discovered that on occasions the reading exceeded 1V so it was necessary to treat the input as a 0-5V range, with a corresponding loss of resolution. This transducer was located on the older of the two tug berths (713106N 274823E).

The wave probe consisted of the remaining components from the SUBTLE system. The resolution of the capacitance probe was improved by using a

12-bit A/D convertor instead of the 8-bit version employed by the Tasman Data Logger. This resulted in a resolution of 0.003m (cf. 0.024m). The probe was located on the newer tug berth (713066N 274816E). The output from the voltage regulator was transmitted to the data logger via 175m of coaxial cable. No significant signal losses or interference were determined during testing.

To avoid interference from waves reflected off the tug berth piles a special mounting frame was built to extend the probe 3m out from the end of the berth. Visual observations indicated that reflected waves from other sources were negligible. The major disadvantage of this location was its vulnerability to passing shipping and berthing operations (Plate A3.1).

Both signals were fed into the Apple II+ computer via an Interactive Structures AI13 12-bit A/D convertor. The two channels were sampled alternately, which at high sampling rates (>256Hz) could result in cross-talk between the channels (Interactive Structures, 1981). To minimise this, each channel was read twice and the first reading discarded, although such a high sampling rate was not required. Timing was conducted by software loops so that the timing could not be set exactly to a desired rate.

The readings were stored as 12-bit numbers by separating the high and low order bytes and storing them sequentially. The graphic screen memory of the Apple was utilised, giving 2048 readings per channel. At the completion of a sampling event, the graphic screens were stored on disk. All data sets were automatically assigned a filename determined by the time at which sampling began. All disks were self-booting so that the system would restart in the event of a power failure.

The amount of data collected was limited by the storage space on disk and the availability of people to change disks. The records were collected at hourly intervals with an actual sampling rate of 4.57Hz for 2048 data points per sensor. For Pilot Bay this meant that data could be collected at 1 hour intervals, for 23 hours a day, during the working week.

The data collection system ran from 12/2/85-26/3/85, with the first week being used as a calibration and testing period. During this initial period, a minor fault was discovered in the software which prevented the system from storing more than two sampling periods before requiring

rebooting. Difficulties were experienced with the link to the tide gauge, mainly due to voltage surges. These necessitated altering the gain on the tide gauge A/D channel from 0-1V to 0-5V full range. It was also determined that the wave probe transmitter drew more than the specified 28mA (Robertshaw, 1980) due to the length of coaxial cable used, resulting in a faster than anticipated battery drain.

Revised software and larger capacity batteries were installed on February 19, 1985. The system then operated 5 days a week until March 26, 1985. At that time it was discovered that the voltage regulator and batteries had failed so that the wave probe was no longer operational. The failure appeared to occur progressively, starting on March 13, and was marked by a steady decline in the response from the capacitance probe.

During this sampling period a total of 509 records were collected. Of these, at least 108 were affected by the progressive failure of the power supply, and others were affected by problems during the calibration and testing period. Eventually 360 records were assessed as being suitable for further analysis after conversion from raw data to actual water elevations.

Once the power supply problem had been identified, it was decided to redeploy the system with larger capacity batteries connected to a trickle charger. However, due to a collision with a BOPHB tug, the mounting platform was destroyed, and the transmitter and capacitance probe were damaged. This delayed redeployment until October, 1986, by which time a new system had been developed.

A3.1.1 - Data conversion

For the purposes of deriving a relationship between the raw data and actual elevations, the mean water level was determined from the corresponding Salisbury Wharf tide gauge chart for each sampling period. A comparison of water levels between the Salisbury Wharf tide gauge and the pressure transducer tide gauge made subsequent to the completion of the THS showed no significant deviations (J.C. Stephenson, pers comm., 1985), contrary to reported tidal deviations (Barnett, 1985). Comparison of mean water surface elevations between the pressure transducer and the capacitance probe sites also show no marked

deviation. Hence the Salisbury Wharf tide gauge was suitable for calibration of the mean water levels recorded.

The mean water levels at Salisbury Wharf were regressed against the raw data means for both the tide gauge and the wave probe. The r^2 values were 0.992 and 0.091 respectively. If the sensors behaved in a linear fashion and were stable with time the expected r^2 value would be 1.000. The tide gauge response is close but the wave probe shows a major discrepancy.

Checking back over the period that the recorder was operating, it was determined that the pressure transducer had been shifted by approximately 0.08m at 1230 NZST on March 1, 1985 (J.C. Stephenson, pers comm., 1985). The data were then split into two groups, representing before and after this event, and the regression repeated. The new values were 0.981 and 0.510 respectively before the shift, and 0.998 and 0.070 after the shift. This indicates an improvement in the behaviour of the tide gauge with time and a definite decline in the wave probe, which may be associated with component failures. The data were then regressed in daily groups (Table A3.1).

These results indicate that both sensors behaved irregularly during February 12-19, the calibration and testing period. Subsequent to the modifications made on February 19, the tide gauge operated well with r^2 values of 0.989-1.000. The wave probe showed a good response from February 20 to March 13, except for some strange values for February 28 and the morning of March 1. After March 13 the response of the wave probe declined rapidly and it shows little correlation with Salisbury Wharf tide levels. This period coincides with the failure of the wave probe power supply.

The residuals between predicted and observed values were examined for all regressions performed, to determine if there was any systematic pattern. The wave probe residuals showed no discernable trend other than that associated with the decrease in correlation noted above. The tide gauge residuals did show a consistent behaviour. As the actual water level rose, the magnitude of the residuals increased, so that at high tide the tide gauge was consistently under-reading the level by 3.5% of the total tidal range (about 0.05m for a mean tide).

This suggests that the transducer response is not linear, however the slopes of the regression lines are very close to the theoretical value

Table A3.1 - Wave recorder calibration results

Date	Wave Probe Intercept	Wave Probe Slope	Wave Probe r^2	Tide Gauge Intercept	Tide Gauge Slope	Tide Gauge r^2
12/ 2/85	-2.17776	0.24799E-2	0.962	-0.37938	0.50657E-2	0.998
13/ 2/85	-2.11346	0.23314E-2	0.945	-0.63355	0.53492E-2	0.963
14/ 2/85	-1.77821	0.21375E-2	0.866	-0.44783	0.49328E-2	0.964
15/ 2/85	-0.76972	0.12528E-2	0.856	-0.31851	0.43540E-2	0.989
18/ 2/85	-7.67450	0.72169E-2	0.856	-0.39055	0.49442E-2	0.981
19/ 2/85	-0.86841	0.15099E-2	0.292	-0.42496	0.48965E-2	1.000
20/ 2/85	-2.18465	0.24414E-2	0.923	-0.47435	0.49451E-2	0.999
21/ 2/85	-2.06397	0.22280E-2	0.885	-0.43438	0.48380E-2	0.997
22/ 2/85	-2.46544	0.24207E-2	0.981	-0.47036	0.49349E-2	0.999
25/ 2/85	-2.59487	0.25871E-2	0.995	-0.47988	0.49990E-2	0.999
26/ 2/85	-2.72725	0.46859E-2	0.972	-0.48512	0.49913E-2	0.999
27/ 2/85	-1.83415	0.19807E-2	0.919	-0.59352	0.51786E-2	0.989
28/ 2/85	0.70792	0.34132E-3	0.053	-0.51464	0.47927E-2	0.995
1/ 2/85[a]	-0.27658	0.11882E-2	0.697	-0.61855	0.51408E-2	0.993
1/ 2/85[b]	1.38140	0.15451E-3	0.994	-0.58300	0.52771E-2	0.998
4/ 2/85	-2.61154	0.26298E-2	0.986	-0.46467	0.49336E-2	1.000
5/ 2/85	-2.85485	0.28071E-2	0.982	-0.46899	0.49574E-2	1.000
6/ 2/85	-2.70240	0.26942E-2	0.982	-0.46217	0.49226E-2	0.998
7/ 2/85	-2.83834	0.27687E-2	0.982	-0.45771	0.49201E-2	0.999
8/ 2/85	-2.98403	0.28680E-2	0.991	-0.48930	0.50944E-2	0.999
11/ 2/85	-2.55891	0.25989E-2	0.994	-0.47011	0.50000E-2	1.000
12/ 2/85	-2.87541	0.27917E-2	0.990	-0.47485	0.49905E-2	1.000
13/ 2/85	-2.96517	0.27828E-2	0.963	-0.44369	0.48552E-2	0.996
14/ 2/85	-1.12301	0.18597E-2	0.460	-0.47674	0.49726E-2	0.999
15/ 2/85	-1.01003	0.15995E-2	0.363	-0.49306	0.50382E-2	1.000
18/ 2/85	0.73655	0.40109E-3	0.026	-0.53036	0.52075E-2	0.999
19/ 2/85	-0.23027	0.60200E-2	0.143	-0.54238	0.52748E-2	0.999
20/ 2/85	1.38063	-0.21400E-2	0.039	-0.51017	0.51329E-2	1.000
21/ 2/85	0.78401	0.87016E-3	0.005	-0.51611	0.51354E-2	0.999
22/ 2/85	1.39004	-0.41500E-2	0.087	-0.49446	0.50423E-2	1.000
25/ 2/85	3.68240	-0.18520E-1	0.635	-0.46314	0.49951E-2	0.999
26/ 2/85	-0.36347	0.16360E-1	0.426	-0.51302	0.51065E-2	1.000
Before	-0.99390	0.15339E-2	0.510	-0.44790	0.48458E-2	0.981
After	0.84758	0.22571E-3	0.070	-0.47912	0.50048E-2	0.998
Total	0.75866	0.28046E-3	0.091	-0.46881	0.49477E-2	0.992

On March 1 the tide gauge transducer was adjusted by approximately 0.08m at 1230 NZST; [a] indicates before the adjustment and [b] indicates after adjustment.

of 0.005 for a linear response. There is a marked fluctuation in the position of the intercept which should correspond to the depth of the transducer (-0.25m after March 8). The ability of the sensors to accurately predict the tide levels at Salisbury Wharf is not as important as measuring the amplitude of the waves correctly. Comparing

the tide gauge maxima and minima against Salisbury Wharf values gave good agreement to two significant figures. This is despite not correcting the data for the attentuation in amplitude inherent in pressure sensors (Bowden, 1983).

However, the wave probe values indicated an amplification of the amplitude by a factor of about 10-20. This was surprising, despite the indications of a slight amplification from the earlier data collected by the SUBTLE system, considering the results of Black (1983). The transmitter generates a DC voltage proportional to the difference in the RF waveforms transmitted through a reference capacitor and the capacitance probe (Robertshaw, 1981), and at fast sampling rates with rapidly varying levels it appears this produces an amplified form of the water level fluctuations as output, although averaging will still produce the correct mean water level.

The actual amplification produced was not constant, but varied with battery voltage, showing a steady decline after March 13. Analysis of the gain between the two sensors at 0.2857Hz for 266 records obtained for the period February 20 to March 12 1985, indicated that the amplification of the wave probe relative to the tide gauge was 16.3±1.0. After using this value to compensate for amplification, the wave probe results agreed with visual observations. Therefore it was decided to use the tide gauge spectral density in the vicinity of 0.2857Hz to determine the appropriate gain to correct for the wave probe amplification.

A3.2 - The second Apple II+ wave recording system

After repairing and testing of the capacitance probe and transmitter, a revised form of the wave recording system was developed during October, 1986. In the intervening period, the BOPHB had established a BBC computer as a data logger/processor for the pressure transducer tide gauge. Therefore, it is was decided not to incorporate that sensor into the system. Due to the loss of the mounting platform, a new location for the wave probe was also necessary.

The wave probe was attached to one of the supporting piles for the floating breakwater adjacent to the tug berths (713117N 274808E). The mounting system for the actual capacitance probe had to altered due to

the loss of the former mounting platform. The two rods were separated by plastic spacers at 0.5m intervals giving a 10mm gap. The transmitter was calibrated to operate over a 4.5m range within the total 6m length, starting 1m below the transmitter. This gives a theoretical resolution of 0.0015m (cf. 0.003m in the previous configuration). By reducing the operating range from 4.8 to 4.5m, some difficulties could be experienced with waves exceeding H_{max}=0.60m in conjunction with large spring tides. On the basis of the data collected during the previous periods, this occurrence was deemed to be unlikely.

The two rods were securely taped over the non-operational regions to prevent flexing of the unit. Flexing of the system in response to tidal current and wind stresses were observed in the previous configuration. This could induce additional apparent oscillations in the record, although the effect of the movement of piles was considered to be more significant. The system was then strapped to lengths of 200x50mm timber to provide extra rigidity and a mounting board which could be attached to piles. The spacers used also kept the rods 2mm away from the timber surface, preventing the retention of water in contact with the rods. After a few months, the growth of organisms eliminated this space, necessitating cleaning.

The transmitter was connected to the power supply, located within the BOPHB offices, via spare conductors in the cable connecting the pressure transducer to the Hydrographers Office. Although the transmitter operated over 4-20mA, due to the length of capable involved, the range at the voltage regulator was 15-31mA resulting in a different range of output voltages from the previous configuration.
These were still within the 0-5V full range capabilities of the A/D convertor. Heavy duty batteries were employed, which could be connected to a trickle charger as required. However, despite the longer power cables required, the voltage drain experienced was much lower than with the previous configuration.

Two software systems were employed. The first was a simple extension of the previous system. This sampled the wave probe for 4096 points per sample period and stored the raw data onto disk. The self-booting facility was omitted and twin disk drives were employed, enabling a total of 28 sampling periods before requiring attention.

The system was deployed on October 15 with a sampling frequency of

4.26Hz. Initially some difficulty was experienced with one of the power cable connections coming into contact with sea water. This significantly changed the voltage range, causing out of range errors in the A/D convertor. These problems were rectified, but re-occurred intermittently as the cable fastenings worked loose.

The time series data collected by this system underwent a zero up-crossing analysis by an Apple IIe as part of the pre-analysis, before being transferred to the Vax 11/780. This time the amplification of the wave heights was found to be relatively constant over the period considered, and a standard amplification of 8, derived during calibration, was assumed in all subsequent data analysis. Using the tidal heights from the BBC computer tidal system, the water elevation at the wave probe (Y) was given by:

$$Y = -2.73 + 0.0017X \qquad \ldots A3.1$$

where X = A/D convertor reading.

The zero up-crossing results were scaled from A/D convertor values to real units by multiplying by a scale factor of 2.125×10^{-4}, derived by dividing the slope by the amplification factor. This produced results consistent with visual estimates made with the aid of a stage board.

While this system was operating, new software was developed. The new version collected smaller samples and undertook a zero up-crossing analysis in real time. Most of the parameters derived by the Vax routines for the data collected previously were determined by the Apple, in addition to the variance, skewness and kurtosis of the sea surface elevations. All the data analyses were performed in terms of the raw data obtained from the A/D convertor. The results were then output to disk and a few were converted to real units and displayed on the VDU.

The timing for the data collection routine was changed to an interrupt driven system, which meant that the desired sampling rates could be achieved more accurately. As deployed, the system collected 256 data points at 4Hz every 15min. This gave a total capacity of 9.5 days per disk. A twin disk system was also used, doubling the operating capacity. The machine code version of this software could sample and analyse a set of data within 8min, whereas the BASIC version required

about 12min. These were the only limits on the rate at which samples were collected.

This version of the software was deployed from November 4, 1986, to December 31, 1986. Due to a software error, the initial period of deployment only saved one set of readings per day. This was rectified on November 12. A further development of this software involving spectral analysis was found to be feasible, but was not implemented.

The data collected by this system were converted to real units using the scale factor discussed above. This value was checked occasionally by comparing the value of H_s against visual estimates, and the results were found to be consistent.

During December 31, 1986, the batteries driving the computer clock dropped below the minimum voltage required, and the system shut down. New batteries were installed on January 10, 1987 and the system was reactivated. During the following week, the capacitance probe sustained damage to the teflon insulator, allowing electrical contact between the conducting core and sea water. As a result the wave probe ceased operating and had to be removed.

A3.3 - Wave recorder data analysis algorithms

The final wave recorder system was quite successful in terms of the data logging and analysis functions. The actual transducer used was less than satisfactory. This system was extended slightly to allow limited spectral analysis in addition to the zero up-crossing analysis. Due to the complete failure of the capacitance probe transmitter following the short circuit in the probe, this system was not tested in the field. Therefore only the algorithms used in the extended system are presented here.

After the raw data has been obtained the first step is to remove any tidal components or systematic changes in the still water level. This requires that the data is detrended and the simplest detrending function appropriate for the conditions encountered within Tauranga Harbour, is linear. This is achieved by applying a linear regression to the data to determine the slope of the still water surface. The calculated still water surface is then rotated, adjusted to zero and removed from the original data. The data will then range either side of zero.

A simple algorithm for performing a linear detrend and calculating the mean water level, T_c and H_σ, assuming n data points (y[1..n]) at intervals of Δt, is as follows:

1) $\Sigma x=\Sigma y=\Sigma x^2=\Sigma xy=\Sigma v=c=00$

2) Repeat for x=1 to n.
$\Sigma x=\Sigma x+x$, $\Sigma y=\Sigma y+y[x]$, $\Sigma x^2=\Sigma x^2+x*x$, $\Sigma xy=\Sigma xy+x*y[x]$

3) $A=(\Sigma xy-\Sigma x*\Sigma y/n)/(\Sigma xx-\Sigma x*\Sigma x/n)$
$B=(\Sigma y-A*\Sigma x)/n$
$M=\Sigma y/n$

At this stage we have defined the still water level as y=Ax+B, and the mean position of this surface as M in terms of the wave probe coordinate system.

4) Repeat for x=1 to n.
y'[x]=y[x]-(A*x+B)

Having detrended the data it is then possible to perform a zero up-crossing analysis. The following routine extracts the wave heights from the record and stores them in an array. Wave heights are determined from parabolic fits to the upper and lower parts of the wave record between two consecutive zero up-crossings. These require a minimum of four data points per wave, so that the wave height array requires a dimension of n/4. This routine also determines T_z and T_c and can be modified to calculate statistical wave period parameters (T_s and T_{10}) by using linear interpolation to determine the time of each zero up-crossing within the record.

5) Repeat for x=1 to n
$\Sigma yy = \Sigma yy + y[x]^2$
$H_\sigma = 4*\Sigma yy^{½}$

6) $x' = 1$
$\Sigma yy = c = N_z = y_b = y_t = H_m = H_{rms} = H_s = H_{10} = 0$

7) Repeat until ((y[x']≤0) and (y[x'+1]>0)) or (x'≥n-1)
$x' = x' + 1$
$x_b = x_t = x' + 1$

8) Repeat for x = x'+1 to n-1
If (y[x-1]<y[x]) and (y[x]>y[x+1] Then
$c = c + 1$

If ($y[x] < y_b$) Then
$y_b = y[x]$
$x_b = x$
If ($y[x] > y_t$) Then
$y_t = y[x]$
$x_t = x$
If ($y[x] \leq 0$) and ($y[x+1] > 0$) Then
$u_1 = y[x_t+1] - y[x_t-1]$
$u_2 = y[x_1+1] + y[x_t-1] - 2y[x_t]$
$u_3 = u_1 / (2u_2)$
$H_t = y[x_t] + u_3/2 + u_3^2 u_2/2$
$u_4 = y[x_b+1] - y[x_b-1]$
$u_5 = y[x_b+1] + y[x_b-1] - 2y[x_b]$
$u_6 = u_4 / (2u_5)$
$H_b = y[x_b] + u_6/2 + u_6^2 u_5/2$
$N_z = N_z + 1$
$H[N_z] = abs(H_t - H_b)$
$y_t = y_b = 0$
$x_t = x_b = x$

9) Repeat for $x=1$ to N_z
Repeat for $x'=1$ to $N_z - x$
If $H[x'] < H[x'+1]$ Then
$H_t = H[x']$
$H[x'] = H[x'+1]$
$H[x'+1] = H_t$

10) $T_c = (n-1)*\Delta t/c$
$T_z = (n-1)*\Delta t/N_z$
$N_3 = |N_z/3|$
$N_{10} = |N_z/10|$
$H_{max} = H[1]$

11) Repeat for $x=1$ to N_z
$H_m = H_m + H[x]$
$H_{rms} = H_{rms} + H[x]^2$
If ($x \leq N_3$) Then
$H_s = H_s + H[x]$
If ($x \leq N_{10}$) Then
$H_{10} = H_{10} + H[x]$

12) $H_m = H_m/N_z$
$H_{rms} = (H_{rms}/N_z)^{1/2}$
$H_s = H_s / N_3$
$H_{10} = H_{10} / N_{10}$

Spectral analysis requires two main subroutines; one to calculate the wavenumber for any given frequency, and the second to undertake the Fast Fourier Transform. The wavenumber (k) can be derived by solving the Linear Wave Dispersion relationship numerically using the Newton-Raphson iterative method. The following algorithm performs this analysis, given the water depth (h) and the wave frequency (f), and produces the product

kh, which can be converted to wavenumber by dividing by depth if needed.

s1) h and f transferred to subroutine
g = 9.81

s2) $kh_0 = (2\pi f)^2 h/g$
If ($kh_0 \geq 6.3$) Then
$kh = kh_0$
Exit routine

s3) $kh = kh_0^{½}$

s4) Repeat until abs($\delta kh/kh$)$\leq$0.0001 (0.01% error)
sh = sinh(kh)
ch = cosh(kh)
$ep = kh_0 - kh*sh/ch$
$sl = -kh/ch^2 - sh/ch$
$\delta kh = -ep/sl$
$kh = kh + \delta kh$

s5) Exit routine

The following routine performs fast fourier transforms and inverse fast fourier transforms (FFT and FFT^{-1}) by separating the imaginary and real parts of the complex fourier coefficients into two arrays FI[] and FR[] respectively. This routine will only work for arrays of dimension 2^m, where m = 0,1,2,3,... Normally when entering the routine, FR[] contains the time sequence and the fourier function will be returned in FR[] and FI[]. If a FFT^{-1} transform is required, on entering the routine FR[] and FI[] contain the fourier function and the time series will be returned in FR[]. The routine also requires the value of n ($=2^m$) and a flag to indicate the required analysis as follows:

flag$\geq$0 - FFT

flag<0 - FFT^{-1}

s1) Pass FR[], FI[], n and flag to subroutine

s2) If flag<0 Then
Repeat for i=1 to n
FI[i] = -FI[i]

s3) mr = 0
nn = n-1

s4) Repeat for m=1 to nn
o = n
Repeat until mr+o$\leq$nn

```
                o = o/2
            If mr>m Then
                tr = FR[m+1]
                ti = FI[m+1]
                FR[m+1] = FR[mr+1]
                FI[m+1] = FI[mr+1]
                FR[mr+1] = tr
                FI[mr+1] = ti
```

s5) o = 1

```
s6)  Repeat until o≥n
         inc = 2*o
         eo = o
         Repeat for m=1 to o
             a = π(1-m)/eo
             wr = cos(a)
             wi = sin(a)
             Repeat for i=m to n step inc
                 j = i + o
                 If flag<0 Then
                     tr = wr*FR[j] + wi*FI[j]
                     ti = wr*FI[j] - wi*FR[j]
                 Else
                     tr = wr*FR[j] - wi*FI[j]
                     ti = wr*FI[j] + wi*FR[j]
                 FR[j] = FR[i] - TR
                 FI[j] = FI[i] - TI
                 FR[i] = FR[i] + TR
                 FI[i] = FI[i} + TI
         o = inc
```

```
s7)  an = n

s8)  If flag≥0 Then
         Repeat for i=1 to n
             FR[i] = FR[i]/an
             FI[i] = FI[i]/an

s9)  Exit from routine
```

Using these routines the following algorithm will derive the energy densities at each frequency and scale them to adjust for pressure attenuation. This spectrum will then be used to derive spectral wave parameters. The routine assumes that the data received consists of detrended sea levels with a mean of 0. Further the routine requires the water depth (h) and the height of the transducer above the bottom (b).

13) Call FFT routine with FR[] containing n values of y and flag=1

14) n2 = n/2

freq = $1/((n-1)\Delta t)$

15) Repeat for i=1 to n2
    Sf[i] = FR[i]^2 + FI[i]^2
    f[i] = (i-1)*freq

16) Repeat for i=1 to n2
    Call wavenumber routine with depth and freq[i]
    kb = kh * b / h
    kp = cosh(kb) / cosh(kh)
    Sf[i] = Sf[i] / kp^2

17) $m_0 = m_1 = m_2 = m_3 = m_4 = Q_p = f_p = d_p = 0$

18) Repeat for i=1 to n2
    If Sf[i]>dp Then
        d_p = Sf[i]
        f_p = freq[i]
    If (i=1) or (i=n2) Then
        xdf = freq/2.0
    Else
        xdf = freq
    Q_p = freq[i] * Sf[i]^2 * xdf
    m_0 = m_0 + Sf[i] * xdf
    m_1 = m_1 + Sf[i] * xdf * freq[i]
    m_2 = m_2 + Sf[i] * xdf * freq[i]^2
    m_3 = m_3 + Sf[i] * xdf * freq[i]^3
    m_4 = m_4 + Sf[i] * xdf * freq[i]^4

19) $T_p = 1/f_p$
    $T_c = (m_2/m_4)^{1/2}$
    $T_z = (m_0/m_2)^{1/2}$
    $H_{m0} = 4m_0^{1/2}$
    $H_e = 2^{3/2}(m_0)^{1/2}$
    $Q_p = 2Q_p/m_0^2$
    $\epsilon_s = (1-m_2^2/(m_0m_4))^{1/2}$

Appendix 4 - Hydraulic Behaviour of Tauranga Harbour Sediments

The textural analyses undertaken by both the THS and this study were performed using the University of Waikato Rapid Sediment Analyser (RSA). This device consists of two concentric perspex tubes: the inner being the settling tube; and the outer tube creating a water jacket around the inner tube which minimises temperature fluctuations and provides additional structural rigidity. Samples are mechanically introduced at the top by a cassette fitted with sliding trapdoors. The sediment falling down the tube is collected at the bottom on a plastic tray connected to an electronic balance.

Both the sample cassette and the balance are connected to an Apple II+ computer which samples the output of the electronic balance at ~4Hz when the cassette is opened. These data are analysed by the Apple to produce a range of textural parameters. Since these parameters may need to be compared with results determined by standard seiving techniques, it is necessary to consider the behaviour of sediment within the settling tube and determine what effects the settling behaviour and the RSA analyses may have on the final textural parameters.

The sediment present within Tauranga Harbour covers a wide range of densities (Table A4.1). In most cases, the observed densities are due to variations in the atomic structures of the minerals present so that density is independent of grain size. Pumice, however, shows density variations with grain size (Fig. A4.1) due to the porous structure within each grain (Heiken and Wöhletz, 1985). The grain porosity decreases with decreasing grain size until the density is primarily controlled by the density of the glass shards present (~2400kgm^{-3}).

The RSA derives equivalent sphere diameters from measured settling velocities using the empirical relationship of Gibbs *et al* (1971) with correction factors for grain density as determined by Komar (1981). The RSA only considers one grain density for each analysis, normally taken to be the density of quartz grains (2650kgm^{-3}), so it is necessary to consider the effects of mixed sediment-density variations on the grain size parameters determinated by the RSA.

The relationship between grain radius and settling velocity can be expressed as (Gibbs *et al*, 1971):

$$s = \frac{-3\mu+(9\mu^2+gr^2\rho(\rho_s-\rho)(0.015476+0.19841r))^{\frac{1}{2}}}{\rho(0.011607+0.14881r)} \quad \ldots \text{A4.1}$$

Table A4.1 - Typical clastic materials found within Tauranga Harbour sediments and their densities. Data after Moon (1983), Carmichael (1984) and Tilly (in prep.).

Material	Density (kgm^{-3})
Quartz	2650
Calcite	2710
Aragonite	2930
Feldspar	2570-2710
Ironsand	4680
Volcanic glass	2330-2413
Whole shell	2790-2900
Broken shell	2230
Pumice (saturated)	1120-2370

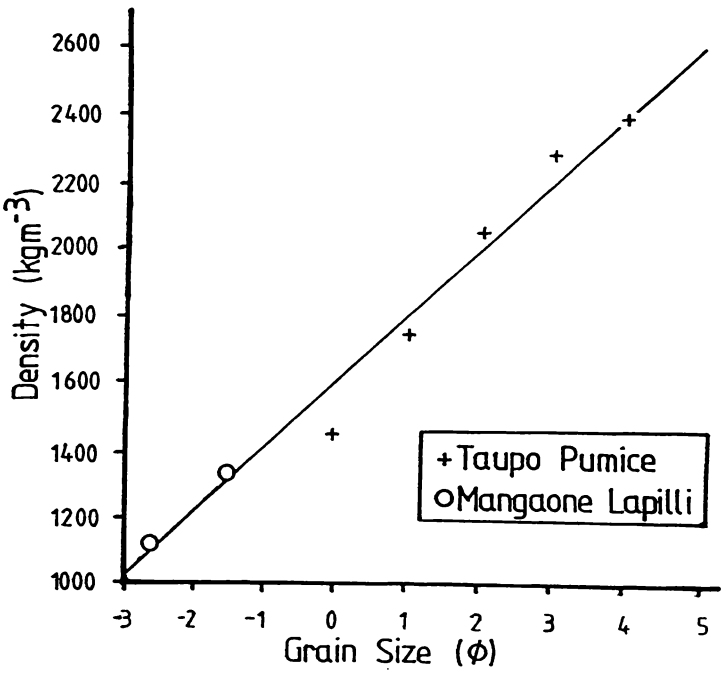

Figure A4.1 - Grain density versus grain size for saturated pumice as determined by Moon (1983) for Mangaone Lapilli and Tilly (in prep.) for Taupo Pumice. The line plotted was determined by linear regression and is given by $\rho=1601+199\phi$ ($r^2=0.97$).

where μ = dynamic viscosity (Poise),

r = grain radius (cm),

ρ = fluid density ($g.cm^{-3}$),

and ρ_s = grain density ($g.cm^{-3}$)

The settling velocities determined by the RSA are expressed as χ units, where χ is defined in terms of a temperature corrected settling velocity given by (May, 1981):

$$s = s_m + k(20-T)*s_m \qquad \ldots A4.2$$

where s_m = measured settling velocity (ms^{-1}),
T = temperature of settling fluid (°C),
and k = a correction factor given by

$s_m > 0.177$	$k = 0$
$0.177 > s_m > 0.002$	$k = -0.00555\ln(s_m) - 0.00961$
$0.002 > s_m$	$k = 0.025$

This equation gives the estimated settling velocity at 20°C, which can then be non-dimensionalised and transformed to give χ as follows (May, 1981):

$$\chi = -\log_2(s/s_0) \qquad \ldots A4.3$$

where s_0 = standard settling velocity ($1ms^{-1}$).

In order to investigate the effect of choosing a density of $2650kgm^{-3}$ for beach sediment containing a range of densities, equations A4.1 and A4.3 were used to determine the expected settling velocities over a range of grain sizes for typical non-carbonate sediments present in Tauranga Harbour (Fig. A4.2). As expected, for most materials the shape of the curve is constant, although it has been translated slightly. This indicates that for minerals with a density $<2650kgm^{-3}$ the RSA under-predicts the size, and for minerals $>2650kgm^{-3}$ the RSA over-predicts the size.

The behaviour of pumice is slightly different from the other materials, mainly due to the density variations associated with different grain sizes. It can be seen that settling velocity does not decrease with decreasing grain size for grains larger than -1.5ϕ (2.83mm). Figure A4.2 is based on saturated pumice clasts. If the clasts are unsaturated, or partially saturated, the density is lower than the corresponding saturated density (Moon, 1983). This effect is more marked with larger clasts due to the increased porosity, and non-saturated large pumice clasts may have densities lower than sea water

(1020-1035kgm^{-3}) so that they float. Due to these density variations, one χ value can correspond to two grain sizes, both of which are significantly under-predicted by the RSA.

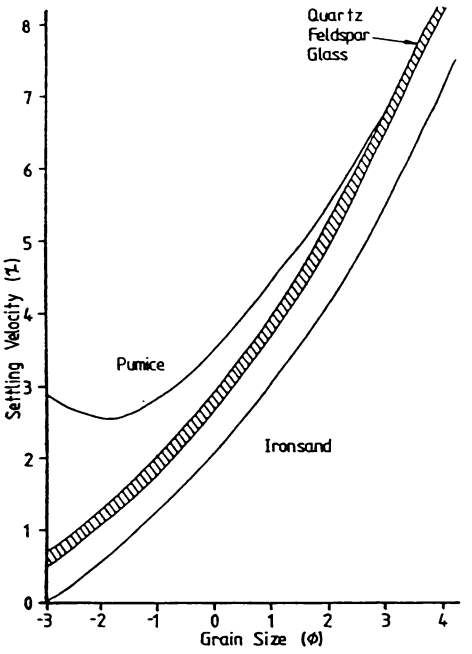

Figure A4.2 - Predicted settling velocity (χ) determined for typical non-carbonate sediments within Tauranga Harbour, using Equation A4.1.

The carbonate sediments within Tauranga Harbour are primarily shells and shell fragments. These clasts are normally platy which causes them to settle in an oscillatory fashion, rather than the linear paths followed by spherical grains (Mehta *et al*, 1980; Leeder, 1982). In general two major modes of settling are identified for carbonate clasts (Fig. A4.3): a stable mode where the clast remains essentially horizontal and traces out a helical spiral; and an unstable mode involving pronounced sliding and tipping. For any given mass, the stable settling mode results in a higher settling velocity than the unstable mode. Usually, as clasts become less platy their settling mode becomes more stable. Therefore, platy carbonate fragments have lower settling velocity than spheres of the same mass.

Three main species of shell occur in Tauranga Harbour sediment samples: *Paphies australis, Chione stutchburyi* and *Atrina zelandica*. It was assumed that these species contributed most of the shell fragments within the sediment. Examination of the sediment samples under a low power binocular

microscope indicated that the shell fragments became less platy with decreasing size, and for <1ϕ they were essentially spherical and could be assumed to settle at the terminal velocity of grains with the appropriate density.

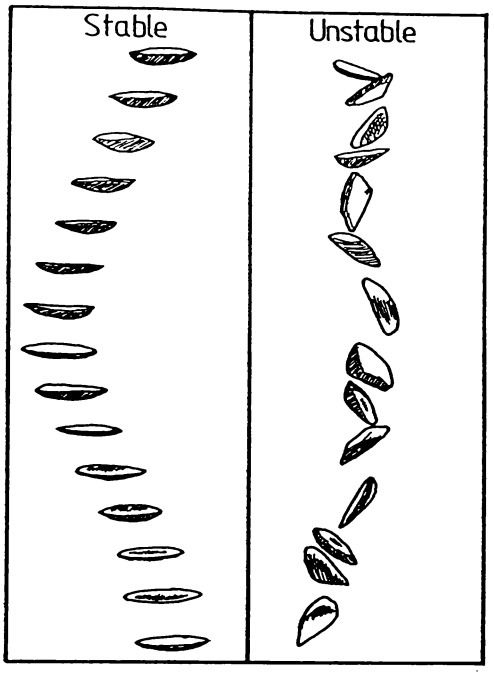

Figure A4.3 - Settling modes for carbonate sediments as determined by observations of whole shells and fragments in the University of Waikato RSA, and after Mehta *et al* (1980).

The settling velocity of larger grains could not be predicted by equation A4.1, with the actual settling velocity being considerably lower than that predicted for a sphere corresponding to the intermediate axis of the shell fragment (Fig. A4.4). Therefore, the carbonate sediments also display a non-linear relationship between grain size and settling velocity, similar to pumice. However, the deviations apparent with shell fragments are due to grain shape and not grain density.

If the actual grain size distributions are required, the grain size dependent deviations discussed above would be critical. This may be the case if sediment textural parameters were used as an environmental indicator by applying an empirically derived relationship determined for quartzose or quartzo-feldspathic sediments (Folk and Ward, 1957; Visher, 1969; Sunamura and Horikawa, 1972; Grace *et al*, 1978; Leeder, 1982). This type of relationship is usually derived from data obtained by seiving. Therefore, the relationship does not consider density or shape variations within the sediment. These variations may

be significant for the sediments encountered within Tauranga Harbour.

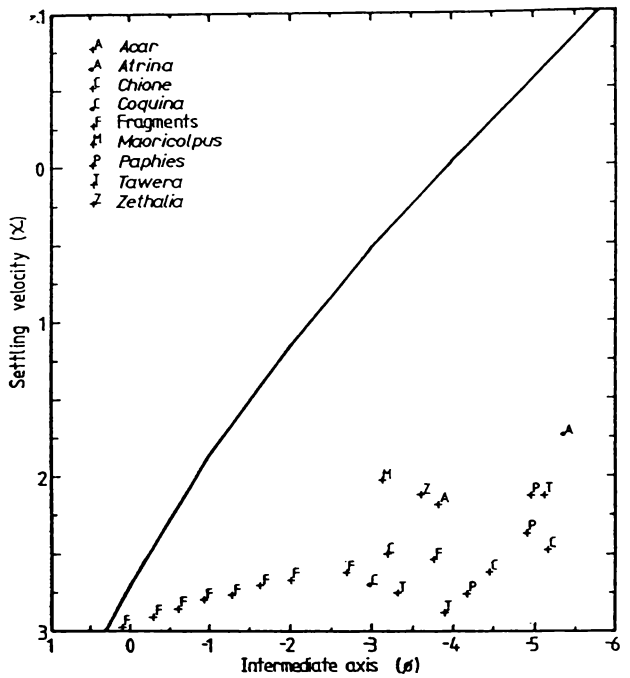

Figure A4.4 - Predicted settling velocity for quartz spheres with diameters corresponding to intermediate axes of carbonate shell fragments, compared to measured settling velocities. Settling velocity data obtained from Mehta *et al* (1980), Black (1984) and measurements in the University of Waikato RSA.

This study was concerned with the question of sediment transport. Most sediment transport equations are a function of grain diameter and grain density (Graf, 1971; Leeder, 1982). These are commonly taken as the median grain diameter (ϕ_{50}) and 2650kgm^{-3} respectively for mixed sediments. The ϕ results produced by the RSA represent the predicted distribution of quartz spheres with settling velocities equivalent to the measured velocity distribution of the sediment. Therefore the value of ϕ_{50} determined by the RSA has been adjusted to compensate for the actual density and shape variations within the sediment. This would not be the case if ϕ_{50} was determined by seiving.

References

Allen, J.R.L., 1977: *Physical Processes of Sedimentation*, 4th edition. George Allen & Unwin Ltd., London. 248p.

Bacchetti, J.A., and Schuler, E., 1985: Electronic principles of radio frequency level sensing. *Automation & Control* 15: 20-24.

Baird, W., and Thompson, E.F., 1977: The presentation of wave data. *Ports '77, 4th annual symposium of the Waterway, Port, Coastal and Ocean Division, ASCE*. Volume 2, pp. 382-393.

Banner, M.L., and Melville, W.K., 1976: On the separation of air flow over water waves. *Journal of Fluid Mechanics* 77: 825-842.

Bardsley, W.E., and Manly, B.F.J., 1983: Regression-based estimation of long-term mean and variance of wind speed at potential aerogenerator sites. *Journal of Climate and Applied Meteorology* 22: 323-327.

Barnett, A.G., 1985: *Overview and Hydrodynamics. Tauranga Harbour Study Part I & III*. A report for the Bay of Plenty Harbour Board.

Barnett, T.P., 1968: On the generation, dissipation and prediction of wind waves. *Journal of Geophysical Research* 73: 513-529.

Barry, R.G., and Chorley, R.J., 1982: *Atmosphere, Weather and Climate*. 4th edition. Methuen & Co. Ltd., London. 407p.

Barthel, V., 1982: Height distributions of estuarine waves. *Proceedings of the 18th International Conference on Coastal Engineering*. 136-153.

Beer, T., 1983: *Environmental Oceanography - An introduction to the behaviour of coastal waters*. Pergamon Press, Oxford. 262p.

Black, K.P., 1983: *Sediment transport and tidal hydraulics*. D.Phil thesis, Earth Science Department, University of Waikato.

Black, K.P., 1984: *Sediment Transport. Tauranga Harbour Study Part IV*. A report for the Bay of Plenty Harbour Board. 150p.

Black, K.P., and Healy, T.R., 1981: Computer programs for wave analysis, wind wave generation, wave refraction diagrams, and fast fourier analysis. *Occasional Report* No.6, Department of Earth Sciences, University of Waikato. 76p.

Blair-Mason, J., 1919: *Report on proposed developments*. Report to the Tauranga Harbour Board. 10p.

Boothroyd, J.C., 1978: Mesotidal inlets and estuaries. In Davis, R.A. (ed.), *Coastal sedimentary environments*. Springer-Verlag. 287-360.

Bouws, E., and Komen, G.J., 1983: On the balance between growth and dissipation in an extreme depth-limited wind-sea in the southern North Sea. *Journal of Physical Oceanography* 13: 1653-1658.

Bouws, E., Gunther, H., Rosenthal, W., and Vincent, C.L., 1985: Similarity of the wind wave spectrum in finite depth water, Part I - Spectral form. *Journal of Geophysical Research* 90C: 975-986.

Bowden, K.F., 1983: *Physical oceanography of coastal waters*. Ellis Horwood Ltd., Chichester. 302p.

Bretschneider, C.L., 1977: On the determination of the design ocean wave spectrum. *Look Lab/Hawaii* 7: 1-23.

Bridgwater, G.D., 1986: Littoral sediment transport at Mangatawhiri Spit, New Zealand. *New Zealand Journal of Marine and Freshwater Research* 20: 147-151.

Bunting, D.C., 1970: Evaluation forecasts of ocean-wave spectra. *Journal of Geophysical Research* 75C: 4131-4143.

Burrows, R., and Hedges, T.S., 1985: The influence of currents on ocean wave climates. *Coastal Engineering* 9: 247-260.

Carmichael, R.S. (ed.), 1984: *Handbook of physical properties of rocks*, Volume 3. CRC Press, Inc., Boca Raton, Florida. 340p.

Carter, D.J.T., 1982: Prediction of wave height and period for a constant wind velocity using the JONSWAP results. *Ocean Engineering* 9: 17-33.

Carter, L., and Mitchell, J.S., 1985: Stability of an artificially nourished beach, Balaena Bay, Wellington Harbour, New Zealand. *New Zealand Journal of Marine and Freshwater Research* 19: 535-552.

Chandrasekar, S., 1961: *Hydrodynamic and hydromagnetic stability*. Oxford University Press, London. 654p.

Chiswell, S.M., and Kibblewhite, A.C., 1980: Ocean wave studies in western Cook Strait. *New Zealand Journal of Marine and Freshwater Research* 14: 417-425.

Chiswell, S.M., and Kibblewhite, A.C., 1981: Spectra of the fully developed wind-generated ocean wave field west of central New Zealand. *New Zealand Journal of Marine and Freshwater Research* 15: 81-84.

Coode, J., 1880: *Report on Tauranga Harbour*. Report submitted to the Marine Department. 10p.

Csanady, G.T., 1982: *Circulation in the coastal ocean*. D. Reidel Publishing Co., Dordrecht, Holland. 279p.

Dahm, J., 1983: *The geomorphic development, bathymetric stability and sediment dynamics of Tauranga Harbour*. M.Sc. thesis, Earth Science Department, University of Waikato.

Davies-Colley, R.J., 1976: *Sediment dynamics of Tauranga Harbour.* M.Sc. thesis, Earth Science Department, University of Waikato.

Davies-Colley, R.J., and Healy, T.R., 1978: Sediment transport near the Tauranga Entrance to Tauranga Harbour. *New Zealand Journal of Marine and Freshwater Research* 12: 237-243.

de Lange, W.P., 1983: *Tsunami hazard: An investigation into the potential tsunami hazards of the Bay of Plenty region using numerical models.* M.Sc. thesis, Earth Science Department, University of Waikato.

de Lange, W.P., 1984: *Wave refraction analysis for No. 1 Reach - Tauranga Harbour.* Report to the Bay of Plenty Harbour Board. 31p.

de Lange, W.P., and Healy, T.R., 1986a: New Zealand tsunamis, 1840-1982. *New Zealand Journal of Geology and Geophysics* 29:

de Lange, W.P., and Healy, T.R., 1986b: Tsunami hazards in the Bay of Plenty, New Zealand: An example of hazard analysis using numerical models. *Journal of Shoreline Management* 2: 177-198.

de Lisle, J.F., and Kerr, I.S., 1963: The climate and weather of the Bay of Plenty region. *N.Z. Meteorological Service Miscellaneous Publication* 115(1). 12p.

Dixon, W.J., Brown, M.B., Engelman, L., Frane, J.W., Hill, M.A., Jennrich, R.I., and Toporek, J.D., 1981: *BMDP statistical software 1981.* University of California Press, Berkley. 726p.

Draper, L., 1966: The analysis and presentation of wave data - A plea for uniformity. *Proceedings of the 10th International Conference on Coastal Engineering.* 1-11.

Eckart, C., 1953: The generation of wind waves on a water surface. *Journal of Applied Physics* 24: 1485-1494.

Englelund, F., and Fredsøe, J., 1976: A sediment transport model for straight alluvial channels. *Nordic Hydrology* 7: 293-306. —

Folk, R.L., and Ward, W.C., 1957: Brazos River Bar, a study in the significance of grain-size parameters. *Journal of Sedimentary Petrology* 27: 3-27.

Fredsøe, J., Andersen, O.H., and Silberg, S., 1985: Distribution of suspended sediment in large waves. *Journal of Waterway, Port, Coastal and Ocean Engineering* 111: 1041-1059.

Gardiner, V., and Dackrombe, R.V., 1983: *Geomorphological field manual.* George Allen & Unwin Ltd., London. 254p.

Garvine, R.W., 1985: A simple model of estuarine subtidal fluctuations forced by local and remote wind stress. *Journal of Geophysical Research* 90C: 11945-11948.

Gibb, J.G., and Aburn, J.H., 1986: Shoreline fluctuations and an assessment of a coastal hazard zone along Pauanui Beach, Eastern Coromandel Peninsula, New Zealand. ***Water and Soil Technical Publication*** 27: 48p.

Gibbs, R.J., Matthews, M.D., and Link, D.A., 1971: The relationship between sphere size and settling velocity. ***Journal of Sedimentary Petrology*** 41: 7-18.

Gilmour, A.E., and Butcher, C.N., 1987a: Free oscillations in Lake Taupo - a triangular lake. ***DMFS Reports*** 1: 11-14.

Gilmour, A.E., and Butcher, C.N., 1987b: Free oscillations in Lake Whakatipu. ***DMFS Reports*** 1: 15-19.

Goda, Y., 1978: The observed joint distribution of periods and heights of sea waves. ***Proceedings of the 16th International Conference on Coastal Engineering***. 227-246.

Gonzalez, F.I., 1984: A case study of wave-current-bathymetry interactions at the Columbia River Entrance. ***Journal of Physical Oceanography*** 14: 1065-1078.

Goodknight, R.C., and Russell, T.L., 1963: Investigation of the statistics of wave heights. ***Journal of the Waterways and Harbours Division, ASCE*** 89(WW2): 29-54.

Grace, J.T., Grothaus, B.T., and Ehrlich, R., 1978: Size frequency distributions taken from within sand laminae. ***Journal of Sedimentary Petrology*** 48: 1193-1202.

Hallermeier, R.J., 1980: Sand motion initiation by water waves: two asymptotes. ***Journal of the Waterway, Port, Coastal and Ocean Division, ASCE*** 106(WW3): 299-318.

Harris, T.F.W., Hughes, T.S., and Valentine, E.M., 1983: Deepwater waves off Hicks Bay and the North-east Coast, North Island. ***Water and Soil Miscellaneous Publication*** 56, Wellington. 82p.

Harris, T.F.W., 1985: ***North Cape to East Cape: Aspects of the physical oceanography***. Auckland University. 178p.

Hasselmann, K.D., Barnett, T.P., Bouws, E., Carlson, H., Cartwright, D.E., Enke, K., Ewing, J.A., Gienapp, H., Hasselmann, D.E., Kruseman, P., Meerburg, A., Muller, P., Olbers, D.J., Richter, K., Sell, W., and Walden, H., 1973: Measurements of wind-wave growth and swell decay during the Joint North Sea Wave Project (JONSWAP). ***Deutschen Hydrographischen Zeitschrift, Reihe A*** 8. 95p.

Hasselmann, K.D., Ross, D.B., Muller, P., and Sell, W., 1976: A parametric wave prediction model. ***Journal of Physical Oceanography*** 6: 200-228.

Hastie, W.J., 1985: Wave height and period at Timaru, New Zealand. *New Zealand Journal of Marine and Freshwater Research* 19: 507-515.

Healy, T.R., 1985: *Field data collection programme and morphological study. Tauranga Harbour Study Parts II and V.* A report for the Bay of Plenty Harbour Board. 37p.

Healy, T.R., and Kirk, R.M., 1981: Coasts. In Soons, J.M., and Selby, M.J. (eds.), *Landforms of New Zealand*, Longman Paul Ltd., Auckland. 81-104.

Heath, R.A., 1985: A review of the physical oceanography of the seas around New Zealand - 1982. *New Zealand Journal of Marine and Freshwater Research* 19: 79-124.

Heiken, G., and Wöhletz, K., 1985: *Volcanic ash.* University of California Press, Berkley. 246p.

Hoffman, J.S., Keyes, D., and Titus, J.G., 1983: *Projecting future sea level rise - Methodology, estimates to the year 2100, and research needs.* U.S. Environmental Protection Agency, Washington.

Holland, L.D., and Kirk, R.M., 1985: Processes of coastal change: Himatangi to Paekakariki. *1985 Australasian Conference on Coastal and Ocean Engineering, Preprints of Papers*, Volume 1: 357-366.

Hubbell, D.W., Stevens, H.H., Skinner, J.V., and Beverage, J.P., 1987: Laboratory data on coarse-sediment transport for bedload-sampler calibrations. *U.S. Geological Survey Water-supply Paper 2299.* 31p.

Hughes, S.A., 1984: The TMA shallow-water spectrum description and applications. *Technical Report CERC-84-7*, Waterways Experiment Station, U.S. Army, Corps of Engineers, Vicksburg. 39p.

Hydraulics Research Station, 1963: *Tauranga Harbour Investigation. Report on First Stage, January 1963.* Report No. EX 201, Hydraulics Research Station, Wallingford, England.

Hydraulics Research Station, 1968: *Tauranga Harbour Investigation. Report on Second Stage, April 1968.* Report No. EX 395 (2 volumes), Hydraulics Research Station, Wallingford, England.

Ikeda, S., and Nishimura, T., 1986: Flow and bed profile in meandering sand-silt rivers. *Journal of Hydraulic Engineering* 112: 562-579.

Interactive Structures, 1981: *AI13 analog input system users manual, November, 1981.* Revision 4. Interactive Structures, Inc., Bala Cynwyd, Pennsylvania. 40p.

Jeffreys, H., 1925: On the formation of water waves by wind. *Royal Society of London, Proceedings, Section A* 107: 198-206.

Jeffreys, H., 1926: On the formation of water waves by wind (2nd paper). *Royal Society of London, Proceedings, Section A* 110: 241-247.

Johnson, N.L., and Kotz, S., 1970: *Continuous univariate distributions,* Volume 1. Houghton Mifflin Co., Boston. pp. 250-267.

Kahma, K.K., 1981: A study of the growth of the wave spectrum with fetch. *Journal of Physical Oceanography* 11: 1513-1515.

Kato, H., and Tsuruya, H., 1978: Experimental study of wind waves generated on currents. *Proceedings of the 16th Conference on Coastal Engineering,* Volume 1. 742-755.

Kelvin, Lord W., 1871: The influence of wind on waves in water supposed frictionless. *Philosophical Magazine* 42: 368-374.

Kitaigorodskii, S.A., Krasitskii, V.P., and Zaslavskii, M.M., 1975: On Phillip's Theory of equilibrium range in the spectra of wind-generated gravity waves. *Journal of Physical Oceanography* 5: 410-420.

Knowles, C.E., 1982: On the effects of finite-depth on wind-wave spectra. 1. A comparison with deep-water equilibrium-range slope and other spectral parameters. *Journal of Physical Oceanography* 12: 556-568.

Komar, P.D., 1976: *Beach processes and sedimentation.* Prentice Hall Inc., Englewood Cliffs, New Jersey. 429p.

Komar, P.D., 1981: The application of the Gibbs Equation for grain settling velocities to conditions other than quartz grains in water. *Journal of Sedimentary Petrology* 51: 1125-1132.

Komar, P.D., and Miller, M.C., 1973: The threshold of sediment movement under oscillatory water waves. *Journal of Sedimentary Petrology* 43: 1101-1110.

Komar, P.D., and Miller, M.C., 1975: On the comparison between the threshold of sediment motion under waves and unidirectional currents with a discussion of the practical evaluation of the threshold. *Journal of Sedimentary Petrology* 45: 362-367.

Komen, G.J., Hasselmann, S., and Hasselmann, K., 1984: On the existence of a fully developed wind-sea spectrum. *Journal of Physical Oceanography* 14: 1271-1285.

Lambrecht, 1983: *Mechanical Wind Recorder, Woelfle Type, No.1482.* Göttingen. 5p.

LeBlond, P.H., and Mysak, L.A., 1978: *Waves in the ocean.* Elsevier Scientific Publishing, Amsterdam. 602p.

Lee, G.A., 1928: *Survey of Harbour.* Report to the Tauranga Harbour Board. 13p.

Lee, T.T, and Black, K.P., 1978: The energy spectra of surf waves on a coral reef. *Proceedings of the 16th International Conference on Coastal Engineering*, Volume 1. 588-608.

Leeder, M.R., 1982: *Sedimentology: Process and product*. George Allen & Unwin Ltd., London. 344p.

Liu, P.C., 1971: Normalised and equilibrium spectra of wind waves in Lake Michigan. *Journal of Physical Oceanography* 1: 249-257.

Longuet-Higgins, M.S., 1952: On the statistical distribution of the heights of sea waves. *Journal of Marine Research* 11: 245-266.

Longuet-Higgins, M.S., 1975: On the joint distribution of the periods and amplitudes of sea waves. *Journal of Geophysical Research* 80: 2688-2694.

Losada, M.A., Desiré, and Merino, J., 1987: An energy approach to non-breaking wave-induced motion of bottom sediment particles. *Coastal Engineering* 11: 159-173.

Madsen, O.S., and Grant, W.D., 1976a: *Sediment transport in the coastal environment*. R.M. Parsons Lab., MIT, Technical Report 209. 105pp.

Madsen, O.S., and Grant, W.D., 1976b: Quantitative description of sediment transport by waves. *Proceedings of the 15th International Conference on Coastal Engineering*. 1093-1112.

McDowell, D.M., and O'Connor, B.A., 1977: *Hydraulic behaviour of estuaries*. The MacMillan Press Ltd., London. 292p.

Mehta, A.J., Lee, J., and Christensen, B.A., 1980: Fall velocity of shells as coastal sediment. *Journal of the Hydraulics Division, ASCE* 106: 1727-1744.

Miles, J.W., 1957: On the generation of surface waves by shear flows. *Journal of Fluid Mechanics* 3: 185-204.

Moon, V.G., 1983: *A flume study of the boundary layer flow over some non-quartzose sediments*. M.Sc. thesis, Earth Science Department, University of Waikato.

Nielsen, P., 1986: Suspended sediment concentrations under waves. *Coastal Engineering* 10: 23-31.

NZ Meteorological Service, 1982: The climatology of Tauranga Airport. *NZ Meteorological Service Miscellaneous Publication* 171(17). 20p.

NZ Meteorological Service, 1983a: Climatological extremes for New Zealand. *NZ Meteorological Service Miscellaneous Publication* 181. 13p.

NZ Meteorological Service, 1983b: Percentiles and extremes of atmospheric pressure at sea level: Stations in New Zealand, the Pacific Islands and Antarctica. *NZ Meteorological Service Miscellaneous Publication* 179. 51p.

NZ Meteorological Service, 1983c: Summaries of climatological observations to 1980. *NZ Meteorological Service Miscellaneous Publication* 177. 172p.

NZ Meteorological Service, 1983d: Wind data listing for New Zealand Stations. *NZ Meteorological Service Miscellaneous Publication* 184. 21p.

NZ Meteorological Service, 1983e: Meteorological Observations for 1981. *NZ Meteorological Service Miscellaneous Publication* 109(1981). 99p.

NZ Meteorological Service, 1984: Meteorological Observations for 1982. *NZ Meteorological Service Miscellaneous Publication* 109(1982). 102p.

NZ Meteorological Service, 1985: Meteorological Observations for 1983. *NZ Meteorological Service Miscellaneous Publication* 109(1983). 104p.

Officer, C.B., 1976: *Physical oceanography of estuaries (and associated coastal waters)*. John Wiley & Sons, New York. 465p.

Pattullo, J.G., Munk, W., Revell, R., and Strong, E., 1955: The seasonal oscillation in sea level. *Journal of Marine Research* 14: 88-155.

Peregrine, D.H., and Jonsson, I.G., 1983: Interaction of waves and currents. *Miscellaneous Report No. 83-6*, Coastal Engineering Research Center, U.S. Army, Corps of Engineers, Fort Belvoir. 88p.

Peregrine, D.H., Jonsson, I.G., and Galvin, C.J. 1983: Annotated bibliography on wave-current interaction. *Miscellaneous Report No. 83-7*, Coastal Engineering Research Center, U.S. Army, Corps of Engineers, Fort Belvoir. 82p.

Phillips, O.M., 1957: On the generation of waves by turbulent wind. *Journal of Fluid Mechanics* 2: 417-445.

Phillips, O.M., 1985: Spectral and statistical properties of the equilibrium range in wind-generated gravity waves. *Journal of Fluid Mechanics* 156: 505-531.

Pierson, W.J., Neumann, G., and James, R.W., 1955: Practical methods for observing and forecasting ocean waves by means of wave spectra and statistics. *Hydrographic Office Publication No. 603*, U.S. Navy Hydrographic Office, Washington. 284p.

Pierson, W.J., and Moskowitz, L., 1964: A proposed spectral form for fully developed wind seas based on similarity theory of S.A. Kitaigorodskii. *Journal of Geophysical Research* 69: 5181-5190.

Putz, R.R., 1952: Statistical distribution for ocean waves. *Transactions, American Geophysical Union* 33: 685-692.

Quayle, A.M., 1984: The climate and weather of the Bay of Plenty Region. *NZ Meteorological Service Miscellaneous Publication 115(1)*, 2nd edition. 56p.

Rance, P.J., and Warren, N.F., 1969: The threshold movement of coarse material in oscillatory flow. *Proceedings of the 11th International Conference on Coastal Engineering*. 487-491.

Raudkivi, A.J., 1976: *Loose boundary hydraulics*, 2nd edition. Pergamon Press, Oxford. 397pp.

Resio, D.T., 1981: The estimation of wind-wave generation in a discrete spectral model. *Journal of Physical Oceanography* 11: 510-525.

Resio, D.T., and Vincent, C.L., 1982: A comparison of various numerical wave prediction techniques. *Society of Petroleum Engineers Journal* 22: 764-774.

Revell, C.G., 1984: Annual and diurnal variation of thunderstorms in New Zealand and outlying islands. *Scientific Report* 3, NZ Meteorological Service. 35p.

Rigler, J.K., and Collins, M.B., 1984: Initial grain motion under oscillatory flow: A comparison of some threshold criteria. *Geo-Marine Letters* 3: 43-48.

Riley, D.S., Donelan, M.A., and Hui, W.H., 1982: An extended Miles Theory for wave generation by wind. *Boundary-Layer Meteorology* 22: 209-225.

Robertshaw, 1980: *Installation and operation instructions - Capacitance transmitter Model 167*. Robertshaw Controls Company, Anaheim, California. 14p.

Robertshaw, 1981: *Technical service and maintenance manual - Capacitance transmitter Model 167*. Robertshaw Controls Company, Anaheim, California. 38p.

Saville, T., 1954: The effect of fetch on wave generation. *Technical Memorandum No. 70*, Beach Erosion Board, Washington D.C.

Seelig, W.N., 1977: A simple computer model for evaluating coastal inlet hydraulics. *Coastal Engineering Technical Aid No.77-1*, U.S. Army Corps of Engineers, Coastal Engineering Research Center, Fort Belvoir.

Seymour, R.J., 1977a: Estimating wave generation on restricted fetches. *Journal of the Waterway, Port, Coastal and Ocean Division, ASCE* 103(WW2): 251-264.

Seymour, R.J., 1977b: Defining the wave climate for a harbour. *Ports '77, 4th annual symposium of the Waterway, Port, Coastal and Ocean Division, ASCE*. Volume 2, 218-235.

Shore Protection Manual, 1984: *Shore Protection Manual*. Coastal Engineering Research Center, U.S. Army, Corps of Engineers, Washington. (2 Volumes)

Southgate, H.N., 1985: A harbor ray model of wave refraction-diffraction. *Journal of Waterway, Port, Coastal and Ocean Engineering* 111: 29-44.

Stive, M.J.F., and Battjes, J.A., 1985: A model for offshore sediment transport. *Proceedings of the 19th International Conference on Coastal Engineering*, Volume 2. 1420-1436.

Stowe, K.S., 1979: *Ocean science*. John Wiley and Sons, New York. 610p.

Sunamura, T, and Horikawa, K., 1972: Improved method for inferring the direction of littoral drift from grain size properties of beach sands. *Annual Report of the Engineering Research Institute, Faculty of Engineering, University of Tokyo* 31: 61-68.

Sverdrup, H.U., and Munk, W.H., 1947: Wind, sea, and swell: Theory of relations for forecasting. *Hydrographic Office Publication No. 6*, U.S. Navy Hydrographic Office, Washington. 44p.

Thompson, E.F., and Vincent, C.L., 1984: Shallow water wave height parameters. *Journal of Waterway, Port, Coastal and Ocean Engineering* 110: 293-299.

Thompson, E.F., and Vincent, C.L., 1985: Significant wave height for shallow water design. *Journal of Waterway, Port, Coastal and Ocean Engineering* 111: 828-842.

Thornton, E.B., 1979: Energetics of breaking waves within the surf zone. *Journal of Geophysical Research* 84C: 4931-4938.

Thurman, H.V., 1985: *Introductory Oceanography*, 4th edition. Charles E. Merrill Publishing Co., Columbus, Ohio. 503p.

Trenberth, K.E., 1977: Surface atmospheric tides in New Zealand. *New Zealand Journal of Science* 20: 339-56.

Ursell, F., 1956: Wave generation by wind. In G.K. Batchelor and R.M. Davies (eds.), *Surveys in mechanics*. Cambridge University Press. 216-249.

Vincent, C.E., Young, R.A., and Swift, D.J.P., 1981: Bed-load transport under waves and currents. *Marine Geology* 39: 71-80.

Vincent, C.L., 1982: Depth-limited significant wave height: A spectral approach. *Technical Report 82-3*, Waterways Experiment Station, U.S. Army, Corps of Engineers, Vicksburg.

Vincent, C.L., 1985a: Depth-controlled wave height. *Journal of Waterway, Port, Coastal and Ocean Engineering* 111: 459-475.

Vincent, C.L., 1985b: Wind wave growth in shallow water. *Journal of Waterway, Port, Coastal and Ocean Engineering* 111: 765-770.

Visher, G.S., 1969: Grain size distributions and depositional processes. *Journal of Sedimentary Petrology* 39: 1074-1106.

Walters, R.A., and Gartner, J.W., 1985: Subtidal sea level and current variations in the Northern Reach of San Francisco Bay. *Estuarine, Coastal and Shelf Science* 21: 17-32.

Walton, T.L., and Dean, R.G., 1982: Computer algorithm to calculate longshore energy flux and wave direction from a two pressure sensor array. *Technical Paper No. 82-2*. Coastal Engineering Research Center, U.S. Army, Corps of Engineers, Fort Belvoir. 33p.

Wiegel, R.L., 1949: An analysis of data from wave recorders on the Pacific Coast of the United States. *Transactions, American Geophysical Union* 30: 700-704.

Graf, W.H., 1971: *Hydraulics of sediment transport*. McGraw-Hill, Inc., New York. 513p.

Sternberg, R.W., 1979: Bottom-current measurements and circulation in Western Port, Victoria. *Marine Geology* 30: 65-83.